University of Southampton

Faculty of Engineering and Physical Sciences

Engineering

The Effect of Fractures in Aquifers on the Performance of Borehole Ground Heat Exchangers

by

Oleksandra Pedchenko

ORCID ID 0000-0003-4802-7846

Thesis for the degree of Doctor of Philosophy

September 2019

University of Southampton

Abstract

Faculty of Engineering and Physical Sciences

Engineering

Thesis for the degree of Doctor of Philosophy

The Effect of Fractures in Aquifers on the Performance of Borehole Ground Heat Exchangers

by Oleksandra Pedchenko

Ground-source heat pump schemes for space conditioning and thermal storage increasingly use vertical borehole heat exchangers (VBHEs) because they can be installed in a wide range of geological conditions. Current models for VBHE performance often assume homogeneous ground conditions. However, in reality, hydrogeological conditions are rarely simple and homogeneous, and bedrock is commonly fractured. Application of the typical design assumption of homogeneous and isotropic ground conditions can give erroneous results.

It is known that for a single fracture in a low hydraulic conductivity matrix, the flow in the fracture increases the apparent thermal conductivity of the ground. Therefore, the presence of a fracture improves the estimated thermal performance of a VBHE and exacerbates downstream thermal impacts. However, studies investigating VBHE performance near to a flowing fracture installed in a matrix with considerable groundwater flow are lacking.

This study uses 2D and 3D numerical modelling to investigate a range of possible hydrogeological scenarios in which an open, flowing fracture may influence the long-term thermal performance of a VBHE. The key question considered by this study is: when does an open fracture improve (and when does it worsen) the thermal performance of a VBHE, compared with the thermal performance estimated assuming a homogeneous host rock? To answer this question, the temperature change at the VBHE wall, the mean temperature change of the heat transfer fluid, the extent of the downstream thermal plume, and the time to reach steady state were all used as the indicators of the VBHE performance. For simplicity, the analysis considered 30 years of the continuous VBHE operation under the constant thermal loading.

The analysis demonstrated that a fracture could have positive or negative effect on the thermal performance of a VBHE. The outcome depends on the interplay of two fracture effects. Firstly, the ability of a fracture to change the local groundwater velocities in the aquifer matrix (which leads to an increase or decrease in the local apparent thermal conductivity of the matrix). Secondly, the ability of a fracture itself to increase the thermal transport from a VBHE. The fracture can reduce the thermal transport from the VBHE if the first fracture effect is dominant and the VBHE is located in the area where the groundwater velocity has been locally reduced. This will lead to the increase in the estimated temperature change at the borehole compared with the case when the aquifer is assumed to be homogeneous. The overall fracture effect on the VBHE depends on which of the two fracture effects is dominant.

The impact of the fracture is the most significant in cases when the groundwater flow is moderate (0.01 - 0.1 m day^{-1}). At the higher groundwater flows, the impact of thermal dispersion in reducing the temperature change at the borehole is greater than the impact of the fracture in most cases. For moderate groundwater flows, significant thermal dispersion will act to exacerbate the adverse fracture impacts and reduce its positive impacts. For slow groundwater flows in an aquifer, a fracture near a VBHE can significantly increase the thermal transport, even when the volumetric flow rate in the fracture is small. Therefore, when groundwater flow in an aquifer is slow, the thermal performance of a VBHE is likely to be beneficially influenced by a fracture.

Fractures in bedrock aquifers potentially can have a positive or negative effect on the thermal performance of a VBHE. Therefore, the uncertainty in the long-term thermal performance of VBHEs and their downstream thermal impacts can be reduced when the assumption of homogeneous and isotropic ground conditions is justified.

Table of Contents

List of Tables

List of Figures

Research Thesis: Declaration of Authorship

Print name: OLEKSANDRA PEDCHENKO

Title of thesis: The Effect of Fractures in Aquifers on the Performance of Borehole Ground Heat Exchangers

I declare that this thesis and the work presented in it are my own and has been generated by me as the result of my own original research.

I confirm that:

1. This work was done wholly or mainly while in candidature for a research degree at this University;
2. Where any part of this thesis has previously been submitted for a degree or any other qualification at this University or any other institution, this has been clearly stated;
3. Where I have consulted the published work of others, this is always clearly attributed;
4. Where I have quoted from the work of others, the source is always given. With the exception of such quotations, this thesis is entirely my own work;
5. I have acknowledged all main sources of help;
6. Where the thesis is based on work done by myself jointly with others, I have made clear exactly what was done by others and what I have contributed myself;
7. Parts of this work have been published as: (Pedchenko O. *et al.* 2019).

Signature: Oleksandra Pedchenko Date: 04.12.2019

Acknowledgements

I thank my supervisors Fleur Loveridge, Nick Woodman and William Powrie for their devotion, tenacity and relentless efforts to develop me as a researcher. I am impressed how they managed as a team to guide and support me during this research journey. I am grateful for their support of my initiatives to enrich this project with courses in shallow geothermics and hydrogeology, conferences, workshops and teaching experience. I also thank my supervisory team for setting up this research project and for the research studentship from the Faculty of Engineering and the Environment.

I thank Keith Daly for valuable support in the construction of my first COMSOL model and learning how to use the COMSOL Multiphysics for my specific research questions. I very much value the contributions of Ian Hawke and Petr Reischig to solve the analytical solution for 3D dispersion for moving finite line source. I greatly appreciate valuable comments of Giles Richardson on the frameworks for mathematical models. The technical assistance of Petr Reischig and his expert advice on the best approaches to programming allowed me to produce more maintainable code versions. Without this essential advice my research experience would be less daring and less enjoyable. I am thankful to the leaders from the TUD COST Action TU1405: Sebastien Burlon, Giovanna Biscontin and Fleur Loveridge for accepting me to participate and contribute to the project GABI action: the European network for shallow Geothermal energy Applications in Buildings and Infrastructures. I am thankful to Peter Bayer, Selcuk Erol, Maria Klepikova, Daniel Schulte and Jaime Rivera for their kind support, thought-provoking discussions and refreshing advice.

I acknowledge the use of the IRIDIS High Performance Computing Facility and associated services, and the financial support of the Faculty of Engineering and Physical Sciences, the University of Southampton.

To overcome myself I lead my countless battles
I bless the light that shines in dark and gloom
I think of wonders in the storm that rattles
I savour moments in the silent room

To overcome the fears my battles will be countless
They'll test my strengths and weaknesses each day
But music will dissolve ever approaching darkness
and someone will remind along my way:
"Make it work and keep it going!
Put your best effort all the way through!
Don't cheat yourself and keep on throwing
Everything you have in everything you do."

to courageous souls who inspire me along the way

Definitions and Abbreviations

Abbreviations

ATC	Apparent thermal conductivity
BTES	Borehole thermal energy storage
COP	Coefficient of performance
DNF	Discrete fracture network
GHG	Greenhouse gas
GSHP	Ground-source heat pump
HDPE	High density polyethylene
HVAC	Heating, ventilating and air conditioning
MFLS	Moving finite line source
MILS	Moving infinite line source
TAF	Numerical model of **T**hermal transport in an **A**quifer with a single discrete open **F**racture near a VBHE installed in a homogeneous aquifer. TAF-2D is variant of TAF in 2D, TAF-3D is TAF in 3D.
TAFpi	The same model as TAF-3D but the heat source is modelled explicitly as a U-pipe with water circulating inside it
TAH	Numerical model of **T**hermal transport in an **A**quifer with **H**omogeneous matrix. TAH-2D is variant of TAH in 2D, TAH-3D is TAH in 3D.
TAHpi	The same model as TAH-3D but the heat source is modelled explicitly as a U-pipe with water circulating inside it
VBHE	Vertical borehole heat exchanger

Symbols

A Pipe cross-sectional area (m^2)

A_f Fracture rotation angle around the VBHE, it is relative to the x-axis (°)

$\boldsymbol{B}$ Hydrodynamic dispersion **tensor** ($m^2\ s^{-1}$)

C_{ef} Effective volumetric heat capacity at constant pressure for meter depth of fracture material, fluid and solid ($J\ m^{-3}\ K^{-1}$)

C_{em} Effective volumetric heat capacity at constant pressure for meter depth of matrix (aquifer) material (for 2D model) and per volume for 3D model, effective meaning it is for both fluid and solid ($J\ m^{-3}\ K^{-1}$)

C_v Volumetric heat capacity ($J\ m^{-3}\ K^{-1}$) or ($W\ s\ m^{-3}\ K^{-1}$)

C_m Volumetric heat capacity of solid material in porous media ($J\ m^{-3}\ K^{-1}$)

C_w Volumetric heat capacity of water ($J\ m^{-3}\ K^{-1}$)

c_f Specific heat capacity at constant pressure of solid material in the fracture ($J\ kg^{-1}\ K^{-1}$)

c_g Specific heat capacity of solid in grout ($J\ kg^{-1}\ K^{-1}$)

c_m Specific heat capacity at constant pressure of solid material in porous media ($J\ kg^{-1}\ K^{-1}$)

c_p Specific heat capacity of the wall material (HDPE) of pipe at constant pressure ($J\ kg^{-1}\ K^{-1}$)

c_w Specific heat capacity at constant pressure of water in porous media ($J\ kg^{-1}\ K^{-1}$).

D_f Orthogonal distance from fracture to the VBHE wall (m)

$\boldsymbol{D_t}$ Thermal diffusion tensor or thermal diffusivity tensor ($m^2\ s^{-1}$) in a hydraulically isotropic medium, has the principal longitudinal $D_{t,L}$, transverse $D_{t,T}$ and vertical $D_{t,V}$ components

D_t^* Thermal diffusion coefficient in a matrix without flow ($m^2\ s^{-1}$)

$D_{t,L}$ Longitudinal thermal diffusion coefficient ($m^2\ s^{-1}$), the longitudinal component of the thermal diffusion coefficient D_t in hydraulically isotropic medium

$D_{t,T}$ Transverse thermal diffusion coefficient ($m^2\ s^{-1}$), the transverse component of D_t in hydraulically isotropic medium

$D_{t,V}$ Vertical thermal diffusion coefficient ($m^2\ s^{-1}$), the vertical component of D_t in hydraulically isotropic medium

d Representative length dimension (m)

d_p Inner diameter of the circular pipe (m)

d_z Thickness of model domain in the out-of-plane direction in the 2D model and equal to VBHE length H_b in the 3D model (m)

E total mechanical energy per unit mass of fluid ($J\ kg^{-1}$)

e_A Surface roughness for drawn tubing (m)

F_o Fourier number (–)

f_D Darcy friction factor (-)

H Hydraulic head (m)

H_b Length of vertical borehole heat exchanger (m)

H_f Fracture height (m)

h Heat transfer coefficient ($W\ m^{-2}\ K^{-1}$)

h_i Internal film heat transfer coefficient (W m^{-2} K^{-1})

g Acceleration due to gravity (m s^{-2})

I_f Fracture inclination relative to the horizontal ground (°)

J Source heat flow rate (W)

K Hydraulic conductivity of material (m s^{-1})

K_f Hydraulic conductivity of fracture (m s^{-1})

K_g Hydraulic conductivity of silica-sand based grout (m s^{-1})

K_m Hydraulic conductivity of matrix (m s^{-1})

L Length scale (m)

L_f Fracture length (m)

M Constant hydraulic gradient in the direction of the x-axis (-)

M_F Mesh size factor (-)

M_i Initial maximum mesh size found by the preliminary mesh refinement (m)

M_s Maximum mesh element size at the heat source (m)

$\boldsymbol{n}$ Normal vector toward exterior (outward) (-)

N_u Nusselt number for turbulent flow (-)

O_f Volumetric flow rate in the fracture per meter of depth (m^3 s^{-1})

O_p Volumetric flow rate in the U-pipe (m^3 s^{-1})

P_e Thermal Peclet number, P_e (-)

P_r Prandtl number (-)

p Pressure (Pa)

p_0 Reference pressure (Pa)

Q Heat source in 3D (W m^{-3})

Q_p Heat transferred through the pipe wall (W m^{-1})

$\boldsymbol{q}$ Heat flux vector (W m^{-2})

$\boldsymbol{q_f}$ Heat flux vector in the fracture (W m^{-2})

q_{tb} Heat flow rate per unit length of the borehole, $q_{tb} = J/H_b$ (W m^{-1})

R Relative difference between the TAF and TAH models (-)

R_b Thermal resistance of borehole for each meter of depth (m K W^{-1})

Re Reynolds number (-)

R_K Ratio of the hydraulic conductivity of the fracture to the matrix (-)

r Radius of the VBHE (m)

r_p Inner pipe radius (m)

r_{s2D} Heat source radius for model in 2D

r_{s3D} Heat source radius for model in 3D

S_f Fracture shift, offset longitudinal to its orientation (m)

S_s Specific storage (m^{-1})

s Shank space between the inlet and outlet pipes (m)

T Temperature (K)

T_0 Initial (undisturbed, reference) temperature (K)

T_d Temperature difference between T_{in} and T_{out} (K)

T_m External temperature outside the pipe (K)

T_{in} Input working fluid temperature entering the U-pipe (K)

T_{out} Output working fluid temperature leaving the U-pipe (K)

ΔT Temperature change, $\Delta T = T - T_0$ (K)

ΔT_b Temperature change at the VBHE wall after 30 years of continuous VBHE operation (K)

ΔT_{max} Maximum difference in temperature change between numerical model (TAH-2D and TAH-3D) and the corresponding analytical solution (MILS and MFLS)

ΔT_{pm} Mean temperature change of the working fluid in U-pipe after 30 years of continuous VBHE operation (K)

t Time (s)

t_{max} Maximum time for simulations (years)

t_n One of calculated time steps (s)

t_{Sb} Time to stabilise the temperature change at the VBHE wall ΔT_b (years)

t_{Sp} Time to stabilise the temperature change of working fluid ΔT_{pm} (years)

t_{S2K} Time to stabilise maximum extent of the +2 K isotherm (years), similar notation for other isotherms, e.g. $t_{S0.5K}$

u Mean flow velocity, $u = v/\phi$ (m s^{-1})

u_t Thermal velocity, $u_t = v\ C_w/C_{em}$ (m s^{-1})

$\boldsymbol{v}$ Darcy velocity **vector** (m s^{-1})

v_b Darcy velocity in the matrix at the VBHE wall (m s^{-1})

$\boldsymbol{v_f}$ Darcy velocity vector in the fracture (m s^{-1})

v_{fmax} Maximum Darcy velocity in the fracture (m s^{-1})

v_L Longitudinal component of Darcy velocity (m s^{-1})

v_p Velocity of the fluid in the U-pipe (m s^{-1})

v_T Transverse component of Darcy velocity (m s^{-1})

v_u Groundwater velocity in an undisturbed matrix (m s^{-1})

W_f Fracture width, aperture (m)

w_p Wall thickness of pipe (m)

X_{2K} Maximum extent of the +2 K isotherm along the x-coordinate axis (m), i.e. in the direction of groundwater flow in the matrix, after 30 years of continuous VBHE operation; similar notation for other isotherms, e.g. $X_{0.5K}$

x Cartesian x-coordinate (m), positive x is downstream

y Cartesian y-coordinate (m)

z Cartesian z-coordinate (m), positive z is downward

z_e Elevation (m)

Z_f Depth from the fracture top edge to the ground surface (m)

Z_{fh} Depth at which horizontal fracture intersects the VBHE (m)

Z Pipe wall perimeter, $Z = \pi d_p$ (m)

α_s Compressibility of solid in the matrix (Pa^{-1})

α_w Compressibility of water (Pa^{-1})

$\boldsymbol{\beta}$ Hydrodynamic dispersivity tensor (m)

β_L Longitudinal (along x-axis) thermal dispersivity of the aquifer (m)

β_T Transverse (along y-axis) thermal dispersivity of the aquifer (m)

β_V Vertical (along z-axis) thermal dispersivity of the aquifer (m)

∇_p Gradient that is taken parallel to the line of the fracture

ϵ Porosity of porous material (-)

ϵ_f Porosity of the fracture (-)

ϵ_m Porosity of the matrix, the fraction of the total matrix volume that is occupied by the pore space, (-)

Θ Dimensionless temperature (-)

κ Permeability of porous material (m^2)

λ Thermal conductivity for isotropic medium (W m^{-1} K^{-1})

$\boldsymbol{\lambda_a}$ Apparent thermal conductivity tensor (W m^{-1} K^{-1})

$\boldsymbol{\lambda_B}$ Dispersive thermal conductivity tensor (W m^{-1} K^{-1})

λ_f Thermal conductivity of solid material in the fracture (W m^{-1} K^{-1})

λ_g Thermal conductivity of solid in the VBHE grout (W m^{-1} K^{-1})

λ_{ef} Effective thermal conductivity of fracture (W m^{-1} K^{-1})

λ_{em} Effective thermal conductivity that accounts for both matrix solid and fluid properties (W m^{-1} K^{-1})

λ_m Thermal conductivity of solid material in the matrix (W m^{-1} K^{-1})

λ_p Thermal conductivity of the wall material (HDPE) of pipe (W m^{-1} K^{-1})

λ_w Thermal conductivity of mobile water in the matrix (W m^{-1} K^{-1})

μ Dynamic viscosity of the fluid (kg m^{-1} s^{-1})

ν Kinematic viscosity of the fluid (m^2 s^{-1})

ρ Mass density (kg m^{-3})

ρ_g Density of the solid material in grout (kg m^{-3})

ρ_f Density of solid material in the fracture (kg m^{-3})

ρ_m Density of solid material in the matrix (kg m^{-3})

ρ_p Density of the wall material (HDPE) of pipe (kg m^{-3})

ρ_w Density of water (kg m^{-3})

φ_r Angular coordinate (polar angle) (-)

ϕ Porosity (-)

ψ Pressure head (m)

Subscripts

0 initial

b borehole

e effective

f fracture

L longitudinal with respect to the direction of groundwater flow in undisturbed matrix (along x-axis)

m matrix

S steady state

T transverse with respect to the direction of groundwater flow in undisturbed matrix (along y-axis)

V vertical (along z-axis)

w water

Chapter 1 Introduction

1.1 Background

Ground-source heat pump (GSHP) schemes for space conditioning and thermal storage increasingly use vertical borehole heat exchangers (VBHEs) because they can be installed in a wide range of geological conditions (Dehkordi *et al.* 2015), require only a small ground area and cause minimal landscape disturbance (Yang *et al.* 2010). Additionally, no licensing for groundwater abstraction or injection is required because it is a closed-loop system. Future use of GSHP systems (including VBHEs) is expected to increase as the market for low-carbon technologies grows (Carvalho *et al.* 2015b). Improved energy efficiency for buildings is required by the EU legislation (Directives: 2018/2002 (EU Council 2018b), 2010/31/EU (EU Council 2010b), 2009/125/EC (EU Council) and 2010/30/EU (EU Council)). Additionally, some government authorities of the EU member states provide financial support for the use of renewable energy sources for heating and cooling to reduce primary energy dependency and greenhouse gas emissions (Cansino *et al.* 2011).

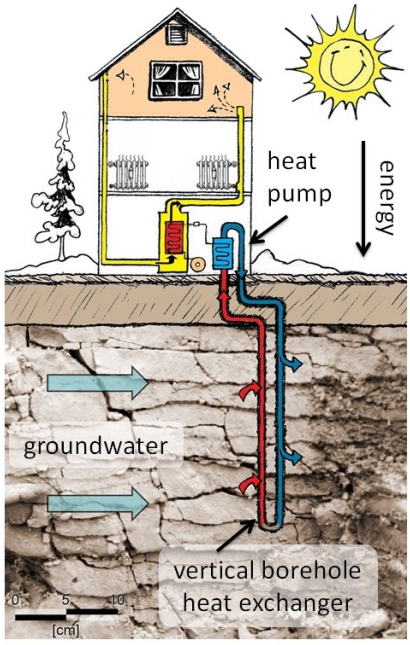

Figure 1.1 Vertical borehole heat exchanger installed in a fractured aquifer. Scheme. House figure from (Plumas-Sierra Rural Electric Cooperative 2016); geology photo from (Lord *et al.* 2002).

The indicators used to estimate the thermal performance of a VBHE include the temporal development and stabilisation of the temperature change at the VBHE wall and / or of the working fluid. Additionally, the thermal impacts of a VBHE on the surrounding ground further afield can be estimated to assess possible thermal interactions. Modelling of the thermal performance of a VBHE is an effective tool to estimate the temperature changes induced by the thermal load demand on a VBHE, the time to reach steady state and

whether the system can be profitable over its whole lifecycle (Retkowski *et al.* 2015).

Consideration of groundwater effects on a VBHE can significantly improve the estimated thermal performance of a VBHE. Capozza *et al.* (2013) quantified the value of considering groundwater flow during the VBHE design as a saving of 16 % on the project investment costs. Additionally, modelling the groundwater flow is useful to estimate interactions between VBHE systems, especially in congested urban environments. Ferguson (2015) points out that if the groundwater velocity exceeds 1×10^{-8} m s^{-1} (8.6×10^{-4} m day^{-1}), it should be accounted for during modelling of a VBHE because it increases the apparent thermal conductivity of the ground as defined by Sauty *et al.* (1982). Therefore, the effectiveness of thermal exchange can be significantly increased by groundwater flow. Groundwater flow also reduces the time needed to reach steady state (Tye-Gingras & Gosselin 2014; Rivera *et al.* 2015b). However, the influence of groundwater flow is frequently ignored, and practical guidelines are lacking (Tye-Gingras & Gosselin 2014).

Current models for the thermal performance of a VBHE often assume homogeneous ground conditions. However, in practice, hydrogeological conditions are rarely simple and homogeneous, and bedrock is commonly fractured. VBHEs are frequently installed in heterogeneous and fractured media, which may have groundwater flow (Dehkordi *et al.* 2015). Application of the typical design assumptions of homogeneous and isotropic ground conditions and the averaged thermal properties in a layered or heterogeneously fractured aquifers can give erroneous estimations of the thermal performance of a VBHE (Loveridge *et al.* 2013; Erol 2016).

Recent research has investigated the effect of fractured aquifers on the thermal performance of a VBHE. Several studies modelled the influence of a single open fracture in a matrix of low hydraulic conductivity material. In these cases, the flow in the fracture increases the apparent thermal conductivity of the ground. Therefore, the presence of a fracture improves the estimated thermal

performance of a VBHE and exacerbates its downstream thermal impacts, even if the flow rate in such a fracture is low (Gehlin & Hellström 2003; Liebel *et al.* 2012; Dehkordi *et al.* 2015). However, studies investigating the performance of a VBHE near to a flowing fracture installed in a matrix with groundwater flow are few. Thus, there is a need for systematic analysis and quantification of the effects of open fractures on the long-term thermal performance of VBHEs for a wide range of hydrogeological conditions, including considerable groundwater flow in the matrix.

1.2 Research objectives

The key research question addressed by this study is how an open fracture in an aquifer influences the thermal performance of a VBHE, compared with the thermal performance estimated assuming a homogeneous host rock.

To address this question, the research approach and methods were structured according to the following objectives:

1) To investigate how groundwater flow and the thermal dispersivity influence the thermal performance of a VBHE installed in homogeneous aquifers using available analytical solutions to the diffusion-advection equation. The indicators used to quantify the VBHE thermal performance were:
   a) the temperature change at the borehole wall as it develops with time;
   b) the longitudinal extent of the isotherm of interest as it changes with time;
   c) the time to reach steady state of a) and b);
2) To set up and validate numerical models to allow investigation of fracture effects on a VBHE, a topic not within the scope of analytical methods.
3) To conduct a single-parameter sensitivity analysis using numerical models to understand how a flowing fracture can influence the long-term thermal performance of a VBHE, estimated assuming a homogeneous host rock.
4) To conduct an uncertainty analysis using the Monte Carlo method to estimate to what extent a nearby fracture can influence a VBHE for a wide range of

hydrogeological scenarios. The hydrogeological scenarios include varying groundwater velocity in the aquifer, thermal dispersivity and fracture parameters (fracture geometry, hydraulic properties and relative location to the VBHE and groundwater flow direction).

5) To investigate how the simulation results are affected by different modelling assumptions, such as 2D vs 3D, and the detail of the heat exchanger captured by the model.
6) To provide the practical recommendations to estimate the uncertainty in the long-term thermal performance of a VBHE installed nearby a fracture in an aquifer.

1.3 Thesis outline

This thesis is arranged in 9 chapters, as explained below.

Chapter 1 Introduction

Chapter 2 Literature review

Chapter 2 composed of two parts. The first provides an overview of the current status and prospects of shallow geothermal energy installations. It summarises available technologies and legislation in this low carbon energy field. It introduces the benefits and current challenges of ground heat resource management using vertical borehole heat exchangers (VBHEs).

The second part is the overview of the technical aspects: fundamental heat transfer processes, the physical reality of the fractured aquifers and their conceptual representations (modelling frameworks). Finally, the research literature on the influence of the groundwater flow and fractures on the thermal performance of a VBHE is reviewed.

Chapter 3 Effects of the advective thermal transport on a VBHE installed in a homogeneous aquifer

Chapter 3 analyses the results of calculations to assess how groundwater influences the thermal performance of a VBHE carried out using available analytical solutions, which assume that the VBHE is installed in a homogeneous aquifer. It also considers the role of the VBHE length and thermal load.

Chapter 4 The influence of thermal dispersion on the thermal performance of a vertical borehole heat exchanger

Chapter 4 develops and applies an improved analytical solution for a VBHE installed in a homogeneous aquifer, which accounts for thermal dispersion in 3D, to investigate how thermal dispersion can affect the thermal performance of a VBHE.

Chapter 5 Development and validation of the 2D and 3D numerical models

Chapter 5 describes numerical models built for a VBHE installed in a homogeneous aquifer in 2D and in 3D. It then presents analyses to validate these models against results from relevant analytical solutions. This chapter also includes the description of the numerical models for a VBHE installed in a homogeneous aquifer with a nearby single fracture. The model with explicit representation of pipes inside the VBHE is also described here.

Chapter 6 The influence of a single fracture on a VBHE in 2D

Chapter 6 discusses the results of a single-parameter sensitivity analysis using the 2D numerical model. Here the possible effects of a single permeable fracture on the thermal performance of a VBHE are investigated. The chapter identifies the conditions in which a nearby fracture matters and when it can be ignored in the modelling the long-term thermal performance of a VBHE.

Chapter 7 Uncertainty and parameter sensitivity analysis

Chapter 7 presents the results of the Monte Carlo analysis using the 2D numerical model. It investigates when and how a single permeable fracture can affect the uncertainty in the thermal performance of a VBHE, to which fracture parameters the model is sensitive, and how this sensitivity changes for different groundwater velocities and thermal dispersivities in an aquifer.

Chapter 8 Fracture influence on a VBHE modelled in 3D

Chapter 8 discusses the implications of uneven heat exchange along the length of the VBHE, based on results from the 3D model with explicitly modelled pipes in the VBHE. The thermal performance of a VBHE is analysed for different groundwater velocities and compared with the results of the 3D model without pipes, which was validated against the analytical solutions. The single-parameter sensitivity analysis was carried out using the 3D numerical model of a VBHE with pipes. The influence of the additional fracture parameters (which can only be modelled in 3D) and their possible effects on the thermal performance of the VBHE are discussed.

Chapter 9 Conclusions, recommendations for practice and future work

Chapter 9 draws the overall conclusions of this work and offers recommendations for practice and suggestions for further research.

Chapter 2 Literature review

2.1 Shallow geothermal energy applications

2.1.1 Benefits, obstacles and popularity

The space heating, cooling and hot water use account for approximately 63 % of the EU final energy consumption (European Commission 2016). Alternative energy sources are necessary to reduce the carbon emissions, ensure a future reliable energy source, save energy costs and relieve the national energy dependence on fossil fuels.

Ground-source heat pumps (GSHP) are a popular installation type to harvest shallow geothermal energy. The number of countries which use these installations has almost doubled in 15 years, and the quantity of reported installed units worldwide increased more than threefold in the last 10 years (Lund & Boyd 2016). GSHP are the single biggest source of direct geothermal energy accounting for 71 % of installed world-wide capacity (50,258 MW) and 55 % of annual direct geothermal energy use (326,848 TJ/year) (Lund & Boyd 2016). In Europe installed capacity of ground-source heat pumps is 17,700 MW (Lund & Boyd 2016).

The main obstacle for the VBHE market is large installation costs, the major part of which is the construction of geothermal boreholes (Hénault *et al.* 2016). The average capital installation cost of a VBHE around the world is around 24 000 € (+/- 7000 €, incl. 19 % Value added tax), around 1000 € (+/- 400 €) per kW (Blum *et al.* 2011). In Europe a residential VBHE for 10 kW costs 1500-2500 € / kW (European Geothermal Energy Council 2015). This causes a trend to combine smaller VBHE system with supplementary heating or cooling devices (e.g. gas-fired boilers, electrical heaters) (Atam & Helsen 2016). The other reason for such combination is estimated ground characteristics, regulation, estimated thermal loads and payback period (typically 5-10 years) (Atam & Helsen 2016).

2.1.2 Types

Geothermal heat pumps use groundwater temperatures between 5 °C and 30 °C; therefore, their application is universal (Curtis *et al.* 2005). There are many designs of shallow geothermal energy installations which makes this technology applicable to a wide range of conditions (Figure 2.1).

A hybrid system combines a VBHE with conventional heating, ventilating and air conditioning (HVAC) to reduce thermal impacts, high installation costs of the VBHE and provide only during the peak building energy demands (Kuzmic *et al.* 2016).

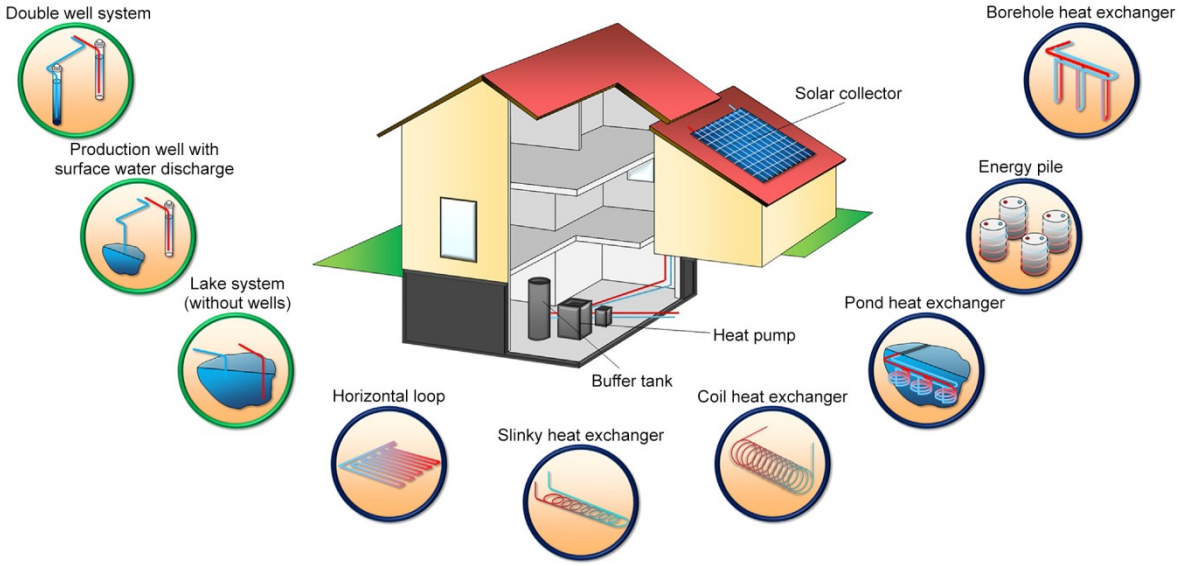

Figure 2.1 Different systems using shallow geothermal energy (Somogyi *et al.* 2017). Energy pile is a VBHE integrated into building foundations to reduce the installation costs.

2.1.3 Legislation in the EU

The spacing for VBHEs is arbitrary and legal requirements are not present in every EU country (Table 2.1).

Table 2.1 Recommended and legally binding minimum distances for the closed and open geothermal systems (Haehnlein *et al.* 2010). The information for the UK is summarized from work by Somogyi *et al.* (2017).

Country	Closed systems	Open systems	Legal status
Austria	2.5 m to the next property line	-	Recommended
China	3-6 m to the next BHE	-	Recommended
Czech Rep.	5 m to the next property line	5 m to next property line	Legally binding
Denmark	300 m to drinking water well	-	Legally binding
Finland	30 m to all wastewaters, 20 m to a onsite wastewater treatment system, 5 m to sewers and water pipes, 20 m to dug or energy well, 40 m to bored well, 3 m to the next building, 10 m to the next property line		Recommended
Germany	5 m to the next property line, 10 m to the next installation	-	Recommended and state-specific
Greece	-	5 m to the neighbouring buildings, 20 m to the next power line	Legally binding, if included in permission
Liechtenstein	3 m to the next property line, 6 m to the next installation	-	Recommended
Sweden	10 m to the next property line 20 m to the next installation 30 m to the next drinking water well	10 m to the next property line 20 m to the next installation 30 m to the next drinking water well	Recommended
Switzerland	3-4 m to the next property line, 5-8 m to the next installation	-	Recommended Legally binding
The United Kingdom	For installation for single domestic property no regulation applies. If the operation of the ground source heat pump interferes with neighbouring installation or environmental feature, the common law of nuisance applies.	Groundwater investigation consent is required before drilling, and full abstraction licence is needed for abstraction above 20 m^3 per day. The temperature difference between the production and injection should be less than 10 °C. The installation should be kept at a minimum distance of 50 m from watercourses, groundwater-dependent natural resources, other groundwater abstraction points	For closed-loop systems and small open-loop system it is advised to carry out an environmental impact assessment, registration or permit is not necessary.

Although the thermal disturbance from the VBHE changes over space and time as thermal loads change, only the distances between the installations are regulated (Haehnlein *et al.* 2010). As VBHEs are installed in the aquifers, the criteria for sustainable use of groundwater should be met even though the VBHE does not directly abstract groundwater (Table 2.2).

Table 2.2 Criteria for a sustainable thermal use of groundwater (Haehnlein *et al.* 2010)

Criterion	Purpose
Technical accurate drilling and installation	Guarantee of operation Protection of groundwater as a resource for drinking water
Backfilling	Avoid leakage of hazardous materials (e.g. heat carrier fluid, drilling fluid, secondary contaminants such as oil of vehicles, drilling apparatus, etc.) Avoid changes in groundwater ecology Avoid hydraulic contacts between different aquifer systems
Minimum distances	Avoid accumulation of temperature changes Avoid interaction with other shallow geothermal systems Avoid influence on other technical systems (drinking water wells, water pipes, neighbouring ground)
Temperature thresholds	Avoid changes in groundwater ecology. Guarantee of operation

2.2 Vertical borehole heat exchangers

2.2.1 Introduction

Vertical borehole heat exchangers (VBHEs) are closed-loop systems coupled with the ground. A VBHE uses a heat pump (Figure 2.2) to exploit deep ground temperatures which is relatively constant (Figure 2.3). A VBHE is usually 45 – 75 m deep for residential but may be over 150 m for the larger industrial applications (Self *et al.* 2013). Therefore, the VBHE provides reliable, consistent performance (Yang *et al.* 2010). The ground temperature is usually not affected by the seasonal changes in ambient air temperature below approximately 15 m depth, whereas geothermal gradient is normally in the range of 0.5 – 3 K per 100 m (Gehlin 2002). The life cycle of a VBHE can span 25 – 50 years.

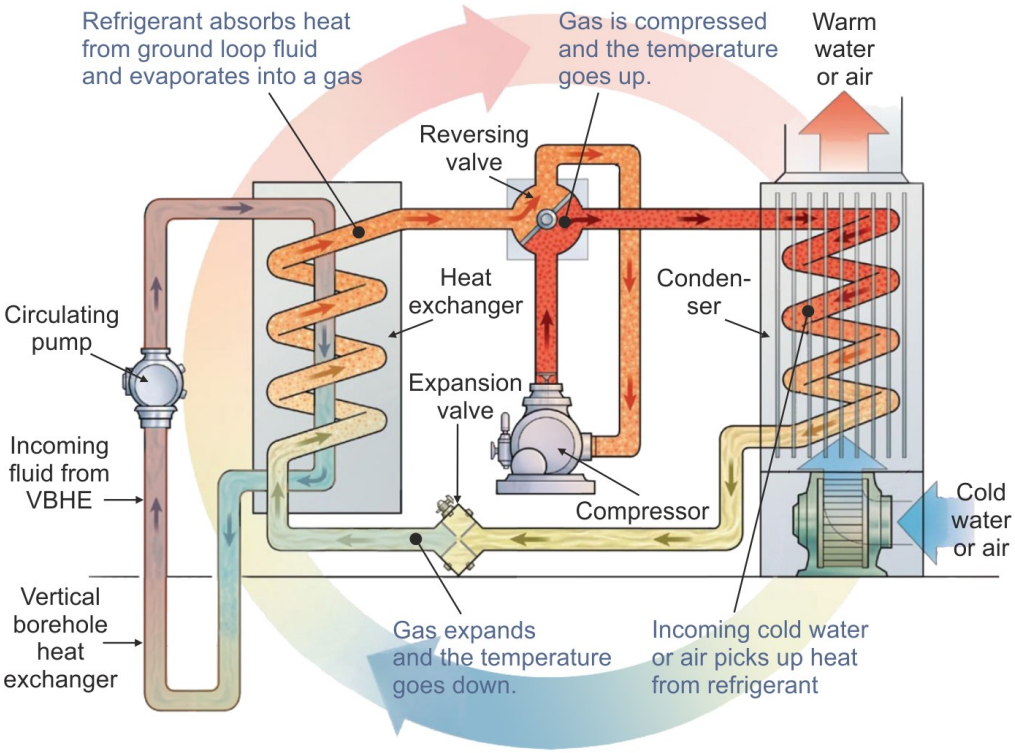

Figure 2.2 Schematic representation of heat pump in a house connected to the vertical borehole heat exchanger used for the space heating. Arrows indicate the direction of movement of the fluid; colour indicates the fluid temperature. Scheme is modified from (Cold Climate Housing Research Center 2016).

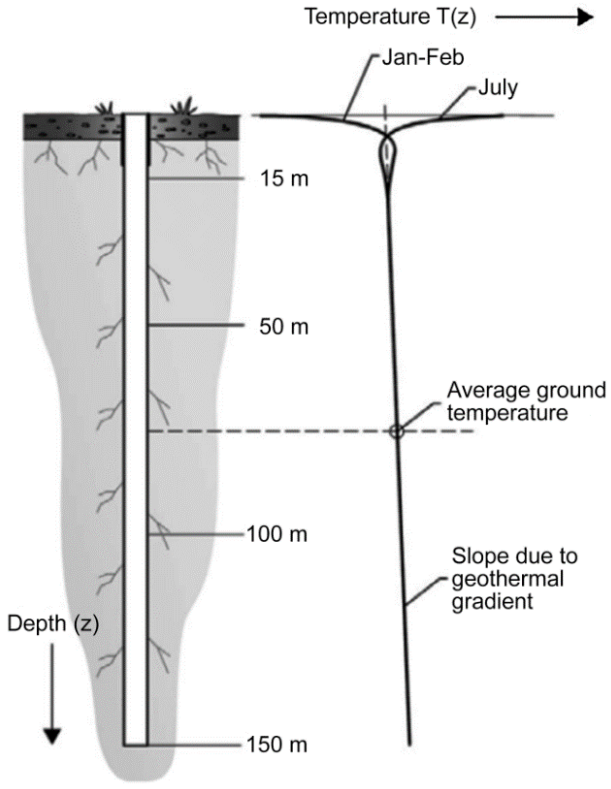

Figure 2.3 Generalised temperature profile in the ground, geothermal gradient is normally in the range of 0.5-3 K per 100 meter (Gehlin 2002).

2.2.2 Benefits and popularity

Ground source heat pump is a leading worldwide direct geothermal energy application by installed capacity (47.2 %) and energy use (68.3 %) (Soni *et al.* 2015). Ground-source heat pump schemes for space conditioning and thermal storage increasingly use vertical borehole heat exchangers (VBHEs) because they can be installed in a wide range of geological conditions (Dehkordi *et al.* 2015). They require a small ground area (Florides & Kalogirou 2007) and cause minimal landscape disturbance (Yang *et al.* 2010). No licencing for groundwater abstraction or injection is required because it is a closed-loop system. An additional advantage of VBHEs includes possibility to integrate it with another energy source or sink (e.g. solar photovoltaics) which can increase the efficiency and reduce the emissions (Busato *et al.* 2015; Soni *et al.* 2016). The seasonal borehole thermal energy storage (BTES) provides more reliability to a VBHE system as well as energy and economic savings (Giordano *et al.* 2016). There are above 1.25 million of installed VBHEs for the residential heating in Europe (Bayer *et al.* 2012), and the number is growing.

VBHEs are not fully exploited. Among the barriers to their use is high installation cost (Soni *et al.* 2015). However, despite the high capital costs of a VBHE, this technology is 20 % cheaper in operational and maintenance costs in the long term (over the 25 years of its lifecycle) compared with the traditional gas boiler heating system (Geological Survey of Ireland 2015).

Future use of the GSHP systems (including VBHEs) is set to increase as the market for low-carbon technologies grows (Carvalho *et al.* 2015b). The government authorities of the EU member states provide financial support for the use of renewable energy sources for heating and cooling to reduce primary energy dependency and greenhouse gas emissions (Cansino *et al.* 2011).

The potential increase in VBHE usage in the future can help to meet the EU Council Clean energy package goals (European Council for an Energy Efficient Economy 2019):

1) to reduce greenhouse gas emissions by at least 40 % by 2030 compared WITH 1990 levels
2) a binding target for at least 32 % of the final energy consumption to come from the renewable sources and
3) a binding target of at least 32.5 % energy efficiency relative to 'business as usual' scenario.

These targets are backed by the revised Energy Efficiency Directive 2018/2002 (EU Council 2018b) and the Directive 2018/2001 on the promotion of the use of energy from renewable sources (EU Council 2018a). The improved energy efficiency for buildings is required by the EU legislation, for example, the Energy Performance of Buildings Directive 2010/31/EU (EU Council 2010b), the Eco-design Directive 2009/125/EC (EU Council) and the Energy Labelling Directive 2010/30/EU (EU Council).

VBHEs have high potential in saving greenhouse gas (GHG) emissions. The Coefficient of performance (COP) defines the efficiency of a VBHE. COP is the ratio between useful thermal energy produced and energy consumed to obtain it (Sarbu & Sebarchievici 2014). During the heating season, a VBHE reduces the temperature of the ground as it takes the heat. As the ground gets colder during the heating season, the COP of a VBHE gradually reduces. Therefore, a seasonal COP is a useful indicator of the VBHE efficiency. To calculate the seasonal COP (sCOP) both usable energy and consumed energy by a VBHE are summed during the full heating season to take the ratio between thermal power (capacity) of the VBHE and its drive power. VBHEs have typical long-term COP range between 2.5 and around 4 (Sarbu & Sebarchievici 2014).

Carvalho *et al.* (2015a) estimated that a replacement of natural gas boilers in the EU used for space heating with the VBHE systems (with sCOP of 4.5) would give a 90 % saving of CO_2 (157 Mt CO_2) emissions due to space heating. Additionally, 60 % of primary energy (520 TWh) was predicted to be saved along with a reduction of 50 % in the dependency of the EU on the externally supplied natural gas. The technology replacement was also predicted to increase the share of renewable energy sources in the total EU energy budget by 5.6 % (Carvalho *et al.* 2015a).

For Europe, GHG emissions of a VBHE is around 63 tons of CO_2 for a lifecycle of 20 years (ca. 0.6 kg CO_2 equivalent per kWh) (Saner *et al.* 2010). Consequently, one VBHE installation can save 1800 and 4000 kg Carbon equivalent per year (Blum *et al.* 2010). During its 20-year lifecycle a VBHE can save between 31 % and 88 % of CO_2 emissions in comparison with the conventional heating systems such as oil-fired boilers and gas furnaces (Saner *et al.* 2010).

2.2.3 Thermal performance and modelling

Models are needed since the design process requires determination of the optimum VBHE length required to service a building heat load while keeping the temperature change within certain limits, either those set by regulations or those appropriate for the efficient operation of a heat pump. They relate the temperature change at the VBHE wall (and sometimes in the ground) to the input of heat (thermal load) of a VBHE. Models can be analytical and numerical. They are solutions to the governing equations for the conductive and advective thermal transport described in section 2.2.4.4. They can also account for the thermal dispersion, governing equation of which described in section 2.2.4.5.

A model is an essential tool to estimate whether the thermal performance of a VBHE system is sustainable, to optimise the design of the system and to provide guidance. Specifically, models can be used before the installation of the VBHE to optimise the system size, depth, spacing and arrangement of VBHEs for a given power demand, installation cost and to estimate the payback for specific

hydrogeological settings. If improperly designed, VBHE systems may lead to overheating of the ground when the VBHE is used for space conditioning or to overcooling of the ground when the VBHE is used for heating purposes.

Considering the long lifespan of GSHP systems (which can reach several decades), a long-term model can be used to estimate whether the thermal performance of the VBHE system will be sustainable during its whole lifecycle (Retkowski *et al.* 2015). If the model estimations for the VBHE system show significant future thermal impacts on the neighbouring installations, the thermal load on the VBHE can be reduced and a hybrid system is installed. This means installation of a conventional auxiliary heating, ventilating and air conditioning (HVAC) system, so the base building load is provided by the GSHP system while HVAC is used during the peak demands (Kuzmic *et al.* 2016).

When a VBHE is used for borehole thermal energy storage (BTES), models are needed to estimate its reliability and whether specific hydrogeological conditions are appropriate for the effective thermal storage. Additionally, models are used to estimate and monitor the thermal influence of BTES on the natural and built environment (Giordano *et al.* 2016).

2.2.4 Governing equations

2.2.4.1 Introduction

The thermal performance of a VBHE can be estimated by the thermal disturbance to the ground caused by the VBHE. Figure 2.4 shows a schematic representation of a VBHE installed in an aquifer with its possible thermal effects on the surrounding ground. The shape of isotherm of interest generated by the VBHE is changed depending on which thermal transport process is present or accounted for in a model. The thermal advection and thermal dispersion can significantly increase the thermal load which the system can sustainably deliver and reduce the thermal impacts of the VBHE on the surrounding ground. However, the presence of these heat transport processes can adversely affect the possibility of thermal storage

(Yang *et al.* 2013). Therefore, models for thermal performance of a VBHE should account for the processes of thermal advection and dispersion (Alcaraz *et al.* 2016).

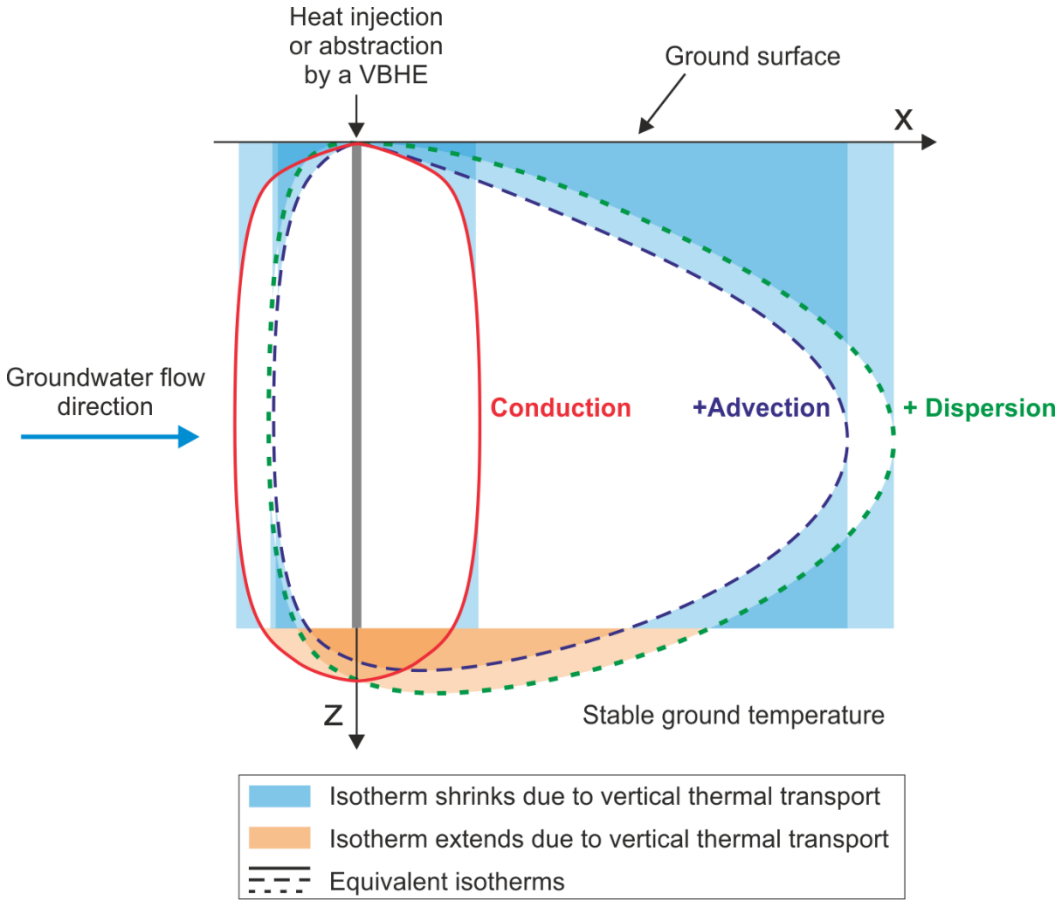

Figure 2.4 The processes of heat transfer from a VBHE installed in a homogeneous aquifer showing how a thermal plume would develop when thermal transport occurs only by conduction, or with conduction with advection or also with dispersion. The effects of vertical conduction and dispersion are shown. Equivalent isotherm of very low-temperature change is shown for the different thermal transport mechanisms after the same time.

The thermal disturbance which a VBHE can cause the surrounding ground is limited by the VBHE design and legislation. The design of a VBHE limits the possible temperature change of the working fluid circulating in the pipes of the VBHE. The legislation can limit the magnitude and the extent of temperature change allowed to be caused by a VBHE to the ground, as was discussed in section 2.1.3. Ground freezing should also be avoided when a VBHE is used for space heating. The thermal performance of a VBHE is estimated with the numerical models or analytical solutions. They solve the problem of heat transfer through the porous media with or without consideration of groundwater flow. The heat transfer and

fluid flow are governed by the principles of conservation of energy, momentum and mass. The heat transfer through porous medium can be modelled using governing equations which are the partial differential equations which express the conservation principles together with empirical laws. When initial, boundary conditions and source function are known, the governing equations can be solved analytically or numerically. In the next section, the governing equations of heat transfer through porous medium are introduced.

2.2.4.2 Conductive thermal transport

This section describes the principles of conductive heat flux. Heat flux is the rate of heat energy transfer through a unit area across the transport path (energy per unit area per unit time, W m^{-2}). Net energy that goes out of control volume equals to a change in energy storage, as illustrated in Figure 2.5.

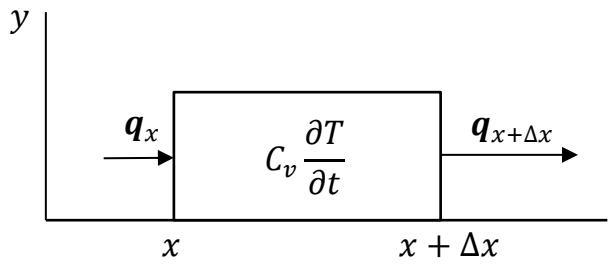

Figure 2.5 Net energy that goes out of control volume equals to a change in energy storage (Lee 1998).

The governing equation for the heat conduction in 3D is

$$\nabla \cdot \boldsymbol{q} = -C_v \frac{\partial T}{\partial t}$$
$$\nabla \cdot \boldsymbol{q} = \frac{\partial q_x}{\partial x} + \frac{\partial q_y}{\partial y} + \frac{\partial q_z}{\partial z} \quad (2.1)$$

where $\boldsymbol{q}$ is the heat flux vector with three independent orthogonal components (W m^{-2}), $\nabla \cdot \boldsymbol{q}$ is a divergence of heat flux, C_v is the volumetric heat capacity (J m^{-3} K^{-1}), T is temperature (K), and t is time.

To solve (2.1) for T another equation is needed – the empirical relationship between the heat flux and the temperature gradient expressed as the **Fourier law** of heat conduction:

$$\boldsymbol{q} = -\lambda \nabla T \tag{2.2}$$

where λ is the thermal conductivity for isotropic medium (W m^{-1} K^{-1}), ∇T is gradient of temperature and equals to $\frac{\partial T}{\partial x} + \frac{\partial T}{\partial y} + \frac{\partial T}{\partial z}$.

The above equations on energy conservation and Fourier's law can be combined into the **heat conduction** equation

$$\nabla \cdot \lambda \nabla T = C_v \frac{\partial T}{\partial t} \tag{2.3}$$

If the material is homogeneous (λ is independent of position), eq. (2.3) can be rewritten as

$$\nabla^2 T = \frac{1}{D_t} \frac{\partial T}{\partial t} \tag{2.4}$$

where ∇^2 denotes the Laplace operator $\nabla \cdot \nabla$, and D_t is thermal diffusivity (m^2 s^{-1}) and equals to λ / C_v.

2.2.4.3 Flow of groundwater

The mass conservation means that the rate of mass flowing out of a control volume equals to the rate of the mass loss from this control volume. The divergence of mass flux equals the declining rate of mass storage.

It can be expressed using the **continuity equation** as follows:

$$\nabla \cdot (\rho \boldsymbol{v}) = -\frac{\partial (\rho \phi)}{\partial t} \tag{2.5}$$

Where $\boldsymbol{v}$ is the volume flux (m^3 s^{-1} m^{-2}), its dimension can be simplified to the dimension of velocity (m s^{-1}). $\boldsymbol{v}$ is called **Darcy velocity**. The mass flux of fluid is $\rho \boldsymbol{v}$

(kg m^{-2} s^{-1}), where ρ is the mass density (kg m^{-3}). The fluid mass per unit bulk volume of porous media is $\rho\phi$, where ϕ is porosity (-).

The total mechanical energy per unit mass of fluid, E (J kg^{-1}), stays constant during flow of the fluid when the energy is not lost via viscous heating. E is expressed with the **Bernoulli equation**:

$$E = \frac{v^2}{2} + gz_e + \int_{p_0}^{p} \frac{dp}{\rho} \tag{2.6}$$

where g is the gravitational acceleration (m s^{-2}), z_e is the elevation (m), p is the pressure (Pa), p_0 is the reference pressure (Pa). The first term in eq. (2.6) is kinetic energy, the second term is potential energy, and the third term is the strain energy (pressure-volume work) per unit mass of fluid.

The flow of groundwater is so slow that the kinetic energy term is negligible. If water is assumed to be incompressible, i.e. water density is constant, then eq. (2.6) can be simplified as

$$E = gz_e + \frac{p - p_0}{\rho} \tag{2.7}$$

The eq. (2.7) can be rewritten by the introduction of new variables $H = E/g$ and $\psi = (p - p_0)/\rho g$ as

$$H = z_e + \psi \tag{2.8}$$

where H is hydraulic head (m), z_e is elevation (m) and ψ is pressure head (m).

Henry Darcy conducted the experiments on the water flow through the sand beds and empirically found that the discharge velocity (Darcy velocity) in a porous medium is proportional to the gradient of hydraulic head ((2.9):

$$\boldsymbol{v} = -K_m \nabla H \tag{2.9}$$

where $\boldsymbol{v}$ is the Darcy velocity vector (m s^{-1}), and K_m is the hydraulic conductivity of porous medium (m s^{-1}). This relationship is called **Darcy's law**, and it assumes that the porous medium is isotropic.

The groundwater flow in porous medium can be formulated with Darcy's law in combination with the mass conservation equation (2.5) as eq. (2.10). This is valid assuming that:

- spatial variation in porosity is negligible,
- grains of porous medium are incompressible,
- the total stress on the surface of the porous medium is constant at a given location. The total stress is a sum of the stress acting on the matrix (effective stress) and the stress acting on the fluid (pore pressure). More details can be found in the work by Lee (1998).

$$\nabla \cdot (K \nabla H) = S_s \frac{\partial H}{\partial t} \tag{2.10}$$

where S_s is the specific storage (m^{-1}) which equals to:

$$S_s = \rho_w g\left(\alpha_w \phi + \alpha_s (1 - \phi)\right) \tag{2.11}$$

where ρ_w is the density of water (kg m^{-3}), α_w is the compressibility of water (Pa^{-1}) and α_s is the compressibility of solid in the matrix (Pa^{-1}).

Note that the eq. (2.10) for groundwater flow in porous medium is valid only for an elastic aquifer where the deformation vanishes once the stress is removed. Darcy's law is valid when the flow is laminar. It is typical for regional groundwater flow which is slow.

2.2.4.4 Convective thermal transport

Total heat flux is composed of the conductive and advective heat fluxes. Together these two fluxes are described by the term convective thermal flux, and it is defined as follows:

$$\boldsymbol{q} = -\lambda \nabla T + C_w (T - T_0)\boldsymbol{v} \tag{2.12}$$

where $\boldsymbol{v}$ is the Darcy groundwater velocity vector (m s^{-1}), C_w is the volumetric heat capacity of water (J m^{-3} K^{-1}) and T_0 is the reference temperature (K).

When the net inflow (negative outflow) is added to the left-hand side of the heat conduction equation (2.3), it gives the equation of the heat transfer:

$$\begin{aligned} \nabla \cdot \lambda_{em} \nabla T - \nabla \cdot (C_w (T - T_0) \boldsymbol{v}) &= C_{em} \frac{\partial T}{\partial t} \\ \lambda_{em} &= \lambda_w \phi + \lambda_m (1 - \phi) \\ C_{em} &= C_w \phi + C_m (1 - \phi) \end{aligned} \tag{2.13}$$

where λ_{em} is the effective thermal conductivity (W m^{-1} K^{-1}). Effective property means property of bulk material, for both matrix solid and water. λ_w and λ_m are the thermal conductivities of water and solid material (W m^{-1} K^{-1}), C_{em} is the effective volumetric heat capacity (J m^{-3} K^{-1}), C_w and C_m are the volumetric heat capacities of water and solid material (J m^{-3} K^{-1}).

Assuming steady state mass flow, i.e. no time dependency in the continuity equation (2.5) and that water is incompressible, then

$$\nabla \cdot \boldsymbol{v} = 0 \tag{2.14}$$

Therefore, the heat transfer equation (2.13) can be reduced to:

$$\nabla \cdot \lambda_{em} \nabla T - C_w \boldsymbol{v} \nabla \mathrm{T} = C_{em} \frac{\partial T}{\partial t} \tag{2.15}$$

2.2.4.5 Dispersive thermal transport

The advection of heat in the porous media is hindered by tortuosity of groundwater flow paths and grains in the solid matrix. Figure 2.6 illustrates different mechanisms of dispersive thermal transport. Mechanical thermal dispersion occurs due to mixing of fluid which advects heat due to taking pathways of different length and velocity. Therefore, in fractured aquifers, the thermal dispersion can be larger than in homogeneous aquifers. The thermal properties of the matrix material (ground) can also differ, for example, in a layered geology. Thermal exchange between the groundwater inside the fractures and the solid rock blocks can also disperse the thermal perturbation in the ground due to

difference in the thermal properties of rock and water in the fractures of the ground.

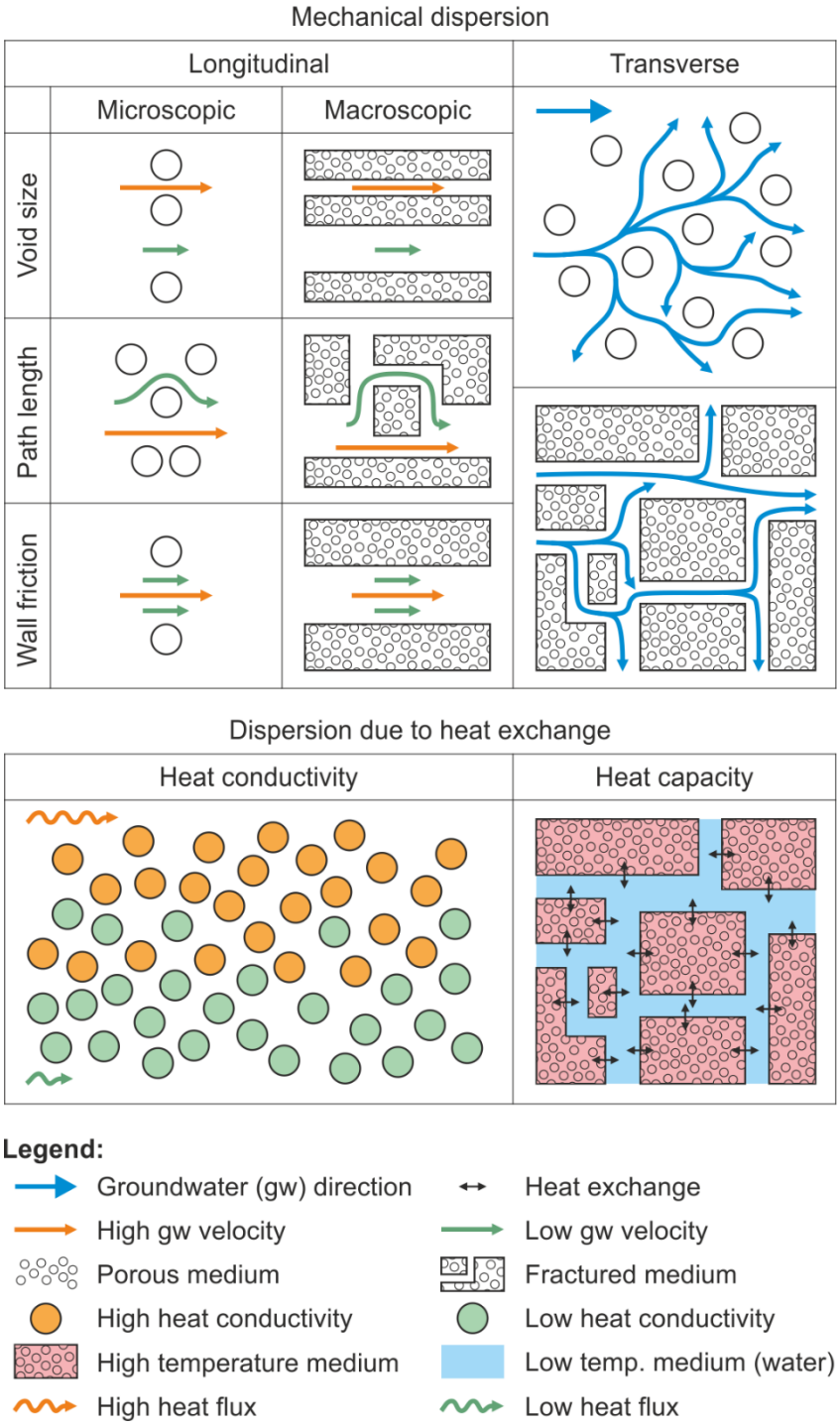

Figure 2.6 Different types of dispersion in homogeneous, heterogeneous and fractured aquifers: longitudinal and transverse mechanical dispersion is adopted from (Fetter 2001), dispersion due to fracture-matrix heat exchange is also shown for case when a VBHE abstracts heat from the ground. Dispersion due to heterogeneity in the thermal conductivity of the ground is shown on an example of a layered aquifer.

The thermal dispersion increases with groundwater flow. The thermal dispersivity in the fractured aquifers gets higher with increasing field scale of measurement compared to the homogeneous aquifers (Figure 2.7).

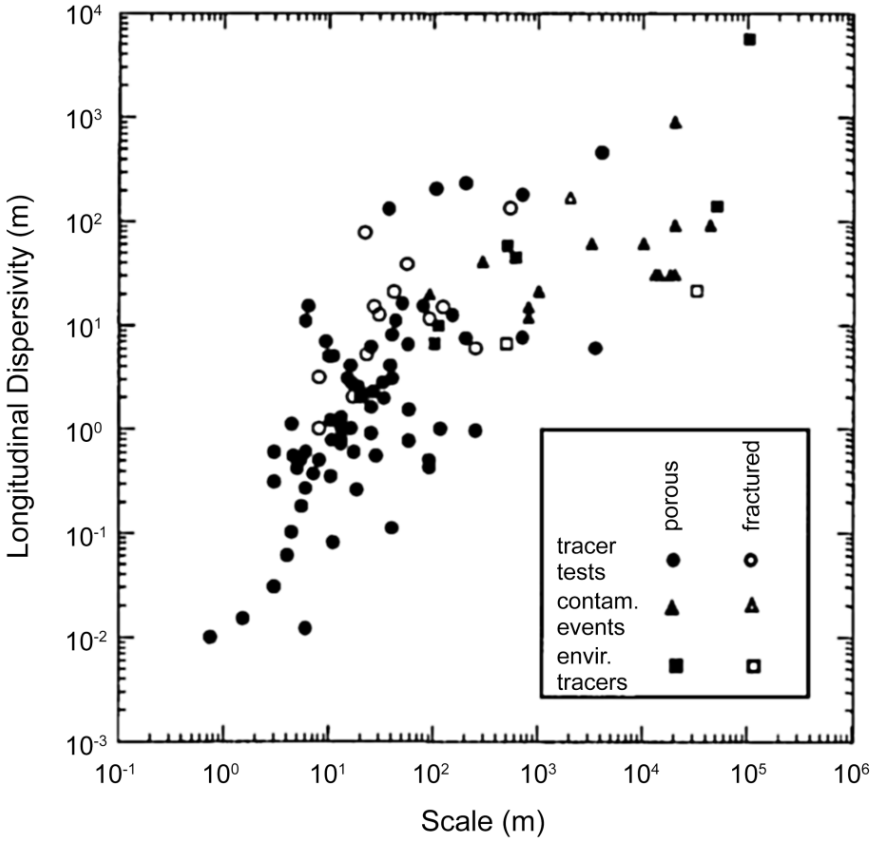

Figure 2.7 The field scale effect on the longitudinal dispersivity in the fractured and non-fractured aquifers (Gelhar *et al.* 1992)

The following governing equations describe the relationship between the advective and dispersive thermal transport. Thermal dispersion can be modelled analogous to dispersion of solute. To account for the dispersive transport, the diffusion coefficient tensor $\boldsymbol{D_t}$ can be added to the heat transfer equation (2.15), which gives:

$$\nabla \cdot (C_{em}\boldsymbol{D_t}\nabla T) - C_w \boldsymbol{v}\nabla T = C_{em}\frac{\partial T}{\partial t} \tag{2.16}$$

where $\boldsymbol{D_t}$ is the diffusion coefficient tensor ($m^2\ s^{-1}$). Thermal dispersive transport depends on the groundwater flow; therefore, it is different in different directions depending on the groundwater flow direction.

The empirical equation for the component of $\boldsymbol{D_t}$ in the x-direction, $D_{t,x}$ ($m^2\ s^{-1}$) is:

$$D_{t,x} = D_t^* + D_{t,d,x} \tag{2.17}$$

where D_t^* is the diffusion coefficient in the matrix without groundwater flow ($m^2\ s^{-1}$)

$$D_t^* = \frac{\lambda_{em}}{C_{em}} \tag{2.18}$$

and $D_{t,d,x}$ is the thermal dispersion coefficient in the x-direction ($m^2\ s^{-1}$)

$$D_{t,d,x} = \frac{\lambda_{B,x}}{C_{em}} = \frac{\beta_x v_x C_w}{C_{em}} \tag{2.19}$$

where $\lambda_{B,x}$ is the component of the dispersive thermal conductivity tensor in the x-direction ($W\ m^{-1}\ K^{-1}$), β_x is the dispersivity in the x-direction (m) and v_x is the x-component of the Darcy velocity ($m\ s^{-1}$).

All components of $\boldsymbol{D_t}$ are described in detail in the section 5.6.3.

The governing equations showed how thermal transport is affected by groundwater flow and the dispersivity of the aquifer. The effect of hydrogeological settings on the thermal performance of a VBHE is discussed in section 2.2.5.

Analytical solutions are preferred due to their versatility and small demands for cost and time compared to computationally intensive numerical models (Rivera *et al.* 2015b). The analytical solutions that solve the described governing equations are described in section 2.2.5. They are used to calculate the thermal performance of a VBHE installed in a ground with or without groundwater flow and thermal dispersivity.

2.2.5 Analytical solutions for a VBHE installed in homogeneous aquifers

The moving infinite line source model (MILS) (Sutton *et al.* 2003; Diao *et al.* 2004) is the simplest analytical model to account for groundwater influence on the VBHE

thermal balance. MILS (Figure 2.8 A) does not account for vertical thermal transport as it models the VBHE as an infinite line (Stauffer *et al.* 2014). The moving finite line source (MFLS) (Molina-Giraldo *et al.* 2011b) model accounts for groundwater advection, radial conduction as well as vertical conduction (Figure 2.8 B). MFLS accounts for constant ground surface temperature and assumes semi-infinite subsurface medium, whereas MILS assumes insulation at top and bottom of the VBHE as the heat source is infinite (Stauffer *et al.* 2014). Both models assume homogeneous fully saturated porous media where the VBHE is installed, with uniformly distributed initial temperature and steady and uniform horizontal groundwater flow (Figure 2.8).

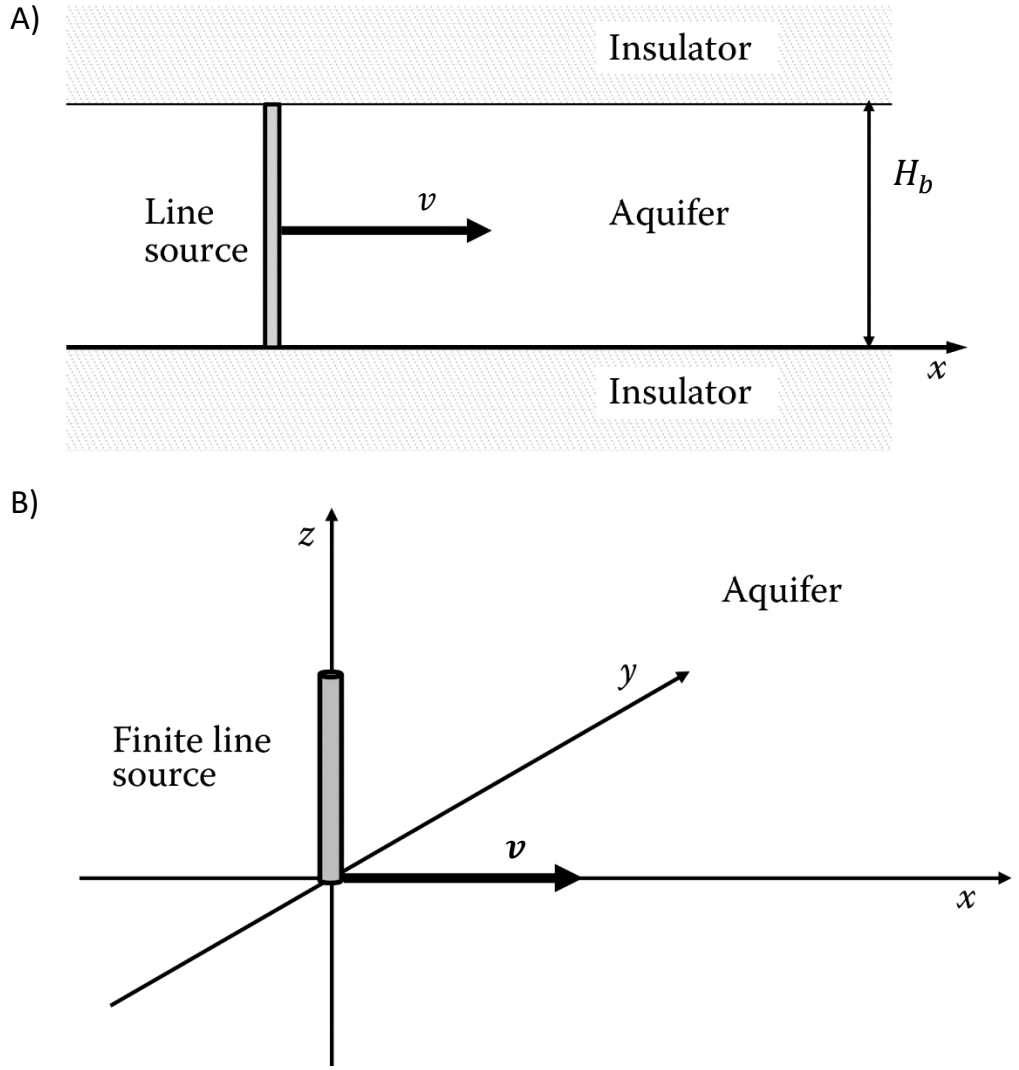

Figure 2.8 Analytical models for a vertical borehole heat exchanger. A) An infinite line source in an aquifer layer with groundwater flow field$v$; B) A finite line source in a semi-infinite aquifer with groundwater flow field v, H_b is a length of the line source (Stauffer *et al.* 2014).

The MILS model was used to calculate the thermal conductivity of the ground, temperature distributions for time-dependent energy extraction/injection, and the effects of groundwater advection on ground-source heat pump systems (Zubair & Chaudhry 1996; Sutton *et al.* 2003; Diao *et al.* 2004). MILS can be expressed as follows (Stauffer *et al.* 2014):

$$T(x,y,t) = T_0 + \frac{q_{tb}}{4\pi C_{em}\sqrt{D_{t,L}D_{t,T}}} \exp\left(\frac{u_t x}{2D_{t,L}}\right) \int_{r_D^2/4D_{t,L}t}^{\infty} \exp\left(-\psi - \frac{{u_t}^2 r_D^2}{16{D_{t,L}}^2\psi}\right)\frac{d\psi}{\psi} \quad (2.20)$$

where $r_D^2 = D_{t,L}\left(\frac{x^2}{D_{t,L}} + \frac{y^2}{D_{t,T}}\right)$, $\psi = r_D^2/\left(4D_{t,L}(t-t')\right)$, $dt/(t-t') = d\psi/\psi$. The heat source is located at $x_0 = y_0 = 0$. Symbols used in this and the following equations are:

C_{em} Effective volumetric heat capacity of the porous medium or aquifer (J m^{-3} K^{-1}) or (W s m^{-3} K^{-1})

C_w Volumetric heat capacity of water (J m^{-3} K^{-1}) or (W s m^{-3} K^{-1})

$\boldsymbol{D_t}$ Thermal diffusion tensor or thermal diffusivity tensor (m^2 s^{-1})

D_t^* Thermal diffusion coefficient in a matrix without flow (m^2 s^{-1})

$D_{t,L}$ Longitudinal thermal diffusion coefficient, component of D_t in hydraulically isotropic medium,
$D_{t,L} = D_t^* + D_{t,d,L} = \lambda_{em}/C_{em} + \beta_L\, v\, C_w/C_{em}$ (m^2 s^{-1})

$D_{t,T}$ Transversal thermal diffusion coefficient, component of D_t in hydraulically isotropic medium,
$D_{t,T} = D_t^* + D_{t,d,T} = \lambda_{em}/C_{em} + \beta_T\, v\, C_w/C_{em}$ (m^2 s^{-1})

F_o Fourier number, $F_o = D_t t/L^2$ (–)

H_b Length of a vertical borehole heat exchanger (m)

J Source heat flow rate (W) or (J s^{-1})

L Length scale (for example a borehole length) (m)

P_e Thermal Peclet number, $P_e = u_t L/D_t = C_w v L/\lambda_{em}$ (–)

q_{tb} Heat flow rate per unit length of the borehole, $q_{tb} = J/H_b$ (W m^{-1})

r_D Adjusted radial distance from the heat source, $r = \sqrt{D_{t,L}\left(\frac{x^2}{D_{t,L}} + \frac{y^2}{D_{t,T}}\right)}$ (m)

R Dimensionless cylindrical radius, $R = \sqrt{x^2 + y^2 + z^2}/L$, z coordinate is only for 3D, note $L = H_b$ (–)

t Time (s)

T Temperature (°C or K; 0°C = 273.15 K)

T_0 Initial or undisturbed temperature (K)

ΔT Temperature change, $\Delta T = T - T_0$ (K)

u Mean flow velocity, $u = v/\phi$ (m s^{-1})

u_t Thermal velocity, $u_t = v\ C_w/C_{em}$ (m s^{-1})

$\boldsymbol{v}$ Specific discharge vector (Darcy velocity), water discharge rate through unit area (m s^{-1})

v_u Darcy velocity of groundwater in an undisturbed matrix (m s^{-1})

Θ Dimensionless temperature (–)

λ_{em} Effective thermal conductivity of the porous medium or aquifer (W m^{-1} K^{-1})

β_L Longitudinal thermal dispersivity of aquifer (m)

β_T Transversal thermal dispersivity of aquifer (m)

φ_r Angular coordinate (polar angle) (–)

ϕ Porosity of the aquifer, volumetric fraction of pores in the aquifer (–)

MILS in a dimensionless form is expressed when the thermal Peclet number P_e and dimensionless radius R (defined above) are introduced (Stauffer *et al.* 2014):

$$\Theta_{MILS} = \exp\left(\frac{P_e}{2} R \cos\varphi_r\right) \int_{R^2/4F_o}^{\infty} \exp\left(-\psi - \frac{{P_e}^2 R^2}{16\psi}\right) \frac{d\psi}{\psi} \tag{2.21}$$

MFLS is derived by Molina-Giraldo *et al.* (2011b) by applying the moving source theory (Carslaw & Jaeger 1959) and the method of images (Eskilson 1987). MFLS is described by Stauffer *et al.* (2014) as follows:

$$T(x,y,z,t) = T_0 + \frac{q_{tb}}{4\pi\lambda_{em}} \exp\left(\frac{u_t x}{2D_t}\right) \cdot \left(\int_0^{H_b} \frac{\Gamma\left({}^1/_2, u_1; u_2\right)}{r'\sqrt{\pi}} dz_0 - \int_{-H_b}^{0} \frac{\Gamma\left({}^1/_2, u_1; u_2\right)}{r'\sqrt{\pi}} dz_0 \right) \tag{2.22}$$

where $r' = \sqrt{x^2 + y^2 + (z - z_0)^2}$, $u_1 = {r'}^2/4D_t t$,

$u_2 = {u_t}^2 {r'}^2/16{D_t}^2$. The heat source is located at x_0 = 0 m, y_0 = 0 m.

MFLS in a dimensionless form is expressed as follows (Stauffer *et al.* 2014):

$$\Theta_{MFLS} = \exp\left(\frac{P_e}{2} R \cos\varphi_r\right) \left(\int_0^{1} \frac{\Gamma\left({}^1/_2, U_1; U_2\right)}{R'\sqrt{\pi}} dZ_0 - \int_{-1}^{0} \frac{\Gamma\left({}^1/_2, U_1; U_2\right)}{R'\sqrt{\pi}} dZ_0 \right) \tag{2.23}$$

with dimensionless variables R, $R' = r'/H_b$, $Z_0 = z_0/H_b$,

$U_1 = {R'}^2/4F_o$, $U_2 = {P_e}^2 {R'}^2/16$.

Generalized incomplete Gamma function formula and its approximation by Chaudhry & Zubair (1994) (in Stauffer *et al.* (2014)) are expressed as:

$$\Gamma\left({}^1/_2, u_1; u_2\right) = \int_{u_1}^{\infty} \frac{1}{\sqrt{\psi'}} \exp\left(-\psi' - \frac{u_2}{\psi'}\right) d\psi' \tag{2.24}$$

$$\Gamma\left({}^{1}/_{2}, u_1; u_2\right) \cong \frac{1}{2}\sqrt{\pi}\left(\exp\left(-2\sqrt{u_2}\right)\operatorname{erfc}\left(\sqrt{u_1}-\frac{\sqrt{u_2}}{\sqrt{u_1}}\right) + \exp\left(2\sqrt{u_2}\right)\operatorname{erfc}\left(\sqrt{u_1}+\frac{\sqrt{u_2}}{\sqrt{u_1}}\right)\right) \quad (2.25)$$

where $\psi' = r'^2/\left(4D_t(t-t')\right)$.

MFLS cannot be used for high groundwater flow (P_e > 0.1) due to groundwater advection effects "inside the borehole" (Tye-Gingras & Gosselin 2014). This means that the groundwater flow directly influences the heat source because the impermeable VBHE grout is not represented in the model. Additionally, formulas for MFLS developed by (Molina-Giraldo *et al.* 2011b) do not account for dispersion; in contrast, MILS accounts for dispersion in 2D. The dispersion effects are discussed in Chapter 4.

Analytical solutions MILS and MFLS approximate the heat source to a point and a line, respectively, however for a short time scale, the steady-state heat transfer inside a VBHE should be accounted for. In this case, the heat transfer between the heat carrier fluid in the pipes of a U-pipe and the borehole wall can be modelled using thermal resistances (Javed & Spitler 2016). A local borehole thermal resistance is defined as follows:

$$R_b = \frac{T_{pm} - T_b}{q_{tb}} \quad (2.26)$$

Where R_b is the thermal resistance of a borehole for each meter of depth (m K W^{-1}), T_{pm} is the local mean fluid temperature at a specific VBHE depth between the two legs of the U-pipe (K), T_b is the borehole wall temperature (K), q_{tb} is the heat flow rate (from the borehole to the ground) per unit length of the borehole (W m^{-1}). Lower values of R_b mean the better thermal performance of a VBHE, thus it can be used as a performance characteristic for a VBHE.

2.2.6 Introduction to groundwater effects

Aestifer is a unit of rock or sediment into which the VBHE is installed, which can store and transmit heat (*aestus* means heat in Latin). Some aestifers can be aquifers (Banks 2015). To estimate a thermal balance of a VBHE, it is important to account for groundwater flow. Figure 2.9 shows different pathways of the heat flux in an aestifer.

Therefore, MILS increasingly overestimates the extent of the isotherms for the long-term simulation and shorter boreholes, because MILS does not consider the thermal exchange with constant surface temperature and groundwater flow below the VBHE (Molina-Giraldo *et al.* 2011b). Vertical conduction can improve the effectiveness of a VBHE. Therefore, it can significantly reduce the required VBHE length, (e.g. by 15 % (Marcotte *et al.* 2010)), number of VBHE installations (Molina-Giraldo *et al.* 2011b) and required spacing between VBHE systems (Liuzzo-Scorpo *et al.* 2015). High groundwater advection can significantly reduce the relative importance of the vertical thermal transport from a VBHE compared with conduction only scenario (Molina-Giraldo *et al.* 2011b). This is because fast groundwater advection results in a very effective thermal exchange between groundwater and the VBHE.

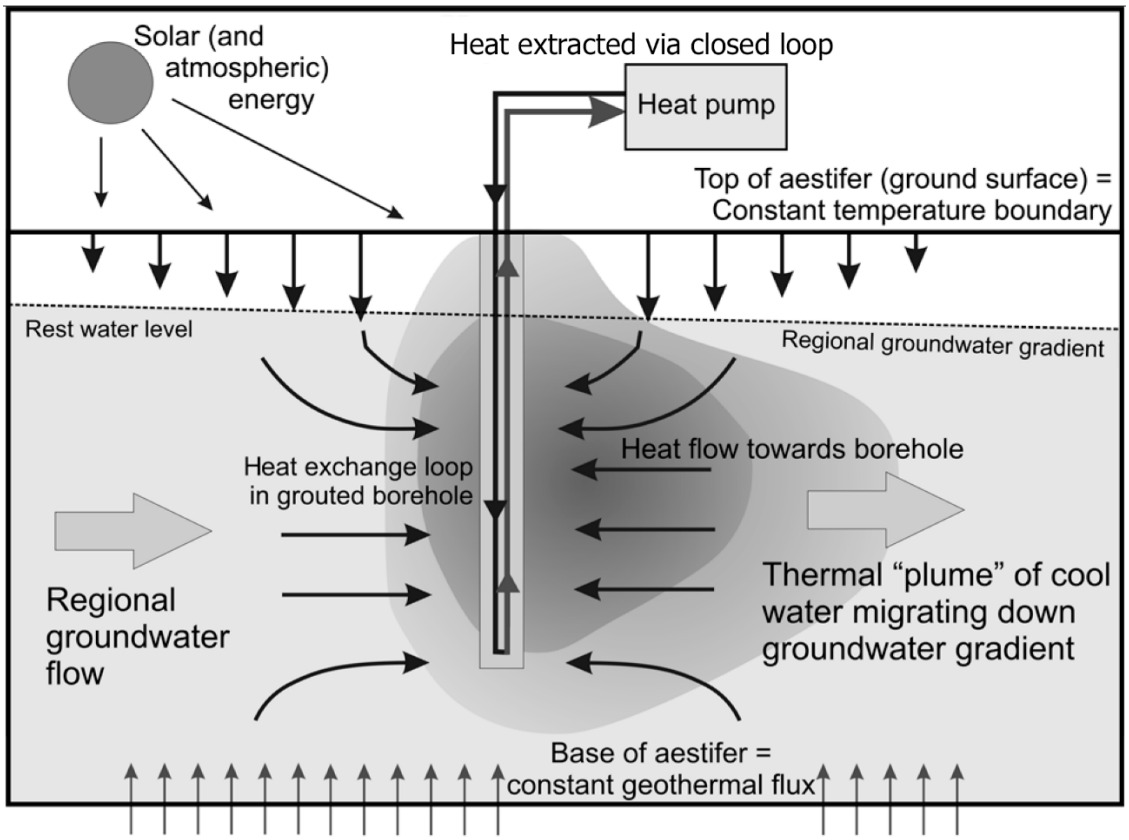

Figure 2.9 Thermal balance for a vertical borehole heat exchanger installed in an aquifer. Thin arrows show heat flow paths; thick arrows show groundwater flow paths and contours show isotherms. (Banks 2015).

In the congested urban environment, numerous users of an aestifer can be in proximity to each other, and the thermal interactions can occur (Figure 2.10). This can either beneficially or adversely influence the thermal performance of the neighbouring GSHP installations. Groundwater flow can change these thermal interactions. For example, Figure 2.10 shows how the extent of the isotherms from three neighbouring installations in an aquifer can change depending on the influence of the upstream thermal users. The upstream thermal users who abstracted the heat from the ground reduced the extent of the generated thermal plume of a downstream installation which injects the heat into the ground. This is a beneficial effect, i.e. the thermal performance is improved.

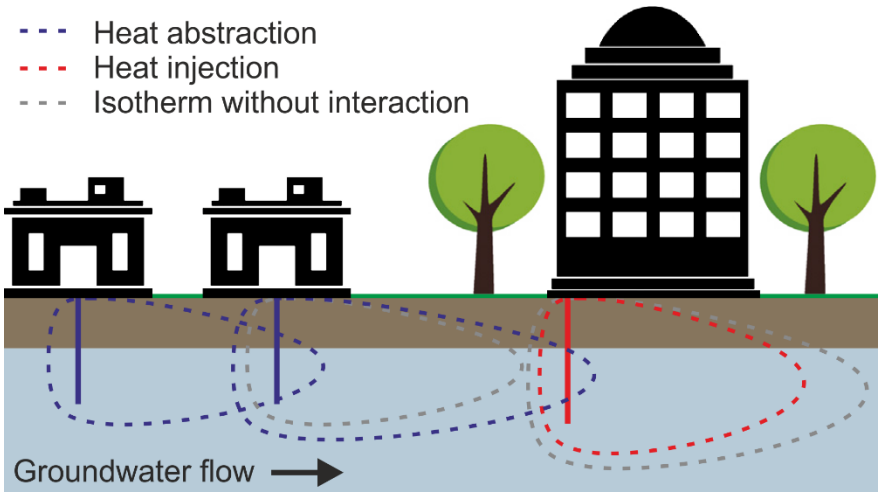

Figure 2.10 Thermal interactions of the vertical borehole heat exchangers installed in an aquifer in an urban environment. Modified from (Rivera *et al.* 2015a).

VBHE systems are usually installed in urban environments where space is limited and accounting for groundwater in models for a VBHE can significantly change the estimated performance and thermal interactions of the systems. Ferguson (2015) points out that if groundwater velocity exceeds $1x10^{-8}$ m s^{-1} then it should be accounted for during modelling of a VBHE because Darcy velocity increases the apparent thermal conductivity of an aquifer (Ferguson 2007):

$$\boldsymbol{\lambda_a} = \boldsymbol{\lambda_{em}} + \boldsymbol{\beta} C_w |v| \qquad (2.27)$$

where $\boldsymbol{\lambda_a}$ is the apparent thermal conductivity (W m^{-1} K^{-1}), λ_{em} is the effective (or overall) thermal conductivity of the porous medium (W m^{-1} K^{-1}), $\boldsymbol{\beta}$ is the dispersivity tensor (m), C_w is the volumetric heat capacity of the fluid (J m^{-3} K^{-1}), v is the Darcy velocity (m s^{-1}).

Soil saturation and groundwater flow are among the important factors to estimate the long-term running costs of a VBHE (Hein *et al.* 2016). For example, specific heat extraction for a VBHE installed in dry sand (< 20 W m^{-1}) increases threefold if the sand is saturated and increases fivefold if groundwater flow is significant (Stauffer *et al.* 2014).

Advection and dispersion can significantly affect the long-term thermal performance of a VBHE (Hein *et al.* 2016). Time to reach steady state by a VBHE is a significant thermal performance indicator of a VBHE. Steady state in the thermal

transport is reached when the thermal plume stabilizes, reaching thermal balance with the environment. Groundwater flow accelerates the time to reach steady state (Dehkordi & Schincariol 2014; Tye-Gingras & Gosselin 2014). Groundwater flow enhances the vertical conductive flux from the thermal plume (Rivera *et al.* 2015b).

Shorter time to reach steady state and reduced thermal disturbance to the ground surrounding a VBHE at steady state means a more efficient and sustainable VBHE system. Knowledge of the system efficiency is important in making the decision on whether to install the system.

A study by Capozza *et al.* (2013) showed that when groundwater flow is considered, it can save 16 % on the VBHE design cost. Even low groundwater velocity (0.017 m day^{-1}) is sufficient to influence the optimum distance between the VBHE systems (Liuzzo-Scorpo *et al.* 2015). However, the groundwater influence is frequently ignored by practitioners because the guidelines applicable to a range of hydrogeological settings are missing (Tye-Gingras & Gosselin 2014). Recognition of the groundwater influence on the thermal performance of a VBHE and their thermal interactions stimulated the development of maps of shallow geothermal potential that account for the groundwater influence at the regional scale (Fujii *et al.* 2007; García-Gil *et al.* 2015; Alcaraz *et al.* 2016; Department of Communications Energy and Natural Resources of Ireland 2016).

An isotropic and homogeneous medium is usually assumed in the models for thermal performance of a VBHE. However, VBHEs are frequently installed in the heterogeneous and fractured media, which may have a groundwater flow (Dehkordi *et al.* 2015). Improved representation of the geological characteristics in models has three main advantages.

Firstly, hydraulically open fractures can be fast conduits for groundwater flow. If groundwater flow is ignored in a VBHE model, so the thermal performance of a VBHE can be underestimated. Owing to high installation costs (Hein *et al.* 2016),

decisions on VBHE installation are very sensitive to any underestimation of its efficiency (Hein *et al.* 2016). The groundwater speeds up ground thermal recovery (i.e. return to the previous undisturbed ambient temperature), allows reduced VBHE length (Erol *et al.* 2015; Hein *et al.* 2016), and therefore reduces the installation costs. The overestimation of efficiency may cause the unsustainable thermal performance of a VBHE.

Secondly, modelling the local hydrogeological conditions will help to estimate the long-term thermal interactions and environmental impacts of a VBHE (Koohi-Fayegh & Rosen 2013). Such models may also permit for the improved monitoring and prevention of possible significant thermal impacts of the system. These may include thermal disturbance to ecosystems (Brielmann *et al.* 2011), long-term thermal interactions with other VBHE systems (Retkowski *et al.* 2015) and the impacts on groundwater quality caused by the induced changes to the physicochemical and microbial processes (Saito *et al.* 2016).

Thirdly, the legislation and guidance for the installation of a VBHE is currently very diverse and sometimes lacks scientific basis (Haehnlein *et al.* 2010). The current guidance could be supported by a better understanding of the conditions when the assumptions of homogeneity in the aquifer are justified.

The effects of thermal advective transport on the long-term thermal performance of a VBHE are quantified in Chapter 3. The effects of the thermal dispersive transport are quantified in Chapter 4. To further discuss the effects of fractures on the thermal performance of a VBHE, the next section introduces the geological fractures and their conceptual representations for modelling purposes.

2.3 Understanding fractured aquifers

2.3.1 Introduction

The depth of a typical VBHE is usually 45 – 75 m for residential and over 150 m for the larger industrial applications (Self *et al.* 2013). At that depths fractures in the

bedrock can be present near a VBHE and can affect its thermal performance. The fracturing in a bedrock can significantly increase the hydraulic permeability of the top layers of a bedrock without changing the porosity (Figure 2.11, Figure 2.12).

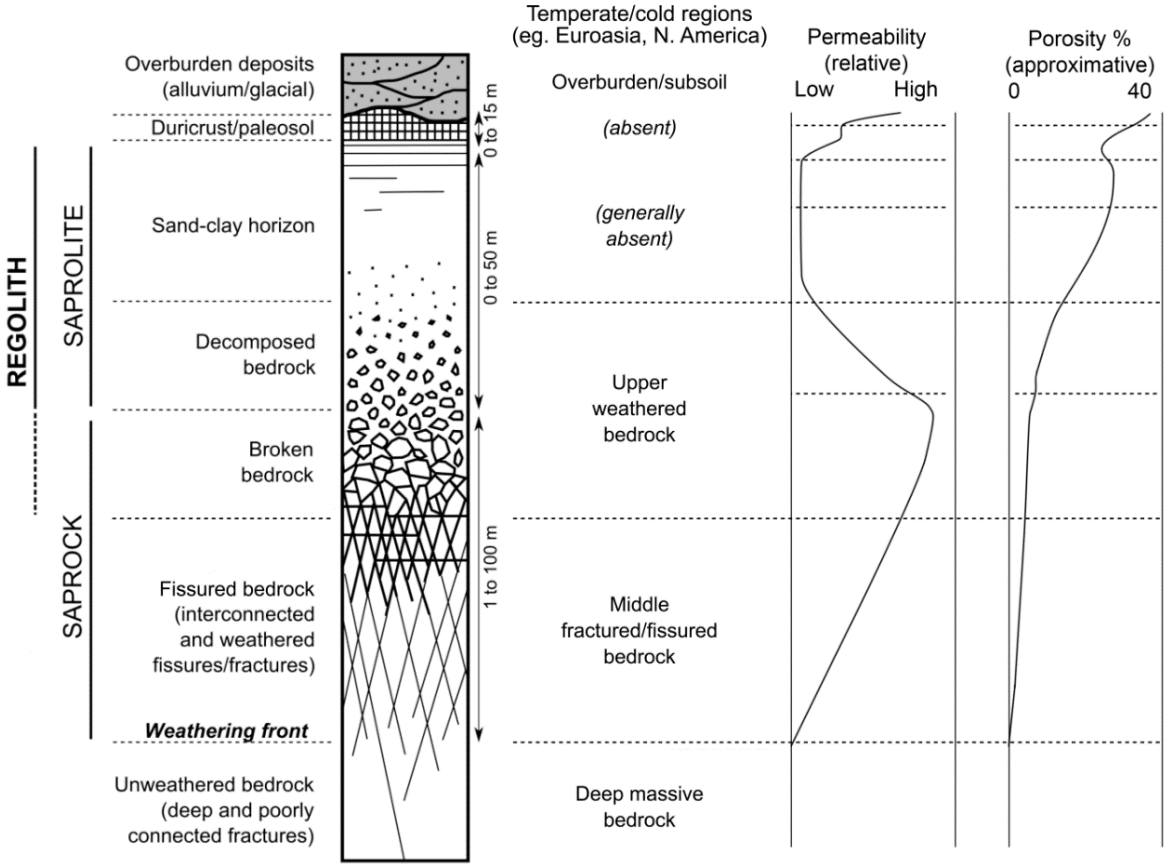

Figure 2.11 Generic layered conceptual model of a weathered/fractured bedrock aquifer. Modified by Comte (2016) from Comte *et al.* (2012) for the lithology and descriptions and from Acworth (1987) for the permeability/porosity profiles with scale modified to match the soil profile typical for Ireland.

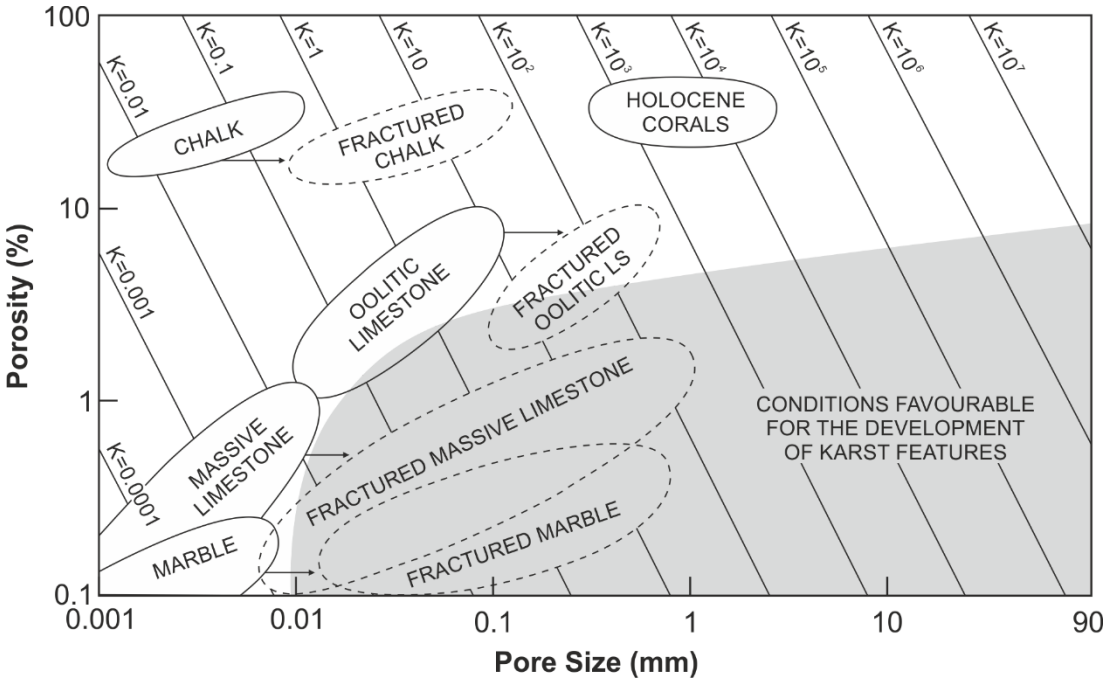

Figure 2.12 Porosity, pore size, and the theoretical hydraulic conductivity (m day^{-1}) of the unfractured (solid ellipses) and fractured (broken ellipses) carbonate rocks. The shaded area depicts conditions favourable for development of the karst features, from Brahana et al. (1988) in Cook (2003).

The physical reality within a fractured aquifer can significantly differ even within a single type of bedrock, for example, chalk (Figure 2.13).

A) B)

Figure 2.13 An example of fractured chalk bedrock (Lord *et al.* 2002): A) Offsets on conjugate faults (marked X) in the Newhaven Chalk Formation, Sussex; B) Frequency of horizontal joints predominates over the vertical ones, trial pit, A27 Brighton Bypass, The Upper Newhaven Chalk.

2.3.2 Methods to identify and characterise fractures

Geological investigations can inform about the likelihood of fracture presence in the bedrock. Geophysical techniques can be used to locate hydraulically significant fractures. Application of several geophysical methods reduces the uncertainty of result (Singhal & Gupta 2010). Fracture parameters can be estimated by various techniques. Well tests are performed to assess the hydraulic significance of a fracture as well as to estimate the fracture connectivity (National Research Council 1996). Fracture density can be determined statistically from the geological exposure (Singhal & Gupta 2010). Field measurements involve large uncertainty therefore statistical analysis is conducted. Fracture spacing can be estimated from the geological outcrops and is adjusted due to fracture rotation (Singhal & Gupta 2010). Fracture length is difficult to quantify, it can be assessed from the geological exposures. Fracture aperture can be measured by various methods, for example feeler gauge, fluorescent dyes, impression packer, tracer test, hydraulic test or exposure of rock surfaces (Singhal & Gupta 2010).

2.3.2.1 Geophysical methods

Geophysical fracture detection methods have three scales: 1) large scale surface investigations 2) intermediate scale borehole investigations and 3) small scale measurements of sampled bedrock material (National Research Council 1996). The inhomogeneities in bedrock can be detected by geophysical methods, which can find them by recognising the anomalous rock properties remotely, such as elastic or electrical properties. The rock matrix can be itself anisotropic and heterogenous which complicates the fracture detection (National Research Council 1996). However, even in this case, a hydrologically active fracture can be effectively located with geophysical methods when the flow regime in the rock is changed and the measurement is taken before and after the change. For example, a radar tomography can be used before and after the injection of saline solution which is very conductive (National Research Council 1996).

Cross-hole and surface-to-borehole tomographic surveys use either seismic or electromagnetic waves to image the velocity and attenuation properties of rock. These methods allow to identify fractures from less than 1 meter up to few hundred meters long, in case the rock does not effectively attenuate these waves. The hydrologically active fractures delay seismic waves and increase attenuation (National Research Council 1996). Surface reflection seismic methods can be used for 3D images; however, they are expensive (National Research Council 1996).

Borehole logging methods allow to estimate the local hydrological properties of the rock and flow in the fractures along the borehole. The results are relevant only locally to the borehole. Therefore, these methods should be used as a complimentary rather than stand alone. Borehole logging involve imaging and flowmeters. Borehole imaging logs include optical, acoustic or electrical techniques. They help to describe the local hydrogeological conditions in the borehole (National Research Council 1996). Fracture connectivity and hydrogeological settings on the larger scale can be estimated with help of geochemical analyses of groundwater samples, radar and seismic tomography and a number of high-resolution flowmeter techniques, for example heat pulse flowmeter in combination with inflatable packer (National Research Council 1996).

2.3.2.2 Hydraulic and tracer tests

Hydraulic and tracer tests artificially induce perturbations into the subsurface (i.e. fluid abstraction or solute injection) to measure the response. Packers can be used to isolate a significant fracture in a borehole and measure its hydraulic response to support a specific conceptual model of a hydrogeological system (National Research Council 1996). The parameters of hydrogeological models can be calibrated based on the results of hydraulic tests. Adjustment of conceptual model and estimation of its parameters are two steps of an iterative process. When the hydrogeological conceptual model is insufficiently constrained by the field measurements, the estimated parameter set of the model can be non-unique (National Research Council 1996).

Tracer tests can be used to investigate the connectivity of the fracture network and transport properties of the fractured aquifer, for example thermal dispersivity. There are several types of tracer tests (National Research Council 1996), including natural gradient tracer test, divergent flow tracer test and convergent flow tracer test. During the divergent flow tracer test the water is injected at a constant rate into the well and when the steady state is reached the tracer is injected, as a pulse or step increase, and its breakthrough is logged further away from the well. Convergent flow tracer test involves pumping from the well until the steady state is reached and then injection of a tracer at certain distance from the well and logging the tracer breakthrough at the pumping well. Thermal dispersivity can also be estimated from the two-well tracer test with pulse injection of tracer. Borehole dilution test can be used in an aquifer to estimate the volumetric rate of groundwater flow through the packed-off borehole section (National Research Council 1996). The thermal and solute tracer tests can be used together to estimate the fracture aperture and geometry (de La Bernardie *et al.* 2018).

Thermal response tests were used to detect fractures in a bedrock and estimate their influence on the thermal transport (Gehlin & Hellström 2003; Liebel *et al.* 2012; Pambou *et al.* 2019). The recent improvements to the thermal response test methods include improved temperature sensors, improved methods for temperature profiling of the borehole and active line source method: the use of electrical heating cable to quickly increase the temperature inside the borehole that can be used to detect hydraulically active fractures (Pehme *et al.* 2013). Multi-injection rate thermal response test can be used to determine whether a borehole is surrounded by fractured rocks (Gustafsson & Westerlund 2010).

2.3.3 Conceptual models

The purpose of a conceptual model for thermal transport in a specific hydrogeological setting is to capture the key thermal transport processes. Figure 2.15 summarizes the classifications of the geological conditions based on the connectivity (density) of the fracture network and the permeability of the bedrock.

A conceptual model is constructed based on the understanding of dominant processes of thermal transport for a specific case. The significance of the heat transfer processes depends on the hydrogeological characteristics of the medium. An increase in the hydraulic conductivity of the medium (for example due to fracturing) increases possible groundwater velocity, hence the heat advection. The patterns of fracture network can be homogeneous or heterogeneous due to a distribution of the fracture orientation, geometry, density and connectivity (Figure 2.14). In a heterogeneously fractured aquifer, the thermal dispersivity is high, the extent of the thermal plume increases during the long time of the VBHE operation. A fracture network in an aquifer can make it heterogeneous with anisotropic thermal and hydraulic properties. An aquifer with low heterogeneity can be represented as a single or double continuum. A region in an aquifer with high localised flow (a fracture) can be represented discretely in a conceptual model.

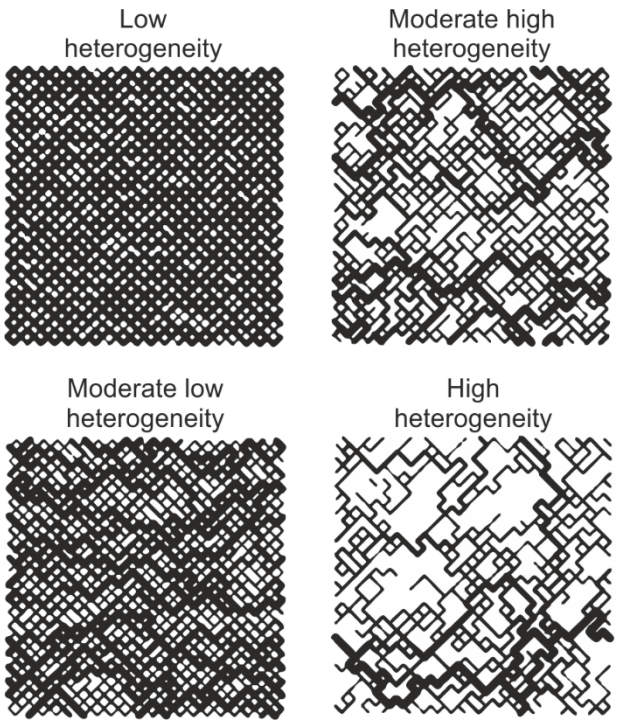

Figure 2.14 Heterogeneous medium and localised flow, thickness of lines represents the flow magnitude (Bruderer & Bernabé 2001).

The discrete conceptual models represent the flow and heat transport on a microscopic level. However, the geometry of fractured rocks is usually too complex to be described and measured. Therefore, the continuum model frameworks are

used when possible. The conceptual model for a homogeneous aquifer is a single continuum illustrated in row I in Figure 2.15. It is the simplest approach, when the matrix is assigned isotropic values for thermal and hydraulic properties which are constant throughout the aquifer. A continuum model framework takes macroscopic approach, where measurable averages of the microscopic values are used (Bear *et al.* 1993). The representative elementary volume is used to define the area of an aquifer which is appropriate to model by a continuum framework (Bear *et al.* 1993).

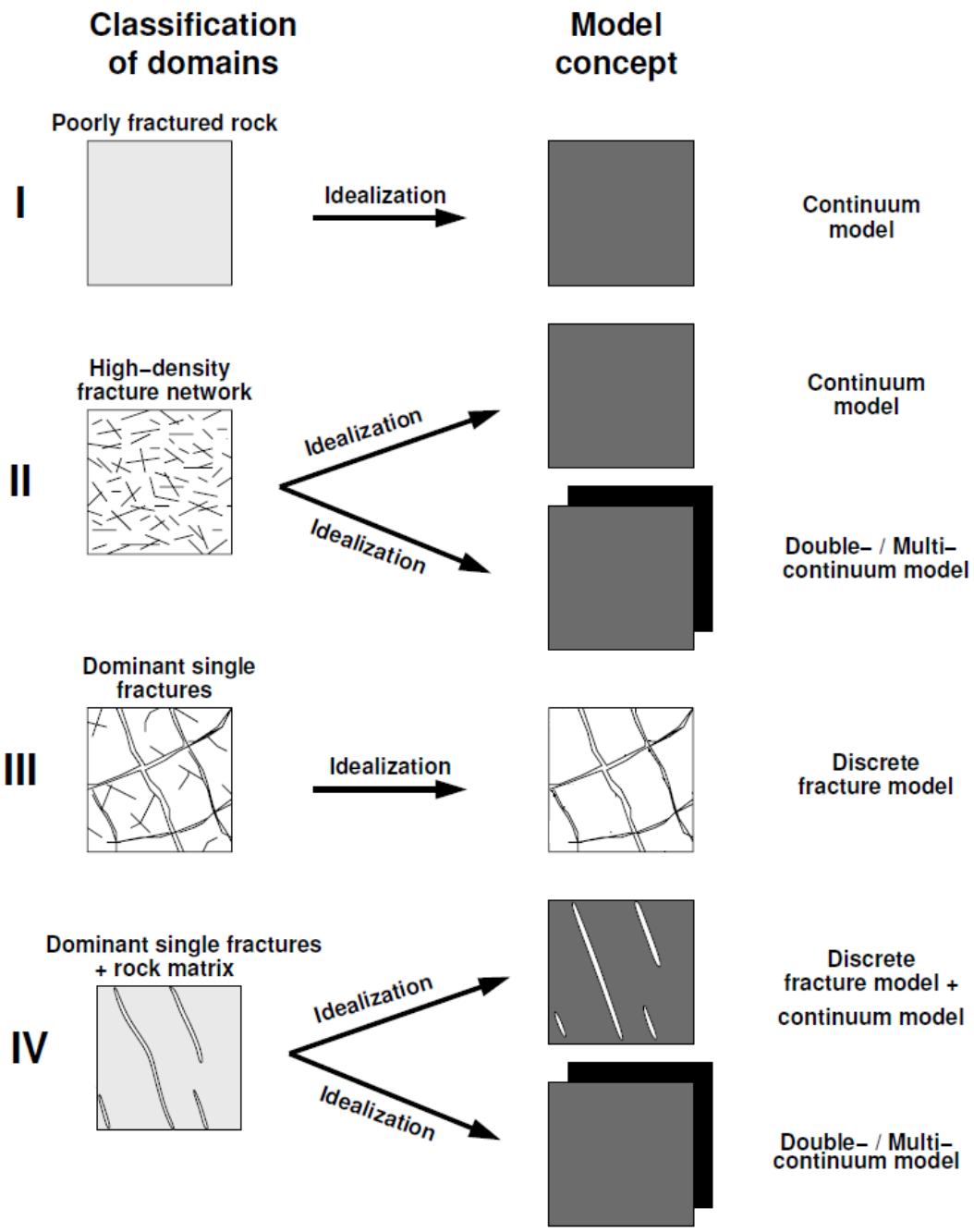

Figure 2.15 The classification of the fractured bedrock and the relevant modelling concepts by Dietrich *et al.* (2005) based on works by Krohn (1991) and Helmig (1993). Grey colour of the domains in the first column (Classification of domains) means the matrix has high hydraulic conductivity; white colour means the matrix with low hydraulic conductivity.

If the matrix of an aquifer is densely fractured (row II, Figure 2.15), it can also be simplified to a single continuum. The single continuum model for a fractured aquifer assumes representative elementary volume, which is possible only when fracturing is homogeneous that does not change the aquifer properties with scale.

Another approach would be to model it as a double continuum where the fracture network is represented by one continuum and the matrix by the other, each

having their own properties. The fractured aquifer can be represented by a dual continuum with an assumption that each continuum is present at every point within the entire domain (Bear *et al.* 1993). The macroscopic flow and heat transfer properties can be estimated from the averaged equations derived with the multiscale homogenisation techniques that allow to study the effects of fractures on the heat transport in a fractured aquifer (Daly & Roose 2014).

Double-continuum models can be divided into dual porosity and dual permeability. Figure 2.16 illustrates how these two types differ. Dual permeability model accounts for groundwater flow through both matrix and fracture network, while dual porosity assumes the matrix has low hydraulic permeability.

Homogenisation has been widely used to describe flow in single porosity materials (Ene & Poliserverski 1987) as well as to describe macroscopic flow and diffusion in the dual-porosity models (Arbogast *et al.* 1990; Panfilov 2000).

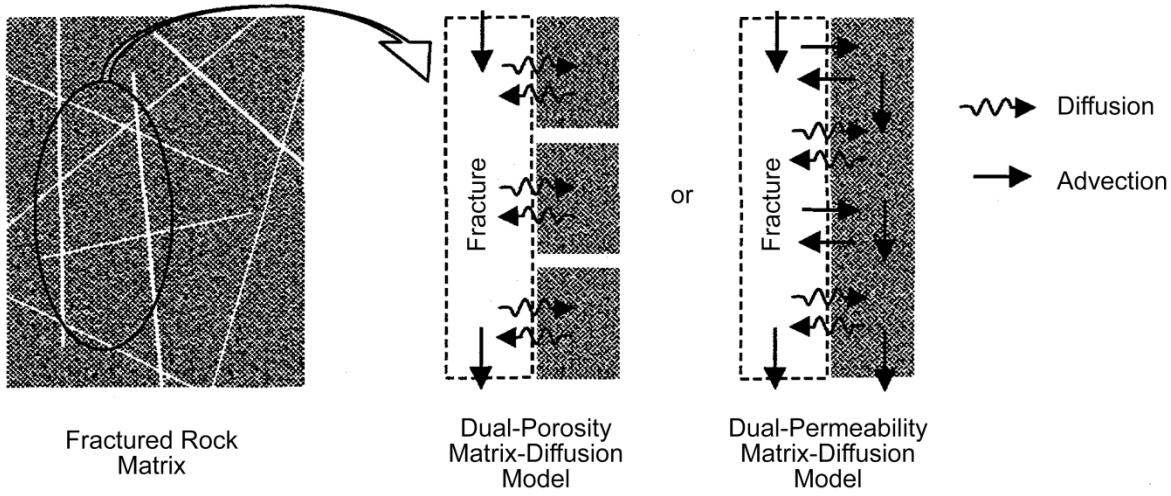

Figure 2.16 Heat transport in the fractured aquifers with dual permeability and dual porosity (Ho 2000). Advection can be regional (groundwater flow) or local (fluid exchange between domains), thermal diffusion occurs due to the local gradient of temperature.

In the case when an aquifer has only a few dominant fractures, it can be conceptualised as a discrete fracture model with or without hydraulic permeability in the matrix (illustrated in rows III and IV, Figure 2.15). The Darcy equation is used for flow in the matrix, hydraulic permeability of fractures in porous medium can be

estimated by linear Stokes equation or local cubic law (Reynolds equation) (Zimmerman & Yeo 2000).

Considering the relatively small size of the area of thermal disturbance to the ground caused by a VBHE operation, when a VBHE is located near a dominant fracture, the fracture might be discretely represented in a model of a VBHE.

The heterogeneities in an aquifer (fractures) cause varying convection velocities, which produce a broad spectrum of thermal transport rates. This results in the wider thermal breakthrough curves with long tailing and early peak. The Fourier type equation cannot capture this behaviour, especially for the heterogeneous fracturing with significant advection where heat transfer rate can span orders of magnitude (Geiger & Emmanuel 2010). Despite the fact that the continuum model framework assumes homogeneous distribution of fractures, the non-Fourier thermal transport can be accounted for if the spatially varying scale-dependent macrodispersivity is deduced from the temporal moment analysis (Suresh Kumar 2014). A time-dependent non-Fourier macrodispersion coefficient can be derived from spatial moment analysis (Suresh Kumar 2014).

Models for thermal transport in fractured aquifers could adopt different frameworks: mechanistic framework (based on advection-dispersion equation), stochastic (partially mechanistic) or artificial intelligence (machine learning) (Figure 2.17). Mechanistic frameworks are the most commonly used. Stochastic frameworks can account for a non-Fourier thermal transport (Neuman & Tartakovsky 2009). The artificial intelligence framework needs a lot of input data for the learning process resulting in a black-box model.

The first subgroup of a mechanistic framework is a continuum model framework (Figure 2.17) which can be deterministic or stochastic. The stochastic approach to a continuum framework uses a Monte Carlo analysis for a probabilistic solution to a flow and transport problem, which is more appropriate given the high uncertainty

of the field measurements and the assumptions of conceptual model of a fractured aquifer.

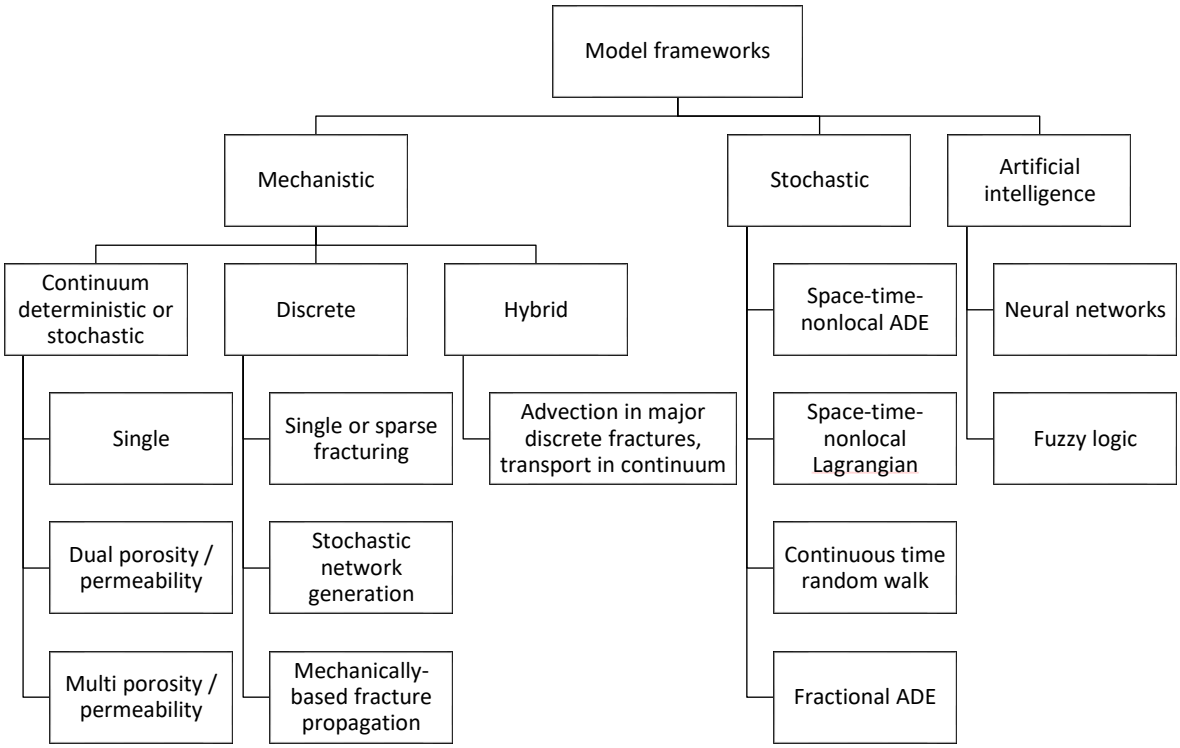

Figure 2.17 Examples of the modelling frameworks for thermal transport in a fractured aquifer. ADE means Advection-Dispersion Equation. Stochastic frameworks were taken from Neuman & Tartakovsky (2009). The main mechanistic frameworks were taken from Beyer & Mohrlok (2007). Examples of the artificial intelligence frameworks were taken from Chen *et al.* (2008).

One of the main advantages of a continuum framework is its high practical applicability and small investigation effort compared with the discrete modelling framework (Figure 2.18). The analytical solutions for a VBHE (described in Chapter 3) assume homogeneous ground and use the continuum modelling approach. To account for heterogeneity in an aquifer requires more investigation effort and computing resources, therefore, its practicality should be justified.

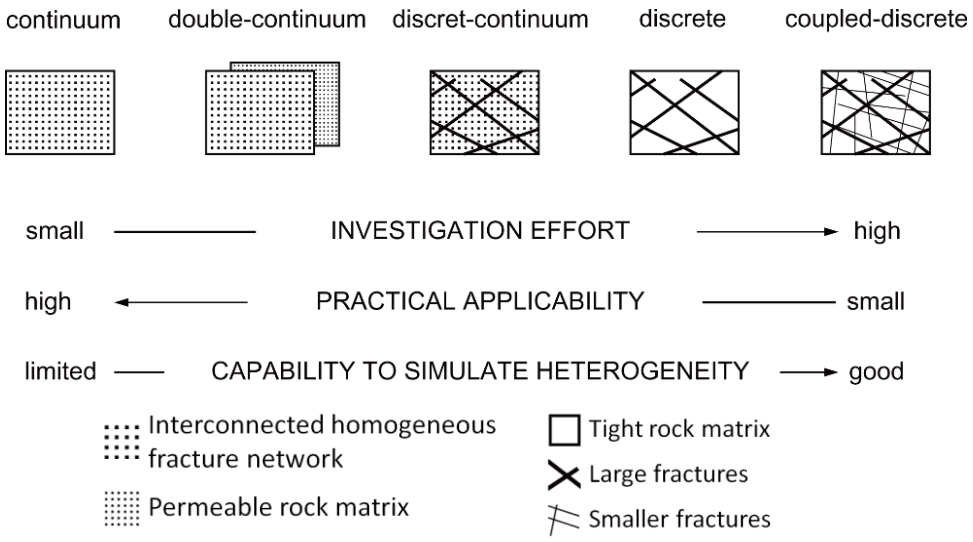

Figure 2.18 The scale of practicality and resource demand for different approaches to conceptual modelling of the fractured aquifers, after work by Teutsch et al. (1991) in Beyer & Mohrlok (2007).

2.3.4 Modelling the effects of fractures on a VBHE

Currently applied models for a VBHE assume homogeneous aquifers. Advection-influenced thermal response tests could potentially be used to determine the integral hydraulic conductivity for heterogeneous or layered aquifer (Wagner *et al.* 2014). However, consideration of the averaged thermal properties in a layered or heterogeneously fractured aquifer can give significantly erroneous results about the thermal performance of a VBHE (Loveridge *et al.* 2013; Erol 2016). Hydrogeological conditions may significantly influence the decision about the design of a VBHE system according to its estimated thermal impacts. Convenient tools are needed to design and plan a multi-VBHE field installed in a range of the hydrogeological conditions (Erol *et al.* 2015). There is a need for a spectrum of models to estimate and optimise the thermal performance of a VBHE in different hydrogeological settings (Lee & Lam 2012). This can include layered, fractured and heterogeneous aquifers. For example, the top layer of bedrock can be fractured due to weathering and can have a higher hydraulic permeability. This top layer could be represented by a separate homogeneous medium with different thermal and hydraulic properties than the rest of the bedrock. An analytical model for a VBHE in a horizontally layered aquifer was developed (Erol 2016; Erol & François).

It is based on a model for multilayer conduction from a VBHE developed by Abdelaziz *et al.* (2014). The model assumes different thermal properties, advection and 2D dispersion separate for each layer, without groundwater exchange or vertical dispersion. The model could be used to investigate the effect of the heterogeneous aquifers on a VBHE rather than considering a homogeneous groundwater flow across the whole VBHE length.

The long-term behaviour and efficiency of a VBHE can be optimised if the heterogeneous geology is considered even for a non-productive aquifer (Radioti *et al.* 2016). The groundwater flow (even through a single open horizontal fracture with a small volumetric flow rate) can significantly increase the apparent thermal conductivity of a fractured hard rock, with a low hydraulic permeability of the rock matrix (Liebel *et al.* 2012).

Figure 2.19 illustrates how even a single vertical hydraulically permeable fracture close to a VBHE installed in a hydraulically impermeable rock can significantly influence the thermal performance of a VBHE (Figure 2.19 A and B) and its thermal interactions (Figure 2.19 C). This work is carried out by Dehkordi *et al.* (2015). The isotherms shown in Figure 2.19 are modelled for a VBHE after 25 years of operation installed near a fracture of two different apertures and at two different distances. The rock type is crystalline and hydraulically impermeable with low porosity (2.5 %), volumetric heat capacity of 2.25×10^6 J m^{-3} K^{-1}, and the thermal conductivity of 4.5 J m^{-1} s^{-1} K^{-1}. A fracture in the bedrock is open and vertical. It is represented as two parallel smooth plates with laminar flow. The groundwater velocity inside the fracture is calculated from the aperture and hydraulic gradient (0.01) using a cubic law. The heat abstraction by a VBHE is seasonal, 9 months on / 3 months off, it is sinusoid of a specific heat extraction peaking at 75 W m^{-1} (Dehkordi *et al.* 2015).

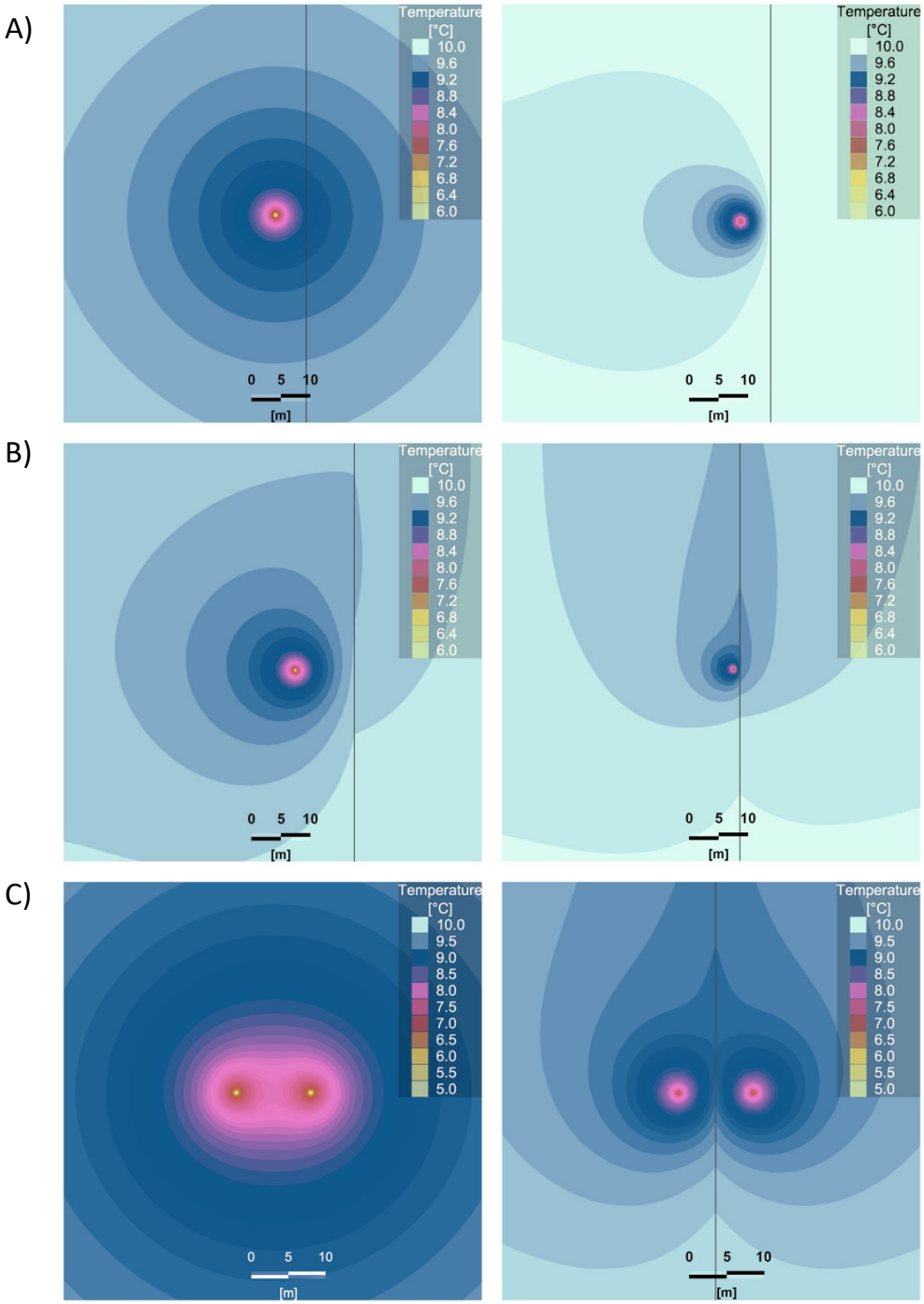

Figure 2.19 Plan of modelled isotherms around a vertical borehole heat exchanger (VBHE) installed near an open vertical fracture with: (A) different apertures: 0.1 mm, tight (left plot) and 10 mm, moderately wide (right plot). Both at the same distance from the VBHE: 5 m; (B) different distances between a fracture and the VBHE: 10 m (left plot) and 1 m (right plot). Both with the same fracture aperture of 1 mm. The thermal interactions between two VBHEs is shown in (C): for homogeneous bedrock (left plot) and for bedrock with one open vertical fracture of 1 mm aperture passing between two VBHEs, at 5 m distance from each VBHE (Dehkordi *et al.* 2015).

A single major open vertical fracture near a VBHE (with aperture 1 to 10 mm) can significantly alter the extent of the thermal plume (Figure 2.19). The classification

of fractures by apertures is given in Appendix B. The results for a single horizontal fracture intersecting a VBHE showed smaller effect on the thermal transport from the VBHE than the results for a vertical fracture. However, the influence became more significant when the number of horizontal fractures intersecting a VBHE was increased (Dehkordi *et al.* 2015).

The apparent thermal conductivity of the ground can significantly increase due to high groundwater flow through a single hydraulically open fracture (Liebel *et al.* 2012). Therefore, it can improve the estimated thermal performance of a VBHE. However, a presence of a fracture also can exacerbate the downstream thermal impacts of a VBHE installed in an aquifer, even if the groundwater flow in the fracture is relatively slow (Gehlin & Hellström 2003). A thermal response test can be used to identify where the water-bearing fractures are located and to inform the decision on the further investigations required and modelling approach for a VBHE installation (Liebel 2012).

Fractured aquifers can have increased thermal advection and macro-dispersion. Different optimum heat extraction rates for a VBHE are necessary for different hydro-geological conditions (Erol *et al.* 2015). A few studies were conducted to test the influence of fractures on the VBHE efficiency and its thermal impacts (Gehlin & Hellström 2003; Dehkordi *et al.* 2015).

2.4 Key messages

- Vertical borehole heat exchangers (VBHE) offer a low carbon technology with increasing popularity due to numerous benefits.
- The main challenge of the technology of the closed-loop ground source heat pump is the installation costs of a VBHE.
- Legislation and guidance for the VBHE installations should reflect the hydrogeological conditions where VBHEs are installed.

- Models are necessary tools to estimate the long-term thermal performance of VBHE systems. Improved models may lead to the improved estimation of the installation costs and provide the basis for the improved legislation.
- A single continuum modelling approach can be selected for a densely fractured aquifer to model the heat transfer from the VBHE, with adjusted parameters for groundwater flow and the thermal dispersivity.
- Current analytical models used for the design of a VBHE system assume the ground is homogeneous.
- Groundwater flow in fractures can significantly alter the thermal interactions and efficiency of the VBHE installations.
- Consideration of a flowing fracture near a VBHE will allow to better estimate the thermal performance and thermal interactions of a VBHE, to decide on the feasibility of an installation and to improve the optimisation for efficiency, sustainability and thermal interactions between the VBHE installations.
- Quantification is needed on how fractures influence VBHE installed in aquifers.

Chapter 3 Effects of the advective thermal transport on a VBHE installed in a homogeneous aquifer

This chapter discusses the influences of the advective thermal transport on the thermal performance of VBHEs in homogeneous aquifers. This provides a useful background before the subsequent analysis of effects of a fracture on a VBHE. It also acts as a base case for the subsequent results of this thesis to be compared against. In this chapter, analytical solutions to the advection-diffusion equation (2.15) are applied to determine how the groundwater flow can influence the thermal performance of a VBHE in terms of the temperature change to the surrounding ground. The analysis of the effects of dispersive thermal transport using analytical solutions in 2D and 3D is carried out in Chapter 4.

3.1 Methods

3.1.1 Models

Two analytical solutions were used: MILS (moving infinite line source) and MFLS (moving finite line source). A complete description of MILS and MFLS models was given in Chapter 2. The analysis was developed using the Matlab software (The MathWorks Inc.). The starting point was the code by Molina-Giraldo published as a supplement in (Stauffer *et al.* 2014).

3.1.2 Parameters and assumptions

In addition to the assumptions listed in Chapter 2 for the relevant analytical solutions, the following assumptions were made. The thermal load (heat injection) to a VBHE is constant. The groundwater flow in the homogeneous and isotropic matrix is constant and horizontal along the x-axis in the positive direction. The surface temperature for the MFLS model is assumed to be constant and equals to the initial temperature of the aquifer. If not stated otherwise, base parameter

values for the models are listed in Table 3.1. The parameters for the aquifer matrix material (density, effective volumetric heat capacity and effective thermal conductivity) were based on the typical sandstone values (Stauffer *et al.* 2014). The tested Darcy groundwater velocities v_u are classified into three categories: fast groundwater flow for $v_u \geq 0.1$ m day^{-1}, slow groundwater flow for $v_u \leq 0.01$ m day^{-1} and medium for the values in between. The hydraulic conductivities in the Permo-Triassic sandstones in the UK can reach 100 m day^{-1} (Allen *et al.* 1997). Most of the analysis was carried out for the groundwater flow velocities selected from each of these three categories. This chapter focuses on the effects of advective and conductive thermal transport. The effects of the dispersive thermal transport are discussed in Chapter 4.

Table 3.1 The base values of parameters for analytical solutions MFLS (Moving Finite Line Source) and MILS (Moving Infinite Line Source). The parameters for the aquifer matrix material (density, effective volumetric heat capacity and effective thermal conductivity) were based on the typical values for a sandstone (Stauffer *et al.* 2014).

Parameter, symbol	Base value
Heat flow rate per unit length of the VBHE, q_{tb}	50 Wm^{-1}
VBHE radius, r	0.05 m
VBHE length, H_b	100 m (for MFLS)
Effective volumetric heat capacity of the aquifer, C_{em}	2.8x10^6 J m^{-3} K^{-1}
Volumetric heat capacity of water, C_w	4.2x10^6 J m^{-3} K^{-1}
Effective thermal conductivity of the aquifer, λ_{em}	2.5 W m^{-1} K^{-1}
Darcy velocity, v_u	Range from 0 m day^{-1} to 0.5 m day^{-1}
Dispersivity in longitudinal β_L, transverse β_T and vertical β_V direction	0.0 m; 0.0 m; 0.0 m

3.1.3 Presentation format

The analysis of the effects of advection on the thermal performance of a VBHE is structured according to the indicators of the VBHE thermal performance as follows:

1) The temperature change at borehole wall ΔT_b determined after continuous heat injection by a VBHE during 30 years at point x = 0.05 m (downstream side of the VBHE), y = 0 m and z = 50 m (z is relevant to the MFLS model only, which is in 3D);

2) The time to stabilise ΔT_b denoted as t_{Sb}. The time needed to a reach the steady state is defined as a time when the temperature change at a specific location (for example at the VBHE wall) reaches 99 % of the temperature change value calculated at time of 300 years. This approach is used because the temperature changes asymptotically with time. Note that if temperature is still changing after 300 years, this method returns the time for steady state as 300 years. For the purposes of this analysis it is not practical to model for longer times. This means that if the determined t_{Sb} equals to 300 years then the steady state was not actually reached within the modelled 300 years (it occurs only for MILS when the groundwater flow is absent).
3) The extent of the +2 K and +0.5 K isotherms (X_{2K} and $X_{0.5K}$) after continuous heat injection by a VBHE during 30 years, which are calculated as a maximum x-axis coordinate for the isotherm in the direction downstream of a VBHE (it is not the actual isotherm width). It is located at the mid-length point of a VBHE when the MFLS model is used.
4) The times to stabilise the isotherms (t_{S2K} and $t_{S0.5K}$). The time needed to reach the steady state for an isotherm extent is calculated using the following steps:
    a) the location of the maximum longitudinal extent of an isotherm for a temperature change of interest (for example +2 K, X_{2K}) is found after time of 300 years. It is located at the mid-length point of a VBHE when the MFLS model is used. X_{2K} is assumed to be at steady state after this time.
    b) the time is found when the temperature of interest, reduced by 1 %, is reached at the location of the maximum longitudinal extent (i.e. at X_{2K} after 300 years). The same note about the limitation of the method to estimate the steady state using 300 years applies for X_{2K} similarly as for ΔT_b.

Before analysis of the groundwater flow on the indicators of the VBHE thermal performance, the difference between two analytical solutions (MILS and MFLS) in modelling thermal transport was discussed. Additionally, the discussion of how the design of a VBHE is influenced by the groundwater flow is presented in the Appendix C.

3.2 Results

3.2.1 The role of vertical conduction

The vertical conduction (i.e. conduction parallel to the line of a VBHE) is important to account for in estimation of the long-term energy efficiency of a VBHE (Zarrella & Pasquier 2015). The MILS analytical solution for a single fully-penetrating (infinitely long) VBHE set in an aquifer with a constant groundwater flow is in 2D, and therefore it does not account for the vertical conduction. The MFLS analytical solution is in 3D and it accounts the vertical conduction. Figure 3.1 shows the difference between the MILS and MFLS models in the extent of the isotherms for different groundwater flows. The difference between modelled results in the extent of the isotherms is noticeable for slower groundwater flow (Figure 3.1 A). The role of vertical conduction is significant at the slow groundwater flow velocities in the long term (year-scale). This is because the conduction to the surface with the stable temperature and also to the region below the VBHE is proportionately larger relative to the advection by groundwater flow for the slower flows. Thus, the role of vertical conduction becomes more significant, and models that ignore it (e.g. MILS) overestimate the extent of the isotherms of interest (Figure 3.1).

The difference between MILS and MFLS for the faster groundwater flow can be observed for the isotherms of small temperature change (for example, +0.5 K in Figure 3.1 B). At the midpoint of a relatively long VBHE (100 m), there is no difference in the isotherm extent (and temperature change at the VBHE wall) between MILS and MFLS. However, if the VBHE is shorter, the role of the vertical

conduction becomes more prominent and the difference between MILS and MFLS increases. This is especially the case for the isotherms of smaller temperature change which have more area for the thermal exchange with the surface and the groundwater flowing underneath the VBHE.

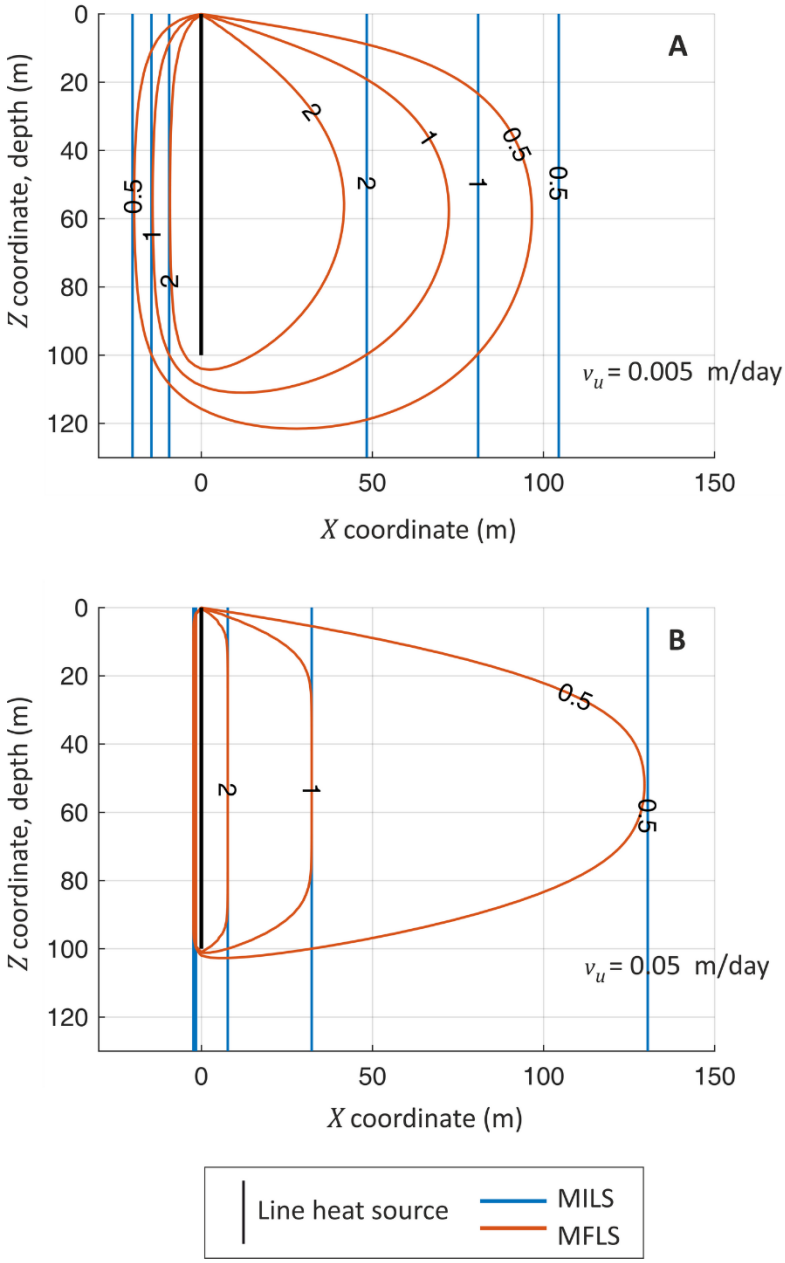

Figure 3.1 The isotherms for temperature change (ΔT in K shown on the isotherm lines) on the vertical cross-section (profile view) along the VBHE centreline (y = 0 m) for the MFLS and MILS models for groundwater flow (A) v_u = 0.005 m day^{-1} and (B) v_u = 0.05 m day^{-1}. Model parameters are given in Table 3.1.

Figure 3.2 shows how the extent of the +2 K isotherm depends on the VBHE length H_b for the same heat input power J = 5000 W (Figure 3.2 A and B) and for the same heat flow rate per unit depth of the VBHE J/H_b = 50 W m^{-1} (Figure 3.2 C and

D). The horizontal lines marking the VBHE lengths H_b in the figure show how much of the +2 K isotherm lies below the VBHE for different groundwater velocities v_u.

For a very short VBHE the role of vertical conduction is significant and the MFLS model is the preferred model choice. For long VBHEs, the role of the vertical conduction is negligible. Therefore, it can be ignored, and MILS analytical solution is an appropriate simplification. If the VBHE is installed in an aquifer with fast to medium groundwater flow, the role of the vertical conduction is reduced (even for a short VBHE), because most of the thermal transport occurs by advection.

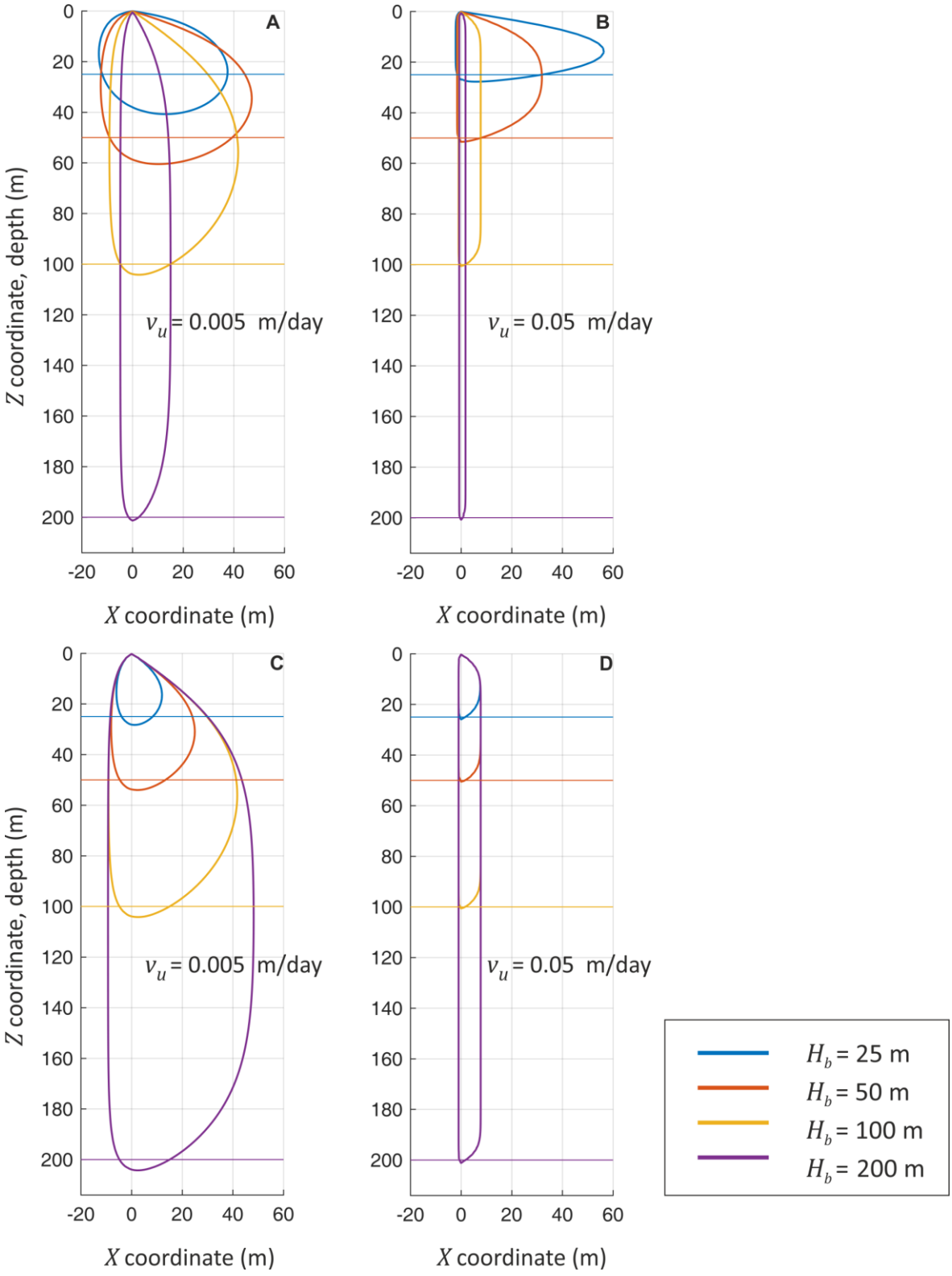

Figure 3.2 Profile view of the +2 K isotherms along the VBHE centreline (y = 0 m) for different VBHE lengths H_b using the MFLS model (A) for constant heat input J = 5000 W and (B) for constant heat input per unit depth of the VBHE J/H_b = 50 W m^{-1}. Model parameters are given in Table 3.1. Two groundwater velocities were used: (A and C) v_u = 0.005 m day^{-1}, and (B and D) v_u = 0.05 m day^{-1}.

3.2.2 Effects of advection on the temperature change at the VBHE wall

Figure 3.3 illustrates the development of the temperature change at the VBHE wall ΔT_b with time for different groundwater flows v_u, modelled using the MILS and MFLS models. Advection significantly reduces ΔT_b even when groundwater flow is slow (0.005 m day^{-1}) compared with the case with no groundwater flow. There is no difference between MILS and MFLS until the time of the VBHE operation is long, about 30 years. Then the difference between the MILS and MFLS models becomes significant for the case with no groundwater flow, because in this case, MILS does not reach steady state. Dimensionless units used in Figure 3.3 B can be used for comparison with the universal thermal response curves (Wagner *et al.* 2014).

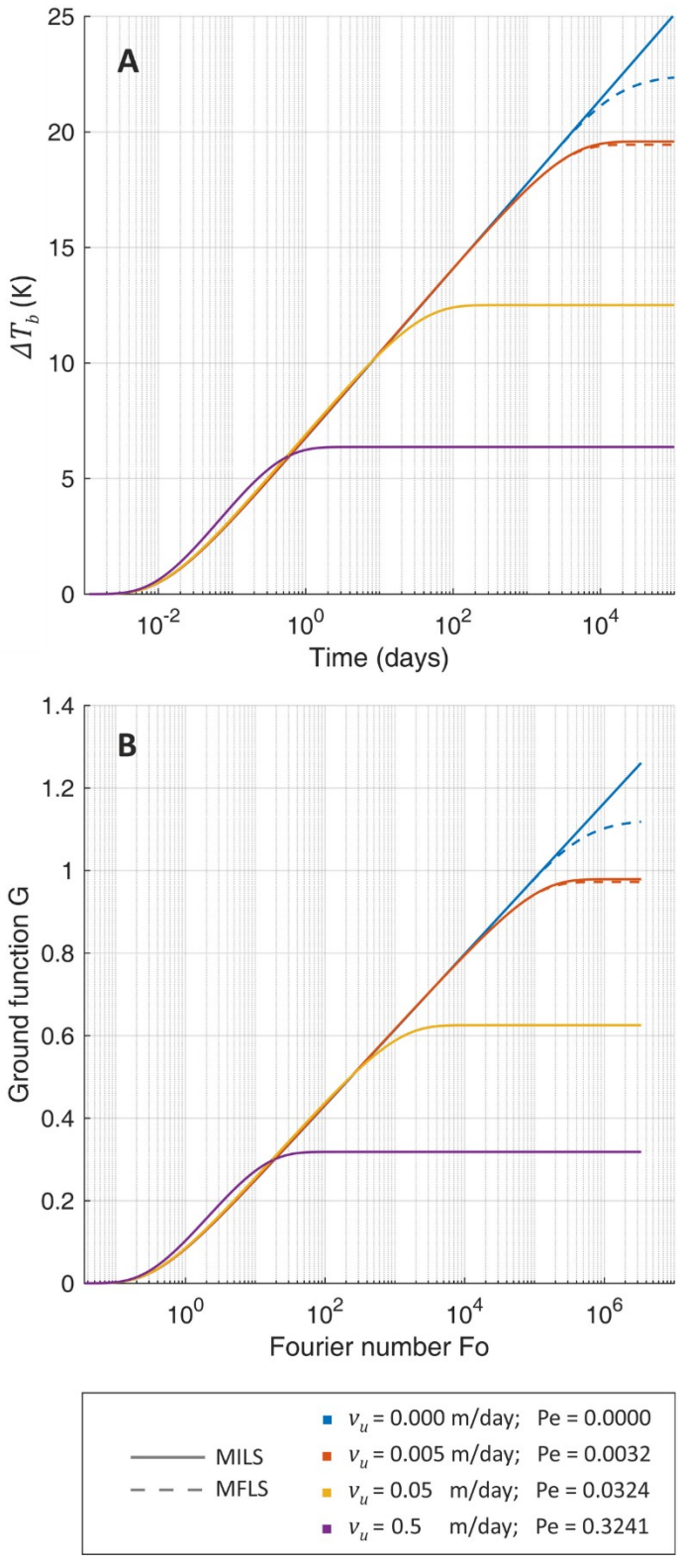

Figure 3.3 The development of the temperature change at the VBHE wall ΔT_b with time for four groundwater flows v_u, using the MFLS and MFLS models (A) in physical units and (B) dimensionless. F_o is dimensionless time, G is dimensionless temperature change at the VBHE wall, $G = \lambda_m T / q_{tb}$ (Rouleau *et al.* 2016), and Pe is Peclet number. Parameters are in Table 3.1. 10^3 days is 2.7 years, 10^4 days is 27.4 years.

Figure 3.4 shows how groundwater flow v_u influences ΔT_b at steady state and the time to reach steady state t_{Sb}. Both ΔT_b and t_{Sb} are significantly reduced with increasing groundwater flow, starting from v_u of 0.001 m day^{-1} (Figure 3.4). Values of ΔT_b and t_{Sb} for slow groundwater flows are higher for MILS because it does not account for the vertical conduction. Due to this reason, the difference between the MFLS and MILS models would grow even larger for cases with negligible groundwater flows if the time of simulation was longer (note that ΔT_b at the steady state was calculated based on 300 years of the continuous VBHE operation). As was discussed in section 3.2.1 the vertical conduction is more important for shorter VBHEs, so if the modelled VBHE was shorter the differences between the MILS and MFLS would be larger.

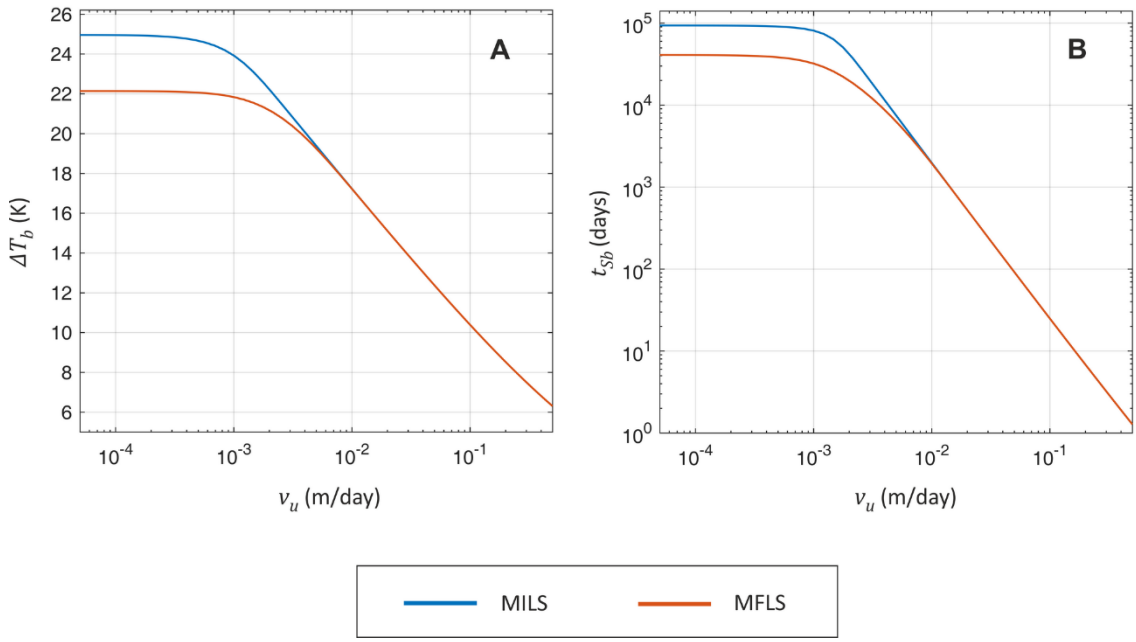

Figure 3.4 (A) The temperature change at the VBHE wall ΔT_b at steady state and (B) the time to reach the steady state at the VBHE wall t_{Sb} for a range of groundwater velocities v_u modelled using the MILS and MFLS analytical solutions.

In this study when the MFLS (model in 3D) is used, the time to stabilise the temperature change at the VBHE wall t_{Sb} is calculated at the mid-length of the VBHE. This is justified as t_{Sb} is more or less similar along most of the length of the VBHE as illustrated in Figure 3.5. However, t_{Sb} differs along the top section of the VBHE which is close to the ground surface. This difference in t_{Sb} is more noticeable

for cases with slow or zero groundwater flows and is negligible for fast groundwater flow. This is because at slower or absent groundwater flow the vertical conduction between the ground and the constant temperature at the surface is significant. Therefore, the steady state is reached quicker at the shallower VBHE depths. At the bottom tip of the VBHE steady state is reached more slowly. This is because it takes time to stabilise the temperature change further away from the VBHE wall.

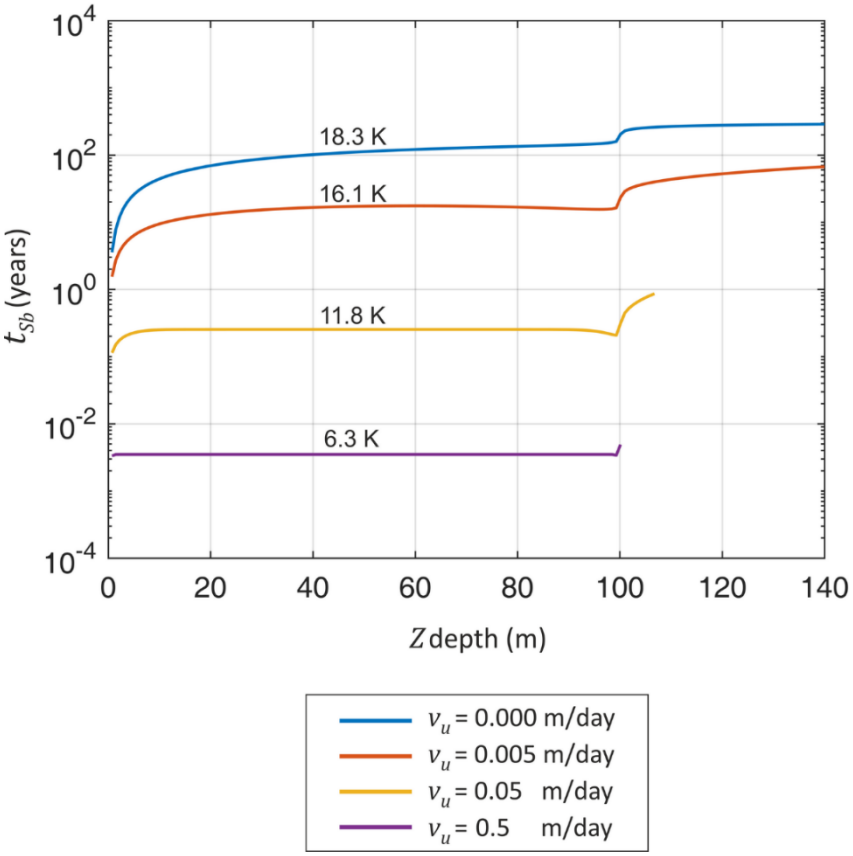

Figure 3.5 The time to reach steady state at the VBHE wall t_{Sb} along the depth for the VBHE (with length of 100 m), for a four groundwater velocities v_u. The numbers on lines show the maximum temperature change at the VBHE wall at the mid-length of VBHE at the steady state. Modelled using MFLS. Other model parameters are in Table 3.1.

3.2.3 Effects of advection on the extent of isotherms

Figure 3.6 shows how groundwater flow can influence the shape of isotherms in plan and profile. Groundwater flow extends the isotherms in the direction of the flow. The exception is fast groundwater flow (0.5 m day^{-1}) when the thermal transport by advection is high enough to reduce the isotherms by spreading the lower temperature change over the large area. Figure 3.6 B also shows how the

vertical conduction differs between different groundwater flows. For slow groundwater flow significant part of the +0.5 K isotherm is below the VBHE, while for the fast groundwater flow (0.5 m day^{-1}) the axial conduction is negligible.

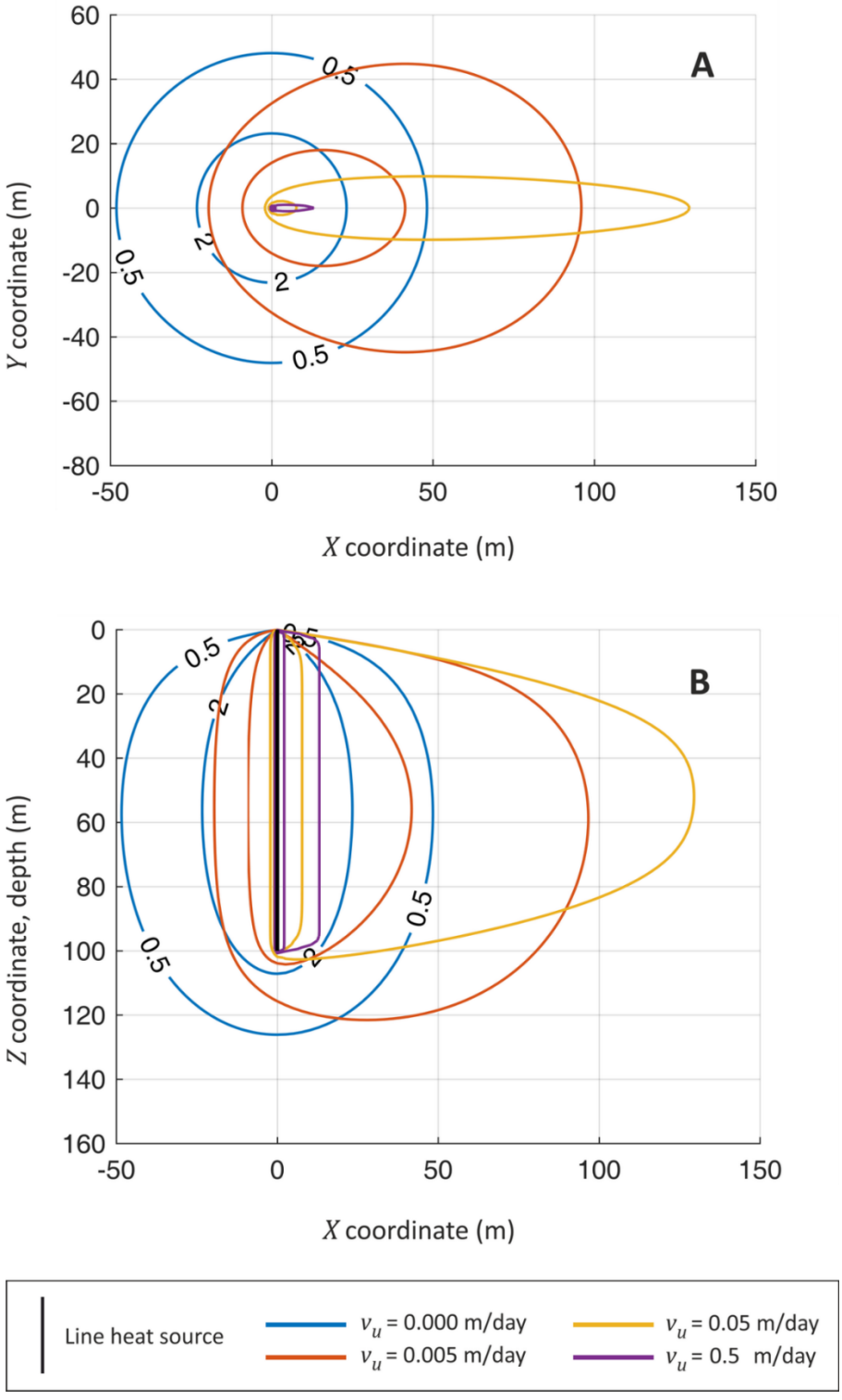

Figure 3.6 Isotherms for ΔT of +0.5 K and +2 K produced by the VBHE after 30 years of continuous operation (heat injection) for a range of groundwater velocities v_u in (A) plan and (B) profile view modelled using MFLS. Model parameters are given in Table 3.1.

As was discussed in section 2.2.6, the estimation of the extent of the isotherm of interest X_T and the time for it to reach steady state is necessary for estimation of the thermal interactions between the VBHE systems, to optimise their spacing and to assess the thermal impacts at specific hydrogeological settings. Figure 3.7 shows how the effective thermal conductivity λ_{em} and the groundwater velocity v_u can change the extent of different isotherms X_T after 30 years of the VBHE continuous operation. The effect of an increase in λ_{em} is similar to the effect of an increase in v_u because the increase of these model parameters increases the apparent thermal conductivity of the ground (discussed in Chapter 2). The increase in these parameters increases the thermal transport from the VBHE.

When λ_{em} and v_u are increased from low values, the modelled extent of the isotherms X_T is increased. When λ_{em} and v_u are increased further it reduces X_T. This is because the further increase in the thermal transport causes the spreading of the thermal disturbance caused by a VBHE over the larger area. The VBHE heat flow rate J is fixed; therefore, the increase in the thermal transport reduces the temperature change at and near the VBHE wall by transporting it further away. Figure 3.7 illustrates how the extent of the isotherms of high ΔT (e.g. +5 K) is decreased by groundwater flow because it increases the extent of the isotherms of low ΔT (e.g. +0.5 K).

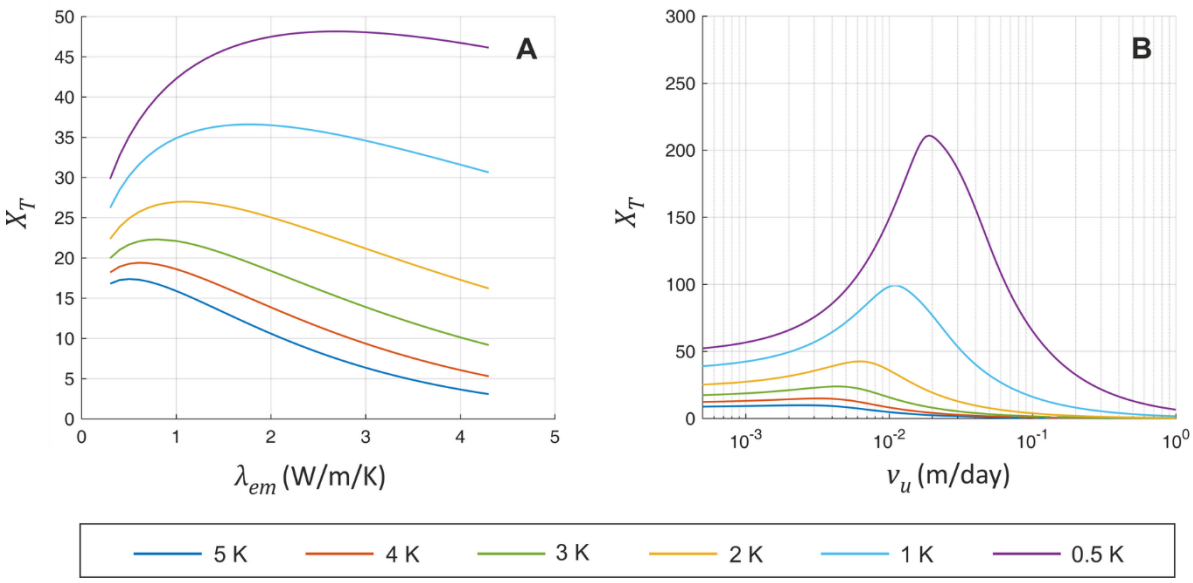

Figure 3.7 The longitudinal extent in x-coordinate for a range of the isotherms X_T produced by a VBHE after 30 years of continuous operation installed in the ground with (A) different thermal conductivities λ_{em} for absent groundwater flow and (B) with various groundwater flows v_u and fixed λ_{em} = 2.5 W m^{-1} K^{-1}. Modelled using MFLS. Model parameters are listed in Table 3.1.

The results presented in Figure 3.7 were only for MFLS. Figure 3.8 shows how the results in the extend of different isotherms (+0.5 K and +2 K, noted as $X_{0.5K}$ and X_{2K}) differ between MILS and MFLS for a range of groundwater flows and for a range of the VBHE heat flow rates J. The result resembles the relationship shown in Figure 3.7 B. The $X_{0.5K}$ and X_{2K} increase with increasing v_u until a specific v_u value. The threshold of v_u at which the extent of the isotherms starts to shrink depends on the VBHE heat flow rate J. For example, for the +0.5 K isotherm this threshold v_u is 0.01 m day^{-1} for J = 2500 W and 0.04 m day^{-1} when J = 10000 W.

The results differ between MILS and MFLS. The extent of the isotherms modelled using MILS for groundwater velocities that maximally extend the isotherm is longer compared with MFLS. This is because MFLS accounts for the vertical conduction. When the VBHE heat flow rate J is increased, the vertical thermal transport between the surface and the ground around the VBHE is also increased due to higher thermal gradient. The role of the vertical conduction is the highest for groundwater flows when the extent of an isotherm is maximally increased by the advection.

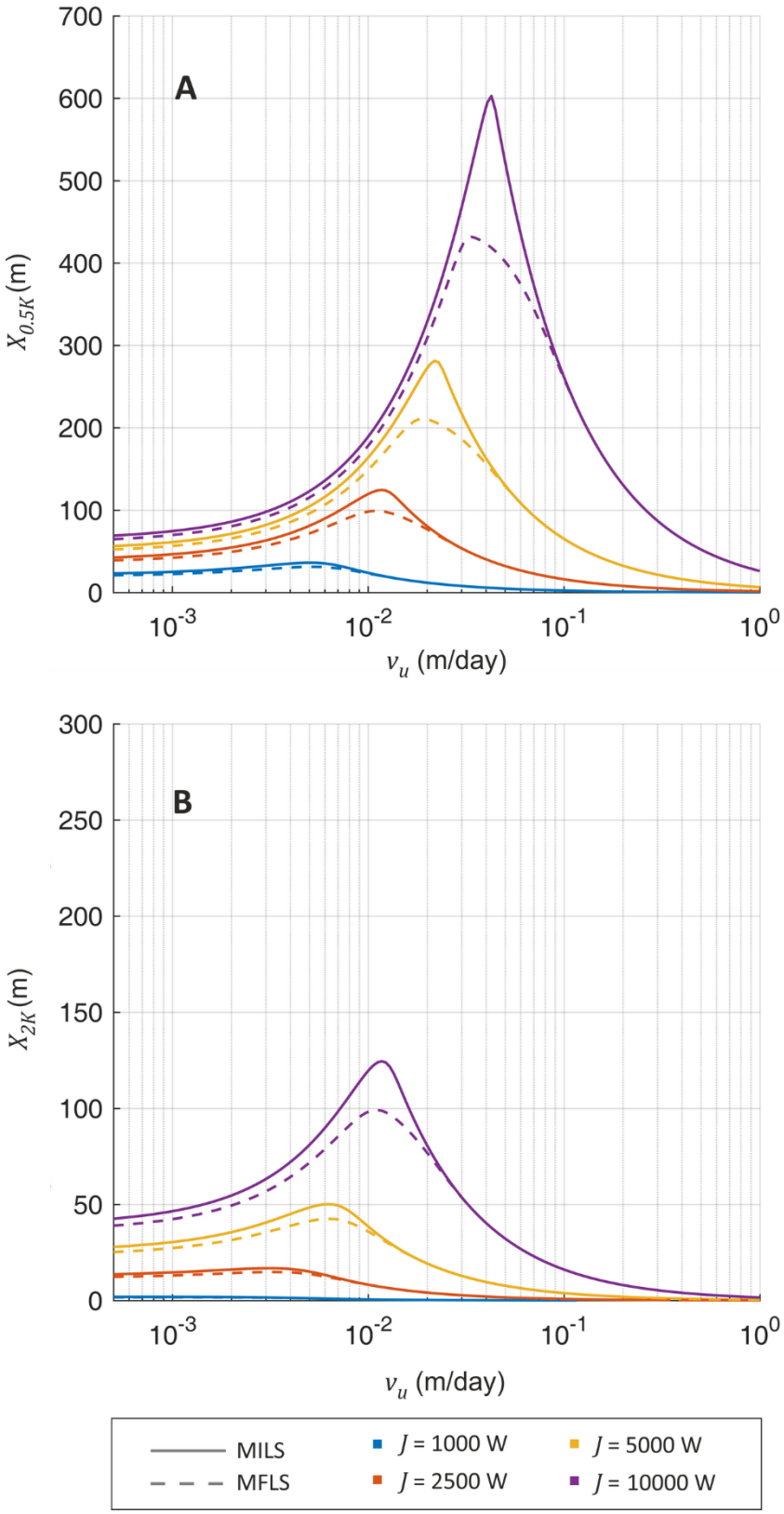

Figure 3.8 The longitudinal extent of the (A) +0.05 K and (B) +2 K isotherm produced by the VBHE after 30 years of continuous operation with different VBHE heat flow rates J for various groundwater velocities v_u. Modelled using MFLS and MILS. The model parameters are listed in Table 3.1.

The practical implication of the results shown in Figure 3.8 advises that MILS can significantly overestimate the thermal disturbance to the ground, increasingly so for a VBHE with high thermal load and installed in an aquifer with medium groundwater flow. Therefore, at groundwater flows that can significantly extend the isotherm compared to no groundwater flow condition it is preferable to account for the vertical thermal transport in modelling the VBHE thermal performance.

3.2.4 Effects of advection on a multi-VBHE field

In practice, ground source heat pump systems can be installed as a field of multi-VBHE installations. The effects of groundwater on a multi-VBHE field are illustrated on Figure 3.9 and Figure 3.10. The figures show the plan view of thermal disturbance to the ground from a set of 9 VBHEs after 30 years of continuously injecting heat (5000 W for each VBHE) into the aquifer with different groundwater velocities as modelled using both MILS and MFLS models. The enclosed table shows ΔT_b after 30 years of operation for each of the VBHEs, mirroring the VBHE layout, the highest value is highlighted in red. When groundwater flow is absent (Figure 3.9 A) the thermal performance of a VBHE located at the centre of the VBHE field can be undermined due to thermal influence of the neighbouring exchangers. While when groundwater flow is slow (Figure 3.9 B) the VBHE located downstream has the highest value of ΔT_b. For both absent and slow groundwater flows the relative difference in isotherm extent between the results of MILS and MFLS are not as significant as their difference in the ΔT_b. However, at medium groundwater flow (Figure 3.10 A) the isotherms (for example, +2 K) generated by the VBHE field are extended the most, while the values of ΔT_b for all VBHEs are significantly reduced by groundwater flow. In this case, the results of MILS and MFLS differ significantly in the extent of isotherms (see values for the maximum extent of +2 K and +0.5 K isotherms for both models on Figure 3.10 A). While the result of MILS and MFLS for ΔT_b are the same. At fast groundwater flow the results by MILS and MFLS for the extent of isotherms and ΔT_b are identical.

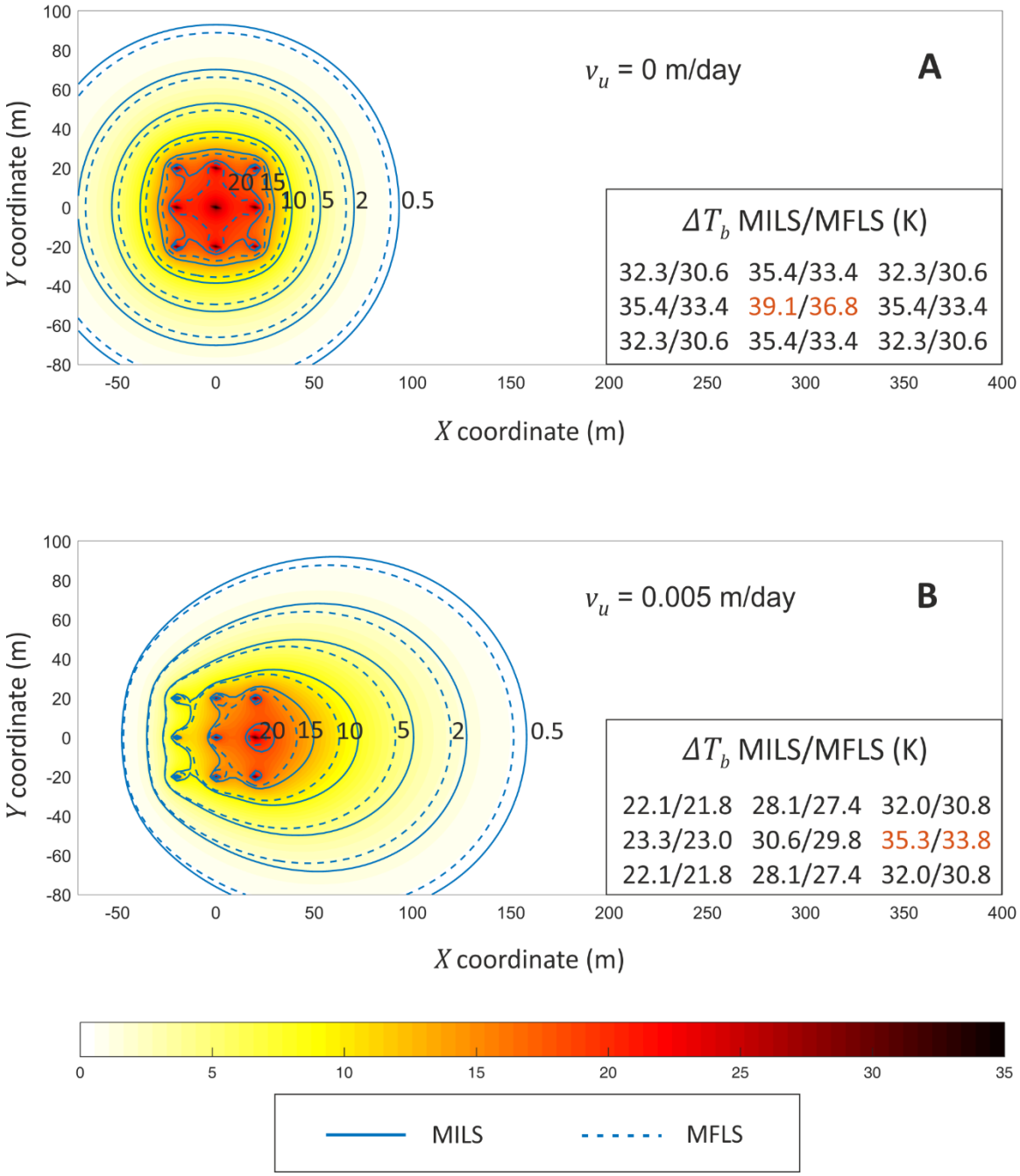

Figure 3.9 A plan view of a multi-VBHE field. Each of nine VBHE is shown as a dot. Modelled using both MILS and MFLS analytical solutions for two groundwater flows v_u: (A) 0 m day^{-1} and (B) 0.005 m day^{-1}. The thermal dispersivity is zero, z coordinate is 50 m, which is the VBHE mid-length. Enclosed table shows the temperature change at the VBHE wall ΔT_b after 30 years of operation for each respective VBHE for each model. The respective temperature changes (K) are shown on the lines of isotherms for MILS and MFLS. The distribution of temperature changes in the field is also shown with colour scheme (K).

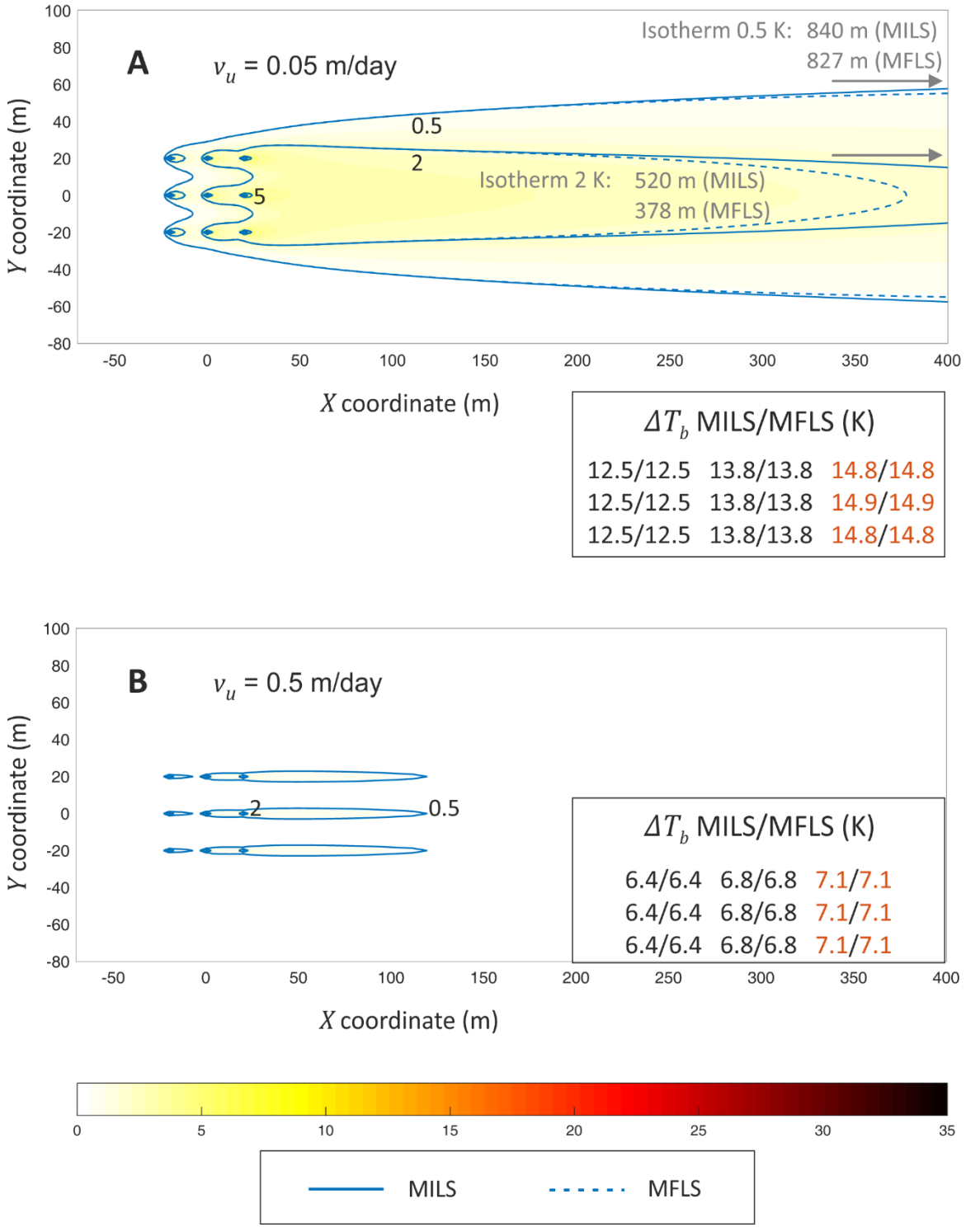

Figure 3.10 A plan view of a multi-VBHE field. Each of nine VBHE is shown as a dot. Modelled using both MILS and MFLS analytical solutions for two groundwater flows v_u: (A) 0.05 m day^{-1} (with values of isotherm extent which go beyond x-range of the figure) and (B) 0.5 m day^{-1}. The thermal dispersivity is zero, z coordinate is 50 m, which is the VBHE mid-length. Enclosed table shows the temperature change at the VBHE wall ΔT_b after 30 years of operation for each respective VBHE for each model. The respective temperature changes (K) are shown on the lines of isotherms for MILS and MFLS. The distribution of temperature changes in the field is also shown with colour scheme (K).

The practical implications of the results shown in Figure 3.9 and Figure 3.10 is that groundwater flow as well as vertical thermal transport can significantly change the estimated thermal performance of a VBHE installation. For slow and absent groundwater flows ignoring the vertical thermal transport in the model of VBHE will lead to significant overestimation of ΔT_b. For medium and fast groundwater flows the vertical thermal transport can be ignored. However, for medium groundwater flows the difference in the isotherm extent between MILS and MFLS is significant. It is supported by Figure 3.8, which illustrates how with increasing thermal load of a single VBHE the role of vertical thermal transport increases, thus it cannot be ignored and MFLS model becomes more appropriate than MILS. Therefore, for multi-VBHE installations and when the downstream thermal impacts have to be taken into account, the disregard of the vertical thermal transport has to be justified.

3.2.5 Time to stabilise temperature change

Figure 3.11 shows how the groundwater flow v_u influences the time to reach steady state t_S for the extent of the +2 K and +0.5 K isotherms (X_{2K} and $X_{0.5K}$) modelled using MILS and MFLS. t_S is significantly reduced with increasing groundwater flow. Note that when t_S equals to 300 years is means that the steady state was not reached within the period of calculation. This happens when it is modelled using MILS at very slow or absent groundwater flows. t_S for X_{2K} is more sensitive to slow groundwater flows (v_u = 0.002 m day^{-1}) compared with t_S for $X_{0.5K}$.

The development of X_{2K} and $X_{0.5K}$ with time is illustrated in the Appendix C.3. With time, the volume of thermal plume grows and stabilises when heat inflow through the VBHE equals heat outflow into the surrounding ground and surface. When the temperature at the VBHE wall and isotherms of high-temperature change are already stabilised, the thermal gradient between the VBHE and the surrounding ground is still steep. With time the thermal perturbance of the ground travels further, and the thermal gradient caused by the continuous heat injection

from the VBHE becomes shallower. Then the isotherms of lower temperature change become also stabilised. Finally, the whole thermal plume reaches the steady state. Therefore, it takes longer to stabilise the extent of the isotherm of smaller temperature change ($X_{0.5K}$) compared with the isotherm of higher temperature change (X_{2K}).

There is a noticeable difference in t_S between MILS and MFLS for both isotherms at slow to medium groundwater velocities when the vertical conduction plays a significant role in the stabilisation of the isotherms (Figure 3.11).

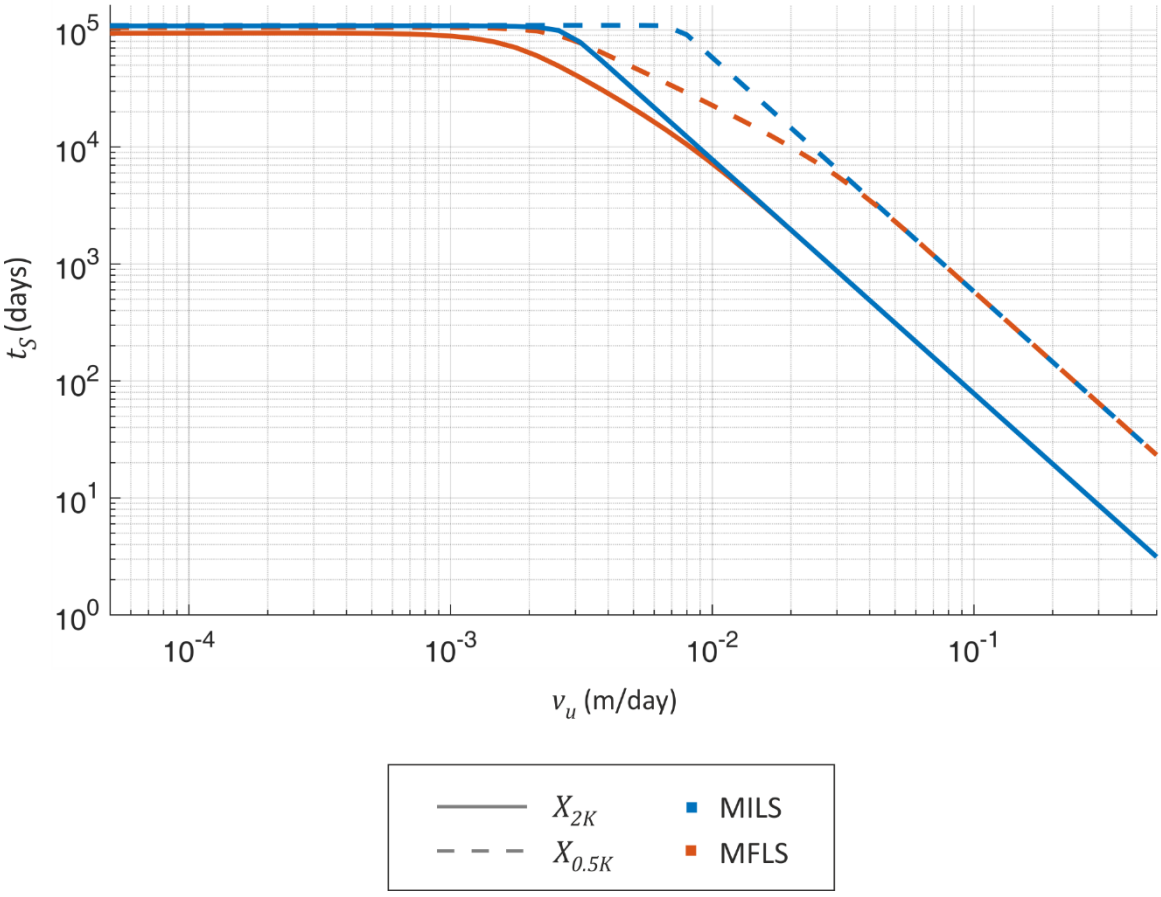

Figure 3.11 The time to reach the steady state t_S for the longitudinal extent in x-coordinate of the +2 K and +0.5 K isotherms (X_{2K} and $X_{0.5K}$) for different groundwater velocities v_u. Modelled using the MILS and MFLS analytical solutions.

Figure 3.12 summarises the influences that groundwater flow can have on the temperature change at the VBHE wall ΔT_b and on the extent of the +2 K isotherm X_{2K}. Slow groundwater flow increases the extent of the +2 K isotherm X_{2K} by advection of heat from the VBHE (therefore ΔT_b is reduced). When groundwater

flow is faster than about 0.01 m day^{-1} (for the given VBHE heat flow rate J), it is able to reduce X_{2K} compared with no groundwater flow scenario. As is shown in Figure 3.12, different groundwater flows can produce the same extent of the isotherm at the steady state. For example, X_{2K} = 40 m is for both groundwater flow v_u = 0.008 m day^{-1} and v_u = 0.0005 m day^{-1}. However, for the case when groundwater flow is faster, the time to stabilise t_{S2K} is significantly shorter compared with the case at slower groundwater flow. This is because the thermal transport at slower v_u is slower compared with the case at faster v_u.

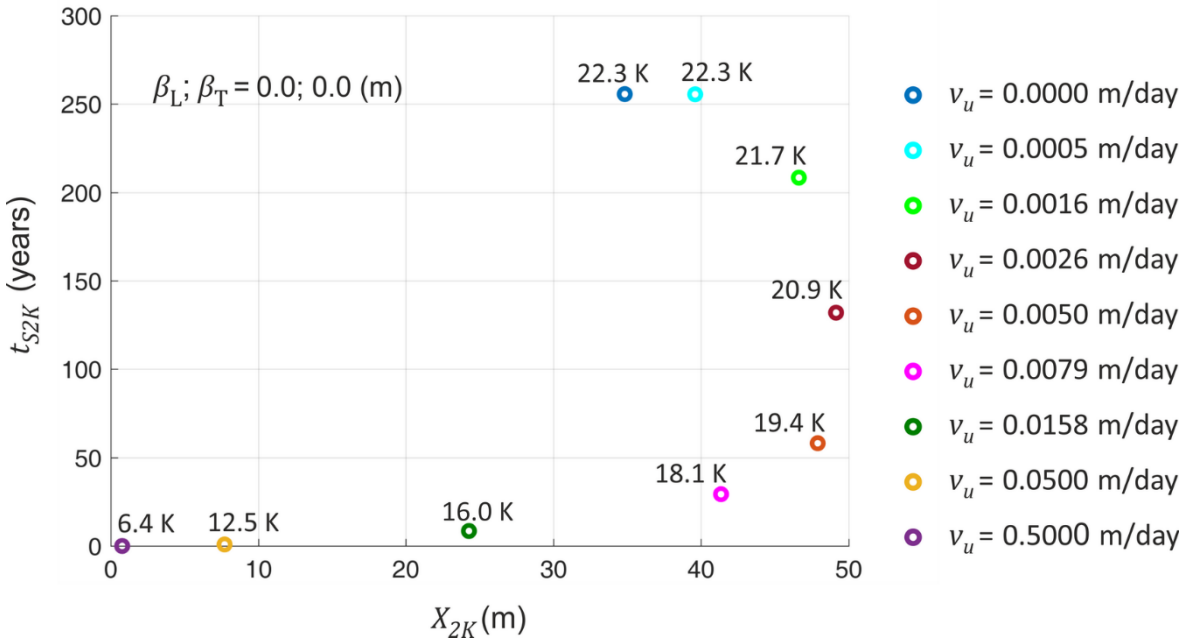

Figure 3.12 The time to stabilise the extent of the +2 K isotherm t_{S2K} versus its longitudinal extent X_{2K} at the steady state for a range of groundwater velocities v_u. The temperature change at borehole wall ΔT_b at the steady state is given near each point. Modelled using MFLS. Model parameters are listed in Table 3.1.

3.3 Key messages

- The groundwater influence on a VBHE in homogeneous aquifer was quantified. The groundwater flow can significantly accelerate the thermal transport. For example, even for very slow groundwater flow v_u = 0.001 m day^{-1}, advection is able to noticeably reduce ΔT_b (by about 1 K) and the time to stabilise it t_{Sb} (Figure 3.4). The discussed analytical solutions were used for validation of the numerical models as discussed in

Chapter 5. The numerical models were used to analyse the effects of fractures near a VBHE.

- The analysis justified the use of the 2D numerical model for a long VBHE to test the effects of fractures; the results are presented in Chapter 6 and Chapter 7. The differences between the MILS and MFLS models in the extent of isotherm increase with increasing role of vertical conduction. The differences between the MFLS and MILS models in ΔT_b and extent of isotherms at the mid-depth of the VBHE are not significant because the role of axial conduction is relatively small for a long VBHE (100 m). Therefore, MILS is an appropriate analytical solution for a long VBHE (100 m). However, the difference is significant for a case without groundwater flow for times longer than 30 years. For all tested groundwater flows, the MILS and MFLS models had similar results in temperature change at mid-depth of the VBHE ΔT_b within 30 years of modelled VBHE operation.
- Depending on the isotherm of interest, its extent can be either reduced or increased by the groundwater flow. This concept is referred to during the analysis of the fracture effects on a VBHE (Chapter 6, Chapter 7, Chapter 8).
- The stabilisation times for isotherms of low-temperature change for slow groundwater velocities can be longer than the planned lifespan of the VBHE installation.

Key messages from the supplementary analysis in the appendices:

- The additional analysis of how advection can influence the optimal design of VBHE is in Appendix C. Specifically, Appendix C.1 explains how the limits in ΔT_b and the generated isotherm of interest can influence the length of VBHE. It also illustrates when the planned length of VBHE should be longer (more expensive) when the extent of the generated isotherm of interest has to be considered.
- Appendix C.2 investigates how time to stabilisation is influenced by the VBHE heat flow rate for both ΔT_b and $X_{0.5K}$. The key message is that fast v_u

stabilises the temperature change quickly both at the VBHE wall and for the isotherms. However, there can be a big difference in the time to stabilisation between ΔT_b and $X_{0.5K}$ for slower v_u (e.g. 0.05 m day^{-1}), and even more so with higher heat flow rates (on the illustrated example their difference can be more than 10 years).

- Appendix C.3 shows how $X_{0.5K}$ and X_{2K} develop with time at a range of groundwater flows. To supplement Figure 3.11 and Figure 3.12 and illustrate how the isotherms of small temperature change (+0.5 K) take long time to develop at slow groundwater flow, while the isotherms of higher temperature change (+2 K) develop quickly.

Chapter 4 The influence of thermal dispersion on the thermal performance of a vertical borehole heat exchanger

4.1 Introduction

Thermal dispersion can significantly alter thermal plumes from a VBHE (Vertical Borehole Heat Exchanger), especially in heterogeneous aquifers where the thermal dispersivity is scale-dependent (Molina-Giraldo *et al.* 2011a). Scale-dependent dispersivity means that the dispersivity increases with the field scale and therefore the dispersion lengths increase too. However, it is often ignored in published analytical models for advective heat transport for VBHE (Chiasson & O'Connell 2011). When thermal dispersion is accounted for in VBHE models, it significantly improves the accuracy of the results (Alcaraz *et al.* 2016).

Molina-Giraldo et al. (Molina-Giraldo *et al.* 2011a) explored the effects of thermal dispersion on the temperature plumes from VBHE with the analytical solution in 2D (MILS). They used two scenarios:

1) Dispersion depends only on the magnitude of groundwater flow (for homogeneous aquifers)
2) Dispersion is scale-dependent (for heterogeneous aquifers).

Their conclusions were that:

- The effect of thermal dispersion on the thermal plume is negligible for homogeneous aquifers, i.e. when thermal dispersion is assumed to be depending only on the magnitude of groundwater flow;
- Thermal transport by dispersion is significant for heterogeneous aquifers when dispersion is scale-dependent. Thermal dispersion cannot be ignored in the estimation of thermal plumes when groundwater flows are faster than 10^{-8} m s^{-1} (> 0.001 m day^{-1});

- Thermal dispersion reduces the extent of thermal plumes (investigated temperature change was -1 K and -0.5 K) at the steady state. For transient conditions, certain isotherm lengths are larger with increasing dispersion.

The authors did not explore how the dispersivity influences the time needed for the system to achieve a steady-state temperature distribution. Also, they used 2D model (MILS) and did not explore when an axial dispersivity is significant in thermal transport. The moving finite line source (MFLS, the analytical solution in 3D) (Molina-Giraldo *et al.* 2011b) is based on the moving point source solution by Carslaw & Jaeger (1959). MFLS does not account for thermal dispersion. It would be useful to examine the role of thermal dispersivity in 3D. VBHEs are frequently installed in fractured bedrock where the thermal dispersivity can be anisotropic.

Hence, this chapter explores the role of the dispersivity on thermal transport from a VBHE with a 3D analytical solution. It first describes the extended solution for MFLS with 3D dispersion, which accounts for the longitudinal, transverse and vertical (axial) aquifer dispersivity. Then this chapter quantifies the possible effects of the aquifer dispersivity on the thermal performance of a VBHE for different groundwater velocities.

This chapter extends the work by Molina-Giraldo et al. (Molina-Giraldo *et al.* 2011a) addressing the following questions:

- When is the influence of vertical dispersivity significant?
- How does its influence relate to transverse and longitudinal dispersion?
- How can thermal dispersion influence the temperature change at the VBHE wall along the length of a VBHE?
- How does thermal dispersion influence the time needed to stabilise the temperature change at the VBHE wall and the isotherms?

4.2 Model assumptions

The following assumptions were used for the aquifer:

- The aquifer is homogeneous and semi-infinite with respect to z-coordinate;
- The initial temperature is homogeneous in the whole aquifer;
- The ground surface temperature is fixed and equal to the initial aquifer temperature;
- Dispersivity can be anisotropic in the principal directions aligned with the co-ordinate axes;
- Thermal conductivity is kept uniform, i.e. there is no contrast between vertical and lateral conduction;
- Groundwater flow is steady, constant and is only in the x-axis direction, parallel to the ground surface;
- Groundwater temperature is in steady state with the temperature of the aquifer's solid;
- There is no geothermal gradient;
- Groundwater flow follows Darcy's law; there is no turbulence;
- Thermal dispersivity is not scale-dependent, because the aquifer is homogeneous. Thermal dispersion is dependent on the Darcy groundwater velocity;

The following assumptions were used for the VBHE:

- Steady equally distributed heat flux along the finite line source
- Continuous heat flow
- Vertical borehole heat exchanger positioned at x = 0 m, y = 0 m, z = 0 m
- Grout is of the same material as the aquifer, i.e. same thermal properties, groundwater can flow through it
- No other heat sources installed in the aquifer other than the VBHE

4.3 Solution

A new analytical solution for MFLS with 3D dispersion was obtained in collaboration Ian Hawke (the Department of Mathematics of the University of Southampton) and Petr Reischig (IT consultant) who entered the equation of the moving point source solution by Carslaw & Jaeger (1959) from Stauffer *et al.* (2014) into the software Wolfram Mathematica 11 to step by step derive the MFLS (as described below) preserving 3D (anisotropic) dispersivity coefficients.

Eq. (4.1) is the moving point source solution by Carslaw & Jaeger (1959) for 3D conduction and advection in an infinite aquifer. The groundwater flow is uniform in the x-direction. The heat source with power J is located at coordinates x, y, z = 0, 0, 0 m.

Anisotropic thermal diffusion/dispersion coefficients $D_{t,L}$, $D_{t,T}$ were modified to allow for independent transverse vertical component $D_{t,V}$. To account for the starting coordinates of the VBHE location being (x, y, z = 0, 0, 0 m), the initial coordinates were excluded from the equation:

$$T(x,y,z,t) = T_0 + \frac{J}{8C_{em}(\pi^3 D_{t,L} D_{t,T} D_{t,V})^{1/2}} \cdot \int_0^t \exp\left[-\left(\frac{(x - v(t-t'))^2}{D_{t,L}} + \frac{y^2}{D_{t,T}} + \frac{z^2}{D_{t,V}}\right)\frac{1}{4(t-t')}\right] \cdot \frac{1}{(t-t')^{3/2}}\, dt' \qquad (4.1)$$

where T is temperature (K), t is time (s), T_0 is initial or undisturbed temperature (K), C_{em} is effective (for both fluid and solid) volumetric heat capacity at constant pressure for meter depth of matrix (aquifer) material for 2D model and per volume for 3D model (J m^{-3} K^{-1}), J is source heat flow rate (W), and v is Darcy velocity (m s^{-1}).

D_t is the thermal diffusion or thermal diffusivity tensor ($m^2\ s^{-1}$), which in a hydraulically isotropic medium has the principal longitudinal $D_{t,L}$, transverse $D_{t,T}$ and vertical $D_{t,V}$ components (thermal diffusion coefficients):

$$D_{t,L} = D_t^* + D_{t,d,L} = \lambda_{em}/C_{em} + \beta_L\,|v|\,C_w/C_{em}$$

$$D_{t,T} = D_t^* + D_{t,d,T} = \lambda_{em}/C_{em} + \beta_T\,|v|\,C_w/C_{em}$$

$$D_{t,V} = D_t^* + D_{t,d,V} = \lambda_{em}/C_{em} + \beta_V\,|v|\,C_w/C_{em}$$

where D_t^* is the diffusion coefficient in the matrix without flow ($m^2\ s^{-1}$), $D_{t,d,L}$, $D_{t,d,T}$ and $D_{t,d,V}$ are the longitudinal, transverse and vertical thermal dispersion coefficients ($m^2\ s^{-1}$), λ_{em} is the effective thermal conductivity that accounts for both matrix solid and fluid properties ($W\ m^{-1}\ K^{-1}$), calculated as the volumetrically weighted average of the combined medium; C_w is volumetric heat capacity at a constant pressure of water in porous media ($J\ kg^{-1}\ K^{-1}$). All water is considered mobile in the fully saturated matrix. β_L, β_T, β_V are the longitudinal, transverse and vertical thermal dispersivity of the aquifer (m).

$D_{t,T}$ and $D_{t,V}$ are used when transverse horizontal (along y-direction) coefficient is different from the transverse vertical (along the z-direction, axial) coefficient, i.e. when β_T and β_V have different values.

The time integral was calculated using Wolfram Mathematica with assumptions that $t \geq 0$, $D_{t,L} > 0$, $D_{t,T} > 0$, $D_{t,V} > 0$, resulting in:

$$
\begin{aligned}
&T(x,y,z,t)\\
&= T_0 + \frac{J}{8\pi C_{em}\sqrt{D_{t,L}D_{t,T}D_{t,V}}\sqrt{\frac{x^2}{D_{t,L}}+\frac{y^2}{D_{t,T}}+\frac{z^2}{D_{t,V}}}}\cdot \exp\left(\frac{\boldsymbol{v}x}{2D_{t,L}}\right)\\
&\cdot\left[\exp\left(-\frac{\boldsymbol{v}\sqrt{\frac{x^2}{D_{t,L}}+\frac{y^2}{D_{t,T}}+\frac{z^2}{D_{t,V}}}}{2\sqrt{D_{t,L}}}\right)\operatorname{erfc}\left(\frac{\sqrt{D_{t,L}}\sqrt{\frac{x^2}{D_{t,L}}+\frac{y^2}{D_{t,T}}+\frac{z^2}{D_{t,V}}}-\boldsymbol{v}t}{2\sqrt{D_{t,L}t}}\right)\right.\\
&\left.+\exp\left(\frac{v\sqrt{\frac{x^2}{D_{t,L}}+\frac{y^2}{D_{t,T}}+\frac{z^2}{D_{t,V}}}}{2\sqrt{D_{t,L}}}\right)\operatorname{erfc}\left(\frac{\sqrt{\mathrm{D_{tx}}}\sqrt{\frac{x^2}{D_{t,L}}+\frac{y^2}{D_{t,T}}+\frac{z^2}{D_{t,V}}}+vt}{2\sqrt{D_{t,L}t}}\right)\right]
\end{aligned}
\tag{4.2}
$$

Using the substitution

$$
r_D = \sqrt{D_{t,L}}\sqrt{\frac{x^2}{D_{t,L}}+\frac{y^2}{D_{t,T}}+\frac{z^2}{D_{t,V}}} = \sqrt{x^2+\frac{D_{t,L}}{D_{t,T}}y^2+\frac{D_{t,L}}{D_{t,V}}z^2}
$$

the equation can be simplified to:

$$
\begin{aligned}
T(x,y,z,t) = T_0 &+ \frac{J}{8\pi C_{em}\sqrt{D_{t,T}D_{t,V}}r_D}\\
&\cdot \exp\left(\frac{vx}{2D_{t,L}}\right)\left[\exp\left(-\frac{vr_D}{2D_{t,L}}\right)\operatorname{erfc}\left(\frac{r_D-vt}{2\sqrt{D_{t,L}t}}\right)\right.\\
&\left.+\exp\left(\frac{vr_D}{2D_{t,L}}\right)\operatorname{erfc}\left(\frac{r_D+vt}{2\sqrt{D_{t,L}t}}\right)\right]
\end{aligned}
\tag{4.3}
$$

To account for axial effects and constant ground surface temperature conditions, the method of images (Carslaw & Jaeger 1959; Eskilson 1987; Stauffer *et al.* 2014) was applied to eq. (4.3), resulting in the MFLS model with anisotropic thermal diffusion/dispersion:

$$T(x,y,z,t) = T_0 + \frac{J/H_b}{8\pi C_{em}\sqrt{D_{t,T}D_{t,V}}} \cdot \exp\left(\frac{vx}{2D_{t,L}}\right) \cdot \left[\int_0^{H_b} \psi dz' - \int_{-H_b}^{0} \psi dz'\right]$$

$$\psi = \left[\exp\left(-\frac{vr'}{2D_{t,L}}\right)\mathrm{erfc}\left(\frac{r'-vt}{2\sqrt{D_{t,L}t}}\right) + \exp\left(\frac{vr'}{2D_{t,L}}\right)\mathrm{erfc}\left(\frac{r'+vt}{2\sqrt{D_{t,L}t}}\right)\right]/r' \quad (4.4)$$

$$r' = \sqrt{x^2 + \frac{D_{t,L}}{D_{t,T}}y^2 + \frac{D_{t,L}}{D_{t,V}}(z-z')^2}$$

where H_b is the length of vertical borehole heat exchanger (m).

This solution in case of isotropic diffusion without dispersion (when $D_{t,L}$, $D_{t,T}$ and $D_{t,V}$ are all equal to D_t) corresponds to MFLS formula by (Molina-Giraldo et al. 2011b) as written in (Stauffer *et al.* 2014), see eq. (2.23).A similar solution was derived by (Erol 2016) for MFLS with anisotropic diffusion, but it did not account for dispersion or different transverse diffusions $D_{t,T}$ and $D_{t,V}$.

4.4 Presentation of results

The adjusted MFLS model, which accounts for the thermal dispersion in 3D, was used to quantify the role of vertical dispersivity on the thermal performance of a VBHE. In this chapter the abbreviation MFLS is used for the adjusted MFLS model, because it is identical to the original equation by (Molina-Giraldo et al. 2011b) as written in (Stauffer *et al.* 2014) except for the possibility to enter different values for $D_{t,T}$ and $D_{t,V}$.The results are discussed with respect to the following:

1) Comparison of MILS with MFLS to estimate the role of aquifer dispersivity;
2) Relative importance of longitudinal and transverse dispersivities on temperature change at the VBHE wall;
3) Influence of dispersivity on the extent of isotherms with time;

4) Influence of dispersivity on time to stabilise temperature change at the VBHE wall and the extent of the isotherms for different groundwater velocities in the matrix;
5) Potential influence of axial dispersivity on the extent of isotherms for different lengths of a VBHE.

4.5 Fixed input parameters

Two models were used and compared to investigate the influence of dispersion: MILS and MFLS. The temperature change at the borehole wall ΔT_b is calculated after 30 years of continuous VBHE operation. The location of ΔT_b is at point x = 0.05 m from the heat source (downstream of groundwater flow direction) with y = 0 m and z = 50 m (z is only relevant for 3D model, MFLS). The influence of dispersivity on the length of the +0.5 K isotherm of $X_{0.5K}$ is determined as the maximum x-axis coordinate of the isotherm in the downstream direction of groundwater flow. It is determined on the horizontal plane at the mid-length of the VBHE (at depth z = 50 m).

The time to stabilise temperature change at the VBHE wall t_{Sb} and the time to stabilise the longitudinal length of the +0.5 K isotherm $t_{S0.5K}$ are also discussed as thermal performance parameters. Steady state is defined as the moment when the temperature change at a specific location (for example at the VBHE wall) reaches 99 % of the temperature change value calculated at time equal to 300 years (when it is already at its “maximum”). This approach is used because the temperatures asymptotically approach steady-state. The transient state solution was chosen (rather than steady state) to keep the same methods as for numerical models, where the steady state can only be determined by modelling for a long time. A 300-year operational time of a VBHE is not of practical interest but is sufficient to reach the steady state for MFLS.

Steady state for the maximum extent of the +0.5 K isotherm $t_{S0.5K}$ is calculated as follows: first the +0.5 K isotherm extent is found after 300 years, then the time is

found when at the point of maximum extent (downstream) the temperature change of +0.5 K (reduced by 1 %) is reached.

If not stated otherwise in the result figures, fixed model parameters are listed in Table 3.1. The dispersivity in each direction was varied during the analysis while keeping the dispersivities in other directions fixed (Table 4.1). The tested range for the longitudinal dispersivity was up to 4 m. The selected range of the longitudinal dispersivity corresponds to values reported in the literature for field scales up to 100 m (Molina-Giraldo *et al.* 2011a). However, for this field scale the longitudinal dispersivity can be higher (Gelhar *et al.* 1992). The transverse dispersivity was assumed to be 0.1 times the longitudinal dispersivity as is commonly assumed for thermal transport. However, it may vary depending on the heterogeneity of aquifer and Peclet number (Molina-Giraldo *et al.*). 2 m is selected as the upper for limit for the transverse dispersivity in the sensitivity analysis. It was reported as viable during investigation for transverse dispersivities (Gelhar *et al.* 1992). The vertical thermal dispersivity is typically one order of magnitude smaller than the transverse dispersivity; however the value can be higher for fractured heterogeneous aquifers (Gelhar *et al.* 1992). A value of 1 m was reported as viable for the vertical (axial) dispersivity (Gelhar *et al.* 1992; Klenk & Grathwohl 2002).

Table 4.1 Values of dispersivities used in the analysis.

Dispersivity, symbol	Range when varied	Value when fixed
Longitudinal, β_L	From 0 to 4 m	2 m
Transverse, β_T	From 0 to 2 m	0.2 m
Vertical, β_V	From 0 to 1 m	0.02 m

4.6 Results

4.6.1 Temperature change at the VBHE wall

Figure 4.1 shows how ΔT_b develops with time as modelled using MILS and MFLS with consideration of the aquifer dispersivity and without it, in aquifers with different groundwater flows. Accounting for the vertical dispersivity by MFLS model has no additional effect on the development of ΔT_b with time. Therefore,

the effects of dispersivity are the same for MILS and MFLS. Neglecting the aquifer dispersivity in a model can significantly overestimate the steady state ΔT_b, which means that the potential thermal performance of the VBHE system in terms of ΔT_b can be underestimated.

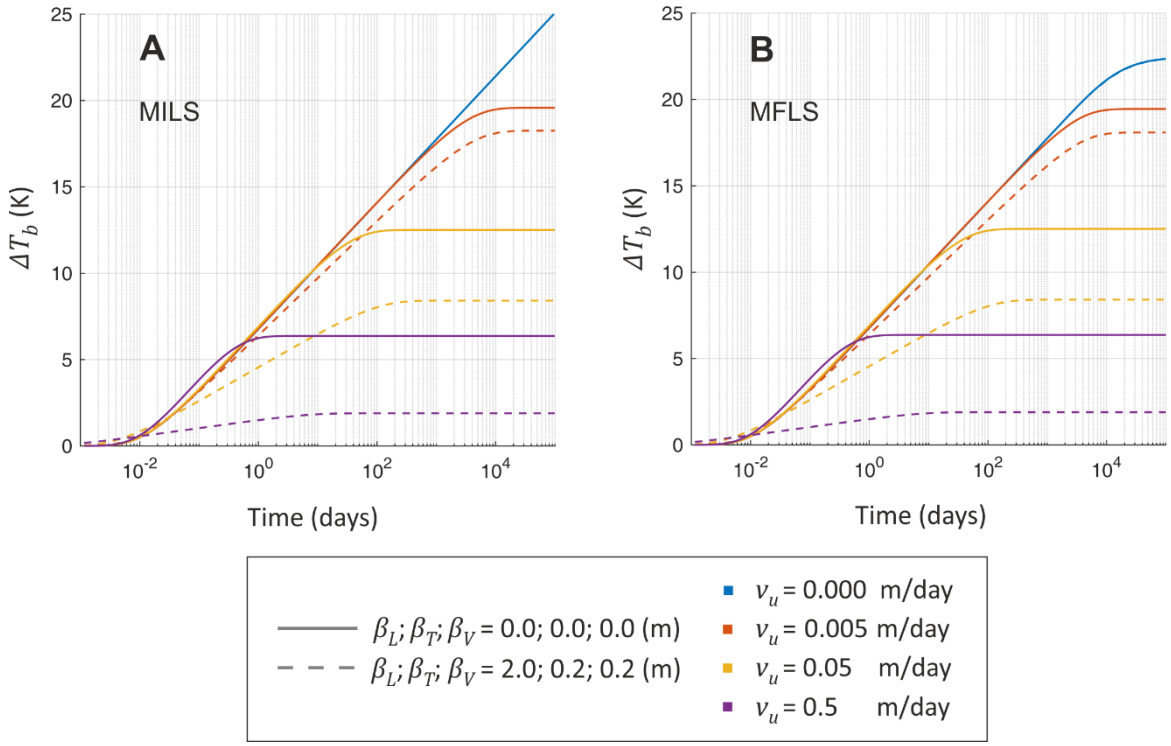

Figure 4.1 Development of temperature change at the VBHE wall (ΔT_b) with time for a range of Darcy groundwater flows (v_u) with and without consideration of longitudinal β_L, transverse β_T and vertical β_V dispersivities (β_V is relevant only for 3D model MFLS). A: MILS (2D) and B: MFLS (3D). 10^3 days equals to 2.7 years, 10^4 days equals to 27.4 years, maximum plotted time is 300 years.

Figure 4.2 shows how the aquifer dispersivity can influence the steady state temperature change at the VBHE wall ΔT_b for a range of groundwater velocities in the aquifer. With increasing longitudinal (Figure 4.2 A) and transverse dispersivity (Figure 4.2 B), the reduction in the estimated ΔT_b is uniform when the dispersivity is increased at slow groundwater velocities in the matrix. For faster groundwater velocity (0.5 m day^{-1}), a small dispersivity value has significant influence on ΔT_b. Therefore, in the presence of groundwater flow, models that neglect dispersivity overestimate the steady state ΔT_b. For example, in case of the longitudinal dispersivity β_L = 2 m (Figure 4.2 A), depending on groundwater velocity the overestimation of ΔT_b when β_L is ignored may vary from about +5 % (for

v_u = 0.005 m day^{-1}) to about +50 % (for v_u = 0.5 m day^{-1}). It is difficult to estimate the dispersivity of an aquifer; however, if a range of relevant values is accounted for in the modelling of the VBHE, it can help to estimate the uncertainty of thermal performance in the long-term.

Change in the axial dispersivity does not affect ΔT_b and therefore is not shown in the figure. ΔT_b is not sensitive to the axial dispersivity for the tested VBHE lengths of 100 and 30 m, both after 30 years of continuous VBHE operation, where ΔT_b is calculated at the VBHE mid-length.

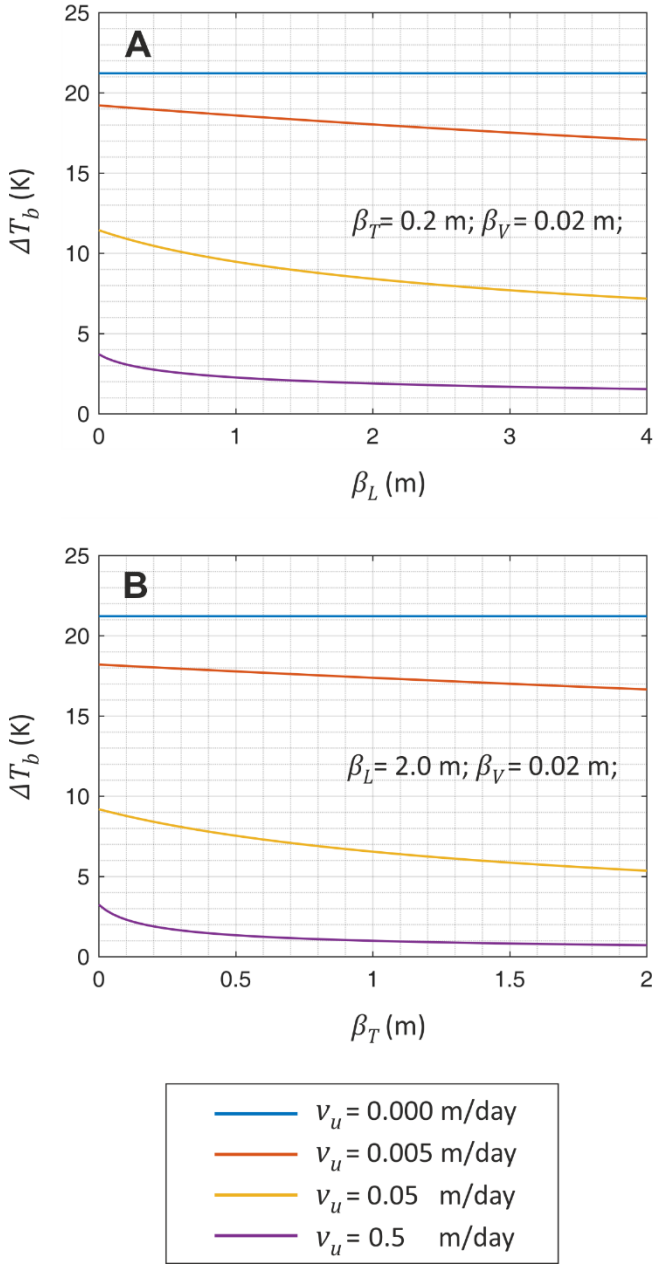

Figure 4.2 Temperature change at the borehole wall ΔT_b after 30 years of continuous operation for changing aquifer dispersivities: longitudinal (A) and transverse (B). Modelled using MFLS – moving finite line source model adapted for 3D dispersion. Longitudinal, transverse and vertical dispersivities are β_L, β_T and β_V. Darcy groundwater flow is v_u.

4.6.2 The effect of thermal dispersivity the development of isotherms with time

Figure 4.3 shows the influence of thermal dispersion on the +0.5 K isotherm in the plan view for different times after the start of VBHE operation. With time dispersion significantly shortens the downstream extent of the isotherm. On the other hand, the upstream extent of the +0.5 K isotherm is increased.

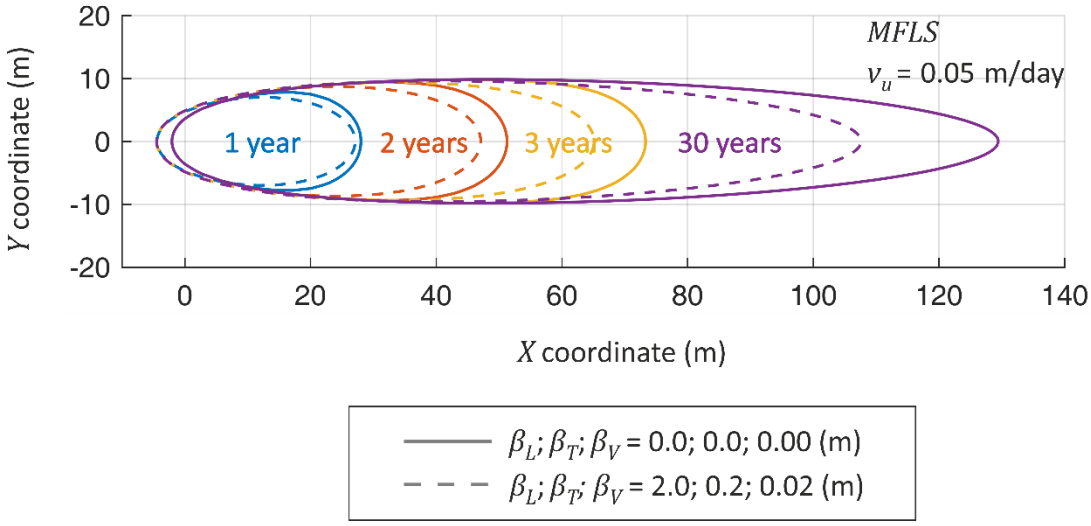

Figure 4.3 Effect of dispersion on the extent of the +0.5 K isotherm at different times after the start of continuous VBHE operation for Darcy groundwater velocity v_u = 0.05 m day^{-1}, modelled using MFLS. Longitudinal, transverse and vertical dispersivities are β_L, β_T and β_V.

Figure 4.4 shows how temperature change differs along the x-axis (the direction of groundwater flow) with and without dispersive thermal transport at two different times since the start of continuous VBHE operation. The groundwater velocity in the aquifer is 0.05 m day^{-1} (medium). When only the thermal transport with advection and conduction is modelled, the presence of dispersive transport increases the apparent thermal conductivity of the aquifer. Therefore, the extent of isotherms of higher temperature change (e.g. +2 K) is reduced by dispersive transport as the isotherms of smaller temperature change (e.g. +0.2 K) are extended, compared with the case without dispersive transport. With time the area of thermal plume spreads and thermal gradient around the VBHE stabilises. With time the role of dispersive transport increases, for example after 200 days of VBHE operation the isotherm of +1 K is only 2 m shorter due to dispersive transport, while after 2 years the difference between cases with and without dispersion for the +1 K isotherm is 8 m (Figure 4.4). With time the extent of isotherms of even smaller temperature change can be reduced by dispersive transport due to significant increase in the area of isotherms of even smaller (negligible) temperature change compared with the no-dispersion scenario.

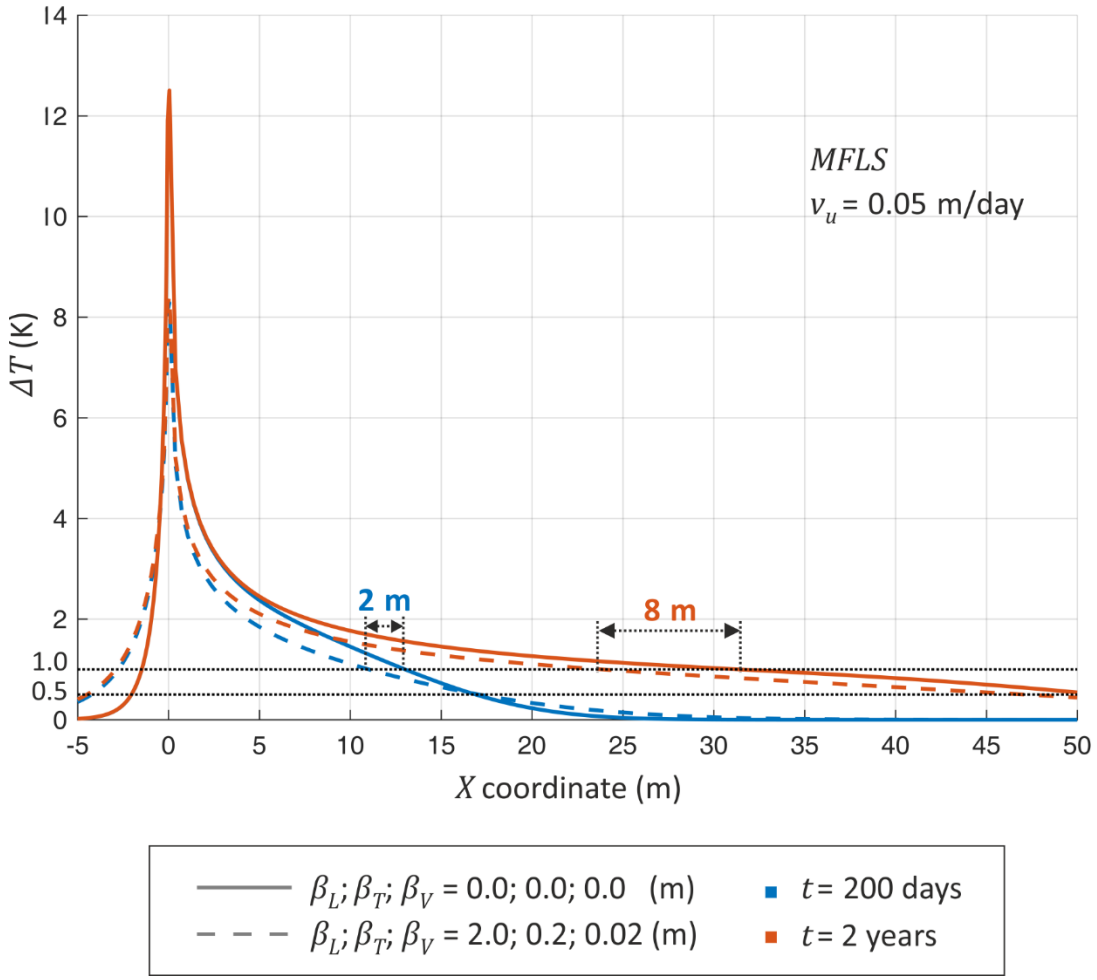

Figure 4.4 Effect of dispersion on the temperature change along the x-axis for two times t (200 days and 2 years). Groundwater flow v_u is 0.05 m day^{-1}. Modelled using MFLS (3D). Horizontal lines mark ΔT of +0.5 K and +1 K. Longitudinal, transverse and vertical dispersivities are β_L, β_T and β_V. Arrows indicate the differences in the longitudinal extent of isotherms for cases with and without dispersivity.

Figure 4.5 shows how the longitudinal extent of the +0.5 K isotherm changes with time with and without dispersivity in the aquifer for different groundwater velocities. When the groundwater flow is slower (0.005 m day^{-1}), the role of dispersivity is negligible within the modelled timescale (30 years). For faster groundwater flows, the extent of the isotherm is significantly reduced by thermal dispersion, with the greatest influence being at steady state.

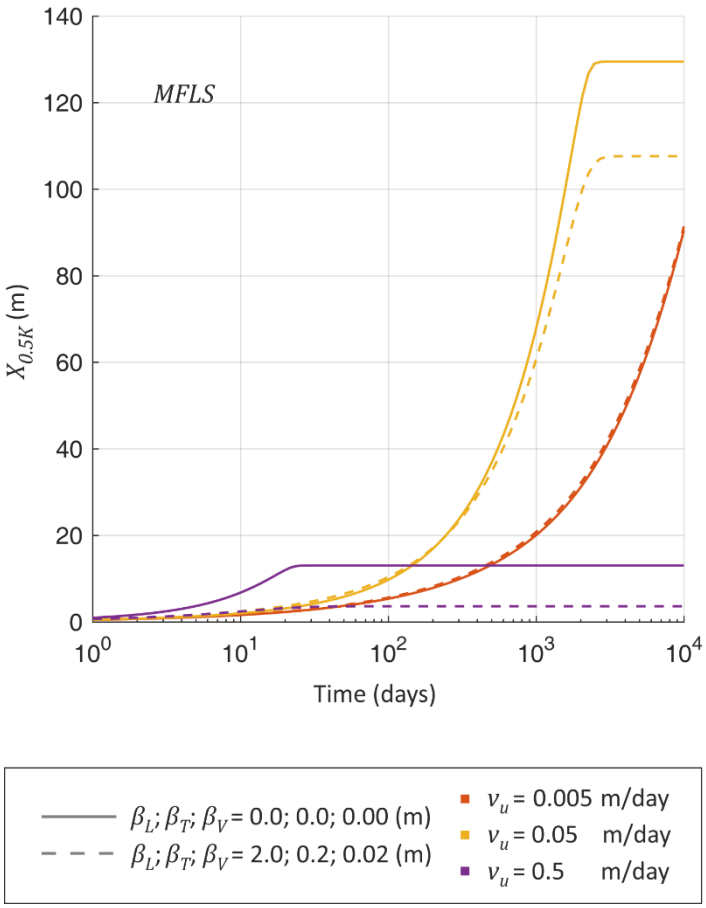

Figure 4.5 The extent of the +0.5 K isotherm for a range of Darcy groundwater velocities v_u using MFLS with and without dispersion. Longitudinal, transverse and vertical dispersivities are β_L, β_T and β_V; 10^3 days equals to 2.7 years, 10^4 days equals to 27.4 years.

4.6.3 The length of isotherm for a range of groundwater velocities and thermal dispersivities

The change in longitudinal and vertical dispersivities does not affect the longitudinal extent of the +0.5 K isotherm $X_{0.5K}$ after 30 years of VBHE operation. Their effect on $X_{0.5K}$ is visible only for velocity 0.016 m day^{-1} and is otherwise insignificant (Appendix D).

The isotherms of higher temperature change than +0.5 K isotherm are reduced by longitudinal dispersivity, while isotherms lower than +0.5 K are extended, as was illustrated in Figure 4.4. The change in longitudinal dispersivity has smaller relative effect on the extent of isotherms compared with the effect of transverse dispersivity. For example, the extent of the +5 K isotherm is reduced by 0.5 m for a groundwater velocity of 0.005 m day^{-1} when the longitudinal dispersivity is

increased from 0 to 2 m. For the same groundwater velocity, the extent of +5 K isotherm is reduced by about 1.5 m when the transverse dispersivity is increased from 0 to 2 m. Therefore, Figure 4.6 only shows the results for the changing transverse dispersivity. The transverse dispersivity can significantly reduce the longitudinal extent of the isotherm for medium groundwater velocities (0.016 m day^{-1} and faster). The relative effect is higher for faster groundwater velocities (0.5 m day^{-1}). However, the actual difference in $X_{0.5K}$ between cases with and without dispersity is largest for a medium groundwater velocity (0.05 m day^{-1}). The modelled isotherm extent is more sensitive to the transverse rather than longitudinal dispersivity because:

- The transport by advection is in x-axis direction while in y-axis direction the thermal transport is by conduction only. This means that when dispersivity is added in x-axis direction its relative role is much smaller compared with the role of dispersivity in the y-axis direction. In the direction of elongated side of the isotherm (the groundwater flow direction) there is smaller thermal gradient compared with that in the transverse direction (see Figure 3.6);
- The isotherm is elongated in x-axis direction (the length of isotherm is longer than its width). Therefore, when dispersivity along the y-axis is included in the model, the thermal transport in the y-axis direction is increased, and it is effective as it occurs along the longer sides on the isotherm.

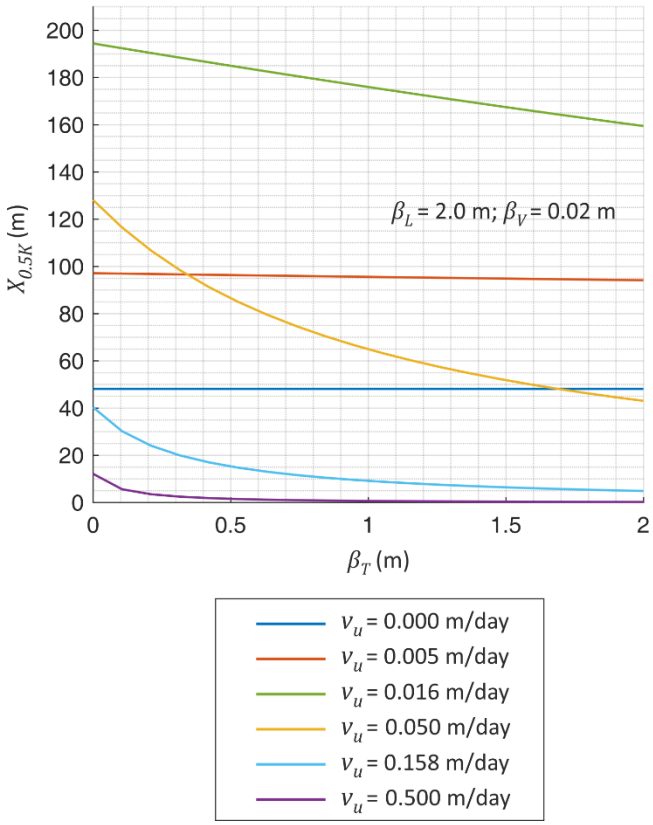

Figure 4.6 Longitudinal extent of the +0.5 K isotherm $X_{0.5K}$ after 30 years of continuous VBHE operation versus changing the transverse dispersivity β_T. Longitudinal and vertical dispersivities are fixed and marked as β_L, and β_V. Modelled using MFLS – the moving finite line source analytical solution, adapted for 3D dispersion. v_u is Darcy groundwater velocity. The pattern of groundwater velocity increase is logarithmic: v_u = 5×10^{-3}, 5×10$^{-2.5}$, 5×10^{-2}, 5×10$^{-1.5}$, 5×10^{-1} m day^{-1}.

4.6.4 Effects of thermal dispersion on the multi-VBHE field

Figure 4.7 shows an example of how various values of thermal dispersivity in the aquifer can influence the +2 K isotherm generated by a field of multi-VBHE modelled using MFLS. The enclosed table shows that ΔT_b is effectively reduced by the thermal dispersivity especially at medium and fast v_u. However, in the illustrated case, the +2 K isotherm is significantly extended only at medium groundwater velocity. Figure 2.4 showed that ΔT_b of a single VBHE without the influence of groundwater flow is 21 K which is significantly lower than ΔT_b for a VBHE in a multi-VBHE field (36.8 K). Thus, especially for a multi-VBHE fields the consideration of groundwater flow and thermal dispersivity can be essential to estimate whether the thermal performance of a VBHE system can be sustainable and whether it is within the design constraints.

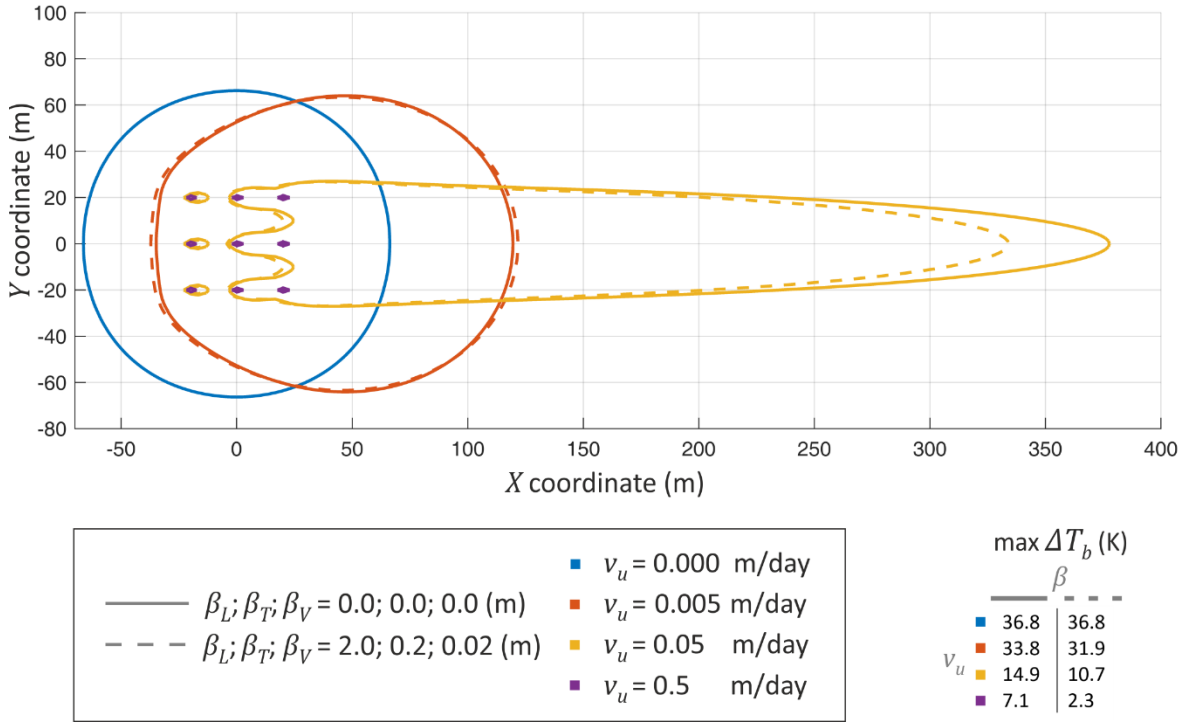

Figure 4.7 Plan view of isotherms for ΔT +2 K produced by a field of multi-VBHE after 30 years of continuous operation (each of nine VBHE continuously injects 5000 W) for a range of groundwater velocities v_u and for two values of thermal dispersivity of the aquifer: longitudinal β_L, transverse β_T and vertical β_V. Modelled using MFLS. Enclosed table shows the maximum achieved value of temperature change at VBHE wall (max ΔT_b) for each combination of v_u and for two values of β (line pattern above each column with results marks the value of β, as noted in the legend). Model parameters are given in Table 3.1.

4.6.5 Time to stabilise temperature change

Figure 4.8 A shows how long it takes to stabilise ΔT_b for different groundwater velocities modelled using MILS and MFLS with and without consideration of aquifer dispersivity. When a model does not account for dispersivity, the time for ΔT_b to reach steady state t_{Sb} for slow groundwater flow in the aquifer is not affected. However, in both models accounting for dispersivity means that the steady state for ΔT_b is reached more slowly when the groundwater velocity is faster (for v_u > 0.01 m day^{-1}), compared with the case without dispersivity. In the relative values, the fastest groundwater velocity causes the largest difference in t_{Sb} between the cases with and without dispersivity in the aquifer. However, the differences in actual values are largest for medium groundwater velocities, for example for v_u = 0.1 m day^{-1} the difference between cases with and without dispersivity is 75 days, while for v_u = 0.5 m day^{-1} the difference is about 10 days.

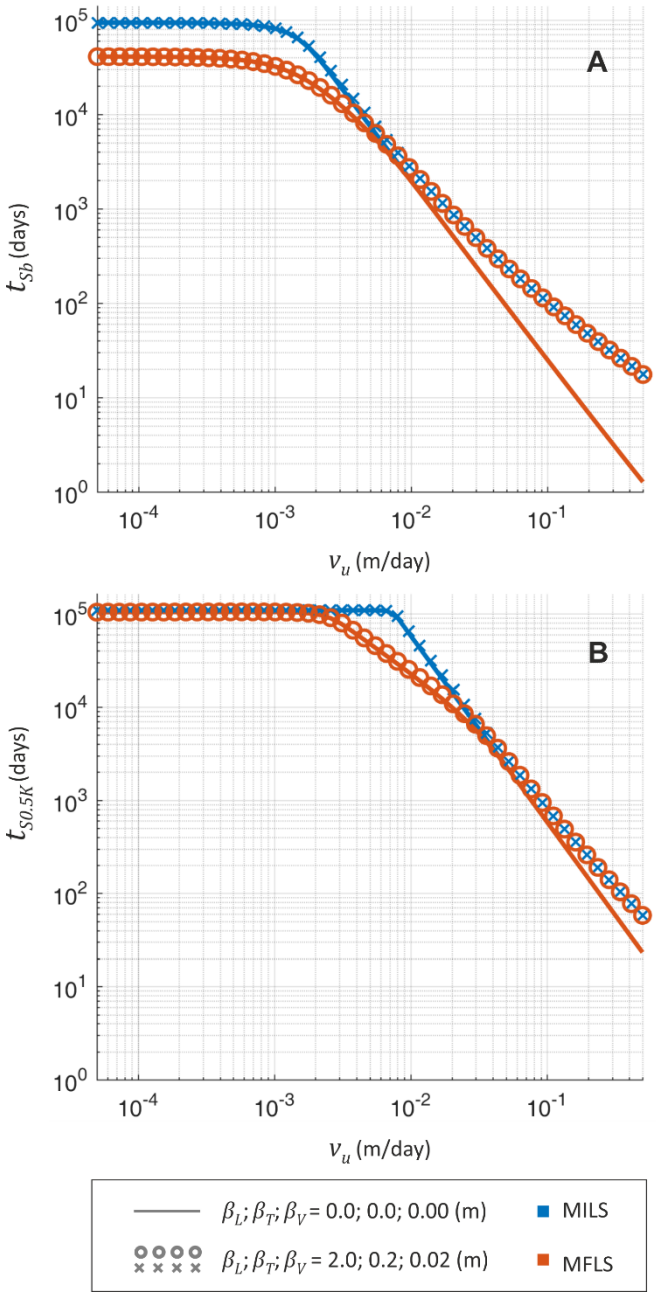

Figure 4.8 Time to reach the steady state for (A) temperature change at the VBHE wall t_{Sb} and (B) in longitudinal extent of the +0.5 K isotherm $t_{S0.5K}$. Both are given for a range of Darcy groundwater velocities v_u, modelled using MILS and MFLS with and without consideration of dispersivity in the aquifer: longitudinal β_L, transverse β_T and vertical β_V, the latter is relevant only for MFLS model. The modelling time for both models (MFLS and MILS) is 300 years; results using MILS do not reach the steady state within 300 years for no/negligible groundwater velocities.

A similar pattern is observed in Figure 4.8 B, which shows the time needed to stabilise the longitudinal extent of the +0.5 K isotherm for different groundwater velocities with and without consideration of dispersivity. It should be noted that for both plots in Figure 4.8 the modelling time was 300 years. The results using

MILS show that ΔT_b and $X_{0.5K}$ are stabilised after 300 years for very slow / negligible groundwater flows, but this is only a limitation of the method (modelling ends after 300 years) and should be ignored. In reality the result using MILS does not reach a steady state in the absence of groundwater flow.

The time to reach steady state at borehole wall (t_{Sb}) does not change with changing vertical and transverse dispersivities for any groundwater velocity, as the temperature is calculated at the mid-point of the VBHE. Therefore, the results are only shown for changing longitudinal dispersivities (Figure 4.9). Increasing longitudinal dispersivity β_L significantly increases t_{Sb} for high and medium groundwater velocities.

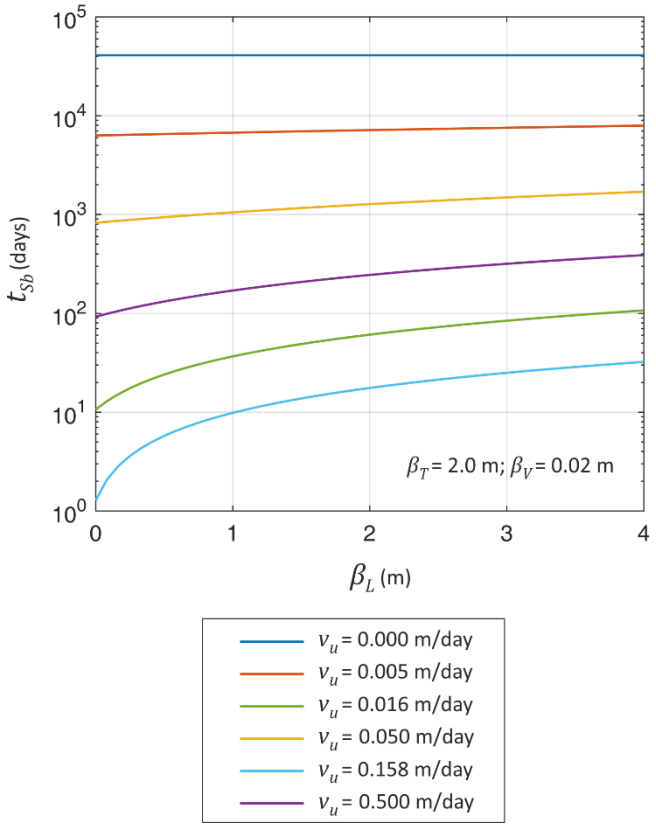

Figure 4.9 Time to steady state for temperature change at borehole wall t_{Sb} versus changing longitudinal dispersivity β_L for a range of groundwater velocities (v_u). Transverse and vertical dispersivities are fixed (β_T and β_V). Modelled using MFLS, the moving finite line source analytical solution adapted for 3D dispersion.

As was discussed the effect of the axial dispersivity on the thermal performance of a VBHE is not significant, given the used model parameters. However, for heterogeneous aquifers, axial dispersivity can become larger than is assumed for

homogeneous aquifers. This is because of the spatial variability of the hydraulic conductivity field (Hidalgo *et al.* 2009) (Ferguson). Therefore, heterogeneous aquifers can have higher dispersivity values because the parameter is scale-dependent.

Figure 4.10 shows the +2 and +0.5 K isotherms in profile view for a VBHE operating continuously for 30 years in an aquifer with and without dispersivity for 2 groundwater velocities in the matrix. In these cases the VBHE lengths are 100 m (Figure 4.10 A) and 50 m (Figure 4.10 B), and the axial dispersivities β_V are 0 m and 1 m. The source heat flow rate J is halved for a VBHE with a length of 50 m (so it remains the same per meter). With a shorter VBHE, the role of axial thermal transport is increased. This is due to the smaller distance between the mid-depth of the VBHE (where the longitudinal extent of the isotherm is determined) and the surface (with constant fixed temperature), and also the groundwater that flows under the VBHE. For example, for a groundwater velocity of 0.05 m day^{-1}, the longitudinal extent of the +0.5 K isotherm for the 50 m long VBHE (Figure 4.10 B) is by accounting for the axial dispersivity reduced by about 20 m (at mid-depth) compared with the case without axial dispersivity. For the 100 m long VBHE the reduction in the extent of the +0.5 K isotherm is about 10 m.

Overestimation of the isotherm of interest by 10 m due to ignoring thermal dispersion can have significant implications for VBHE design, considering that typical legally binding or advised minimum distances between VBHE installations range between 3 to 20 m (Haehnlein *et al.* 2010). This is to ensure sustainable thermal performance and to avoid thermal interactions between VBHEs.

This study assumed that the dispersivity is not scale-dependent. However, in the long term, if the thermal dispersivity is assumed to be scale-dependent, thermal transport by dispersion in heterogeneous aquifers can increase uncertainty in the thermal performance of a VBHE.

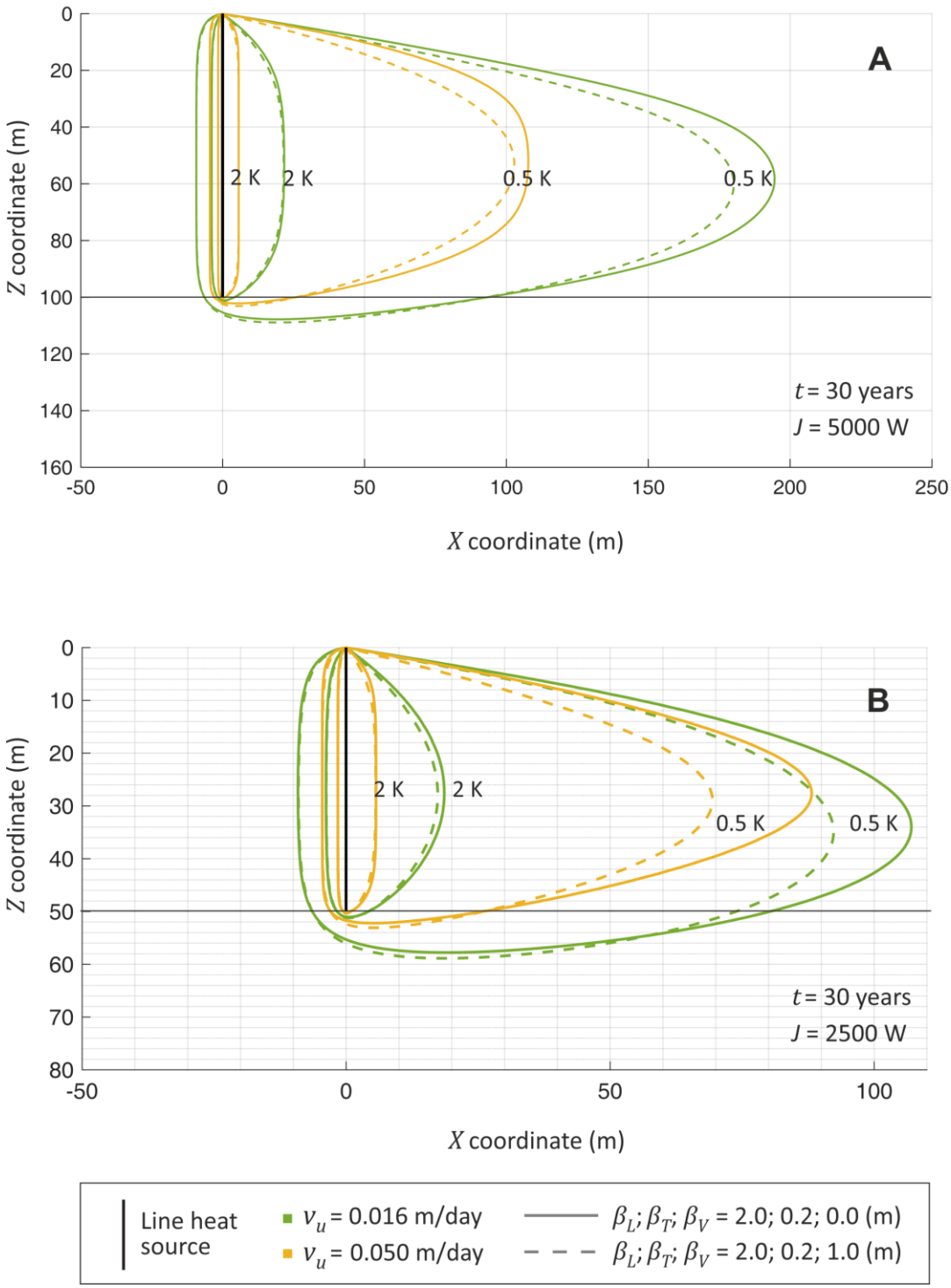

Figure 4.10 Effect of axial dispersion on the extent of the +0.5 K and +2 K isotherms after 30 years of continuous VBHE operation (profile view), modelled using MFLS for two groundwater flows v_u. Longitudinal, transverse and vertical dispersivities β_L, β_T and β_V, are shown in the legend. Length of the VBHE is 100 m (A) and 50 m (B) marked with a horizontal line. Source heat flow rate J = 5000 W (A) and 2500 W (B).

4.7 Key message

This chapter investigated the effects of thermal dispersion on the thermal performance of a VBHE for different groundwater velocities in the matrix. Thermal performance was calculated with respect to the temperature change at the VBHE wall ΔT_b, longitudinal extent (maximum x-coordinate) of the +0.5 K and +2 K isotherms ($X_{0.5K}$, X_{2K}) and times to stabilise them (t_{Sb}, $t_{0.5K}$). The calculation was performed using the analytical solution adjusted to account for thermal dispersion in 3D (MFLS). Thermal dispersion improves the thermal performance of the VBHE. For example, longitudinal thermal dispersion β_L of 2 m for medium groundwater velocity v_u of 0.05 m day^{-1} for the given model parameters reduces the temperature change at the VBHE wall ΔT_b by 3 K (Figure 4.2). The 1 m transverse thermal dispersivity β_T in a matrix with the same groundwater velocity is able to reduce the longitudinal extent of the +0.5 K isotherm $X_{0.5K}$ by 60 m (Figure 4.6). The thermal dispersion can also considerably increase the time of stabilisation for cases with medium groundwater velocities v_u, which are considered to be in a range between 0.01 to 0.1 m day^{-1} (Figure 4.8). The model is not sensitive to the axial dispersivity β_V as was calculated for two VBHE lengths (100 m and 50 m). Although its role can become important for the shorter VBHE in a heterogeneous aquifer as is shown in Figure 4.10.

Ignoring thermal dispersion can result in an underestimation of the modelled thermal performance of the VBHE in the long term (with respect to ΔT_b, $X_{0.5K}$, X_{2K} and times to stabilise them t_{Sb}, $t_{0.5K}$).

Chapter 5 Development and validation of the 2D and 3D numerical models

Consideration of a flowing fracture near a VBHE allows for better estimates of the thermal performance and thermal interactions of a VBHE. It can help to decide on the feasibility of the installation and to improve the optimisation for efficiency, sustainability and thermal interactions between the VBHE installations. Quantification is needed for how fractures can influence VBHE installed in aquifers. This is possible with numerical modelling. Numerical modelling allows the assumption of a homogeneous aquifer to be relaxed and the effects of a fracture on a VBHE can be explored.

This chapter presents the setup and validation of numerical models in 2D and 3D. Both validated numerical models are later used to assess the effect of a single vertical fracture on the thermal behaviour of a single VBHE installed within a permeable rock matrix. Additionally, 3D model allowed to explicitly represent the pipes inside VBHE. This allowed to investigate the relationship between ΔT_b and the mean ΔT of the working fluid inside the U-pipe to make the practical conclusions from the analyses.

5.1 Conceptual models and geometry

5.1.1 Numerical model variants

The developed finite element numerical model in 2D has two variants:

- **TAF-2D** – **T**hermal transport from a VBHE through an **A**quifer in the presence of a single vertical **F**racture.
- **TAH-2D** – **T**hermal transport through an **A**quifer with a **H**omogeneous matrix. This differs from TAF in that the fracture is absent.

The developed 3D numerical model has four variants:

- **TAF-3D** – **T**hermal transport from a VBHE through an **A**quifer in the presence of a single **F**racture.
- **TAFpi** – The same as **TAF-3D** model but the heat source is modelled explicitly as a U-pipe with water circulating inside it.
- **TAH-3D** – **T**hermal transport through an **A**quifer with a **H**omogeneous matrix. It differs from TAF-3D in the aquifer being homogeneous, i.e. the fracture is absent. The moving finite line source (MFLS) analytical solution (Molina-Giraldo *et al.* 2011b) was used for spatial and temporal validation of the TAH-3D model.
- **TAHpi** – is the same as **TAH-3D** model but the heat source is modelled explicitly as a U-pipe with water circulating inside it.

5.1.2 Analytical models

The Moving Infinite Line Source (MILS) analytical solution (Sutton *et al.* 2003; Diao *et al.* 2004) was used to find the optimal mesh for the numerical model and also for spatial and temporal validation of the TAH-2D model, which was used to analyse the comparative performance in more detail. The TAH-3D model was validated against the analytical solution for a moving finite line source (MFLS) (Molina-Giraldo *et al.* 2011b).

5.2 Conceptual models

Conceptualisation of the 2D model is shown in Figure 5.1 and of the 3D model in Figure 5.2.

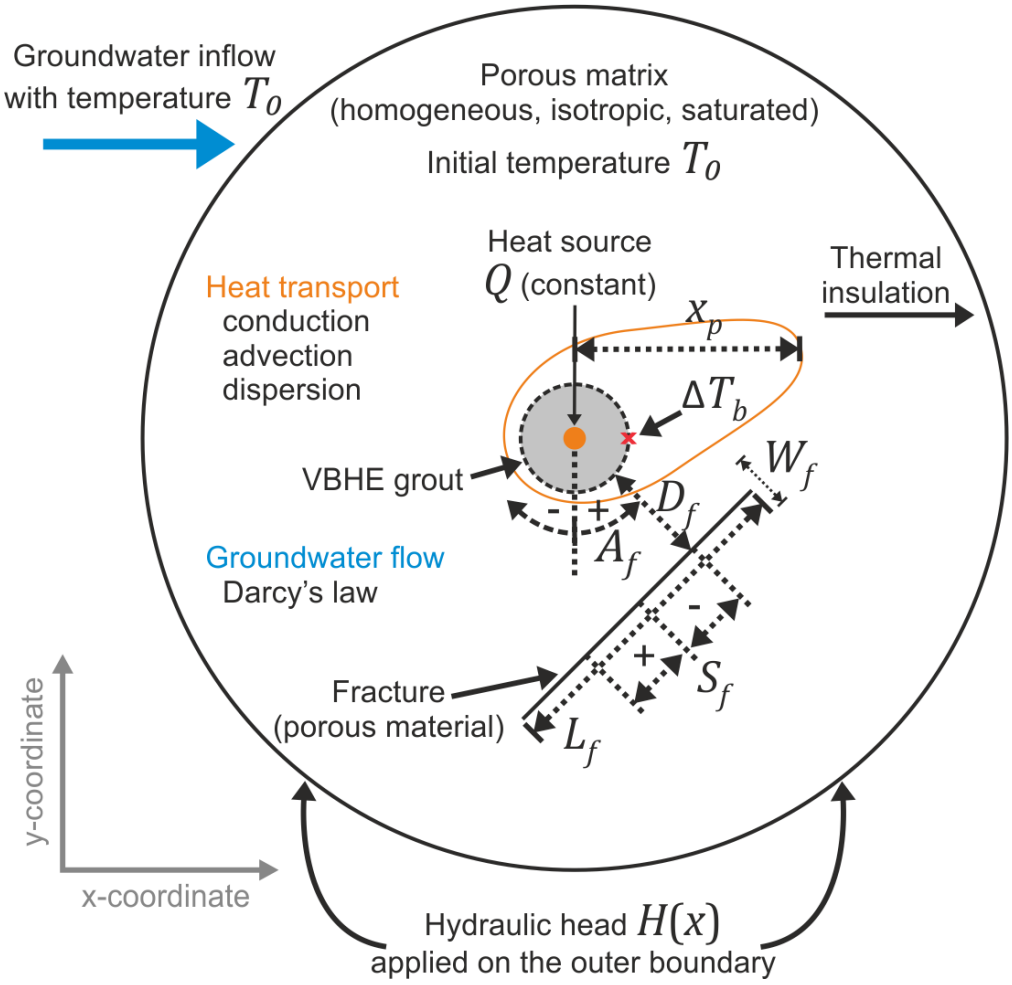

Figure 5.1 Conceptualisation of the TAF-2D numerical model. Not to scale. The red cross identifies the location where the temperature change at the VBHE wall ΔT_b was calculated. The orange line shows an example of the generated isotherm of ΔT = p K (e.g. +2 K) with extent in x-coordinate noted as X_p. $H(x)$ is fixed hydraulic head at the domain boundary.

The following parameters of a fracture near a VBHE are depicted in Figure 5.1 and Figure 5.2:

- D_f – fracture distance from the VBHE wall, perpendicular to fracture line (m);
- S_f – fracture shift specified along the orientation of the fracture from its mid-length. It is positive (+) in the positive direction of the x-axis before rotation;
- A_f – fracture rotation angle around the VBHE. It is relative to x-axis;
- W_f – fracture thickness;
- L_f – fracture length;

Additional fracture parameters for the 3D model (Figure 5.2) are:

- H_f – fracture height,
- Z_f – closest depth from fracture to ground surface.
- I_f – fracture inclination relative to horizontal ground.

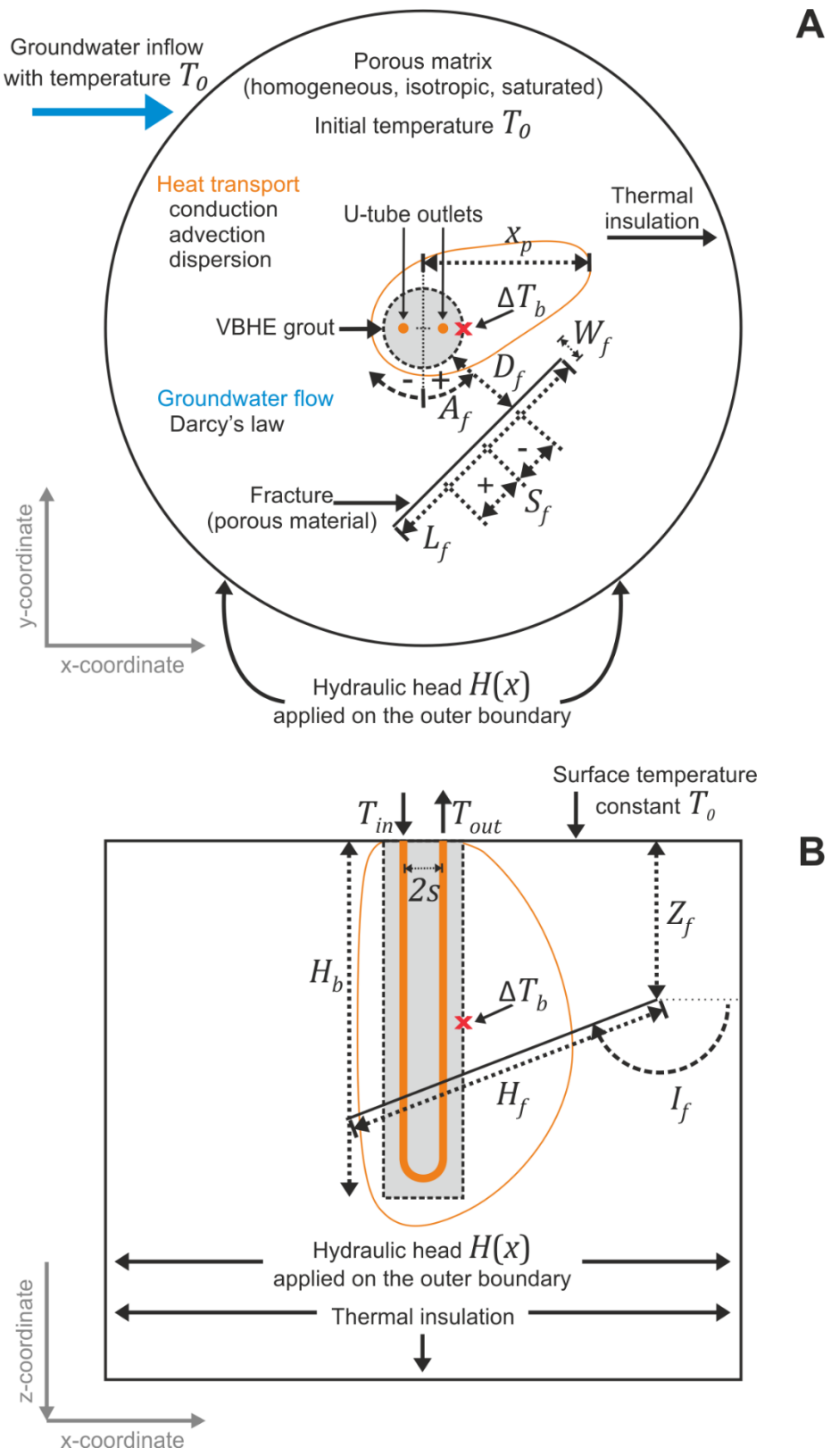

Figure 5.2 Conceptualisation of the TAF-3D numerical model in (A) plan and (B) cross section along x-axis. Fracture is represented by a rectangular plane. Note the fracture rotation angles differ between A and B (A: A_f = 45°; B: A_f = 90°). Not to scale. The red cross identifies the location where the ΔT_b was calculated. The orange line shows an example of an isotherm of ΔT = p K (e.g. +2 K) with extent in x-coordinate noted as X_p. H_b is the height of the VBHE, s is shank space between the inlet and outlet pipes. T_{in} and T_{out} are input and output working fluid temperatures from the U-pipe. $H(x)$ is fixed hydraulic head at the domain boundary.

5.3 Geometry

The model geometry parameters are given in Table 5.1. The large circle (2D) and cylinder (3D), defining the whole domain, had a sufficiently large radius of 400 m (and for 3D the height of 140 m) to allow heat to flow to the distances needed for the isotherms of interest to reach steady-state and to avoid significant temperature change reaching the thermally insulated boundaries (where it would otherwise accumulate), within the maximum simulation run time of 300 years. The heat source circular domain in the 2D model had a radius of 0.02 m. A smaller value could not be used due to the meshing limitations in COMSOL 5.2a. The heat source radius in the 3D model was 0.01 m, which gave slightly better results in validation because it is closer to the assumptions of the analytical solution relating to the linear heat source. However, as the model is focussed on the long-term thermal performance of the VBHE, the radius of the heat source does not play a role in the result.

Table 5.1 Model geometry for the 2D and 3D numerical models

Domain	2D model	3D model
Heat source circle radius (m) centre at $x, y = [0, 0]$ m	0.02	0.01
Domain radius (m) centre at $x, y = [0, 0]$ m	400	
Default position of the fracture centre of rotation at $x, y = [0, 0]$ m	Upstream point $x, y = \left[-L_f/2, -\left(D_f + r\right)\right]$ Downstream point $x, y = \left[L_f/2, -\left(D_f + r\right)\right]$	
Model height (m)		200
Height of the heat source (m)		100

5.4 Assumptions

The analyses assume that:

- The porous medium is divided into two material phases (solid and water) in both in the matrix and the fracture.
- There is local thermal equilibrium between the solid and water.
- All material properties are constant (independent of temperature).

With increase in temperature, the water viscosity reduces and, hence, hydraulic conductivity of the matrix increases. For example, hydraulic conductivity at 20 °C is 1.5 times higher than at 5 °C due to change in water viscosity (Stauffer *et al.* 2014). When temperature is changed by 5 K the hydraulic conductivity is increased by 13 %.

However, the thermal use of shallow subsurface systems produces restricted temperature disturbance to the ground. In this study, the water viscosity is fixed to a value corresponding 10 °C. However, it was checked that for a range of temperature changes involved in the analysis the assumption that water viscosity is constant has negligible effect on the model results. Water density and viscosity are often used as constants in thermohydraulic models for VBHEs and hence temperature dependence is disregarded: water flow is assumed to be not affected by heat transport (Stauffer *et al.* 2014). This is a common assumption for models of thermal transport from VBHE because change in density and viscosity due to temperature changes are negligible under typical hydrogeological and operational conditions of ground source heat pump systems (Hecht-Méndez *et al.* 2010). For example, the temperature change at the VBHE wall can reach temperature change of +20 K but further from the borehole wall the temperature changes are limited (for example the isotherm of +5 K reaches 10 m downstream from the VBHE wall, as illustrated on Figure 6.6). The MFLS analytical solution which models the thermal performance of a VBHE under the influence of groundwater flow also assumes that hydraulic and thermal parameters are independent of the temperature changes (Molina-Giraldo *et al.* 2011b).

- The matrix is saturated, with homogeneous and isotropic thermal and hydraulic properties.
- Thermal dispersivity in the fracture is ignored as advection is the key heat transfer process inside it; groundwater flow inside the fracture is very fast (COMSOL 5.2a 2016).
- All water is considered mobile in the fully saturated matrix.

- The fracture is a plane (represented as a line in the 2D model); it is a homogeneous saturated porous medium with hydraulic and thermal properties that are distinct from the matrix.
- Fluid flow is laminar and described by Darcy's law (Bear 1988).
- Heat is transferred by conduction (according to Fourier's Law), advection and dispersion.
- Thermal expansion is neglected.

Additionally, specific to the 3D analysis:

- The surface temperature is constant and equal to the initial aquifer temperature;
- The bottom of the aquifer is thermally insulated.

5.5 Software

The model was implemented using COMSOL Multiphysics 5.2a, which is a flexible, stable software platform that can couple multiple partial differential equations within a single model and covers a wide range of applications for groundwater modelling (fluid flow, heat and solute transport) (Li *et al.* 2009).

There is still a need to validate the numerical model against the analytical solution because any numerical model can have inaccuracies due to convergence issues and inadequate meshing.

MATLAB R2016a software was used to run the COMSOL models via LiveLink™ for MATLAB. This allowed the model to be run with different parameter sets taken from predefined ranges and the results to be automatically exported as txt files for further data analysis in MATLAB.

5.6 Governing equations

5.6.1 Groundwater flow in the matrix

Steady-state Darcian flow is assumed in the matrix:

$$\boldsymbol{v} = -K_m \nabla H \tag{5.1}$$

where $\boldsymbol{v}$ is the Darcy velocity vector (m s^{-1}), K_m is the hydraulic conductivity of the matrix (m s^{-1}) and H is hydraulic head (m).

In the absence of any fluid sinks or sources, mass continuity is given by:

$$\nabla \cdot (\rho_w \boldsymbol{v}) = 0 \tag{5.2}$$

where ρ_w is the density of water (kg m^{-3}). Substituting (5.1) into (5.2) and noting that the density of water and the hydraulic conductivity are constant, gives the well-known Laplace's equation for hydraulic head:

$$\nabla^2 H = 0 \tag{5.3}$$

Initial values of hydraulic head H for the model domain and hydraulic head boundary condition on the domain outer border were set using the x coordinate with a constant hydraulic gradient M (-) in the direction of the x-axis:

$$\mathrm{H}(x) = -Mx \tag{5.4}$$

The effect of a fracture on heat flow from the VBHE was examined over a wide range of groundwater velocities. For convenience, 'fast' groundwater flow means v_u ≥ 0.1 m day^{-1} and 'slow' groundwater flow means v_u ≤ 0.01 m day^{-1}; 'medium' refers to values in between; v_u is defined as the undisturbed Darcy velocity that would occur in the homogeneous matrix in the absence of a fracture.

The value of matrix hydraulic conductivity K_m is set as

$$K_m = -v_u / M \tag{5.5}$$

The maximum value of K_m *used in the model* was 5.79×10^{-4} m s^{-1} (50.03 m day^{-1}) to achieve the maximum required Darcy velocity in the matrix in the absence of a fracture, of v_u = 0.5 m day^{-1}.

5.6.2 Flow in the fracture

The fracture is coupled to the matrix by continuity of hydraulic head and by conservation of flow into and from the fracture. Steady state Darcian flow was assumed in the fracture. This type of analysis is not suitable for karst geology. The upper limit of the fracture aperture in this analysis was 25 mm and the maximal tested fracture length was 200 m.

Groundwater flow in the fracture was modelled along a line. The fracture was represented as a straight linear object with the fracture aperture as a defined property of the line. Flow in the fracture was modelled parallel to the interior boundary (line) representing the fracture within the matrix. The fracture aperture parameter W_f is part of the fracture geometry; therefore, it is not explicitly stated in the general equation for groundwater flow, like the other geometry parameters such as fracture length.

$$\boldsymbol{v_f} = -K_f \nabla_p H \tag{5.6}$$

$$\nabla_p \cdot (\rho_w \boldsymbol{v_f}) = 0 \tag{5.7}$$

where $\boldsymbol{v_f}$ is the Darcy velocity vector in the fracture (m s^{-1}), K_f is the hydraulic conductivity of the material in the fracture (m s^{-1}) and the subscript *p* means that the gradient is taken parallel to the line of the fracture. K_f is defined in relation to the hydraulic conductivity of the matrix as:

$$K_f = K_m R_K \tag{5.8}$$

where R_K is the ratio of the hydraulic conductivity of the fracture to that of the matrix (-).

5.6.3 Heat transfer physics

Heat transfer is modelled by conduction (according to Fourier's law) and by advection with the fluid flow.

The governing equation for heat transfer in the matrix away from the fracture is:

$$C_{em}\frac{\partial T}{\partial t} + \rho_w c_w \boldsymbol{v}\cdot\nabla T + \nabla\cdot\boldsymbol{q} = Q \tag{5.9}$$

$$\boldsymbol{q} = -\lambda_a \nabla T \tag{5.10}$$

where $\boldsymbol{q}$ is the conductive heat flux vector (W m^{-2}), c_w is the specific heat capacity of water (J kg^{-1} K^{-1}), C_{em} is the effective volumetric heat capacity (J m^{-3} K^{-1}), T is the temperature (K), t is the time (s), λ_a is the apparent thermal conductivity in the matrix (W m^{-1} K^{-1}) defined by an averaging model to account for the properties of both the solid matrix and the liquid (eq. (5.15)) and includes dispersive conductivity (eq. (5.17)), and Q is a constant heat source (W m^{-3}).

The constant heat source Q for the model is

$$Q = \frac{J}{d_z \pi r_s^2} \tag{5.11}$$

where J is the source power (W), d_z is the thickness of the model domain in the out-of-plane direction in the 2D model and equal to VBHE length H_b in the 3D model (m) and r_s is the heat source radius.

The thermal balance equation at the fracture is:

$$-\boldsymbol{q}\cdot\boldsymbol{n} = -W_f C_{ef}\frac{\partial T}{\partial t} - W_f \rho_w c_w \boldsymbol{v}\cdot\nabla_p T - W_f \nabla_p\cdot\boldsymbol{q_f} \tag{5.12}$$

$$\boldsymbol{q_f} = -\lambda_{ef}\nabla_p T, \tag{5.13}$$

where W_f is the fracture aperture (m), C_{ef} is the effective volumetric heat capacity of the fracture material at constant pressure (J m^{-3} K^{-1}), $\boldsymbol{q_f}$ is the heat flux vector in the fracture (W m^{-2}), λ_{ef} is the effective thermal conductivity of the fracture

(W m^{-1} K^{-1}), ϵ_f is the porosity of the fracture material (-), c_f is the specific heat capacity of the solid material in the fracture (J kg^{-1} K^{-1}) and the subscript *p* means that the gradient is taken parallel to the line of the fracture. The term $-\boldsymbol{q} \cdot \boldsymbol{n}$ gives the heat transfer from the fracture to the matrix.

The effective volumetric heat capacity (solid-liquid system) for the matrix C_{em} and for the fracture C_{ef} is calculated as the weighted mean

$$\begin{aligned} C_{em} &= (1-\epsilon_m)\rho_m c_m + \epsilon_m \rho_w c_w \\ C_{ef} &= \left(1-\epsilon_f\right)\rho_f c_f + \epsilon_f \rho_w c_w \end{aligned} \tag{5.14}$$

where the subscript *m* is for matrix (c_{em}) and *f* is for fracture (C_{ef})(, ρ_m and ρ_f are the density of the solid material in the matrix and fracture (kg m^{-3}), c_m and c_f are the specific heat capacities of the solid material at constant pressure (J kg^{-1} K^{-1}), c_w is the specific heat capacity of water at constant pressure (J kg^{-1} K^{-1}).

The effective conductivity of the solid-fluid system for the matrix λ_{em} and the fracture λ_{ef} is calculated as the weighted arithmetic mean of the thermal conductivities of mobile water and solid material (in either the matrix (5.15) or the fracture (5.16)). The weighted arithmetic mean applies to the situation when heat conduction occurs in parallel in the solid and the fluid and provides an upper bound to the effective thermal conductivity. The weighted harmonic mean was not used because it applies to a situation where the heat conduction takes place in series; it provides a lower bound to the effective thermal conductivity. The effective thermal conductivity of solid-fluid system in the matrix, λ_{em}, is therefore calculated as follows:

$$\lambda_{em} = (1-\epsilon_m)\lambda_m + \epsilon_m \lambda_w \tag{5.15}$$

where λ_m is the thermal conductivity of the matrix solid material (W m^{-1} K^{-1}), λ_w is the thermal conductivity of mobile water (W m^{-1} K^{-1}).

As with λ_{em},the effective conductivity of the solid-liquid system in the fracture, λ_{ef}, is calculated as follows:

$$\lambda_{ef} = (1 - \epsilon_f)\lambda_f + \epsilon_f \lambda_w \quad (5.16)$$

where the subscript f denotes the fracture so λ_f is the thermal conductivity of the solid material in the fracture (W m^{-1} K^{-1}).

The apparent thermal conductivity $\boldsymbol{\lambda_a}$ in the matrix includes both effective and dispersive conductivities:

$$\boldsymbol{\lambda_a} = \boldsymbol{\lambda_{em}} + \boldsymbol{\lambda_B} \quad (5.17)$$

where λ_B is the dispersive thermal conductivity tensor (W m^{-1} K^{-1}).

Analogous with hydraulic dispersion (Bear 1988), thermal dispersion was assumed as follows:

$$(\boldsymbol{\lambda_B})_{ij} = \rho_w c_w \boldsymbol{B_{ij}} \quad (5.18)$$

where $\boldsymbol{B}$ is the hydrodynamic dispersion tensor (m^2 s^{-1}) (COMSOL 5.2a 2016):

$$\boldsymbol{B} = \frac{1}{|\boldsymbol{v}|}\begin{bmatrix} \beta_L v_L^2 + \beta_T v_T^2 + \beta_V v_V^2 & (\beta_L - \beta_T) v_L v_T & (\beta_L - \beta_V) v_L v_V \\ (\beta_L - \beta_T) v_L v_T & \beta_T v_L^2 + \beta_L v_T^2 + \beta_V v_V^2 & (\beta_L - \beta_V) v_T v_V \\ (\beta_L - \beta_V) v_L v_V & (\beta_L - \beta_V) v_T v_V & \beta_V v_L^2 + \beta_V v_T^2 + \beta_L v_V^2 \end{bmatrix} \quad (5.19)$$

where β_L is the longitudinal dispersivity along the x-axis (m) , β_T is the transverse along the y-axis dispersivity (m) and β_V is the vertical dispersivity along the z-axis (m); v_L, v_T and v_V are the longitudinal, transverse horizontal and transverse vertical components of the Darcy velocity vector.

The hydrodynamic and therefore thermal dispersivity coefficients are assumed to scale linearly with the components of the Darcy flux. This form of scaling is widely accepted (Bear 1988), especially for the not-too-fast groundwater velocity range in the matrix used in this work (up to 0.5 m day^{-1}). Laboratory studies of very fast groundwater flow in the matrix (20 - 100 m day^{-1}) in coarse sand have shown that thermal dispersion can be described by a square law for groundwater velocities when Re < 2.5 (Rau *et al.* 2012).

5.7 Boundary conditions

Zero conductive flow is assumed over the outer model boundary and over the bottom of the 3D model domain. Note that this boundary condition does not influence the model results because the domain size is large, and heat does not reach these boundaries over the modelled time period of 300 years. The hydraulic head H was fixed on the domain boundary. The ground surface temperature of the 3D model was constant and equal to the initial aquifer temperature T_0. In every simulation, a check was made to ensure that the simulated velocities were low enough to maintain laminar flow. In only a few simulations were the groundwater velocities such that the Reynolds number exceeded 10; these were excluded from consideration of the results.

A boundary condition was applied to the outer domain that allowed heat carried by water at a specified arbitrary reference exterior temperature (T_0 = 273.15 K, 0 °C) to advect into the domain.

The initial temperature T_0 was selected to be 0 °C as a convenient datum to inform about the temperature disturbance to the aquifer caused by a VBHE for both heat injection and heat abstraction operation modes. No water freezing is assumed. All model assumptions are discussed in section 5.4.

The outer boundary was otherwise assumed to have zero conductive heat flux:

$$\begin{aligned} T &= T_o \text{ , if } \boldsymbol{n} \cdot \boldsymbol{v} < 0 \\ -\boldsymbol{n} \cdot \boldsymbol{q} &= 0 \text{ , if } \boldsymbol{n} \cdot \boldsymbol{v} \geq 0 \end{aligned} \tag{5.20}$$

where $\boldsymbol{n}$ is the outward normal vector of the boundary (-), $\boldsymbol{v}$ is the Darcy velocity vector (m day^{-1}), and $\boldsymbol{q}$ is the conductive heat flux vector (W m^{-2}).

5.8 Heat source

The heat source Q delivers a constant input of power to the ground (there is no seasonal variation in the VBHE operation). The heat source was represented as a

circular heated domain (circle for the 2D and cylinder for the 3D model) with a small radius (Table 5.1). This was done both for simplicity and to aid validation of the model against the MILS or MFLS analytical solutions in which the VBHE is approximated as a point source and a line source. The heat source was installed inside the domain of radius r = 5 cm, which represents the grout of the VBHE (Figure 5.1). The hydraulic and thermal properties of the grout material are given in Table 5.3. The temperature probe ΔT_b was located on the borehole wall downstream at r, y = [0.05, 0] m. This point is marked by a red circle in Figure 5.1. For model validation purpose, to be consistent with the assumptions of the analytical solutions, the VBHE grout and heat source had the same material properties as the aquifer. However, for the analysis of the VBHE performance discussed in the following chapters, the grout and heat source materials were changed to impermeable and assigned the typical grout material properties (Table 5.3).

The presence of grout in a VBHE has no influence on the results of the models on a long timescale. This is illustrated by the comparison of the analytical solution to the numerical model without grout (Figure 5.7) and with impermeable grout (Figure 6.2 for 2D and Figure 8.2 for 3D). However, at fast groundwater flow at short times (for up to 5 hours) the numerical model with grout has lower temperature at the VBHE wall than analytical solution. This is due to the time needed for the temperature change to travel by conduction via the grout to the downstream location point of ΔT_b calculation. While for the analytical solution without grout the temperature change from the heat source travels to the VBHE wall location via both conduction and advection. For fast groundwater flows the upstream side of the VBHE wall in the model without grout is effectively cooled by the groundwater directly by advection. This is illustrated on Figure 5.3 which shows how groundwater passes through the VBHE wall for TAH-3D model (line heat source without grout) and for TAHpi model (explicit representation of pipes and with impermeable grout).

Another difference between models with and without grout is the local groundwater velocity at the VBHE wall. In the model without grout the groundwater velocity does not differ around the VBHE wall. In the model with impermeable grout the groundwater velocity differs around the grout as it flows around it (Figure 5.3). However, the mean groundwater flow in the area around the VBHE grout is the same, therefore the groundwater flow has the same influence for both cases.

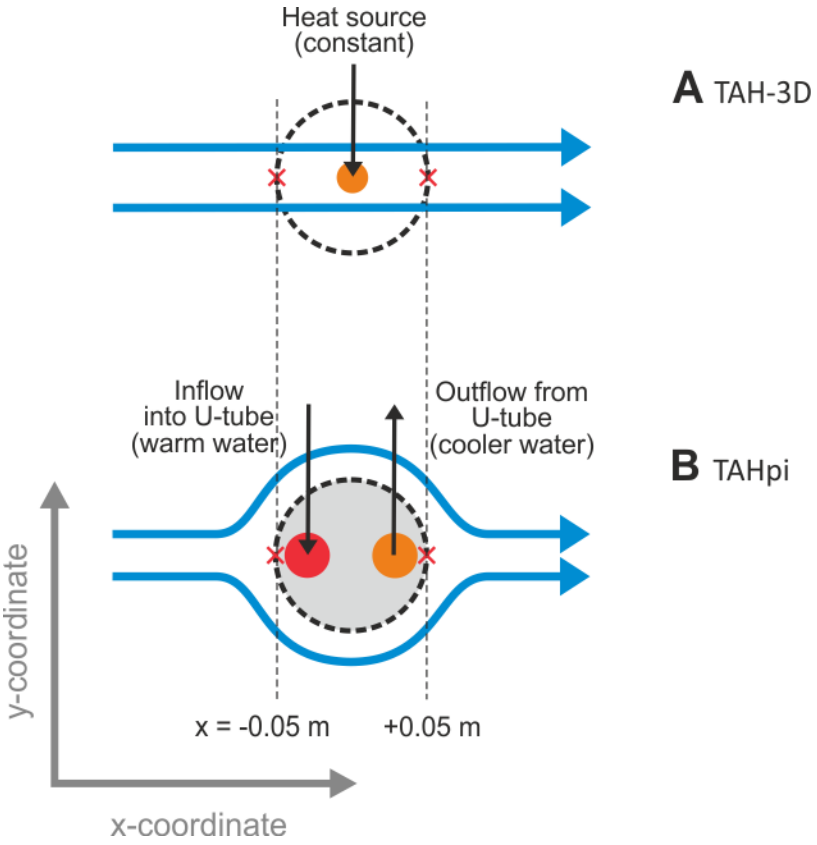

Figure 5.3 Sketch of groundwater flow around plan cross-section of (A) TAH-3D and (B) TAHpi models. Locations where ΔT_b was calculated (at z = 50 m) are marked with red cross. The groundwater flow path is shown with blue arrows.

The heat source for the versions of the 3D model with pipes TAHpi and TAFpi was modelled as a symmetrical U-pipe inside the grouted cylinder (VBHE) with circulating water inside it. In this case, the temperature of water entering the U-pipe was equal to:

$$T_{in} = T_{out} + T_d \tag{5.21}$$

$$T_d = \frac{J}{\rho_w c_w O_p} \tag{5.22}$$

where T_{in} is the working fluid (water) temperature (K) entering the U-pipe, T_{out} is the water temperature (K) leaving the U-pipe, T_d is temperature difference (K) induced by the power input to the fluid before it re-enters the U-pipe, J is the power delivered by the heat pump to the fluid before it re-enters via the U-pipe (W), ρ_w is the density of working fluid (water) in the U-pipe (kg m^{-3}), c_w is the specific heat capacity of the working fluid (J kg^{-1} K^{-1}) and O_p is the volumetric flow rate inside the U-pipe (m^3 s^{-1}).

The U-pipe in the 3D model was implemented via the 'Heat Transfer in Pipes' interface (COMSOL 5.2a 2016). This interface is used to model heat transfer by conduction and advection in pipes. The interface represents pipes in 1D to define the pipe flow and temperature profiles along the pipelines. Pipelines represent simplifications of hollow tubes. The U-pipe was set within the 3D geometry of the borehole and heat is exchanged between the U-pipe and the borehole grout (Figure 5.2). It was checked that the flow inside the U-pipe was turbulent, Re > 1, in accordance with design guidance (Energy Saving Trust). Additional fixed parameters for the models with U-pipe are given in Table 5.2.

5.9 Flow inside pipes

The thermal balance equation in the pipe is (COMSOL 5.2a 2016):

$$\rho_w A c_w \frac{\partial T}{\partial t} + \rho_w A c_w v_p \boldsymbol{e_t} \cdot \nabla_t T = \nabla_t \cdot (A \lambda_w \nabla_t T) + f_D \frac{\rho_w A}{2 d_p} \left| v_p^3 \right| + Q_p \tag{5.23}$$

where T is the temperature of the working fluid in the pipe, ρ_w is the density of the working fluid (water) in the pipe (kg m^{-3}), c_w is the specific heat capacity of the fluid at constant pressure (J kg^{-1} K^{-1}), d_p is the inner diameter of the circular pipe (m), A is the pipe cross-sectional area calculated as $A = \pi d_p^2/4$ (m^2), $v_p \boldsymbol{e_t}$ is the tangential velocity $v_p \boldsymbol{e_t}$ based on the velocity of the fluid in the pipe $v_p = O_p/A$

(m s^{-1}), λ_w is the thermal conductivity of water (W m^{-1} K^{-1}), f_D is the Darcy friction factor (-) and Q_p is the heat transferred through the pipe wall (W m^{-1}).

The Churchill friction model was used for calculating the flow resistance (COMSOL 5.2a 2016):

$$
\begin{aligned}
f_D &= 8\left[\left(\frac{8}{Re}\right)^{12} + (c_A + c_B)^{-1.5}\right]^{\frac{1}{12}} \\
Re &= \frac{\rho_w v_p d_p}{\mu} \\
c_A &= \left[-2.457\ \ln\left(\left(\frac{7}{Re}\right)^{0.9} + 0.27\left(\frac{e_A}{d_p}\right)\right)\right]^{16} \\
c_B &= \left(\frac{37530}{Re}\right)^{16}
\end{aligned}
\tag{5.24}
$$

where Re is the Reynolds number (-), μ is the dynamic viscosity of the fluid in the pipe (Pa s) and e_A is the surface roughness for drawn tubing (m).

Heat transferred through the pipe wall Q_p (W m^{-1}) is calculated as:

$$
\begin{aligned}
Q_p &= (hZ)_e(T_m - T) \\
(hZ)_e &= \frac{2\pi}{\frac{1}{r_p h_i} + \frac{\ln\left((r_p + w_p)/r_p\right)}{\lambda_p}} \\
h_i &= N_u \frac{\lambda_w}{d_p} \\
N_u &= \frac{(f_D/8)(Re - 1000)P_r}{1 + 12.7(f_D/8)^{\frac{1}{2}}\left(P_r^{\frac{2}{3}} - 1\right)} \\
P_r &= \frac{c_w \mu}{\lambda_w}
\end{aligned}
\tag{5.25}
$$

where $(hZ)_e$ is an effective value of the heat transfer coefficient h (W m^{-2} K^{-1}) times the pipe wall perimeter $Z = \pi d_p$ (m), T_m is the external temperature outside the pipe (K), r_p is the inner pipe radius, $r_p = d_p/2$ (m), λ_p is the thermal

conductivity of the pipe wall material (W m^{-1} K^{-1}), w_p is the pipe wall thickness (m), h_i is the internal film heat transfer coefficient (W m^{-2} K^{-1}), N_u is the Nusselt number for turbulent flow (-) and P_r is Prandtl number (-).

The initial temperature in the pipe was set to T_0 (0 C°)

It was assumed that:

- The velocity profile is fully developed across an entire pipe section;
- Empirical functions (friction charts) describe viscous pressure drop for the turbulent flow regime;
- Curvature of the pipe segment gives rise to insignificant pressure loss in comparison with wall friction
- Hydraulic shocks (dynamical effects) were negligible;
- All velocity components normal to the pipe axis were zero inside the pipe.

Table 5.2 Fixed model parameters for the TAFpi model. The material of the U-pipe is high density polyethylene (HDPE).

	Fixed parameter, symbol	Value and units
Heat source geometry	Pipe diameter, d_p (Mottaghy & Dijkshoorn 2012)	0.03 m
	Pipe volumetric flowrate, O_p (Mottaghy & Dijkshoorn 2012)	4×10^{-4} m^3s^{-1}
	Pipe wall thickness, w_p (Mottaghy & Dijkshoorn 2012)	0.0029 m
	Shank space for U-pipe, distance from VBHE centre to pipe centre, s (Zeng *et al.* 2003)	0.03 m
	U-pipe half-length	100 m
	Grout length (grout is also below the U-pipe bend)	100.025 m
	Radius of U-pipe bottom end loop	0.025 m
Heat input	Power delivered to fluid by heat pump, J	5000 W
	Corresponding temperature difference between inlet and outlet pipe, $T_d = T_{in} - T_{out} = J/c_w q_p$	2.98 K
Material properties	Thermal conductivity of solid in the VBHE grout, silica-sand based material (Erol & François 2014), λ_g	2.3 W m^{-1} K^{-1}
	Density of the solid material in grout (Erol & François 2014), ρ_g	1800 kg m^{-3}
	Specific heat capacity of solid in grout (Erol & François 2016), c_g	1500 J kg^{-1} K^{-1}
	Porosity of silica-sand based grout (Erol & François 2016), ϵ_g	0.12
	Hydraulic conductivity of silica-sand based grout (Erol & François 2014), K_g	6×10^{-10} m s^{-1} (5.2×10^{-5} m day^{-1})
	Thermal conductivity of HDPE of U-pipe, λ_p within the range from (Raymond *et al.* 2015)	0.33 W m^{-1} K^{-1}
	Surface roughness for drawn tubing (default COMSOL value), e_A	1.5×10^{-6} m
	Density of HDPE of U-pipe, ρ_p within the range from (British Plastics Federation 2019)	960 kg m^{-3}
	Specific heat capacity of HDPE of U-pipe at constant pressure (Erol & François 2016), c_p	2100 J kg^{-1} K^{-1}

5.10 Hydrogeological scenarios

A range of scenarios was investigated to examine how an open fracture may influence the thermal performance of a VBHE. The analysed fracture geometry parameters are shown in Figure 5.1 and Figure 5.2 (for 2D and 3D models). Parameter for the ratio of the fracture to the matrix hydraulic conductivity R_K is also included. The analysis was conducted for a wide range of groundwater velocities in the matrix v_u, and for different aquifer dispersivities β_L, β_T and β_V. Single-parameter sensitivity analyses and Monte Carlo uncertainty and sensitivity analyses were conducted. Single-parameter analysis involved running the numerical model with the individual fracture parameters changed for each model run, while the remaining parameters were fixed to the base values.

5.11 Parameters and material properties

The time intervals for the analysis ranged from 1.095×10^{-3} to 1.095×10^{5} days (95 s to 300 years), with the total time of 300 years divided logarithmically into 128 time steps. All fixed parameters are given in Table 5.3. Thermal properties for the aquifer matrix material (density, effective volumetric heat capacity and effective thermal conductivity) were based on typical sandstone values (Stauffer *et al.* 2014). The matrix hydraulic conductivity K_m was based on the target groundwater velocity in a homogeneous matrix v_u and a constant hydraulic gradient in the x-axis direction M. This allowed the model to be run for specified groundwater velocities in an undisturbed matrix v_u.

The maximum value of v_u was selected to be 0.5 m day^{-1} because this is large enough to significantly cool the VBHE wall, rendering the effect of a nearby flowing fracture insignificant. For example, hydraulic conductivities in the Permo-Triassic sandstones in the UK reach 100 m day^{-1} (Allen *et al.* 1997). In the results, medium (v_u = 0.05 m day^{-1}) and slow (v_u = 0.005 m day^{-1}) aquifers are selected and compared in testing the effects of a fracture on the VBHE. Fixed model parameters are listed in Table 5.3.

Hydraulic and thermal material properties are listed in Table 5.3, together with the symbols used in the governing equations. The numerical models use the same material properties and default fixed parameters as the analytical solutions that were used for validation.

Table 5.3 Fixed model parameters used in all models

	Fixed parameter, symbol, formulas	Value and units
Heat input	Source power J	5000 W (corresponds to 50 W m^{-1})
Geometry	Domain radius	400 m
	VBHE radius, r	0.05 m
	Heat source radius (2D), r_{s2D}	0.02 m
	Heat source radius (3D), r_{s3D}	0.01 m
	VBHE length (for 3D model), H_b, U-pipe half-length (3D model with U-pipe), thickness of domain (2D model), d_z	100 m
Material Properties	Effective volumetric heat capacity of aquifer, $C_{em} = (1-\epsilon_m)\rho_m c_m + \epsilon_m \rho_w c_w$	2.8×10^6 J m^{-3} K^{-1}
	Effective volumetric heat capacity of fracture material, (fluid and solid) $C_{ef} = (1-\epsilon_f)\rho_f c_f + \epsilon_f \rho_w c_w$	3.4×10^6 J m^{-3} K^{-1}
	Specific heat capacity of water, c_w	4.2×10^3 J kg^{-1} K^{-1}
	Specific heat capacity of solid in the matrix, c_m	814.8 J kg^{-1} K^{-1}
	Thermal conductivity of water, λ_w	0.56 W m^{-1} K^{-1}
	Effective thermal conductivity of aquifer, $\lambda_{em} = (1-\epsilon_m)\lambda_m + \epsilon_m \lambda_w$	2.5 W m^{-1} K^{-1}
	Thermal conductivity of solid in the matrix, λ_m	3.33 W m^{-1} K^{-1}
	Porosity of the matrix, ϵ_m (Morris & Johnson 1967)	30 %
	Porosity of the fracture, ϵ_f	60 %
	Density of solid material in the matrix, ρ_m	2700 kg m^{-3}
	Density of solid material in the fracture, ρ_f	2700 kg m^{-3}
	Density of water, ρ_w	999.9 kg m^{-3}
	Constant hydraulic gradient in the x-axis direction in the case of a homogeneous matrix, M	0.01 m m^{-1}
	Hydraulic conductivity of matrix material that would achieve the target groundwater velocity in a homogeneous matrix, $K_m = -v_u/M$	Maximum K_m value 5.79×10^{-4} m s^{-1} (50.03 m day^{-1}) was used to achieve maximum v_u of 0.5 m day^{-1}
Time	Reporting time for thermal performance, t	30 years
	Maximum time for simulations (used to calculate steady state), t_{max}	300 years

5.12 Solver settings

A time-dependent solver with a BDF (Backward Difference Formula) time stepping method was used for both 2D and 3D models. The Backward Euler (COMSOL default) was used to perform consistent initialization using a small artificial step. The fraction of the initial step (0.001 days) for the Backward Euler step was 0.001.

A linear system parallel sparse direct solver (PARDISO) was used. Default solver settings were used except that strict time stepping rather than unspecified.

5.13 Temperature interpolation

Analysis of model results was performed in MATLAB. A general function that returns temperatures at desired points (x, y, z coordinates) and times for the specified model (2D, 3D, 3D with U-pipe) and model parameters was implemented. Results were retrieved from hundreds of scenarios pre-calculated in separate runs in COMSOL. The COMSOL results exported as text files for each run contained temperatures at mesh nodes for all time steps. To later determine the temperature in MATLAB at any desired point (not only at mesh nodes), Delaunay triangulation and Barycentric coordinates were used to calculate the weighted average of temperatures from the three nodes around each desired point. The nodes define the element (mesh triangle) in which the desired point is located. For this, the inbuilt MATLAB Delaunay triangulation class was used to define the mesh element list by creating a 2-D triangulation from a set of COMSOL mesh nodes with calculated temperatures. This allowed evaluation of temperature at arbitrary points for further analysis, comparisons and plots in MATLAB.

5.14 Spatial discretization for processing of numerical model results

Spatial discretisation is needed to calculate temperatures along a single axis or over the 2D domain at defined points (locations) independent of mesh node locations and model used. The developed spatial discretisation allows a higher density of points to be specified for locations with quickly changing temperatures near the VBHE wall and a reduced density further away (to reduce computational time). The coordinates of the points for temperature evaluation were created based on the desired ranges for x and y-coordinates (for 2D calculation) or for the range for x-coordinate (1D). Ranges were based on the expected thermal plume extents for the relevant times. The ranges used to calculate RMSE (root mean

squared error) and MAE (mean absolute error) for temperature difference between the analytical and numerical models (model validation) are given in Table 5.4.

Table 5.4 Spatial and temporal discretization for RMSE/MAE calculation used for model validation

Discretization parameter	Value
Number of discretization points for each coordinate	100 (i.e. 100x100 points for x-y plan view)
Range for x-coordinate	From -50 to 250 m
Range for y-coordinate	From -80 to 90 m
Limit of exponential spatial discretisation method	50 m
Optimal step growth rate	1.1
Fixed starting step size	0.01 m
Excluded range around origin point (0,0)	0.05 m (VBHE radius)
Time intervals	From 1.095×10^{-3} to 1.095×10^{5} days (95 seconds to 300 years), divided logarithmically into 32 time steps

The spatial discretization for these ranges was calculated using exponential and linear methods with the required number of discretization points (Figure 5.4). The following rules were followed:

- VBHE diameter was excluded from the spatial discretization.
- Discretization with exponentially increasing spacing was used for points up to 50 m distance from the VBHE, to have more points near the borehole where the temperature changes rapidly.
- The required number of points was split between two ranges (one for negative coordinates, one for positive) in proportion to their relative lengths. The number of points was further split between exponential (up to 50 m) and linear (50 m and more) method of discretization. More points were used for the exponential region, with the proportion based on optimal meshing with a growth rate of 1.1 and 100 required points for the range from 0 to 250 m.

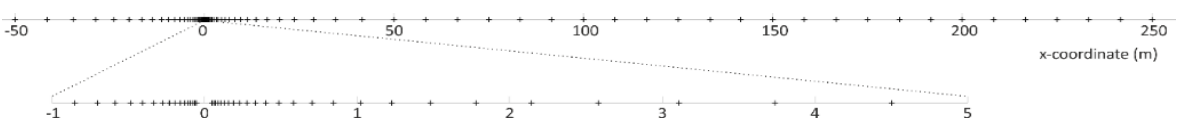

Figure 5.4 Example of space discretization with default parameters as defined in Table 5.4.

5.15 Meshing

Free triangular meshing with the COMSOL default options and automatic tessellation was used. The mesh size parameters used for each domain are specified in Table 5.5. The complete 2D mesh consists of around 2.5×10^4 elements (differing slightly, depending on the fracture location). The complete mesh for the 3D model without U-pipe TAH-3D consists of around 1.7×10^6 elements and of around 2.4×10^6 elements for the 3D model with U-pipe. All elements for a given domain are smaller than or equal to the maximum element size specified for the domain. The maximum element growth rate was the maximum rate at which the element size can grow from a region with small elements to a region with larger elements. The curvature factor determines the size of boundary elements compared with the curvature of the geometric boundary (the ratio between the element size and the radius of curvature). The curvature radius multiplied by the curvature factor gives the maximum allowed element size along the boundary. Resolution of narrow regions controls the number of layers of elements that are created in narrow regions (COMSOL 5.2a Multiphysics Application Library Manual, (COMSOL 5.2a 2016)).

Table 5.5 Mesh size parameters

Mesh parameter / Model and domain		Minimum element size (m)	Maximum element size (m)	Maximum element growth rate (-)	Curvature factor (-)	Resolution of narrow regions (-)
2D	Heat source	-	0.01	-	-	-
	Medium	-	5	1.4	-	-
	Large (remaining)	10	20	1.2	0.9	0.4
3D	Heat source	-	0.04	-	-	-
	Medium	0.04	16	1.28	-	-
	Large (remaining)	16	40	1.2	0.9	0.4

Not specified values "-" use value from large domain (remaining)

The mesh parameter definition achieves fine meshing around the heat source (Figure 5.5) and for the medium domain where accurate model results are required, while avoiding unnecessary elements in the rest of the domain.

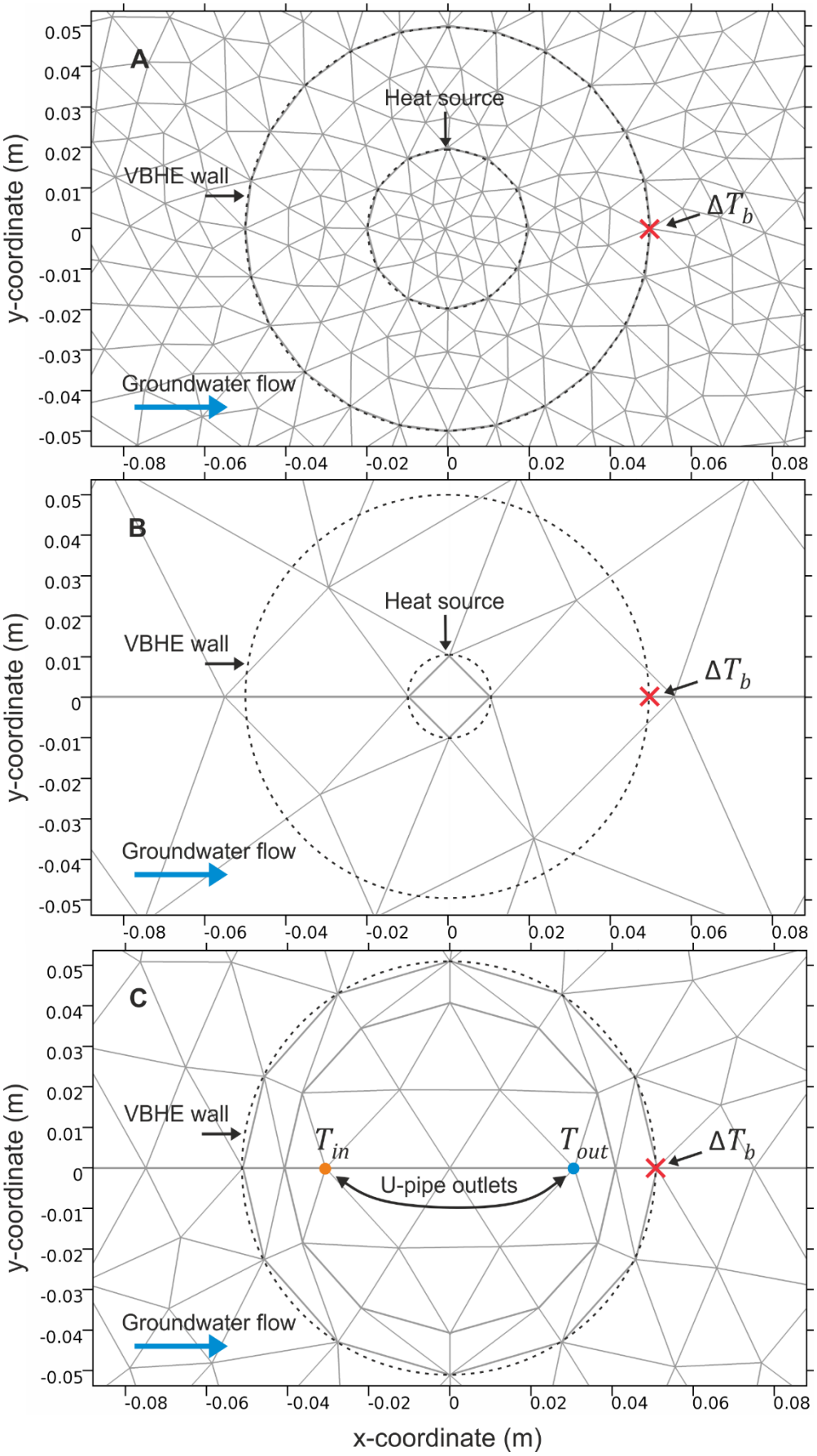

Figure 5.5 Mesh sizes around the heat source for (A) the 2D model, (B) the 3D model and (C) the 3D model with U-pipe. The red cross identifies the location where the temperature change at the VBHE wall ΔT_b was calculated.

5.16 Mesh refinement

During mesh refinement, different meshing variants were tested to produce acceptable model results in comparison with the analytical solution. The mesh was changed by changing the maximum element size at the heat source M_s (Table 5.6). Each tested M_s was used to calculate the mesh size factor M_F as follows:

$$M_F = \frac{M_s}{M_i} \tag{5.26}$$

where M_i is the initial maximum mesh size found by the preliminary mesh refinement and is set to 0.01 m for 2D and 0.05 m for 3D.

M_F was then used to change meshing parameters during mesh refinement to find the optimal mesh (Table 5.6).

Table 5.6 Mesh size parameters as set in COMSOL during mesh refinement. M_s is the maximum mesh size value for mesh parameter, M_F is the mesh size factor.

Model	Model domain	Mesh parameter		
		Minimum element size (m)	Maximum element size (m)	Maximum element growth rate (-)
2D	Heat source	-	M_s	-
	Medium	-	min(50, 5×M_F)	1.1
	Large (remaining)	min(50, 10×M_F)	min(100, 20×M_F)	1.2
3D	Heat source	-	M_s	-
	Medium	M_s	min(50, 20×M_F)	max(1.2, min(1.6, 0.8+0.6×M_F))
	Large (remaining)	min(50, 20×M_F)	min(100, 50×M_F)	1.2

Not specified values "-" use value from large domain (remaining)

5.16.1 Criteria for mesh convergence

To determine the optimal mesh settings, the following criteria were evaluated when comparing the results of the analytical and numerical models for different M_s values and 4 different groundwater velocities in the matrix v_u:

- The difference between models in temperature change at the VBHE wall after 30 years ΔT_b reported as actual and relative values. The borehole wall point is at location x = 0.05 m, y = 0 and z = 50 m (i.e. half the VBHE length,

relevant to 3D model only), downstream of the VBHE. The differences between models are calculated as the value from the numerical model minus the analytical model result.

- The maximum temperature difference ΔT between the numerical and analytical models for all tested locations and all time steps.
- The mean absolute error (MAE) and Root mean square error (RMSE) were selected as the statistical criteria. $\mathrm{RMSE}_{\mathrm{total}}$ and $\mathrm{MAE}_{\mathrm{total}}$ were calculated for the differences between the numerical and analytical models in ΔT for each point and each time (eq. (5.27)). MAE is a good metric for average model performance (but might be affected by large quantity of averaged error values), and RMSE is effective in revealing the differences in model performance during parameter sensitivity analysis because it highlights large errors (Chai & Draxler 2014).

$$\mathrm{RMSE}_{total}^{2D} = \sqrt{\frac{\sum_{xy,t_n}\left(\Delta T_{xy,t_n}^{TAH_{2D}} - \Delta T_{xy,t_n}^{MILS}\right)^2}{N}}$$

$$\mathrm{RMSE}_{total}^{3D} = \sqrt{\frac{\sum_{xy,t_n}\left(\Delta T_{xy,t_n}^{TAH_{3D}} - \Delta T_{xy,t_n}^{MFLS}\right)^2}{N}} \qquad (5.27)$$

$$\mathrm{MAE}_{total}^{2D} = \frac{\sum_{xy,t_n}\left|\Delta T_{xy,t_n}^{TAH_{2D}} - \Delta T_{xy,t_n}^{MILS}\right|}{N}$$

$$\mathrm{MAE}_{total}^{3D} = \frac{\sum_{xy,t_n}\left|\Delta T_{xy,t_n}^{TAH_{2D}} - \Delta T_{xy,t_n}^{MILS}\right|}{N}$$

where $\Delta T_{xy,t_n}^{model}$ is temperature change at location (x, y) for time t_n modelled using specified $model$, t_n is one of 128 calculated time steps, xy is one of 10000 tested locations on a horizontal plane (for 3D model the horizontal plane is at a depth of mid-length of the VBHE), N is total number of compared temperature changes (N = 1 280 000).

A combination of these metrics is used to assess model performance. Relative error could not be used for comparison, as the initial temperature value in the model was zero (°C).

5.17 Criteria for the thermal performance of a VBHE

For the selected optimal mesh for 2D and 3D models, the following criteria were tested to show how the numerical model matches the relevant analytical solution:

- The temperature change at the borehole wall ΔT_b after 30 years of continuous VBHE operation for four different groundwater velocities in the matrix v_u.
- The temperature change along the x-axis (for 3D at z = 50 m) for four different groundwater velocities in the matrix v_u and for two dispersivities β.
- The plan and profile views for several isotherms for both the analytical and numerical models for two groundwater velocities in the matrix v_u.

5.18 Mesh refinement results

5.18.1 Criterion 1: Differences between modelled temperature change at the VBHE wall

The differences in ΔT_b between the numerical models (TAH-2D and TAH-3D) and the respective analytical solutions for 2D and 3D (MILS and MFLS) are shown in Figure 5.6. The differences are shown in terms of temperature difference at the borehole wall after 30 years of continuous VBHE operation ΔT_b for a range of mesh densities of the numerical model. The differences in ΔT_b between the models are shown as absolute actual and absolute relative values. The absolute actual difference between models (K) is defined for 2D as $\left|\Delta T_b^{TAH_{2D}} - \Delta T_b^{MILS}\right|$ and for 3D as $\left|\Delta T_b^{TAH_{3D}} - \Delta T_b^{MFLS}\right|$. The absolute relative difference between models (%) is defined for 2D as $\left|\Delta T_b^{TAH_{2D}} - \Delta T_b^{MILS}\right| / \Delta T_b^{MILS}$ and for 3D as $\left|\Delta T_b^{TAH_{3D}} - \Delta T_b^{MFLS}\right| / \Delta T_b^{MFLS}$.

The mesh was controlled by the mesh parameter for the maximum mesh size on the heat source M_s, Figure 5.6 A (for the 2D model) and Figure 5.6 C (for the 3D model). The aquifer dispersivities used were β_L ; β_T ; β_V = 2 ; 0.2 ; 0.2 m to validate

also the correct modelling of dispersion effects. Note that small changes of the mesh parameter for fine mesh correspond to large changes in the number of mesh elements.

Additionally, the number of mesh elements for the 2D and 3D models is also shown in Figure 5.6 B and Figure 5.6 D. In all cases, ΔT_b *for the* numerical model is lower than for the analytical solution. The maximum mesh size at the heat source M_s was selected to be 0.01 m as the optimal for the TAH-2D model and 0.04 m for the TAH-3D. Increasing the number of mesh elements above the optimum values does not significantly improve the accuracy of model results, while the calculation time and memory requirements grow. The number of mesh elements for the complete optimal mesh was 24 522 for TAH-2D and 1 658 972 for TAH-3D. Note that for the TAF models (where a fracture is present), the number of mesh elements increases as the fracture is moved closer to the heat source, where the meshing parameters are finer compared with the outer domain.

The maximum difference in the absolute value of ΔT_b between the optimally meshed TAH-2D and MILS is 0.06 K. It occurs for medium groundwater flow in the matrix v_u = 0.05 m day^{-1}, and corresponds to a relative difference of 0.7 % (Figure 5.6 A). The relative difference in ΔT_b between TAH-2D and MILS is maximum when groundwater flow is fastest (v_u = 0.5 m day^{-1}). It is -2.6 %, with a corresponding difference in the absolute values of -0.05 K. In this case, the actual value of ΔT_b reaches 1.89 K for MILS.

For the 3D model, the absolute difference in ΔT_b between TAH-3D and MFLS (Figure 5.6 C) varies from -0.2 to -0.07 K for 0 and 0.5 m day^{-1} groundwater velocities. This corresponds to relative differences of 1 and 3.6 %. The largest relative difference occurs when groundwater flow in the matrix is fast (0.5 m day^{-1}). As shown in Figure 5.6 C, the relative difference can be further reduced by refining the mesh; however, the finer mesh also requires more time steps, a longer computational time and more computer memory.

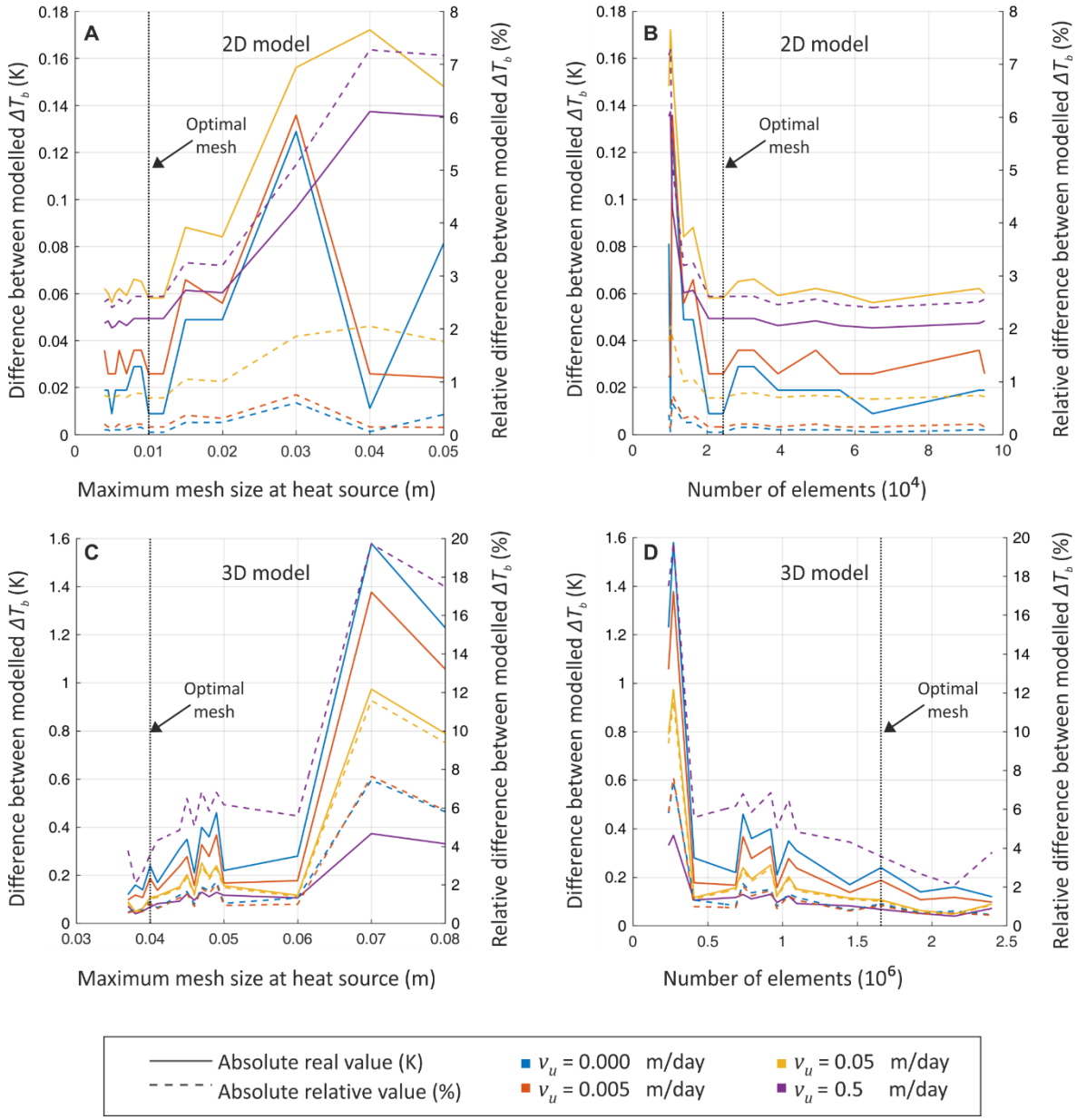

Figure 5.6 Differences between the modelled temperature change at the VBHE borehole wall ΔT_b as an absolute actual (K) and absolute relative value (%) versus maximum mesh size on heat source (A and C) and number of required mesh elements (B and D) for a range of Darcy velocities in undisturbed matrix v_u (marked by different colours). Dotted vertical line denotes the selected optimal meshing parameter (A, C) and corresponding number of mesh elements (B, D). Aquifer dispersivity is β_L ; β_T ; β_V = 2 ; 0.2 ; 0.2 m.

Model calculations were performed using High Performance Computing (HPC) facility IRIDIS, the fourth and fifth generation computer clusters at the University of Southampton. The computational time for TAH-3D with the optimal mesh is about 4 hours on a compute node (computer) of IRIDIS 4. Each job is run on a single IRIDIS 4 compute node, which has 16 CPUs and 64 GB of memory. The computation of the 3D numerical models (TAH-3D, TAF-3D) requires up to 50 GB of memory. 3D models with explicit modelling of working fluid circulation through

the U-pipe instead of a linear heat source (TAFpi and TAHpi) were calculated on IRIDIS 5 compute nodes with 40 CPUs and 192 GB of memory each, the model requires up to 120 GB of memory and the calculation time is up to 14 hours. The computation requirements of the 2D numerical models (TAH-2D, TAF-2D) are much smaller - up to 2 GB of memory with calculation time up to 2 minutes.

5.18.2 Criterion 2: Maximum differences between modelled temperature changes

Table 5.7 summarises the comparative criteria between numerical models with optimal mesh and the analytical solutions for 2D and 3D for four groundwater velocities v_u and for aquifer dispersivity, β_L = 2 m, β_T = 0.2 m (and β_V = 0.2 m for 3D model).

The maximum difference in temperature change ΔT_{max} between optimally meshed numerical model (TAH-2D and TAH-3D) and the corresponding analytical solution (MILS and MFLS) was checked for all time steps and for all tested x, y locations (in the case of the 3D model the horizontal plane was at the VBHE mid-depth z = 50 m). Table 5.7 summarises the comparison for 2D and 3D models for four groundwater velocities (from absent to fast flow), with aquifer dispersivity β_L ; β_T ; β_V = 2; 0.2; 0.2 m. The difference in ΔT_{max} for 2D varies from -0.05 K to -0.16 K ($\Delta T_{max}^{TAH_{2D}} - \Delta T_{max}^{MILS}$) depending on groundwater velocity. The highest difference in ΔT_{max} between TAH-2D and MILS occurs for the fastest groundwater flow of 0.5 m day^{-1}. It occurs at the VBHE wall for short initial times of up to 126 seconds from the start, where the actual ΔT_b is still small, 0.2 K.

The maximum difference in temperature change ΔT_{max} between TAH-3D and MFLS ranges from -0.41 K to -0.16 K ($\Delta T_{max}^{TAH_{3D}} - \Delta T_{max}^{MFLS}$) depending on groundwater velocity (Table 5.7). The largest difference occurs for no groundwater flow (v_u = 0 m day^{-1}), near the upstream VBHE wall at (x; y; z) = (-0.05; -0.0709; 50) m at long simulation time of 169 years.

In this case, the relative value of ΔT_{max} (-0.41 K) is -2 % (calculated as $\left(\Delta T_{max}^{TAH_{3D}} - \Delta T_{max}^{MFLS}\right)/\Delta T_{max}^{MFLS}$). The temperature change modelled using MFLS at the location of maximum ΔT_{max} (for v_u = 0 m day^{-1}) is 20.5 K.

5.18.3 Criteria 3: Differences between models in RMSE$_{max}$ and MAE$_{max}$

The maximum Root-Mean-Square Error RMSE_{max} was calculated as the maximum RMSE at all tested locations on the horizontal plane. RMSE_{xy} for each location was calculated comparing ΔT for all time steps. For 3D model this horizontal plane is at a depth of mid-length of the VBHE.

$$\mathrm{RMSE}_{max} = \max_{xy}\left(\mathrm{RMSE}_{xy}\right)$$

$$\mathrm{RMSE}_{xy}^{2D} = \sqrt{\frac{\sum_{n=1}^{N}\left(\Delta T_{xy,t_n}^{TAH_{2D}} - \Delta T_{xy,t_n}^{MILS}\right)^2}{N}} \qquad (5.28)$$

$$\mathrm{RMSE}_{xy}^{3D} = \sqrt{\frac{\sum_{n=1}^{N}\left(\Delta T_{xy,t_n}^{TAH_{3D}} - \Delta T_{xy,t_n}^{MFLS}\right)^2}{N}}$$

where RMSE_{xy} is RMSE calculated for location (x, y) for 2D or 3D, xy is one of 10000 tested locations on the horizontal plane, $\Delta T_{xy,t_n}^{model}$ is temperature change at location (x, y) for time t_n modelled using specified $model$, t_n is one of N calculated time steps (N = 128).

The reason why RMSE was calculated for each location separately and then taken the maximum was to identify locations with maximum error (difference between models).

Values of RMSE_{max} for 2D and 3D models for four groundwater flows with aquifer dispersivity, β_L; β_T; β_V = 2; 0.2; 0.2 m is shown in Table 5.7.

For TAH-2D, RMSE_{max}^{2D} varies between 0.03 and 0.06 K for groundwater velocities between 0 and 0.5 m day^{-1}. For TAH-3D, RMSE_{max}^{3D} varies between 0.3 and 0.07 K for groundwater velocities between 0 and 0.5 m day^{-1}. RMSE continues to reduce further for mesh size finer than the selected optimal for all groundwater velocities.

However, a finer mesh requires longer computational times. The model accuracy is satisfactory for all groundwater velocities for the selected optimal mesh M_s (when maximum mesh size at heat source is 0.04 m), Figure 5.6 C, D.

Like for RMSE, the maximum value of mean absolute error MAE_{max} was calculated as

$$\mathrm{MAE}_{max} = \max_{xy}\left(\mathrm{MAE}_{xy}\right)$$

$$MAE_{xy}^{2D} = \frac{\sum_{n=1}^{N}\left|\Delta T_{xy,t_n}^{TAH_{2D}} - \Delta T_{xy,t_n}^{MILS}\right|}{N} \tag{5.29}$$

$$MAE_{xy}^{3D} = \frac{\sum_{n=1}^{N}\left|\Delta T_{xy,t_n}^{TAH_{3D}} - \Delta T_{xy,t_n}^{MFLS}\right|}{N}$$

where MAE_{xy} is MAE calculated for location (x, y) for 2D or 3D.

For the 2D model for all time steps across all tested points varies between 0.03 K and 0.06 K for groundwater velocities between 0 and 0.5 m day^{-1}.

For TAH-3D $\mathrm{MAE}_{max}^{3\mathrm{D}}$, for all time steps at all tested points on the horizontal plane at a depth of the VBHE mid-length, varies between 0.2 and 0.07 K for groundwater velocities between 0 and 0.5 m day^{-1}.

Additionally, Table 5.7 lists the differences between the modelled extent of the +5 K, +2 K, +1 K and +0.5 K isotherms after 30 years of continuous VBHE operation (X_{5K}, X_{2K}, X_{1K} and $X_{0.5K}$) calculated as the maximum coordinate for these isotherms on the x-axis.

Table 5.7 Comparative criteria for model validation for four groundwater velocities v_u and for aquifer dispersivity β_L; β_T; β_V = 2; 0.2; 0.2 m (β_V only valid for 3D). Differences between models are calculated as the numerical model minus the analytical solution. Relative differences (%) are calculated as (TAH-2D - MILS) / MILS and in similar way for the 3D model. The maximum isotherm extents X_{5K}, X_{2K}, X_{1K} and $X_{0.5K}$ as well as ΔT_b are given after 30 years of continuous VBHE operation. ΔT_{max} , RMSE_{max} and MAE_{max} are calculated for all time steps and for all tested locations.

	TAH-2D				TAH-3D			
v_u (m day^{-1})	0	0.005	0.05	0.5	0	0.005	0.05	0.5
ΔT_b (K)	- 0.01	-0.03	-0.06	-0.05	- 0.2	-0.2	-0.1	-0.07
ΔT_b (%)	- 0.04	- 0.1	- 0.7	- 2.6	- 1.1	- 1.04	- 1.26	- 3.56
ΔT_{max} (K)	-0.05	-0.05	-0.11	-0.16	- 0.41	- 0.31	- 0.18	- 0.16
X_{5K} (m)	0.003	-0.01	-0.002	-	-0.1	-0.1	-0.01	-
X_{5K} (%)	0.03	-0.1	-0.5	-	-1.3	-1.9	-2.5	-
X_{2K} (m)	0.03	0.1	-0.03	-	-0.04	-0.14	-0.07	-
X_{2K} (%)	0.1	0.2	-0.5	-	-0.17	-0.34	-1.30	-
X_{1K} (m)	0.04	-0.04	-0.3	-0.004	0.2	-0.45	0.35	-0.05
X_{1K} (%)	0.1	-0.05	-1.1	-0.7	0.4	-0.6	1.3	-8.2
$X_{0.5K}$ (m)	0.02	-0.5	-1.4	-0.03	0.3	0.3	0.5	-0.05
$X_{0.5K}$ (%)	0.04	-0.4	-1.3	-0.9	0.6	0.3	0.5	-1.3
RMSE_{max} (K)	0.03	0.03	0.07	0.06	0.27	0.23	0.14	0.07
MAE_{max} (K)	0.03	0.03	0.06	0.06	0.24	0.20	0.13	0.07

5.19 Performance of numerical model compared with the analytical solution

5.19.1 Differences between modelled temperature change at the VBHE wall

There is no significant difference between the numerical model and the analytical solution in terms of temperature change at the borehole wall ΔT_b with time (Figure 5.7). For all tested groundwater velocities and for two dispersivity values, the numerical model results in both 2D and 3D match well with the corresponding analytical solutions.

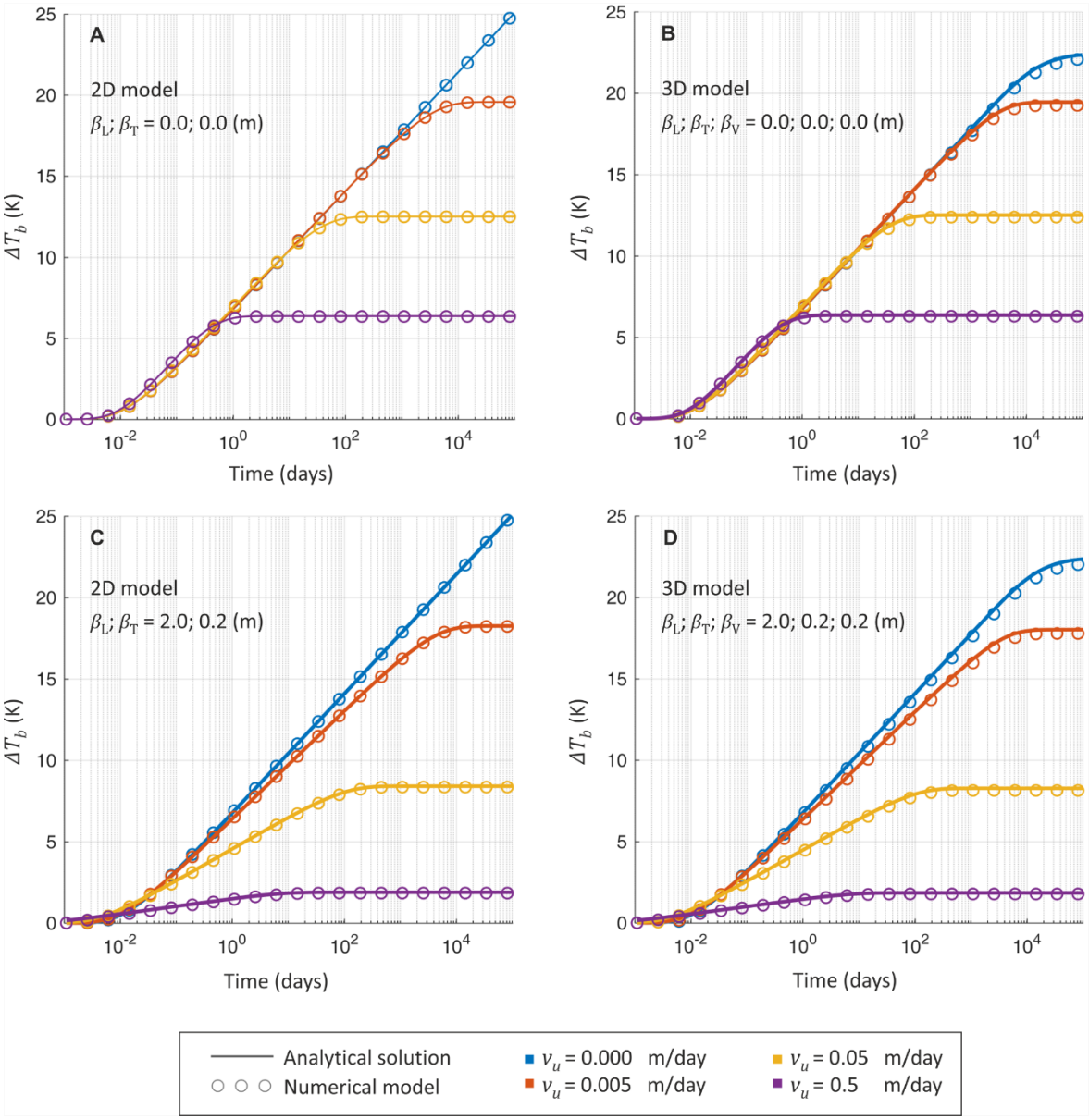

Figure 5.7 Temperature change at the VBHE wall (x = 0.05 m, y = 0 m, for 3D z = 50 m) for a range of groundwater velocities v_u versus time for the analytical solution and the numerical model for 2D (A, C) and 3D (B, D). Aquifer dispersivity (with subscripts L, T, V being longitudinal, transverse and vertical) $\beta_L; \beta_T; \beta_V$ is 0; 0; 0 m (A, B) and 2; 0.2; 0.2 m (C, D), where β_V is only relevant for the 3D model.

5.19.2 Differences between modelled temperature changes at other locations around VBHE

Figure 5.8 shows the difference between the numerical model and the analytical solution in terms of the temperature difference along the x-coordinate axis for 2D and 3D for fast groundwater flow (v_u = 0.5 m day^{-1}) for two values of aquifer dispersivity.

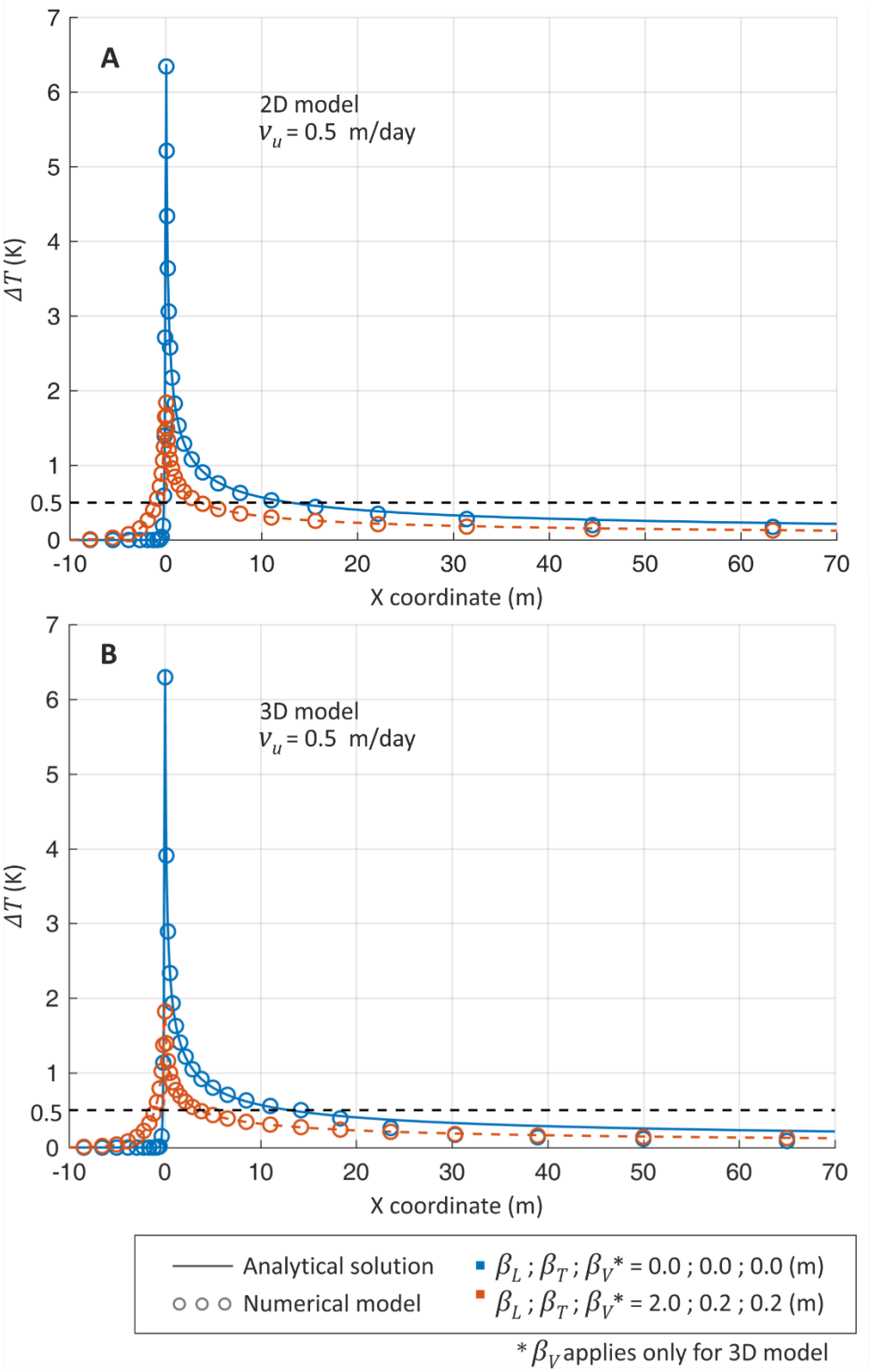

Figure 5.8 Temperature change ΔT along the x-coordinate axis (where x = 0 m is the location of the VBHE) after 30 years of continuous VBHE operation with and without aquifer dispersivity β_L, β_T, β_V and for fast groundwater flow of 0.5 m day^{-1} (v_u) for the analytical solution and the numerical models in 2D (A) and 3D (B). Dashed black line represents ΔT = 0.5 K.

For other tested groundwater flows (0, 0.005 and 0.05 m day^{-1}) the numerical model matched the analytical solution well; the results are not shown, for brevity. When groundwater flow is fast, the 3D numerical model result (TAH-3D)

underestimates the MFLS solution starting from 25 m downstream of the VBHE, especially for case with absent aquifer dispersivity. The 2D numerical model matches MILS relatively better. However, the discrepancy between the 3D model and the MFLS solution is small (i.e. no greater than -0.07 K for ΔT_b after 30 years of VBHE operation), and therefore acceptable for the purpose of the model. The x-coordinate extents of *the +0.5 K and higher isotherms* match the analytical solution well. The extent of isotherms for ΔT *smaller than 0.5 K* (Figure 5.8 B, below 0.5K line) is not of practical interest for VBHE thermal performance. These very small temperature changes were not considered in the further analysis of the VBHE performance.

Isotherms from the TAH-3D model were also compared with the analytical solution in the vertical direction. The comparative profiles of isotherms are illustrated for slow and medium groundwater flows in Figure 5.9. For all four groundwater flows the isotherms compare relatively well; there is only a small difference for medium and fast groundwater flows between the results for the extent of the +0.5 K isotherm.

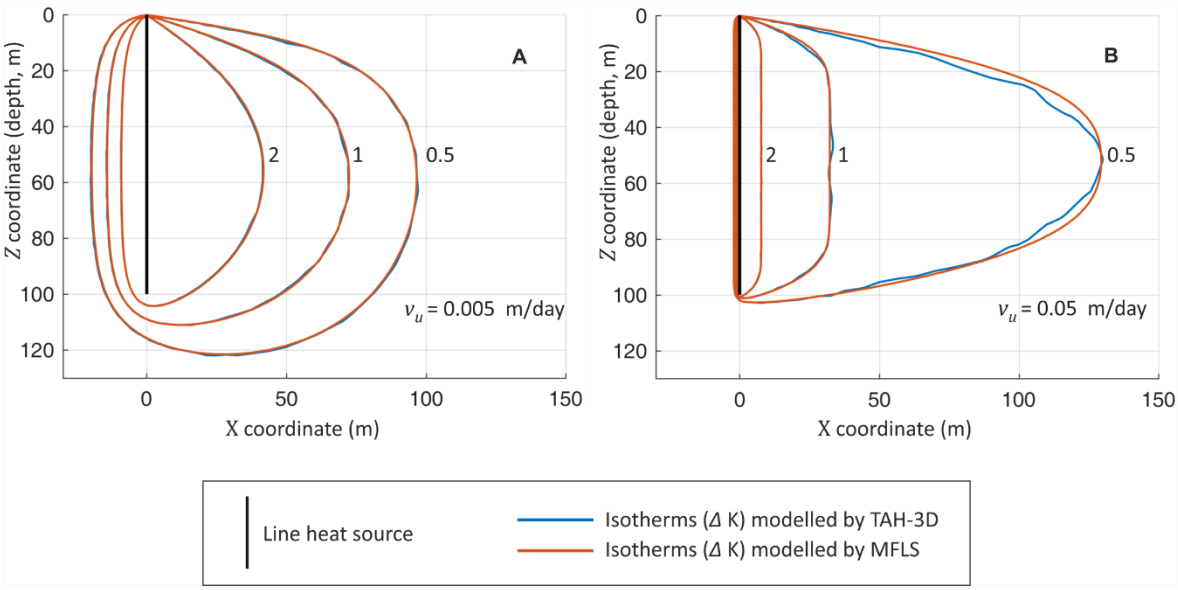

Figure 5.9 Profile view of isotherms of ΔT = 0.5, 1 and 2 K after 30 years of continuous VBHE operation for the numerical model (TAH-3D) and the analytical solution (MFLS) for groundwater velocity v_u = 0.005 m day^{-1} (A) and 0.05 m day^{-1} (B).

5.20 Key message

The numerical models TAH-2D and TAH-3D have been successfully validated against the corresponding analytical solutions (MILS and MFLS). The mesh has been optimised to account for accuracy, calculation speed and memory usage. The following criteria were used for the model validation:

1) The difference between the modelled temperature change at the VBHE wall ΔT_b;
2) The maximum difference between models in the temperature change calculated as a maximum at all tested locations for all calculated time steps ΔT_{max};
3) The differences between models in the calculated RMSE_{max} and MAE_{max};
4) The difference between the modelled maximum extent in x-coordinate of isotherms of ΔT = +5, +2, +1, +0.5 K, and isotherm shapes in plan (2D and 3D) and profile views (3D).

The comparison with the analytical solutions was carried out for two values of aquifer dispersivity and four values of groundwater velocity in the matrix (both in 2D and 3D).

As can be seen in Table 4.1, the largest difference between modelled temperature changes at the VBHE wall ΔT_b occurs for fast groundwater flow of 0.5 m day^{-1}). For TAH-2D it is -0.05 K (-2.6 %). The relative difference for TAH-3D is higher (-3.6 %), but its corresponding actual difference is only -0.07 K. For slower groundwater flows the difference in ΔT_b significantly reduces to -0.04 % for 2D and -1.13 % for 3D (in the absence of groundwater flow). In all cases, the numerical models give slightly lower ΔT_b than the analytical solution.

The largest actual temperature difference at any simulation time (up to 300 years) at any point for fast groundwater flow (0.5 m day^{-1}) was -0.16 K for both TAH-2D and TAH-3D. The largest actual difference for the 3D model occurs in the absence

of groundwater flow at times >100 years, but its relative value of -2 % is acceptable.

The accuracy of the 2D and 3D numerical models is satisfactory for the tested groundwater velocities. The conclusion is that both the 2D and 3D numerical models can be used as the base models to analyse the influence of a fracture on the thermal performance of a VBHE, which is discussed in the following chapters.

Chapter 6 The influence of a single fracture on a VBHE in 2D

6.1 Method

This chapter investigates the effects of a single fracture on the thermal performance of a VBHE installed in an aquifer. The thermal performance of a VBHE is expressed in terms of the temperature change at the VBHE wall and the resulting extent of the isotherms. The effects of different fracture parameters on the adjacent VBHE are considered using a 2D numerical model. The numerical model has two variants:

- **TAF-2D** –**T**hermal transport from a VBHE through an **A**quifer in the presence of a single vertical **F**racture in 2D.
- **TAH-2D** –**T**hermal transport through an **A**quifer with **H**omogeneous matrix. It differs from TAF-2D only in the aquifer being homogeneous, i.e. the fracture is absent. The moving infinite line source (MILS) analytical solution (Sutton *et al.* 2003; Diao *et al.* 2004) was used to optimise the mesh and for spatial and temporal validation of the TAH-2D model (Chapter 5).

In the single-parameter analysis, the numerical model was run with individual fracture parameters changed for each model run and the remaining parameters fixed to the base values. Both the base values of parameters and their ranges are given in Table 6.1. The thermal performance indicators for the VBHE are:

- temperature change at the VBHE wall ΔT_b,
- the maximum extent in x-coordinate of the +2 K isotherm X_{2K},
- time to stabilise ΔT_b and X_{2K} denoted as t_{Sb} and t_{S2K}

Both ΔT_b and X_{2K} are calculated after 30 years of continuous VBHE operation. The results in performance indicators are then compared with the results of the

TAH-2D model without fracture. The methods for single-parameter analysis are outlined in Figure 6.1.

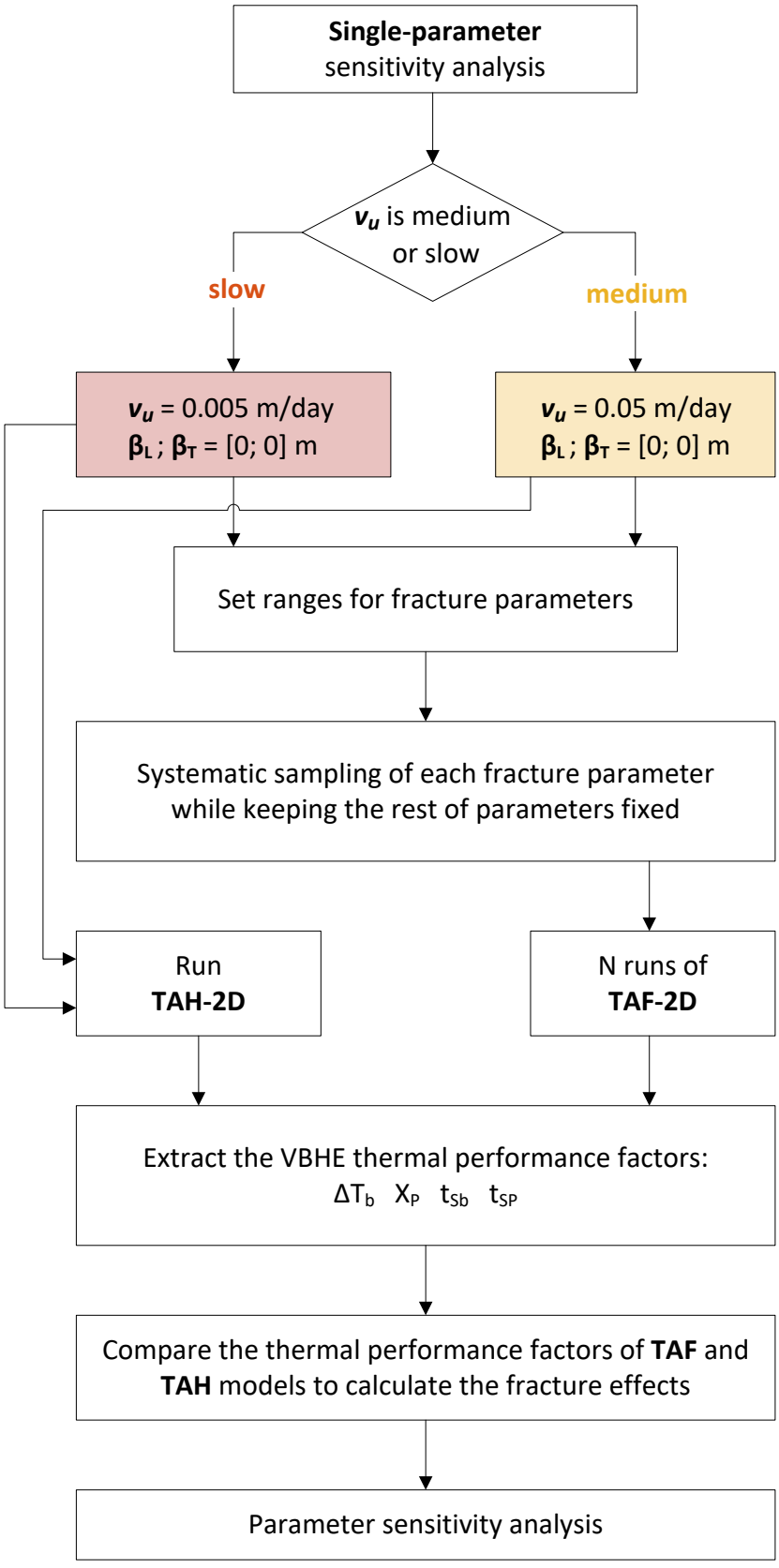

Figure 6.1 The methods outline of the single-parameter sensitivity analysis in 2D. Parameter combinations are in Table 6.1.

The single-parameter sensitivity analysis was done for two groundwater velocities in the undisturbed matrix v_u of 0.005 m day^{-1} (slow) and 0.05 m day^{-1} (medium) to test how the fracture effect will change for different groundwater velocities in the aquifer. The models used in this chapter have zero aquifer dispersivity β. Subsequently, the same fracture parameters (with the same ranges) were varied in a multi-parameter analysis to cover the full range of possible scenarios (discussed in Chapter 7). Effects of fast groundwater flow in the aquifer, and the effects of thermal dispersion are also examined in Chapter 7.

In every simulation, a check was made to ensure that the simulated velocities were low enough to maintain laminar flow. Reynolds numbers inside the fracture and in the matrix were calculated for each simulation to monitor compliance with the assumptions for Darcy's law. Darcy's law is valid as long as the flow remains laminar; Reynolds number Re based on average grain diameter does not exceed 10 (Bear 1988). Re is calculated using the representative length dimension d calculated according to Collins 1961 from (Bear 1988):

$$Re = \frac{vd}{\nu} \tag{6.1}$$

$$d = \sqrt{\frac{\kappa}{\epsilon}} \tag{6.2}$$

$$\nu = \frac{\mu}{\rho} \tag{6.3}$$

$$\kappa = \frac{K\mu}{\rho g} \tag{6.4}$$

Where Re is the Reynolds number (-), v is the Darcy velocity (m s^{-1}), ν is the kinematic viscosity of the fluid (m^2 s^{-1}), d is the representative length dimension (m), κ is the (intrinsic) permeability of porous material (m^2), ϵ is the porosity of porous material (-), μ is the dynamic viscosity of the fluid (kg m^{-1} s^{-1}), ρ is the density of the fluid (kg m^{-3}), K is the hydraulic conductivity of material (m s^{-1}), g is the acceleration due to gravity (m s^{-2}).

6.2 Model parameters

The base values for the fracture parameters were selected following initial manual trials which identified which values have a noticeable influence on the VBHE thermal performance parameters. The base values of fracture parameters are shown in Table 6.1. The fracture thickness was selected to be "moderately wide" (i.e. 0.005 m) based on the classification of fractures by openness (ISRM 1978). The selected base value for fracture length is 50 m. It reflects the mode from the fracture length distribution found by Hardebol *et al.* (2015) from investigation of the size distributions of fractures in a carbonate platform from Dolomites, Italy. The fracture shift S_f is specified along the orientation of a fracture (along the x coordinate) from a point at the fracture mid-length. The base value for fracture shift S_f is 0 m, i.e. the fracture is centred relative to VBHE. Fracture shift is positive if the shift is in the positive direction of x (downstream of the VBHE) (Figure 5.1). The fracture distance from the VBHE D_f is determined perpendicular to the line of the fracture. The base value of the fracture angle A_f is 0° meaning that fracture is parallel to the groundwater flow direction. Positive angle values mean that fracture is rotated in such a way that it is downstream of the VBHE.

Table 6.1 Base values of fracture parameters and their ranges used in the single-parameter sensitivity analysis.

Parameter	Symbol	Base value	Range (Number of steps)
Fracture rotation angle relative to x-axis direction	A_f	0° (parallel to the x-axis)	-90° to 90° (13)
Fracture aperture (thickness)	W_f	0.005 m	0.1 mm to 25 mm (22)
Fracture distance from the VBHE wall	D_f	1 m	0.5 m to 40 m (30)
Shift of fracture mid-length point along its length (parallel to its direction),	S_f	0 m (centred with VBHE)	-160 m to 160 m (29)
Fracture length	L_f	50 m	1 m to 200 m (29)
Ratio of hydraulic conductivity of aquifer material to fracture material	R_K	10000	10 to 1000000 (16)

R_K was sampled on a logarithmic scale because the range for this parameter goes over several orders of magnitude. Using a logarithmic scale ensures that sampling evenly covers each order of magnitude of the sampled range.

In this analysis, the grout of the VBHE in numerical model TAH-2D and TAF-2D is assumed to be impermeable (its material properties are described in Table 5.2), unless stated otherwise. The TAH-2D model with impermeable grout is compared with the analytical solution MILS in Figure 6.2. The presence of hydraulically impermeable grout results in a difference with the analytical solution only for fast groundwater flow (0.5 m day^{-1}) for very small simulation times.

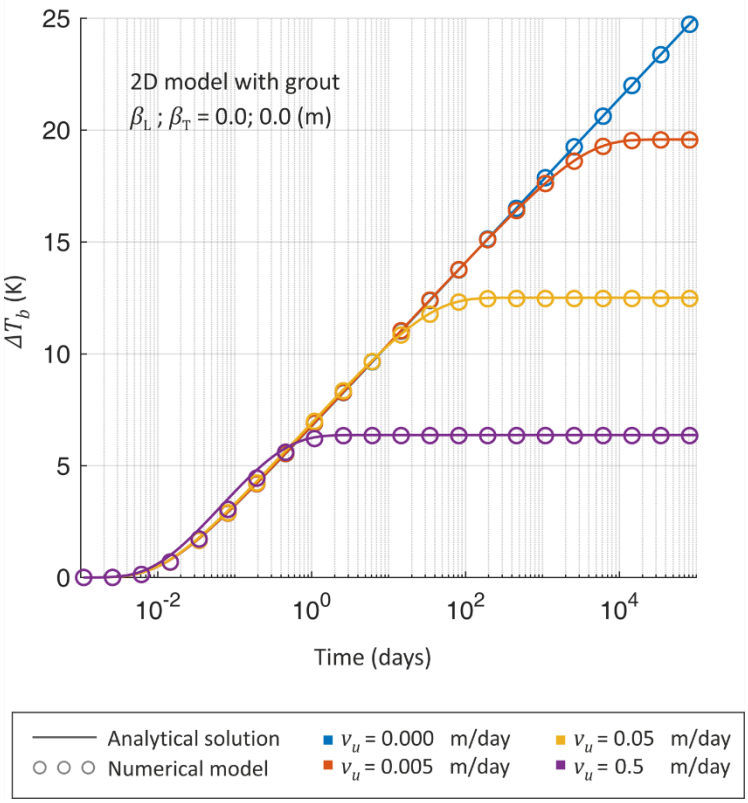

Figure 6.2 Temperature change at the VBHE wall ΔT_b for four groundwater velocities v_u versus time. The analytical solution is MILS, and the numerical model is TAH-2D with impermeable grout. Both models are in 2D.

6.3 Presentation of the results

The results are presented in terms of the performance indicators for the VBHE:

- temperature change at the VBHE wall ΔT_b,
- the maximum extent in x-coordinate of the +2 K isotherm X_{2K},
- time to stabilise ΔT_b and X_{2K} denoted as t_{Sb}, t_{S2K}.

ΔT_b and X_{2K} were determined after 30 years of continuous operation of the VBHE. ΔT_b was determined on the downstream side of the VBHE (i.e. at x = 0.05 m, y = 0 m). Note that if a fracture is present, the isotherms may be not symmetrical along y-axis and the point for the maximum extent of the +2 K isotherm may have a non-zero y-coordinate.

These criteria were estimated for each set of fracture parameters and for different groundwater velocities in undisturbed aquifer matrix v_u. The results were compared with the TAH-2D model (a model without a fracture). In the results that

follow, relative performance indicators R are reported, i.e. the relative difference between the TAF-2D and TAH-2D models:

$$R = \frac{F^{TAF_{2D}} - F^{TAH_{2D}}}{F^{TAH_{2D}}} \tag{6.5}$$

where F is the performance indicator of interest, for example ΔT_b, and the superscripts represent the models.

The final section discusses examples of how a fracture can alter the shape of the isotherm.

6.4 Results of the single-parameter analysis

6.4.1 Effect on temperature change at the VBHE wall

6.4.1.1 Effect of volumetric flow rate in the fracture

The relative difference between models TAH-2D and TAF-2D in ΔT_b is shown in Figure 6.3 for varying fracture parameters K_f, W_f, L_f and A_f. In all cases ΔT_b is reduced because the fracture increases thermal transport from the VBHE. Each fracture parameter reduces ΔT_b differently depending on the groundwater velocity in the matrix v_u.

If groundwater flow in the matrix is slow (0.005 m day^{-1}), the fracture reduces ΔT_b thus improving the thermal performance of the VBHE. The fracture cooling effect is more significant for larger values of fracture length L_f, hydraulic conductivity K_f and aperture W_f. Also, the fracture effect is more significant when the fracture is parallel to the groundwater flow direction (A_f = 0°).

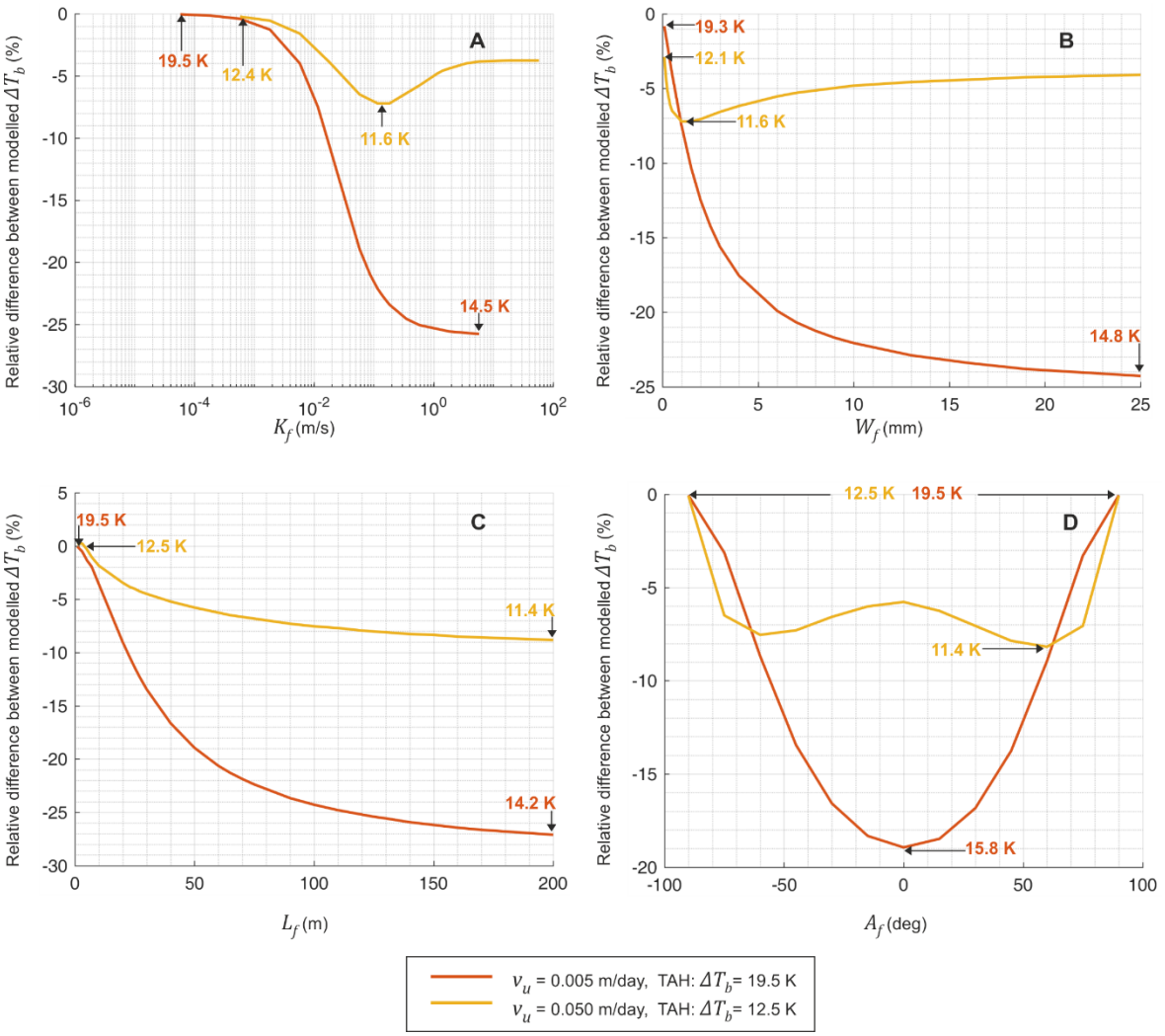

Figure 6.3. Relative difference in temperature change at the VBHE wall ΔT_b after 30 years of continuous operation between models TAF-2D and TAH-2D for (A) Changing hydraulic conductivity in the fracture K_f, (B) Fracture aperture W_f, (C) Fracture length L_f and (D) Fracture rotation relative to x-axis A_f.

The effects of a fracture in a matrix with medium groundwater flow of 0.05 m day^{-1} differ from the results for slow groundwater flow. It is still a beneficial effect as the fracture enhances the thermal performance of the VBHE by reducing ΔT_b. However, the magnitude of this effect does not consistently increase with the increase in the fracture aperture W_f and the hydraulic conductivity K_f. Also, when the fracture is parallel to groundwater flow direction (A_f = 0°), the fracture effect on the VBHE is not as significant compared with other fracture angles.

These patterns of fracture effects on the VBHE are due to the change in the volumetric flow rate inside fracture O_f and depend on the ratio of hydraulic permeabilities of the matrix and fracture R_K. The change in O_f is shown in Figure

6.4 and Figure 6.5 for the same four fracture parameters. O_f is higher with increase in W_f, L_f and K_f. O_f reaches the highest value when the fracture is rotated parallel to the groundwater flow direction (A_f = 0°, Figure 6.5 B). The fracture serves as a preferable fast flow route for groundwater. A fracture with high O_f takes groundwater from the surrounding matrix, and therefore it influences velocities in the surrounding matrix. In addition to a change in O_f, Figure 6.4 and Figure 6.5 show how the groundwater velocity changes inside and near the fracture v_f. Increase in O_f reduces the groundwater velocities in the matrix around the mid-length of the fracture, e.g. at the VBHE wall v_b.

Whatever the value of the fracture hydraulic conductivity K_f, the hydraulic conductivity in the matrix K_m determines how much water can go into the fracture in response to the change in the hydraulic gradient. Therefore, the O_f for slower groundwater flow in Figure 6.4 A is much lower than for medium groundwater flow.

With increasing fracture length (Figure 6.5 A), the maximum groundwater velocity inside the fracture v_f and O_f both increase due to additional lateral inflow of groundwater into the fracture. The slowest groundwater velocity in the matrix around the fracture mid-length (v_b) occurs when L_f is about 10 m rather than the maximum value. This is because the increase in O_f is achieved by lateral flow of groundwater into and from the fracture, which is distributed along the fracture length. Note that the TAF-2D model used for this plot is without grout for the heat source, so that the groundwater velocity determined at the VBHE wall downstream is representative of the mean value around the VBHE wall.

While the increase in O_f is greater for the faster groundwater velocity, the relative impact of the fracture on the ΔT_b is greater for slower groundwater velocities. This is because at a higher groundwater flow, there is a smaller benefit from the increase in the thermal transport due to the fracture.

Note that for fracture angles +/-90° the velocity in the fracture v_f is zero and cannot be shown on the logarithmic scale in Figure 6.5 B.

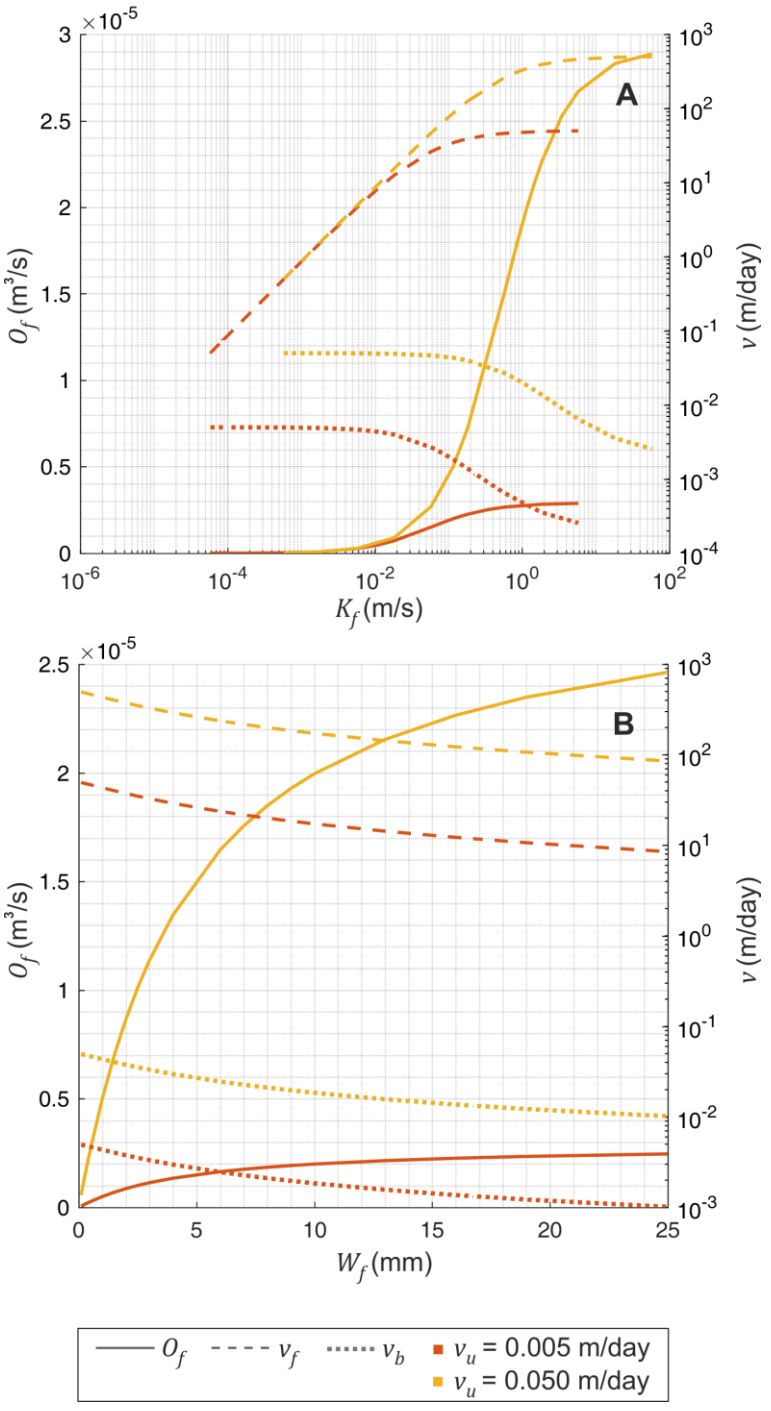

Figure 6.4 Volumetric flow rate in the fracture O_f per unit depth versus (A) the fracture hydraulic conductivity K_f and (B) the fracture aperture W_f for two groundwater velocities in the undisturbed matrix v_u. v_f is the maximum Darcy velocity in the fracture, v_b is Darcy velocity at the location where ΔT_b was calculated.

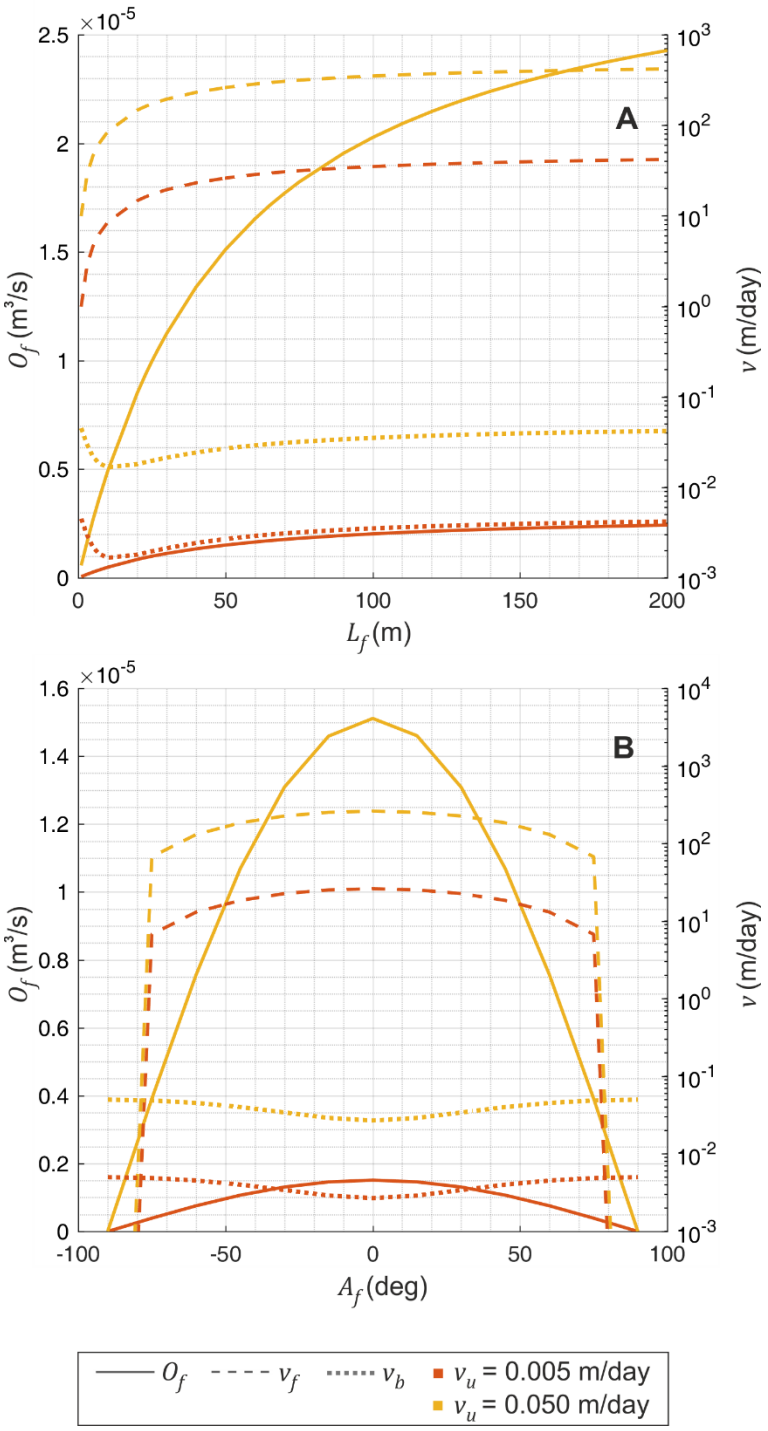

Figure 6.5. Volumetric flow rate in the fracture O_f per unit depth versus (A) fracture length L_f and (B) fracture rotation with respect to matrix groundwater flow direction (x-axis) (A_f) for two groundwater velocities in the undisturbed matrix v_u. v_f is the maximum Darcy velocity in the fracture, v_b is Darcy velocity at the location where ΔT_b was calculated.

6.4.2 Effect of fracture position

Figure 6.4 and Figure 6.5 showed that as the fracture takes water from the surrounding matrix, the velocity of groundwater in the matrix close to the fracture reduces. The effect of the fracture on the surrounding groundwater velocities is

explained using the following case studies for varying fracture distance from the VBHE. Each case is tested for slow and medium groundwater flow in the undisturbed matrix.

In the first case the fracture is close to the VBHE (D_f = 1 m, Figure 6.6 A) and in the second case it is further away from the VBHE (D_f = 10 m, Figure 6.6 B). All other model parameters are kept and the same at base values (Table 6.1). The fracture that is closer to the VBHE (Figure 6.6 A) effectively increases heat transport from the VBHE. This significantly reduces the temperature change at the borehole wall and reduces the spatial extent of the +5 K isotherm, while it extends the isotherms of smaller ΔT (+2 K, +1 K, +0.5 K), see table enclosed in Figure 6.6. The fracture that is further away from the VBHE (D_f = 10 m, Figure 6.6 B) is less effective.

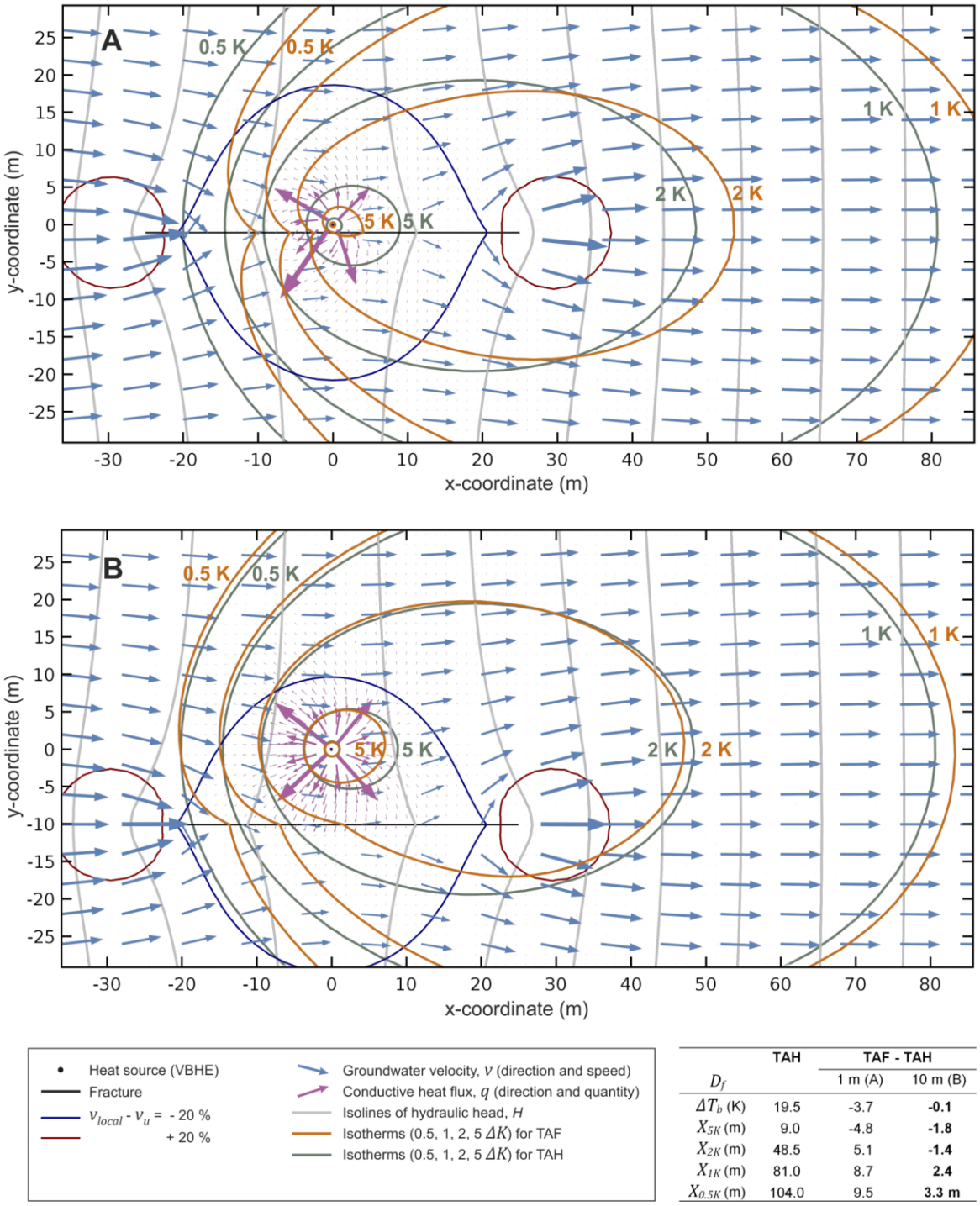

D_f	TAH	TAF - TAH	
		1 m (A)	10 m (B)
ΔT_b (K)	19.5	-3.7	**-0.1**
X_{5K} (m)	9.0	-4.8	**-1.8**
X_{2K} (m)	48.5	5.1	**-1.4**
X_{1K} (m)	81.0	8.7	**2.4**
$X_{0.5K}$ (m)	104.0	9.5	**3.3 m**

Figure 6.6 Groundwater flow vectors, heat flux vectors and isotherms for a VBHE after 30 years of continuous operation installed near a vertical flowing fracture, where (A) fracture distance D_f = 1 m and (B) D_f = 10 m away from the VBHE. Groundwater velocity in the undisturbed matrix v_u = 0.005 m day^{-1}.

A similar case, but when groundwater flow in the matrix is faster, is shown in Figure 6.7 (D_f = 1 m in Figure 6.7 A and D_f = 10 m in Figure 6.7 B). All other model parameters are the same. The fracture that is closer to the VBHE (Figure 6.7 A) effectively increases heat transport from the VBHE. This significantly reduces the

temperature at the borehole wall and reduces the spatial extent of the isotherms of interest (see table enclosed in Figure 6.7). The fracture that is further away from the VBHE (Figure 6.7 B) affects mainly the local groundwater flow velocities near the VBHE; the thermal transport by the fracture is less apparent. In these examples, where the VBHE was centred on the fracture mid-length, the presence of the fracture slowed down the groundwater velocities in the location of the VBHE (see differences in local groundwater velocities caused by the fracture in Figure 6.7). This increases the extent of isotherms with small ΔT (e.g. +2 K isotherm in Figure 6.7, which is small enough to be located in the affected area), as well as ΔT_b compared with the results for the scenario without a fracture (see Table enclosed in Figure 6.7).

In conclusion, for medium groundwater flow of 0.05 m day^{-1}, the dominant fracture effect can either be cooling of the VBHE (increased thermal transport) or change in local groundwater velocities (in this case slowing down), thereby changing the apparent thermal conductivity (ATC, in this case reducing).

For the results presented in Figure 6.3, the fracture distance from the VBHE is 1 m. At this close position, the fracture increases thermal transport from the VBHE, thus decreasing ΔT_b. However, if the VBHE is further from the fracture, then the slowed local groundwater flow at the VBHE leads to an increase in ΔT_b compared with the homogeneous case as is illustrated in Figure 6.7. The effect of D_f on the fracture influence on ΔT_b is systematically studied in Figure 6.8.

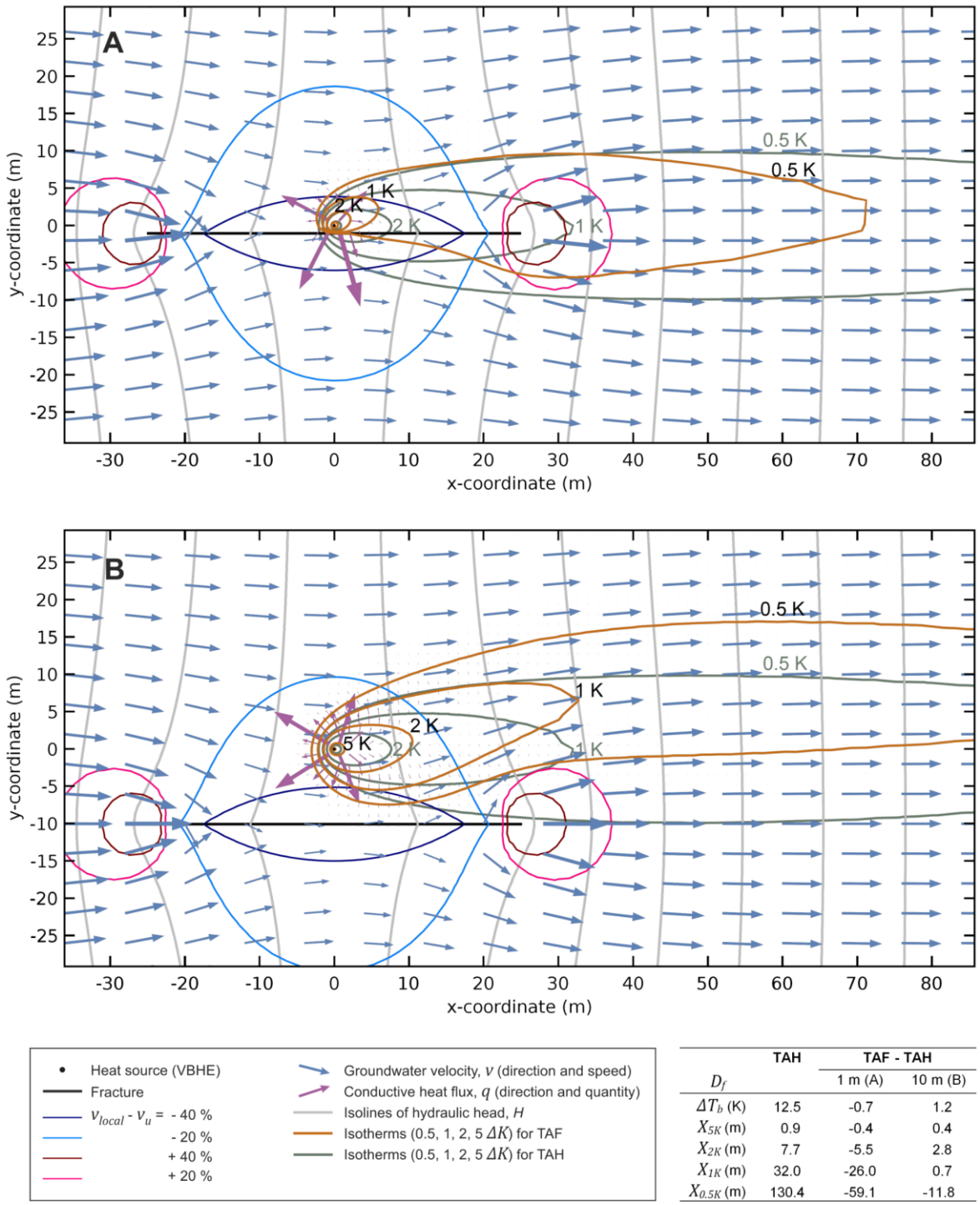

D_f	TAH	TAF - TAH	
		1 m (A)	10 m (B)
ΔT_b (K)	12.5	-0.7	1.2
X_{5K} (m)	0.9	-0.4	0.4
X_{2K} (m)	7.7	-5.5	2.8
X_{1K} (m)	32.0	-26.0	0.7
$X_{0.5K}$ (m)	130.4	-59.1	-11.8

Figure 6.7. Groundwater flow vectors and temperature contours for a vertical borehole heat exchanger (VBHE) after 30 years of continuous operation installed near a vertical flowing fracture, where fracture distance (D_f) is 1 m (A) and 10 m (B) away from the VBHE. Groundwater flow in undisturbed matrix, v_u (far away from the fracture) is 0.05 m day^{-1}. Table gives the difference between models (TAF-2D – TAH-2D) for VBHE performance parameters (ΔT_b and extent of isotherms) for two values of D_f.

6.4.2.1 Effects of the fracture distance from the VBHE in an aquifer with slow groundwater flow

The fracture effects for changing D_f are shown in Figure 6.8 for performance indicator ΔT_b (temperature change at the VBHE wall after 30 years of continuous operation) slow (0.005 m day^{-1}) and medium (0.05 m day^{-1}) groundwater flow in the matrix. The influence of the fracture distance from the VBHE D_f is discussed for cases when the VBHE is centred with the fracture (S_f = 0 m).

The effects of the fracture distance for cases when the VBHE is not centred with the fracture mid-length, but rather is shifted parallel to the fracture (S_f varies) are discussed in the Appendix E to analyse the effects of faster local groundwater velocities around the fracture edges on the thermal performance of the VBHE. The areas of the increased local groundwater velocities around the fracture edges are shown in Figure 6.7.

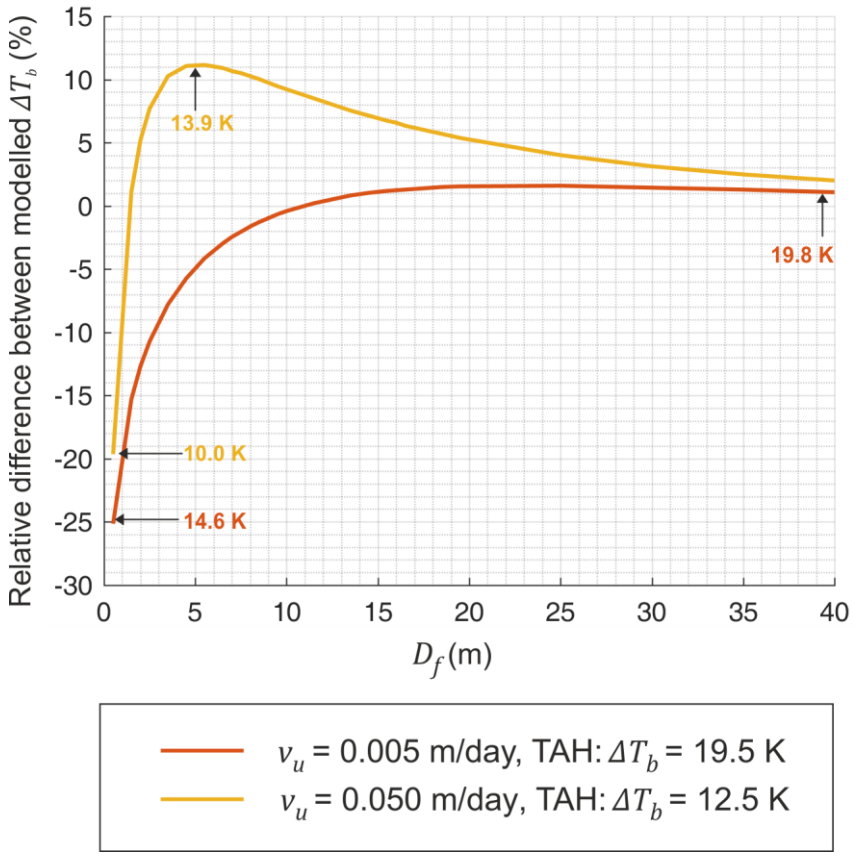

Figure 6.8. Relative difference $\left(\Delta T_b^{TAF} - \Delta T_b^{TAH}\right)/\Delta T_b^{TAH}$ in temperature change at the VBHE wall after 30 years of continuous operation.

The result in Figure 6.8 for slow groundwater flow in the undisturbed matrix (v_u = 0.005 m day^{-1}) shows that compared with the scenario without fracture there is a reduction in ΔT_b when the fracture is close to the VBHE (D_f = 0.5 to 10 m away). However, for D_f > 14 m ΔT_b is slightly higher for the scenario with fracture (TAF-2D). This fracture effect diminishes as the fracture is moved further away from the VBHE (D_f > 30 m). When the matrix groundwater flow is slow (v_u = 0.005 m day^{-1}) the fracture does not significantly reduce the local groundwater velocities near the VBHE compared with its undisturbed value. Thus, a nearby fracture is beneficial to the VBHE installed in an aquifer with slower groundwater flow when the fracture distance is relatively small (i.e. D_f from 0.5 to 9 m) (Figure 6.8). For cases with slower groundwater flow a fracture near the VBHE is more beneficial for thermal performance of the VBHE than for the cases with identical D_f but with faster groundwater flow in the matrix (Figure 6.8). This is because a nearby fracture increases thermal transport from the VBHE installed in a matrix with slower groundwater flow. Therefore, in these cases, a nearby fracture significantly reduces ΔT_b compared with the homogeneous case (TAH-2D).

In a matrix with slow groundwater flow, a fracture that is further away from the VBHE (12 m to 40 m away, Figure 6.8 A) also slightly increases ΔT_b (by 0.3 K) compared with TAH-2D. For these larger fracture distances, while the fracture is less effective in transporting heat from the VBHE, it is still able to reduce the local groundwater velocities in the area of the VBHE (for example, for D_f = 40 m by about 5 % from the undisturbed value 0.005 m day^{-1}). If the fracture distance from the VBHE is increased further, this effect becomes insignificant as well.

6.4.2.2 Effects of the fracture distance from the VBHE in an aquifer with medium groundwater flow

For medium groundwater flow v_u = 0.05 m day^{-1} the fracture improves thermal performance of the VBHE (i.e. reduces ΔT_b) only when it is located very close to the VBHE (D_f < 1.5 m). Figure 6.8 shows that for increasing fracture distance D_f the cooling effect of the fracture decreases, and the position of the borehole in the

region of slow v_u becomes more important, leading to an increase in ΔT_b. Thus, the presence of the fracture worsens the thermal performance of the VBHE (increases ΔT_b). The maximum increase in ΔT_b due to the presence of the fracture for tested scenarios is 1.4 K. However, the effect of the fracture diminishes as it is moved further away from VBHE. The relative differences in ΔT_b between TAH-2D and TAF-2D when D_f = 40 m are 2 % and 3 %. As was discussed in the case study (Figure 6.7), reduced Darcy velocity due to a fracture near the VBHE (which is located close to the fracture mid-length) reduces the local ATC, and hence reduces thermal transport. The consequence for a matrix with medium groundwater flow of 0.05 m day^{-1} can be a significant increase in ΔT_b (Figure 6.8) relative to the TAH-2D model.

6.4.3 Time to stabilise temperature change at the VBHE wall

The relative difference between models in time needed to stabilise the temperature change at the VBHE wall t_{Sb} (Figure 6.9) follows a similar pattern as for the change in temperature at the borehole wall ΔT_b (Figure 6.3) for every tested fracture parameter. For cases when the fracture significantly slowed the groundwater velocities around the VBHE, the time t_{Sb} to stabilise ΔT_b was significantly increased relative to the scenario without fracture (Figure 6.9, A and B). This is consistent with Figure 4.8 that shows how t_{Sb} reduces with increasing groundwater velocity in a homogeneous aquifer.

With increasing fracture length L_f, the ΔT_b is more effectively cooled by the fracture (Figure 6.3). However, at certain fracture lengths (L_f from 10 to 50 m, Figure 6.9 C) the slowed groundwater velocities near the VBHE influence t_{Sb}. The slower the local groundwater flow is, the longer t_{Sb} is. As was shown in Figure 6.5, when fracture length L_f is greater than about 50 m, the groundwater velocity at the VBHE approaches the undisturbed value. However, the volumetric flow rate inside fracture O_f continues to increase for longer fractures. This significantly reduces t_{Sb} as can be seen in Figure 6.9 C.

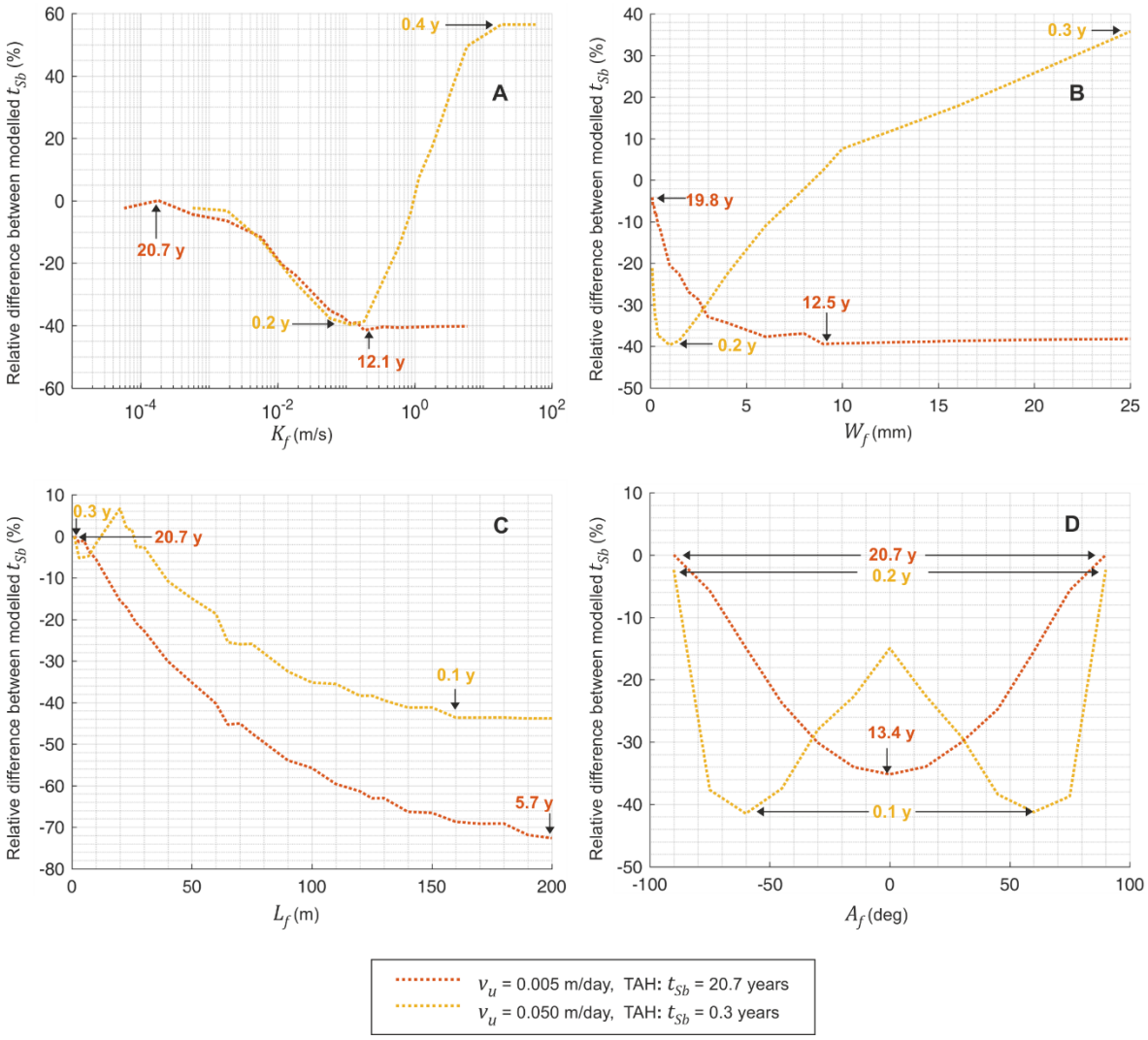

Figure 6.9 Relative difference in time to stabilise the temperature change at the VBHE wall $\left(t_{Sb}^{TAF_{2D}} - t_{Sb}^{TAH_{2D}}\right)/t_{Sb}^{TAH_{2D}}$ for (A) changing hydraulic conductivity in the fracture K_f, (B) fracture aperture W_f, (C) fracture length L_f and (D) fracture rotation relative to groundwater flow direction A_f. Lines are annotated with the maximum and minimum t_{Sb} for the TAF-2D model. t_{Sb} values for the TAH-2D model are in the legend.

Fracture distance from the VBHE D_f influences t_{Sb} (Figure 6.10) similarly to ΔT_b (Figure 6.8). Only the relative values for t_{Sb} are more significant. The greater flow rates allow for faster stabilisation of ΔT_b due to presence of a nearby fracture; however, it also allows for significantly slower stabilisation time (compared with the TAH-2D model) when the fracture is further away from the VBHE and its cooling effect is diminished. It should be noted that the fracture influence on the absolute value of t_{Sb} for slow groundwater in the matrix can be significant. Figure 6.10 (red line) shows how the change in fracture distance from the VBHE D_f

changes t_{Sb} relative to TAH-2D: it reduces t_{Sb} by 7 years when the fracture is close and increases t_{Sb} by 2 years when the fracture is far away.

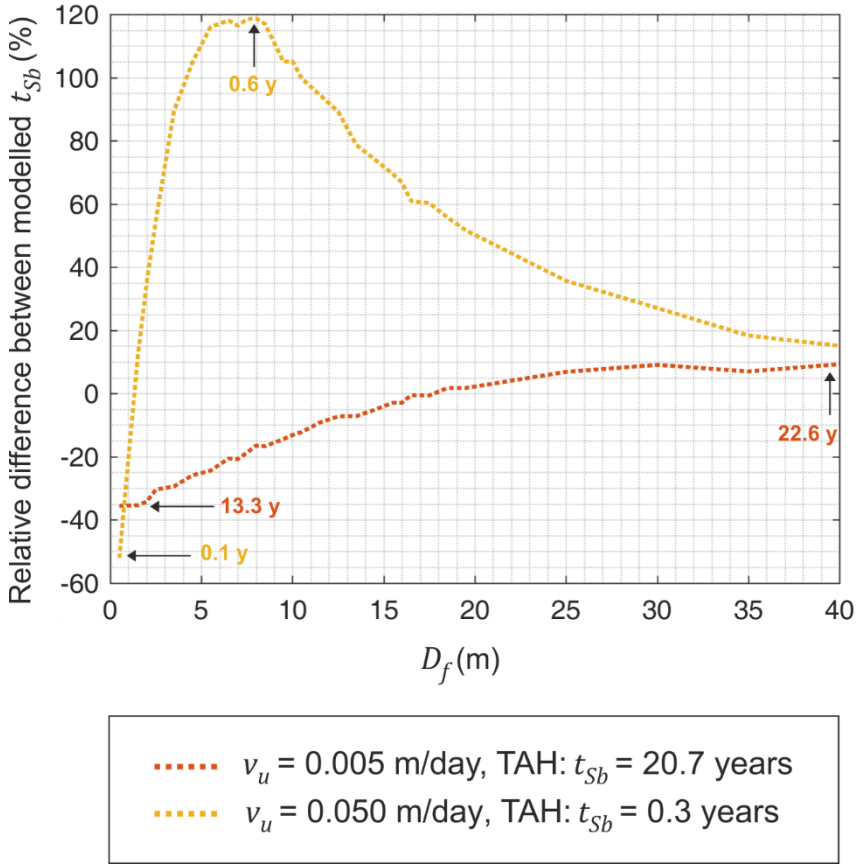

Figure 6.10 Relative difference in time to stabilise temperature change at the VBHE wall t_{Sb} between TAH-2D and TAF-2D models $\left(t_{Sb}^{TAF_{2D}} - t_{Sb}^{TAH_{2D}}\right)/t_{Sb}^{TAH_{2D}}$ for different distances of fracture from the VBHE D_f. Lines are annotated with the maximum and minimum t_{Sb} for the TAF-2D model. t_{Sb} values for the TAH-2D model are in the legend.

6.4.4 Extent of the +2 K isotherm

In a homogeneous aquifer, the longitudinal extent of the +2 K isotherm X_{2K} has a non-linear dependence on groundwater flow velocity v_u (Figure 6.11). As v_u increases the extent of the +2 K isotherm X_{2K} first increases, but then decreases, as discussed in Chapter 4.

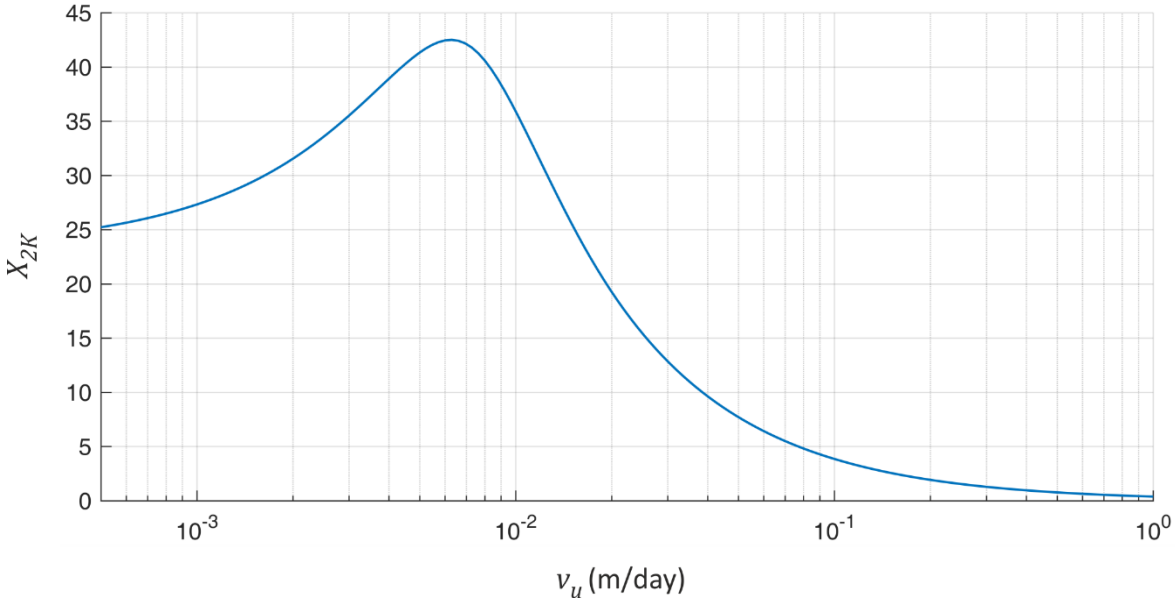

Figure 6.11 Longitudinal extent (x-coordinate) of +2 K isotherm X_{2K} produced by a VBHE installed in an aquifer with various groundwater flows v_u after 30 years of continuous operation. Zero aquifer dispersivity β is assumed. Modelled using MFLS, parameters are listed in Table 3.1.

Figure 6.12 shows the response of X_{2K} to the changes in the fracture hydraulic conductivity K_f (A), width W_f (B), length L_f (C) and angle A_f (D). Results are shown for two groundwater flows v_u. When a fracture is present in the matrix with medium groundwater flow, the isotherm extent X_{2K} will decrease, in some cases substantially (Figure 6.12). However, for slower groundwater flow, X_{2K} will first increase and then decrease as the volumetric flow rate in the fracture O_f increases with change in individual fracture parameter (see Figure 6.4 and Figure 6.5). For slow v_u, the fracture extends the +2 K isotherm X_{2K} by transporting the heat from the VBHE wall thus reducing ΔT_b (Figure 6.3). For cases when K_f and L_f are large (Figure 6.12, A and C), the volumetric flow rate in the fracture O_f is high enough to

reduce X_{2K}. For example, when L_f = 120 m, the +2 K isotherm extent X_{2K} is at its longest, and it starts to shrink when the fracture length L_f is increased further, i.e. when O_f is increased.

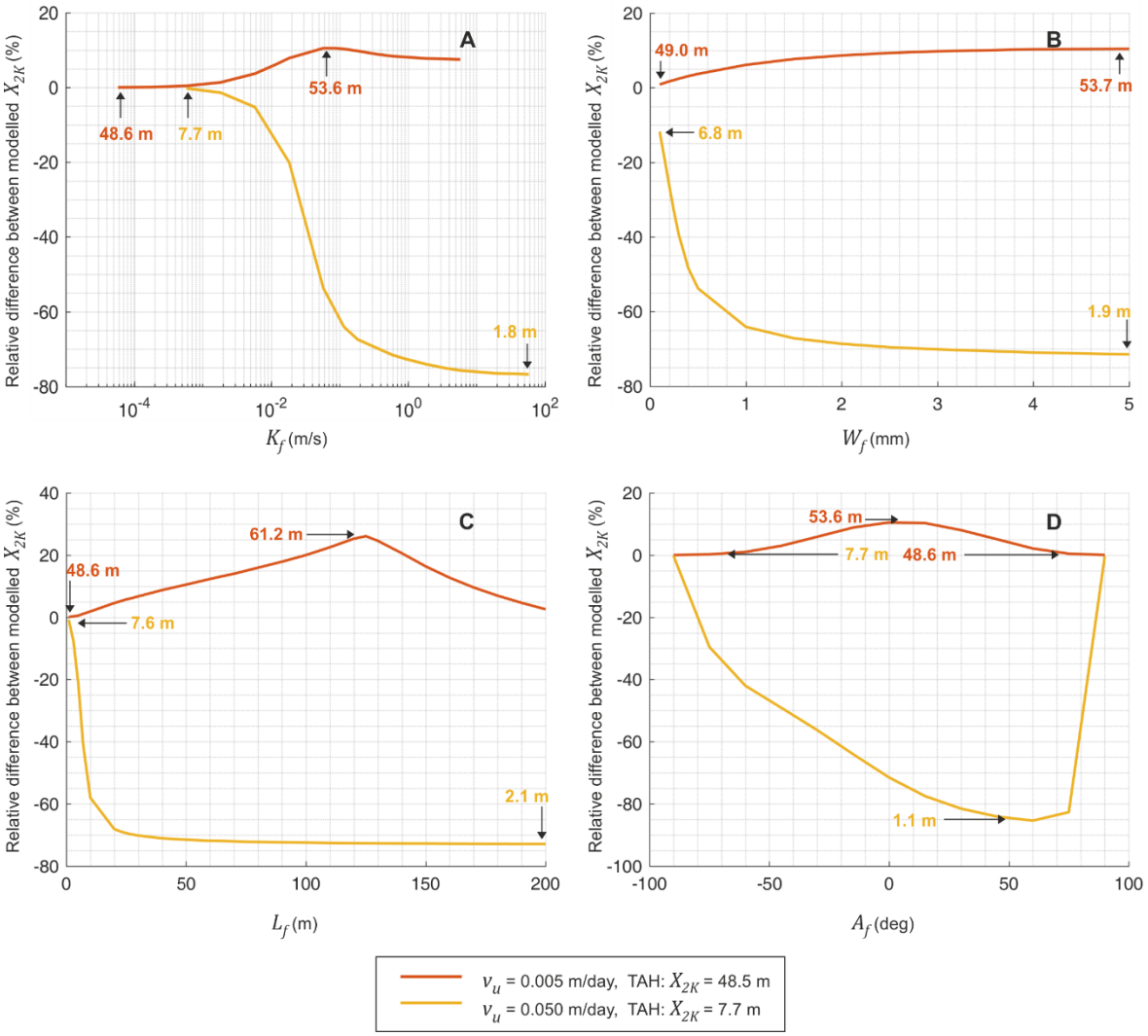

Figure 6.12 Relative difference between TAF-2D and TAH-2D models in longitudinal extent of the +2 K isotherm after 30 years of continuous VBHE operation $\left(X_{2K}^{TAF_{2D}} - X_{2K}^{TAH\_2D}\right)/X_{2K}^{TAH_{2D}}$ for different values of (A) fracture hydraulic conductivity K_f, (B) fracture thickness W_f, (C) fracture length L_f and (D) fracture angle to direction of groundwater flow A_f. Lines are annotated with the maximum and minimum X_{2K} for the TAF-2D model. The value of X_{2K} for the TAH-2D model are in the legend.

Figure 6.13 shows results for the maximum extent in x-coordinate for the +2 K isotherm X_{2K} depending on the fracture distance from the VBHE D_f after 30 years of continuous VBHE operation. The results for slow groundwater flow v_u = 0.005 m day^{-1} show that X_{2K} compared with TAH-2D is extended when the fracture is close to the VBHE (D_f < 5 m). This is because fracture cools down the VBHE wall,

but the volumetric flow in the fracture is not enough to reduce $X_{2K,}$ so the heat is advected downstream by the fracture, which effectively takes heat from the VBHE. Note that slow groundwater flow in the matrix v_u causes a longer X_{2K} (for TAH-2D it is 48.5 m, compared with 8 m for medium groundwater flow). Therefore, the presented relative model differences in X_{2K} due to fracture are not as significant as for the case with medium groundwater flow of 0.05 m day^{-1} in the matrix.

When groundwater flow is faster (v_u = 0.05 m day^{-1}) the fracture significantly reduces X_{2K} compared with TAH-2D (by up to -85 %) for D_f < 4 m. However, for cases when D_f > 4 m, the presence of a fracture increases X_{2K}. The maximum increase in X_{2K} due to the presence of a fracture for tested scenarios with v_u = 0.05 m day^{-1} is about +3 m (+37 %, when D_f = 10 m). This is because if the fracture is close (0.5 m away) it effectively cools down the +2 K isotherm and advects groundwater with lower temperatures. If the fracture is 10 m away its cooling effect is weaker than its effect on local groundwater velocities around the VBHE wall. The +2 K isotherm extent X_{2K} is short enough to fall into the zone of significantly reduced groundwater velocities. Therefore, the extent of the +2 K isotherm increases. The fracture effect diminishes as the fracture is moved further away from the VBHE (D_f > 35 m, Figure 6.13).

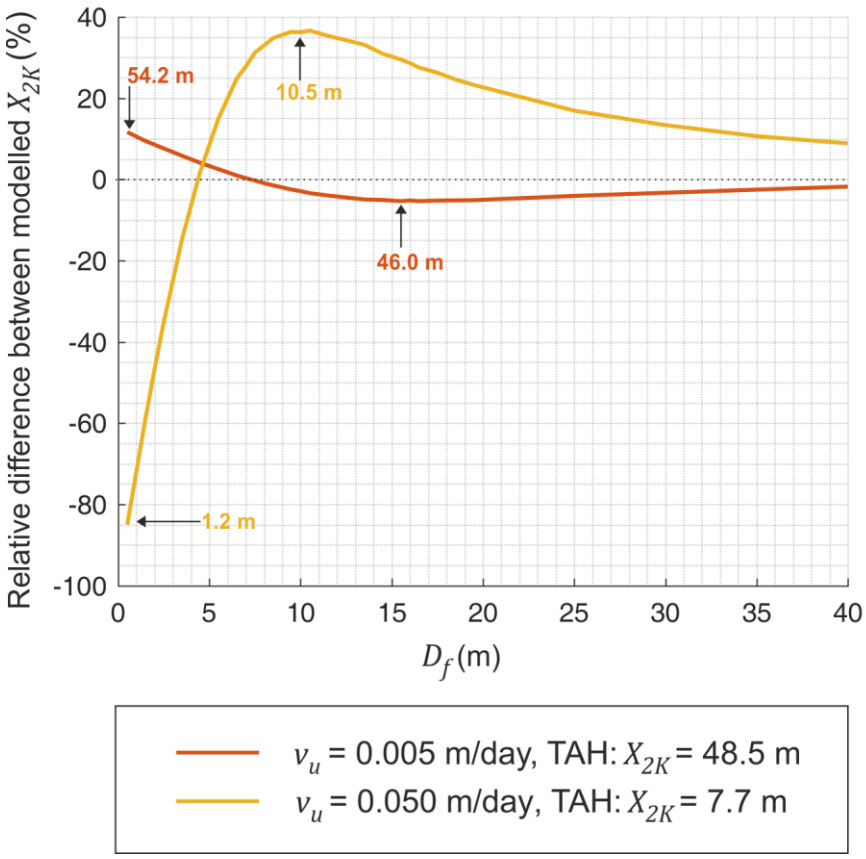

Figure 6.13 Relative difference between models $\left(X_{2K}^{TAF_{2D}} - X_{2K}^{TAH_{2D}}\right)/X_{2K}^{TAH_{2D}}$ in the maximum extent in x-coordinate of the +2 K isotherm after 30 years of continuous VBHE operation. Lines are annotated with the maximum and minimum X_{2K} for the TAF-2D model. X_{2K} values for the TAH-2D model are in the legend.

6.4.5 Time to stabilise extent of the +2 K isotherm

When the matrix is homogeneous, time to stabilise an isotherm will decrease with increasing groundwater velocity (Figure 4.8). The time when the extent of the +2 K isotherm stabilises (t_{S2K}) is sensitive to the volumetric flow rate in the fracture O_f. Therefore, in cases when a fracture reduces local groundwater flow, it increases t_{S2K} . This can be observed for medium groundwater flow (Figure 6.14). This is due to reduced local groundwater velocities, as was discussed in section 6.4.3 for ΔT_b *(*Figure 6.9*)*. The major difference compared with t_{Sb} is that the effect of fracture angle A_f on t_{S2K} for medium groundwater flow (Figure 6.14 D) is not symmetrical. This is because the thermal transport from the VBHE is significantly increased by the fracture. The fracture intersects the isotherms of higher temperature change downstream of the VBHE.

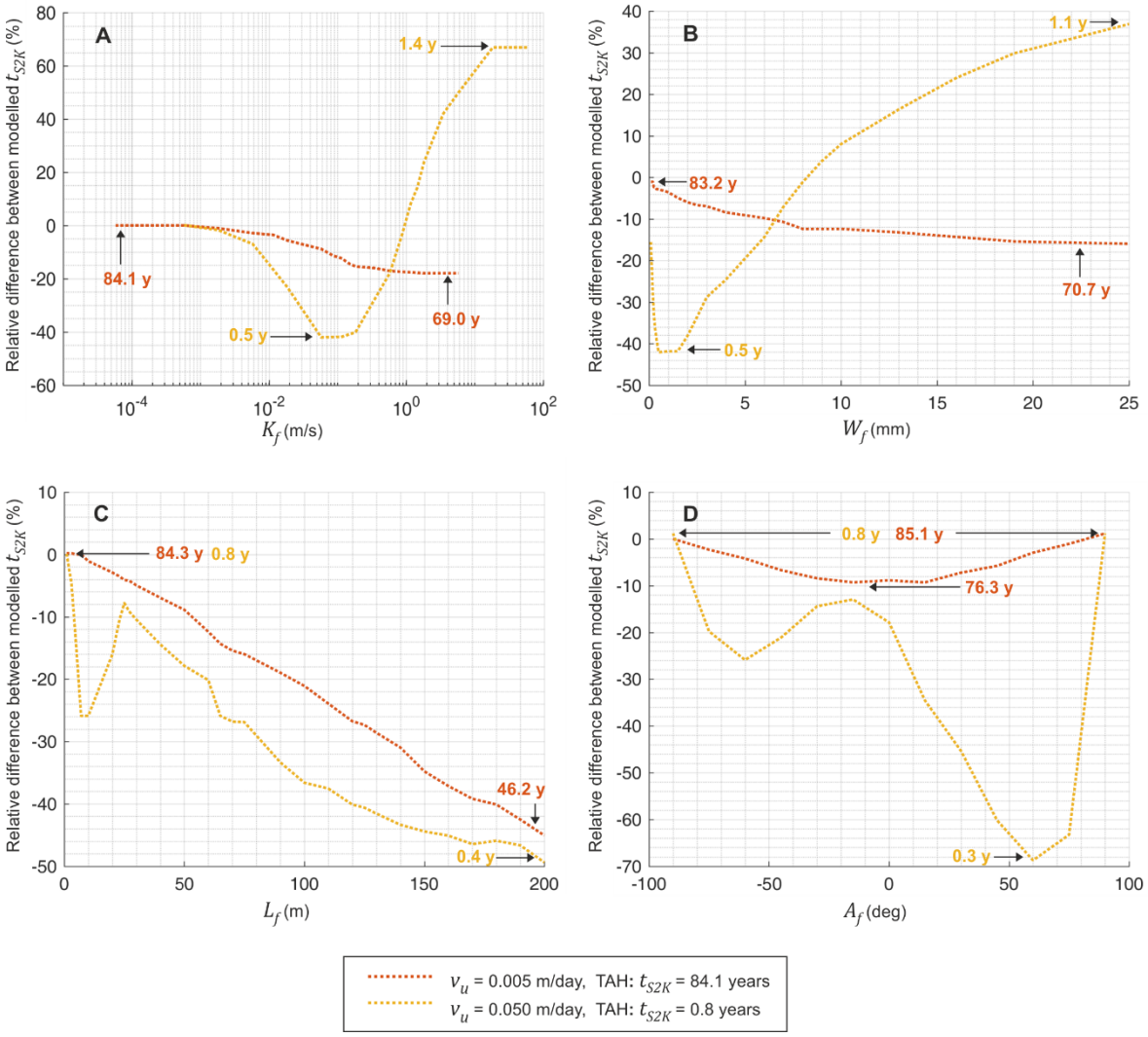

Figure 6.14 Relative difference between TAF-2D and TAH-2D in time needed to stabilise the extent of the +2 K isotherm $\left(t_{S2K}^{TAF_{2D}} - t_{S2K}^{TAH_{2D}}\right)/t_{S2K}^{TAH_{2D}}$ for changing (A) fracture hydraulic conductivity K_f, (B) fracture aperture W_f, (C) fracture length L_f and (D) fracture rotation relative to groundwater flow direction A_f. Lines are annotated with the maximum and minimum t_{S2K} for the TAF-2D model. t_{S2K} values for the TAH-2D model are in the legend.

Figure 6.15 shows how the fracture distance from the VBHE, D_f, influences the time to stabilise X_{2K} for medium and slow groundwater flows. The relationship is similar to that described for ΔT_b (Figure 6.10). The maximum relative difference between models in t_{S2K} (time needed to stabilise the +2 isotherm) for v_u = 0.05 m day-1 is about +100 %.

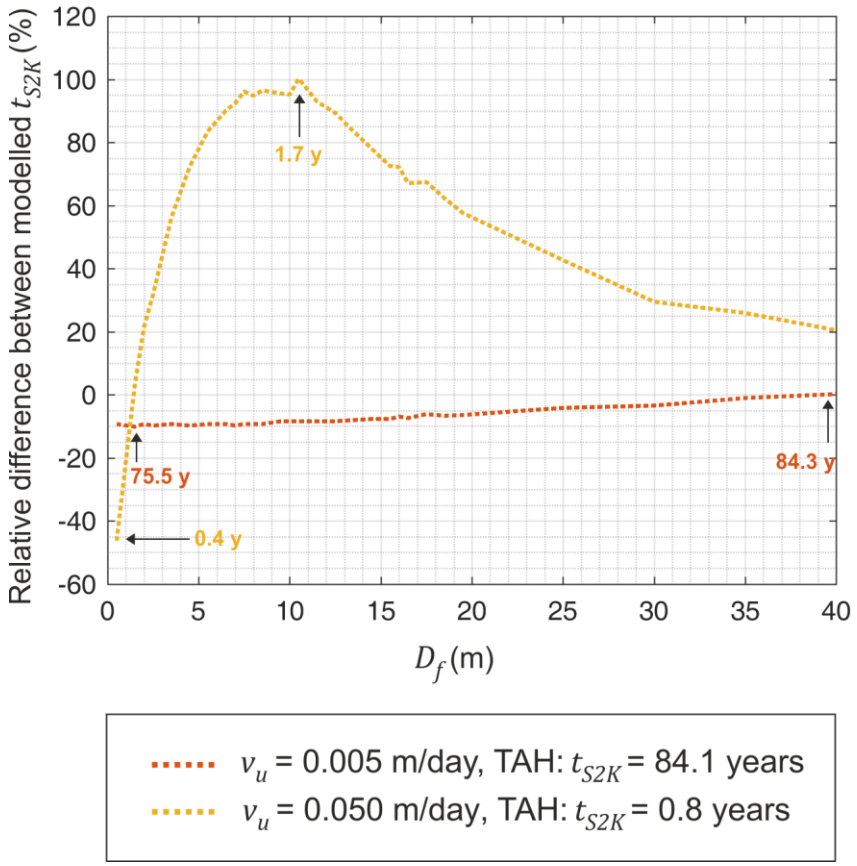

Figure 6.15 Relative difference between TAF-2D and TAH-2D models in time needed to stabilise the maximum extent of the +2 K isotherm $\left(t_{S2K}^{TAF_{2D}} - t_{S2K}^{TAH_{2D}}\right)/t_{S2K}^{TAH_{2D}}$ for different fracture distances from the VBHE D_f. Lines are annotated with the maximum and minimum t_{S2K} for the TAF-2D model. t_{S2K} values for the TAH-2D model are in the legend.

6.4.6 Shape of the isotherms

To illustrate the results from section 6.4.4, two examples of how the fracture can affect the shape of isotherm are presented. Figure 6.16 shows the effect of the fracture length L_f on the +0.5 and +2 K isotherms. The fracture is 1 m away from the VBHE, and all other model parameters are set to the base values given in Table 6.1. The only parameter which is changed is the fracture length L_f from 50 m (Figure 6.16 A) to 65 m (Figure 6.16 B).

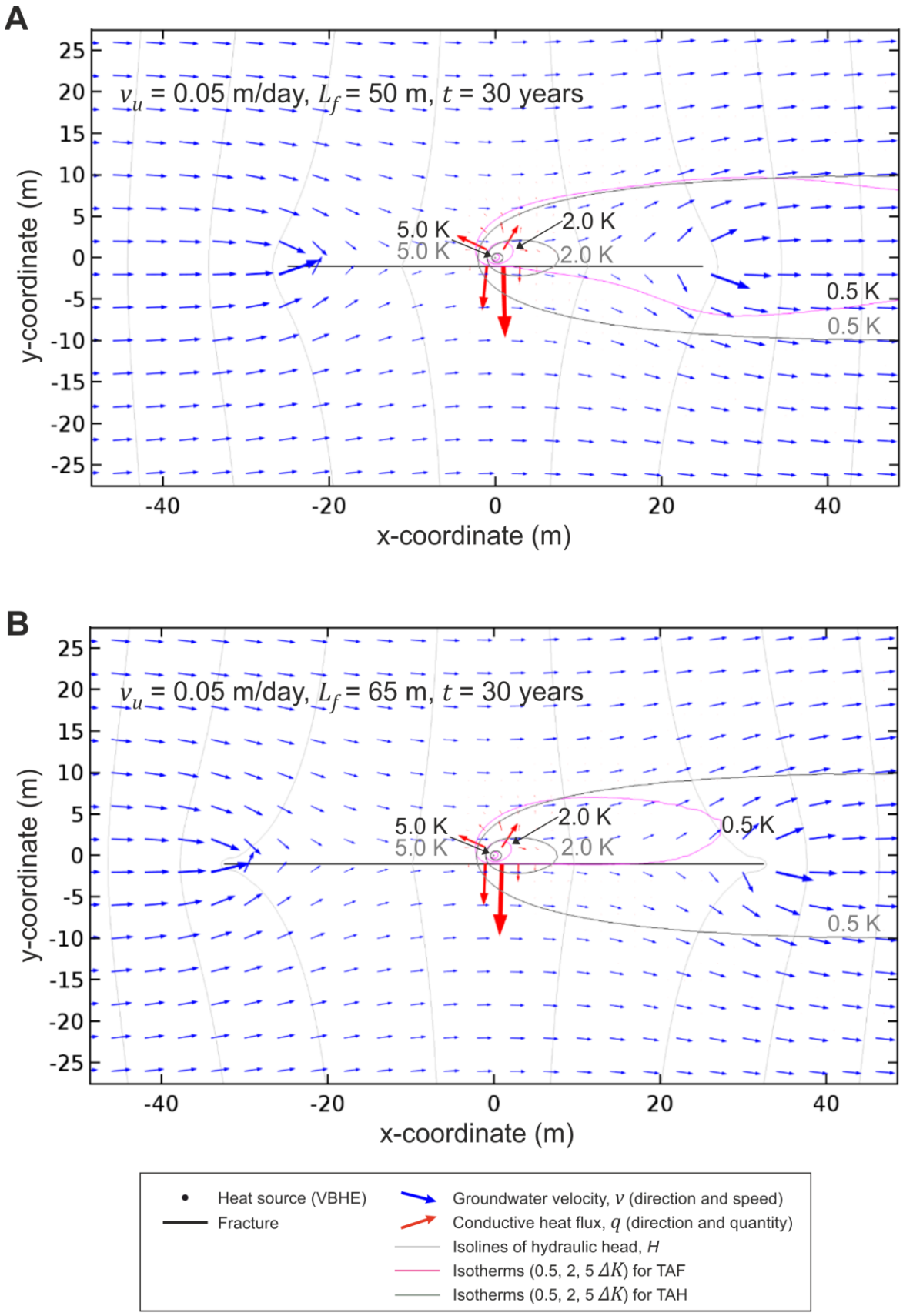

Figure 6.16 Isotherms (+0.5, +2, +5 K) around VBHE, groundwater flow vectors and conductive heat flux vectors after 30 years modelled using TAF-2D, for (A) fracture length L_f = 50 m and (B) L_f = 65 m. Grey isotherms are base scenario (TAH-2D, without fracture and grout). Magnitude of heat flux and groundwater velocity is proportional to the arrow size.

The shape of the +0.5 K isotherm differs between these two cases. In both cases, the longitudinal extent is reduced compared with that predicted by the TAH-2D model. The shape of the +0.5 K isotherm is distorted by the fracture in Figure 6.16 A due to increased groundwater velocities in the direction sideways out of the fracture edge downstream of the VBHE. The extent of the +0.5 K isotherm is sharply reduced by the 65 m long fracture (Figure 6.16 B). This is because volumetric flow rate O_f is higher compared with the 50 m long fracture. It causes more effective cooling of the VBHE wall and reduction of isotherms of interest. In this specific case (Figure 6.16 B) the ΔT of +0.5 K is advected inside the fracture and is exchanging heat with the matrix by conduction. As groundwater exits the fracture its temperature ΔT is already lower than +0.5 K thus this leads to rapid reduction of the +0.5 K isotherm extent for L_f = 65 m. If L_f is increased further, it does not significantly reduce the extent of the +0.5 K isotherm. A similar effect of cooling by a fracture edge for the +2 K isotherm occurs when L_f is about 20 m (Figure 6.12 C).

The second example concerns the fracture distance, D_f, from the VBHE. It is logical to assume that the closer the fracture is to the VBHE, the smaller is the +0.5 K isotherm extent $X_{0.5K}$. That is, the isotherm which is large enough to be unaffected by the slowed groundwater flow local to the VBHE (as was discussed for the +2 K isotherm). However it is not completely the case; the +0.5 K isotherm is maximally reduced by the fracture when it is 2 m from the VBHE (Figure 6.17 B), not 0.5 m away (Figure 6.17 A). This is because as D_f reduces, the fracture starts to intersect isotherms of higher and higher temperature change. The model result becomes even more sensitive to the parameter of fracture distance for a specific isotherm of interest when the isotherm can also be cooled by advection from the fracture edge (Figure 6.17 B). As D_f is reduced further, this effect of fracture edge is not relevant, because the fracture carries inside temperatures larger than the ΔT of interest (+0.5 K). Thus, the effect of the fracture edge only helps to extend the

+0.5 K isotherm around the fracture edge (Figure 6.17 A). Note the differences in effective ranges between the +2 K and +0.5 K isotherms.

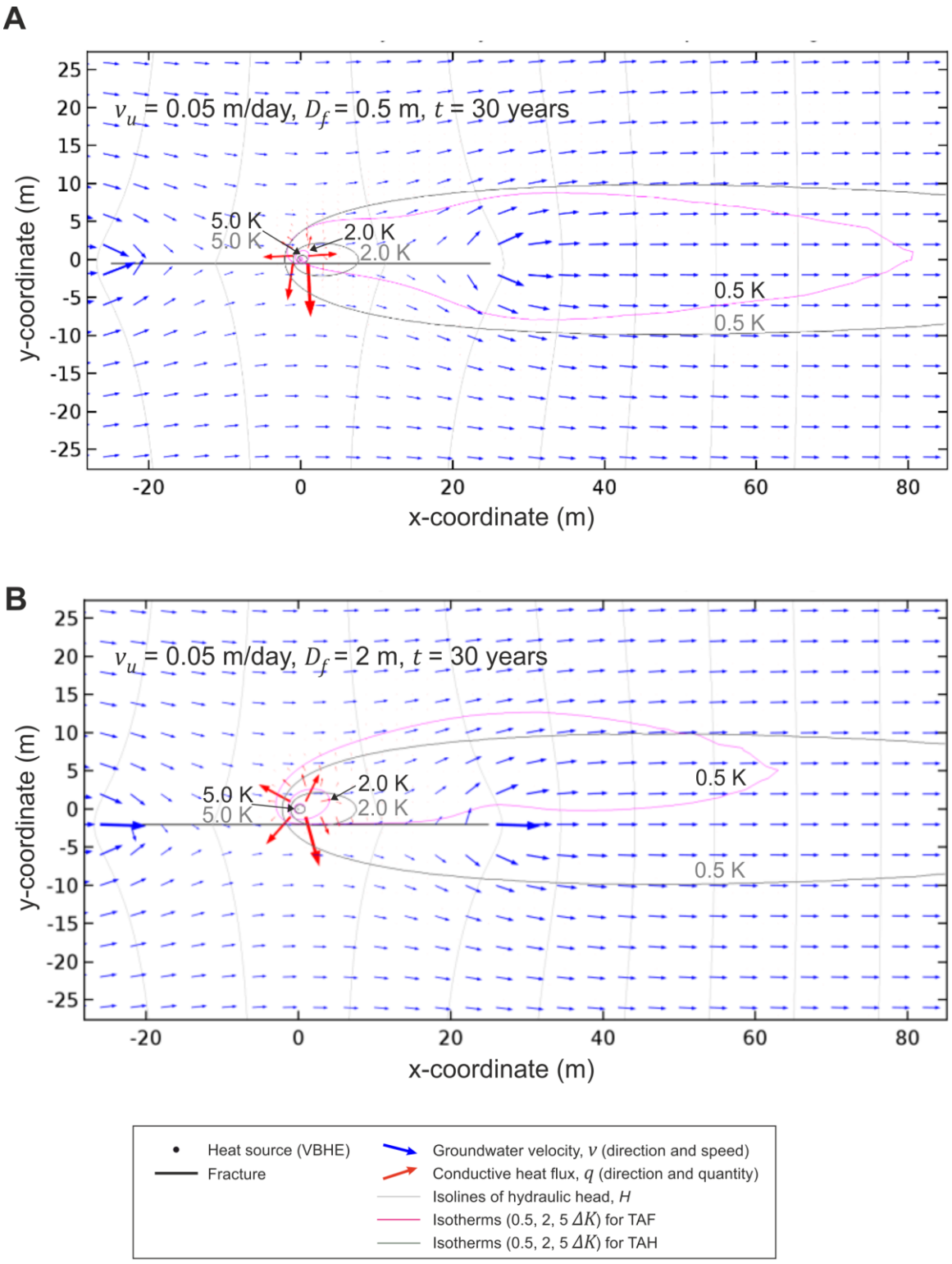

Figure 6.17 Isotherms (+0.5, +2, +5 K) around the VBHE with groundwater flow vectors and conductive heat flux vectors after 30 years modelled using TAF-2D, for different fracture distances from the VBHE, (A) D_f = 0.5 m and (B) D_f = 2 m. Grey isotherms are base scenario (TAH-2D, without fracture). Magnitude of heat flux and groundwater velocity is proportional to the arrow size.

Figure 6.17 illustrates how the zone of increased local groundwater flow at the edge of the fracture influences the shape of the isotherms. Location of a VBHE in the zones of fracture edge also has significant influence on the thermal behaviour due to locally increased groundwater flow. This is further discussed in the supplementary analysis (Appendix E).

6.5 Summary

In conclusion, a negative effect of a fracture on the VBHE performance (increase in temperature change at the VBHE wall ΔT_b compared with a scenario without fracture) is much more significant for scenarios when the matrix has medium groundwater flow (0.05 m day^{-1}) than for slower groundwater flow (0.005 m day^{-1}). This is because for medium groundwater flow the fracture significantly changes nearby local groundwater velocities and is able to increase ΔT_b by 1.4 K compared with the scenario without fracture (TAH-2D). The cooling effect of the fracture can be more than countered by the slowing of local groundwater velocities in the matrix, so the temperature change at the VBHE wall ΔT_b (when VBHE is located in the affected area) can be significantly increased by the influence of the fracture.

In a matrix with slow groundwater flow (0.005 m day^{-1}), the beneficial effect of a fracture (i.e. a reduction in the temperature change at the VBHE wall ΔT_b compared with the homogeneous case, TAH-2D) is larger in both relative and absolute terms than for a matrix with faster groundwater flow (0.05 m day^{-1}). This is because in case of v_u = 0.05 m day^{-1}, the groundwater flow in the matrix already significantly reduces ΔT_b, therefore the thermal gradient created between the VBHE and the nearby fracture is not as steep compared with the slower groundwater flow in the matrix.

The influence of a vertical fracture on the thermal performance of a VBHE was examined under different hydrogeological settings: for two groundwater velocities in the matrix (medium and slow), and for different fracture locations relative to the VBHE as well as for different fracture properties. The effects of fast groundwater

flow are examined in Chapter 7. The thermal performance of the VBHE was examined via the temperature change at the VBHE wall ΔT_b and extent of the +2 K isotherm X_{2K} after 30 years of continuous operation, as well as time needed to stabilise them, t_{Sb} and t_{S2K}.

A fracture can have a positive or negative effect on the thermal performance of a VBHE. It depends on the interplay of the two effects of a fracture:

1) The fracture changes the local groundwater velocities. Thus, it can change (increase or decrease) the conductive and advective thermal transport between the VBHE and the surrounding matrix.
2) The fracture changes the local thermal gradient between the VBHE and the surrounding matrix by advection of the thermal disturbance downstream. Thus, it increases the conductive thermal transport between the VBHE and the matrix.

The overall fracture effect on the VBHE depends on which of the two fracture effects is dominant. The fracture reduces the thermal transport from the VBHE if the first fracture effect is dominant and the VBHE is located in the area of slowed down groundwater flow. The thermal performance of the VBHE is reduced by the fracture (compared with the case when the fracture is not modelled, but groundwater flow in a homogeneous matrix is assumed and included in the model). In cases when the groundwater flow in the model is ignored, the thermal performance of the VBHE can be significantly underestimated. If the groundwater flow is accounted for in the model as the apparent thermal conductivity (ATC) of the matrix, then a fracture present near the VBHE can make the estimated value of ATC smaller.

The extent of an isotherm of high-temperature change (e.g. +2 K) can also be increased by a fracture if the isotherm is contained within the area of reduced local groundwater flows caused by the fracture. The effect of the fracture edge can significantly shrink the extent of the isotherm due to advection from the fracture

into the matrix, which increases the thermal transport between the matrix and the fracture.

The isotherms of interest can be extended (advected) by a fracture in the matrix with slow v_u. It occurs when the volumetric flow rate in the fracture O_f is insufficient to effectively reduce the ΔT of interest.

Figure 6.18 summarises the results of the single-parameter analysis presented in this chapter. The adverse, beneficial and insignificant fracture effects on ΔT_b are shown for each fracture parameter for both slow and medium groundwater flows. In relative terms, ΔT_b is reduced the most by a fracture at slow groundwater flow in the aquifer (ΔT_b is reduced by more than 15 % compared to the case without fracture). At medium groundwater flow the fracture effect is relatively smaller (< 15 %) for the tested sets of parameters of the single parameter analysis. The adverse fracture effect (increase in ΔT_b) occurred only for the medium values of D_f from the tested parameter range. However, the fracture in the single parameter analysis was centred with the VBHE. At the fracture shift relative to a VBHE which positions the VBHE just near the fracture edge, the fracture beneficially influence the thermal transport from the VBHE even at medium distance from the VBHE for medium groundwater flows, as illustrated in Figure E.2 (in Appendix).

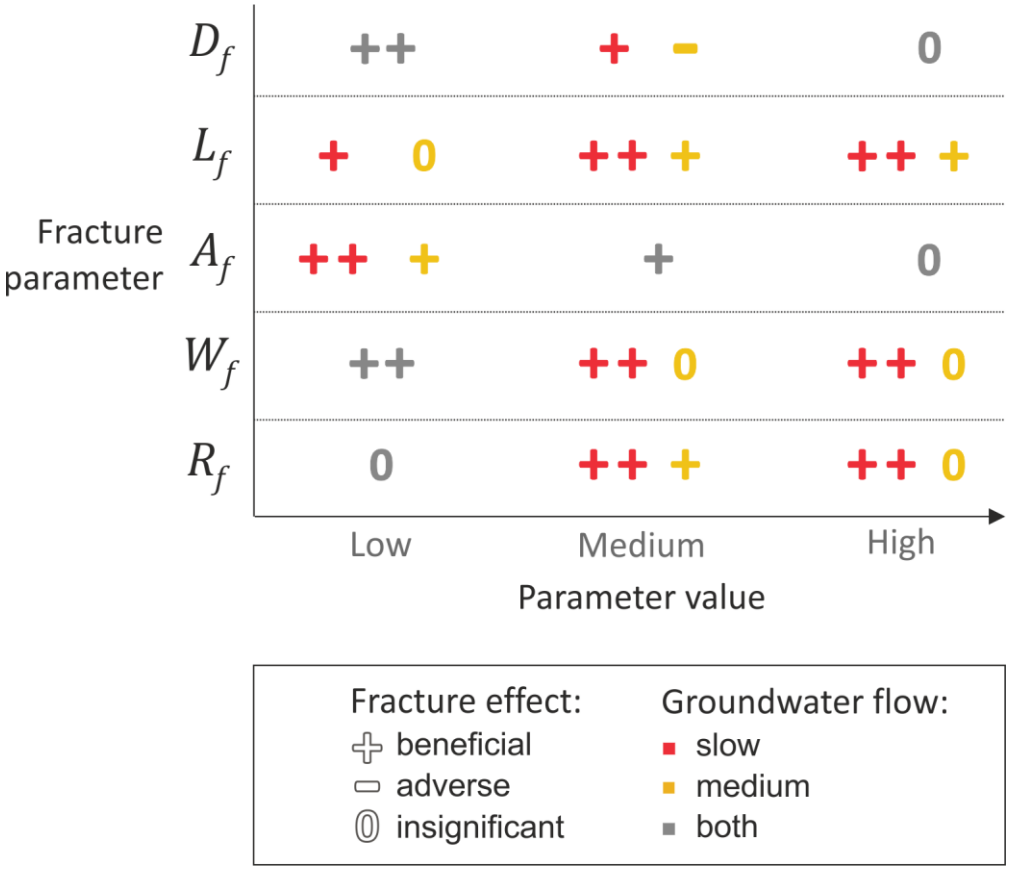

Figure 6.18 Summary of the fracture effects on the thermal transport in the nearby matrix (calculated as the temperature change at the VBHE wall, ΔT_b) based on the results in Chapter 6 for each fracture parameter: D_f fracture distance from VBHE, L_f fracture length, A_f fracture rotation with respect to groundwater flow direction, W_f fracture aperture and R_f fracture hydraulic conductivity. The illustrated groundwater flows are slow (0.005 m day^{-1}) and medium (0.05 m day^{-1}). Adverse fracture effect increases ΔT_b while beneficial fracture effect reduces it. Insignificant fracture effect on the VBHE (noted as 0) causes a change to ΔT_b by less than 5 %, significant beneficial effect (++) changes ΔT_b by more than 15 %, medium adverse and beneficial effects (denoted as – and +) cause a change in ΔT_b between 5 and 15 %.

6.6 Key message

The presence of a fracture is associated with concentrated flow inside that fracture and the change in the groundwater velocities in the nearby matrix. The interplay between the cooling by a fracture and the changes in the local groundwater velocities in the matrix influences the thermal performance of the VBHE installed near the fracture.

If the impact of the cooling is the dominant effect, then there will be:

- Reduction in the temperature change at the borehole wall
- Reduction in the time to stabilise that temperature change

The opposite effect occurs at certain fracture distances from the VBHE. This occurs if the reduction of the groundwater velocities in the matrix local to a VBHE is a dominant effect of a fracture.

If the VBHE is located near the edge of the fracture, then the local Darcy velocity is increased, improving the thermal performance of the VBHE (see Appendix E). These effects on a VBHE are relevant to fractures within permeable matrices. The previous work on the thermal performance of a VBHE installed near a fracture assumed an impermeable matrix, hence these interactions were not shown (see discussion in section 2.3.4).

Chapter 7 Uncertainty and parameter sensitivity analysis

7.1 Methods

This chapter investigates the effect of a fracture on a VBHE for a wide range of hydrogeological scenarios using Monte Carlo analysis (MC). Hydrogeological scenarios include varying the groundwater velocity in the matrix, thermal dispersivity, and all of the fracture parameters in the 2D model to test the effect of the fracture location, hydraulic properties and geometry in relation to the VBHE. Parameter sensitivity analysis was carried out in MATLAB using the Monte Carlo Analysis Toolbox (MCAT) (Wagener & Kollat 2007).

In Chapter 6, it was shown how a fracture can significantly affect the thermal performance of a VBHE. However, the geometrical parameters of a fracture can be difficult to measure. Monte Carlo analysis allows estimation of the uncertainty in thermal performance of a VBHE due to a nearby fracture for different hydraulic properties of matrix.

As in the previous chapter, the numerical model has two variants:

- **TAF-2D** –**T**hermal transport from a VBHE through an **A**quifer in the presence of a single vertical **F**racture in 2D.
- **TAH-2D** –**T**hermal transport through **A**quifer with a **H**omogeneous matrix in 2D.

The method for MC analysis is outlined in Figure 7.1. Single-parameter analysis (Chapter 6) was conducted for two groundwater velocities and zero thermal dispersivity. The current chapter additionally investigates how an open fracture may influence the thermal performance of a VBHE using the Monte Carlo analysis over a wide range of possible fracture parameters to investigate the uncertainty in the modelled thermal performance parameters of a VBHE: the temperature

change at the VBHE wall ΔT_b and the maximum downstream location (x-coordinate) of the ΔT = +2 K isotherm (X_{2K}), both after 30 years of VBHE operation.

The uncertainty in the performance metrics was examined for a wide range of groundwater velocities (v_u) in the matrix and for different values of thermal dispersivity (β). Regional average groundwater velocities can be established by a number of methods. Aquifer pumping tests provide in situ measurements of aquifer transmissivity and storativity averaged over a large aquifer volume (Freeze & Cherry). Therefore, groundwater velocity is treated as a known parameter, although it has an uncertainty around it.

In addition, the MC analysis was also carried out for two fixed values of v_u: 0.005 m day^{-1} and 0.05 m day^{-1}. These are taken as examples of 'slow' (< 0.01 m day^{-1}) and 'medium' (0.01 to 0.1 m day^{-1}) groundwater velocities. Analysis settings are divided into four different pathways (Figure 7.1), each of which leads to the next method step called "Set ranges for fracture parameters". Building on the results from Chapter 6, and taking into account that a fracture is an uncertain geological feature and cannot be precisely measured, this chapter investigates how the uncertainty in thermal performance of a VBHE due to a nearby fracture can be narrowed.

This chapter addresses the following three questions:

1) When and how can knowledge of the groundwater velocity in the matrix refine the uncertainty in VBHE performance due to a nearby vertical flowing fracture?
2) How does thermal dispersivity influence this uncertainty?
3) What is the extent to which determining the uncertainty in a particular fracture parameter can narrow the uncertainty in VBHE performance?

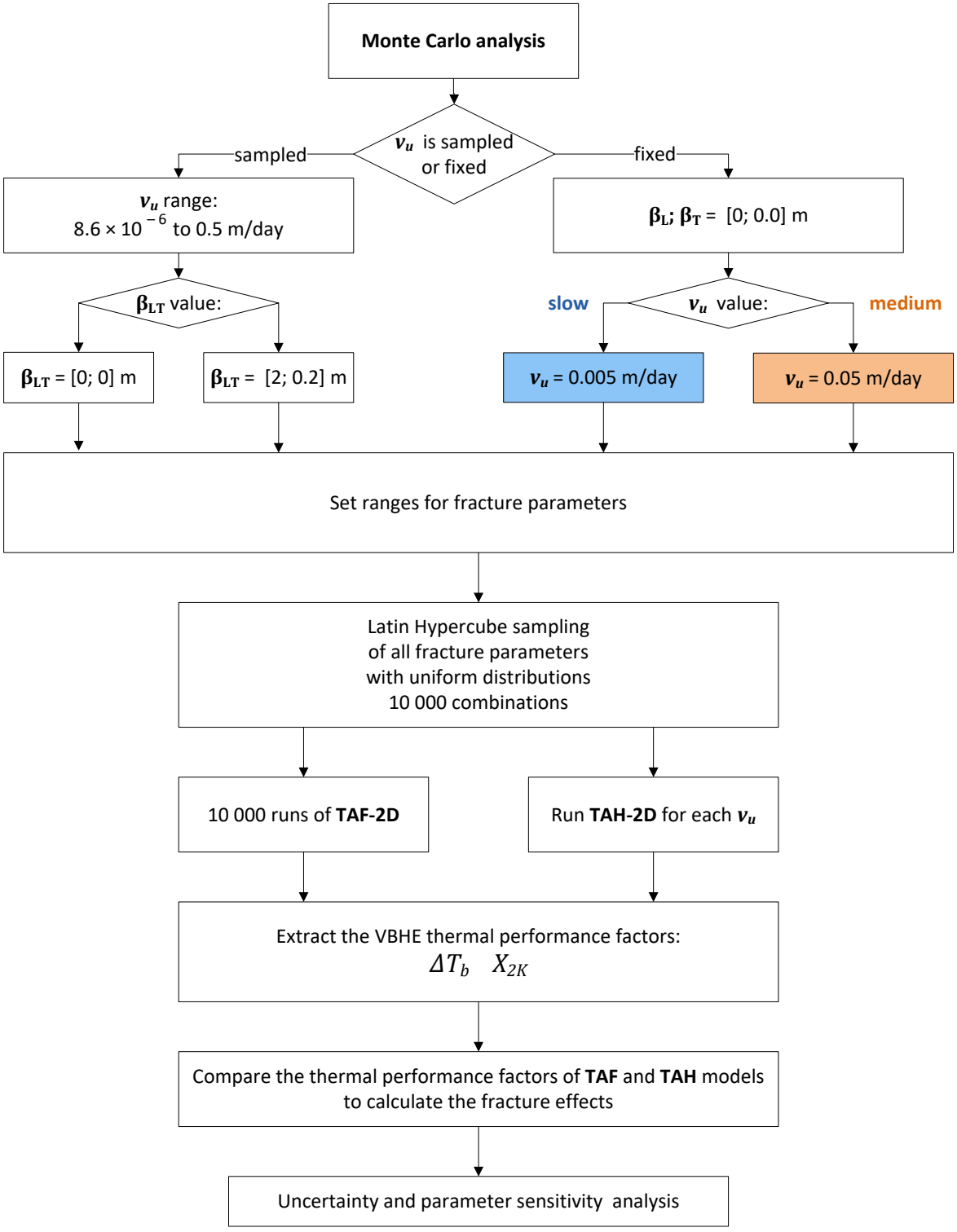

Figure 7.1 Method outline for the Monte Carlo analysis.

The same parameter ranges were used for the MC analysis as for single-parameter sensitivity analysis described in Table 6.1. The MC realisations were generated based on Latin Hypercube sampling of uniform probability density distributions for each fracture parameter. Log-uniform distributions were used for the groundwater velocity v_u and the ratio of the fracture to matrix hydraulic conductivity, R_K. This

was because the ranges for these two parameters span several orders of magnitude. Using a log-uniform distribution provides the same number of samples to each order of magnitude of the sampled range. The sampling was carried out for a wide range of parameters to test the fracture influence over a wide range of hypothetical hydrogeological scenarios rather than to model for a specific hydrogeological case.

Both the TAH-2D and TAF-2D models in this chapter do not explicitly model the VBHE grout (i.e. the grout hydraulic and thermal properties are assumed to be the same as for the aquifer matrix), since the presence of grout does not influence the results (see Chapter 6 for details). In every simulation, a check was made to ensure that the simulated velocities in the fracture and matrix were low enough to maintain laminar flow. Reynolds numbers inside fracture and in the matrix were calculated for each simulation for each time in order to monitor compliance with the assumptions in Darcy's law (similarly to single-parameter analysis, Chapter 6).

The longitudinal dispersivity was fixed to one of two values: 0 m (physically implausible, but it is a reasonable minimum value to test) and 2 m, a medium value from the dispersivity range used in Chapter 4, based on field results for scales of about 100 m (Gelhar *et al.* 1992). The transverse dispersivity was assumed to be 0.1 times the longitudinal dispersivity, as is common in thermal transport (Molina-Giraldo *et al.*).

It should be noted that the sampling pattern has a big influence on the 95% confidence limits of the results from the Monte Carlo analysis, and for a specific hydrogeological case the uncertainty would be much smaller. Since the investigation was theoretical and not bound to any particular hydrogeological condition, the parameter ranges were kept wide. Once the parameters of the particular geology is known, the uncertainty limits will be narrower but the patterns of fracture influence and conclusions still hold.

7.2 Results of uncertainty analysis: The role of groundwater velocity and dispersivity

Figure 7.2 shows the results of MC runs for a wide range of undisturbed groundwater velocities in the matrix (v_u). Table 6.1 lists the fracture parameters varied and their ranges. Vertical lines classify groundwater velocities for reference (slow, medium and fast). The performance indicator is the temperature change at the VBHE wall after 30 years of continuous operation (ΔT_b). Figure 7.2 represents a projection of the parameter space into one dimension (Wagener & Kollat 2007). Each dot is a MC run result of ΔT_b. Matrix dispersivity (β) (the subscripts L and T denote longitudinal and transverse) was included in this analysis as one of two fixed values to show its effect. There are 20 000 MC runs in total: 10 000 runs for the matrix dispersivity β = 0 m and 10 000 runs for longitudinal and the transverse matrix dispersivity β_L; β_T = 2 ; 0.2 m. The TAH-2D lines on the plot represent the results without a fracture for a range of groundwater velocities and the two tested dispersivities. The uncertainty in ΔT_b due to presence of a fracture near the VBHE is quantified by the 95% confidence interval (the distance between the lower 2.5 % and upper 97.5 % percentiles). The uncertainty discussed here arises only from the presence of a fracture (with varying properties), not from the matrix properties.

The minimum values of ΔT_b were obtained for MC runs with the fastest groundwater velocity and with present matrix dispersivity. Knowledge of the groundwater velocity and the thermal dispersivity in the aquifer significantly reduces the uncertainty in the thermal performance of a VBHE due to the presence of an uncharacterised fracture.

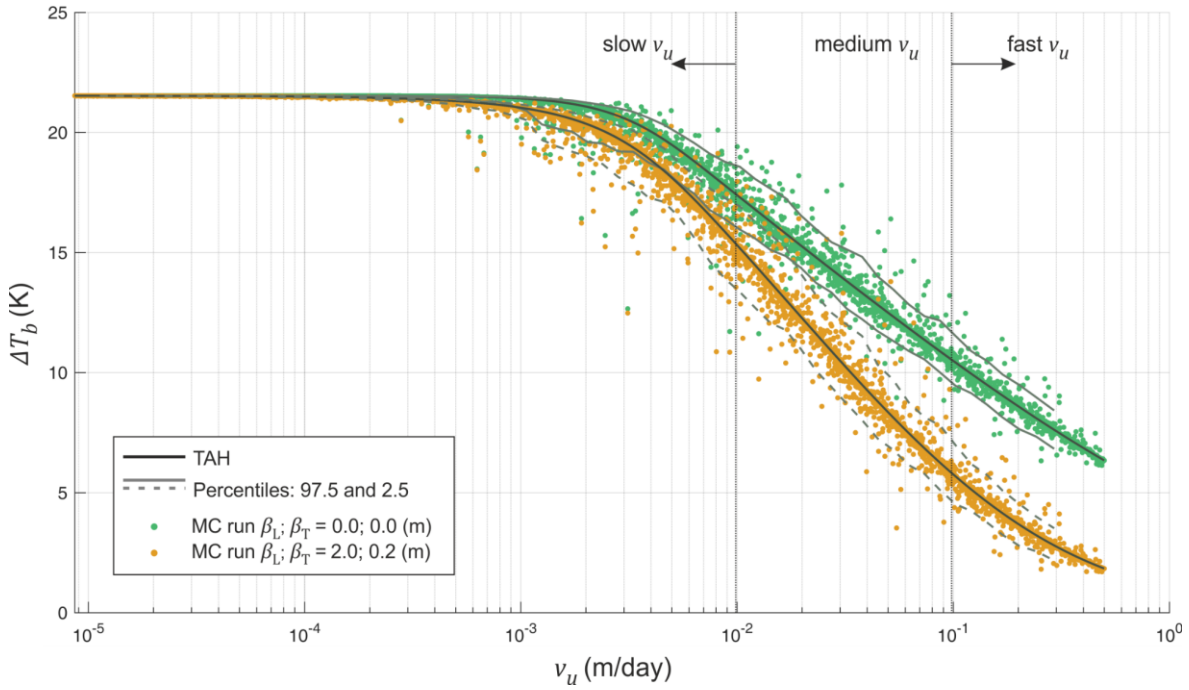

Figure 7.2 Monte Carlo (MC) simulations for the temperature change at the borehole wall, ΔT_b, after 30 years of continuous VBHE operation versus undisturbed groundwater velocity in the matrix, $v_u v_u$ (m day^{-1}). Range of fracture parameters is shown in Table 6.1.

The confidence intervals for the thermal performance of the VBHE vary depending on the groundwater flow. The fracture does not significantly influence ΔT_b in a matrix with slow (< 0.0005 m day^{-1}) and fast (> 0.4 m day^{-1}) groundwater velocity. The uncertainty in the temperature change at the borehole wall ΔT_b due to a nearby fracture is by visual inspection narrowed for a slow groundwater velocity in the matrix and may be insignificant for groundwater flows less than 0.001 m day^{-1} and faster than 0.4 m day^{-1} (Figure 7.2).

The difference in results between two tested dispersivities is significant: increased dispersivity causes a smaller ΔT_b (which means an improved thermal performance of the VBHE). Prior knowledge of the matrix dispersivity can in theory significantly reduce the uncertainty of the VBHE performance for cases with 'fast' groundwater flow (see difference between the TAH-2D lines for the two dispersivities across different groundwater velocities, Figure 7.2).

When groundwater flow in the matrix is fast, the uncertainty in the thermal performance of a VBHE due to matrix dispersivity may be significantly wider than the uncertainty due to the presence of a nearby fracture (compare the difference

between the TAH-2D lines in Figure 7.2 with the width of uncertainty around the single TAH-2D line due to influence of a fracture). The TAH-2D line coincides with the median line for the distribution because most of the fracture parameter sets resulted in no influence from the fracture on the VBHE. If one fracture parameter is ineffective (for example the fracture length is too short or the hydraulic conductivity is low), then the whole fracture parameter set becomes ineffective too. Chapter 6 investigated the values of individual fracture parameters which make the influence of a fracture on ΔT_b negligible.

Figure 7.3 presents the MC results for the maximum x-coordinate extent of the +2 K isotherm (X_{2K}) for a range of undisturbed matrix groundwater velocities (v_u).

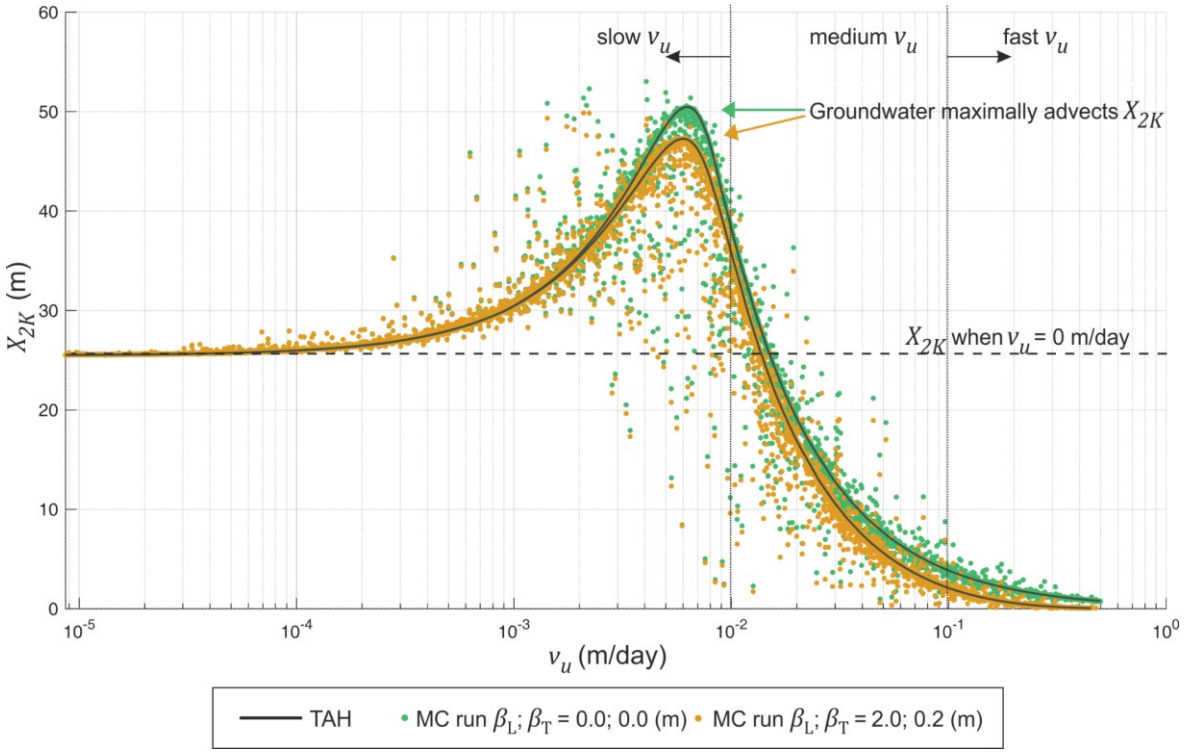

Figure 7.3 Monte Carlo simulations for maximal extent in x-coordinate of the ΔT = +2 K isotherm X_{2K} after 30 years of continuous VBHE operation versus undisturbed groundwater flow in the matrix, v_u (m day^{-1}).

Slow to medium groundwater velocities (v_u from 0.0002 to 0.02 m day^{-1}) in the TAH-2D model led to an increase in X_{2K} due to advection compared with no flow in the matrix. In most cases with a fracture, the extent of the isotherm is reduced compared with TAH-2D for v_u faster than that which maximally extends X_{2K}. The 'maximally extending' groundwater velocity means that it is able to extend the

given isotherm maximally. The maximum X_{2K} occurs at a matrix groundwater flow of about 0.006 m day^{-1}. If the groundwater is faster than this value, the extent of the isotherm will become shorter. For slower groundwater velocities the maximum X_{2K} can be significantly increased by the presence of a flowing fracture (compared to TAH-2D result) (Figure 7.3). For groundwater flows faster than the 'maximally extending' groundwater flow, the presence of an effective fracture can significantly reduce the extent of the +2 K isotherm X_{2K} (compared with the TAH-2D result). Knowledge of the matrix dispersivity can reduce the uncertainty of the modelled X_{2K} for cases when groundwater maximally advects X_{2K} (more so for isotherms with smaller ΔT, e.g. +1 K isotherm). The uncertainty in X_{2K} due to the presence of a fracture also varies with groundwater flow in the matrix.

If the groundwater is slow or fast (slower than 0.001 m day^{-1} or faster than 0.1 m day^{-1}) the uncertainty in the isotherm extent due to the presence of fracture or thermal dispersivity is negligibly small (Figure 7.3). To know how likely it is that a site with a particular groundwater velocity might be on one side or the other of the TAH-2D line for X_{2K} depends on the spread of the distribution. The change percentile values (95 % confidence interval) for X_{2K}, depending on groundwater velocity, is discussed in Figure 7.5.

Figure 7.4 presents the same results as Figure 7.2, but expressed as a difference (in real and relative terms) between TAF-2D and TAH-2D. This allows examination of the effect of the same fracture with different values of the dispersivity in the matrix but the same groundwater velocity v_u.

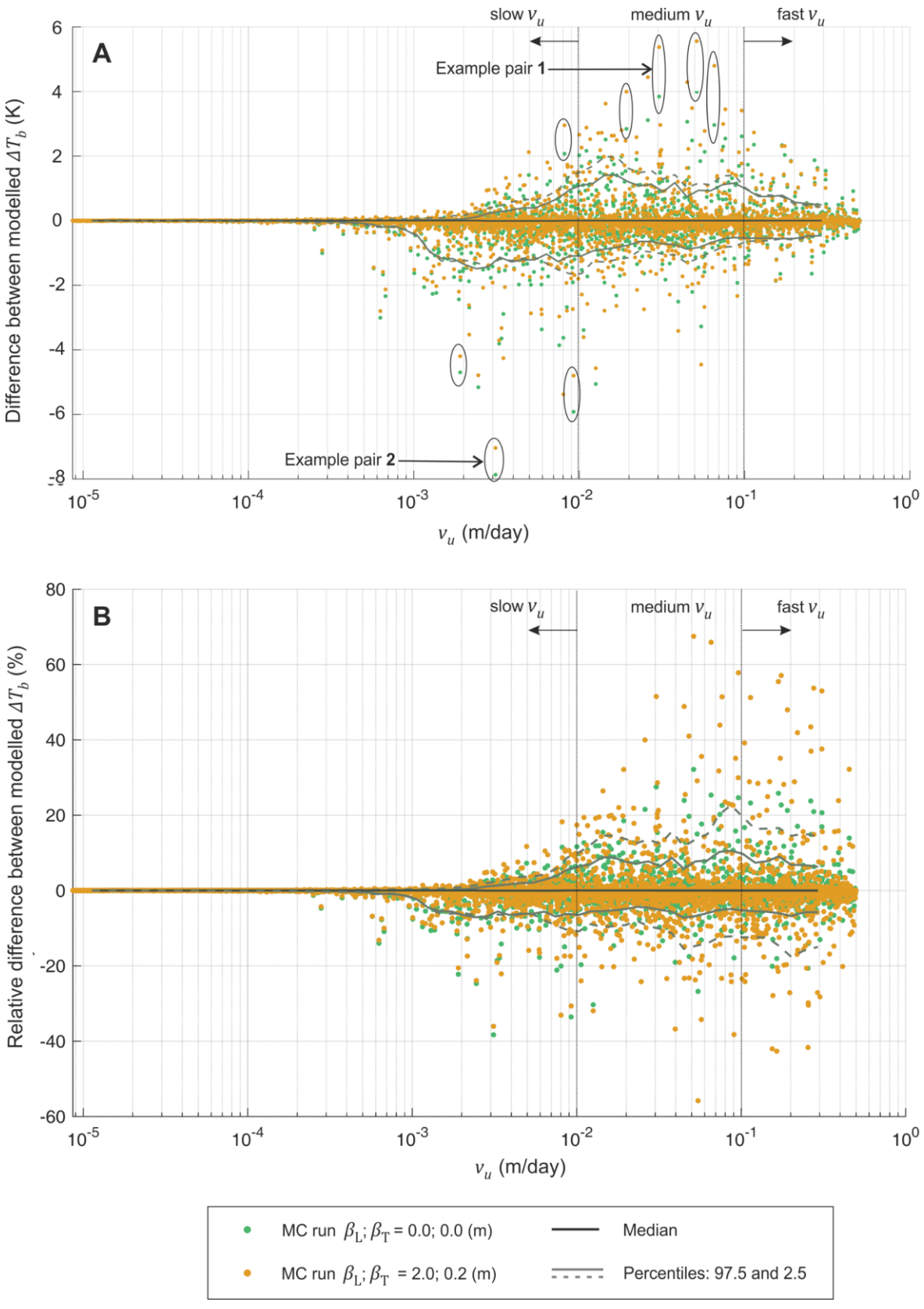

Figure 7.4 Monte Carlo results for temperature change at the borehole wall, ΔT_{bb}, after 30 years on continuous operation expressed as difference between models with and without fractures, $\Delta T_b^{TAF_{2D}} - \Delta T_b^{TAH_{2D}}$ (A) and relative difference, $\left(\Delta T_b^{TAF_{2D}} - \Delta T_b^{TAH_{2D}}\right)/\Delta T_b^{TAH_{2D}}$ in percentage (B). Each of the circled example pairs (A) are two MC runs with the same fracture parameters for the same v_u but different β_L, β_T values.

It shows that over a wide range of groundwater velocities 95% of all the data lie within 2 K of the result for the no-fracture scenario (homogeneous matrix). Results for the no-fracture scenario coincide with the median lines because a wide range of fracture parameters were sampled, and the majority of the combinations of parameters were ineffective because they contained at least one ineffective fracture parameter value.

The uncertainty in ΔT_b due to presence of a fracture near the VBHE is quantified by the 95% confidence interval (the distance between the lower 2.5 % and upper 97.5 % percentiles. For slow groundwater flows (v_u < 0.01 m day^{-1}) the estimated ΔT_b near an uncharacterized single fracture may be significantly lower than the value estimated assuming homogeneous geology (Figure 7.4 A). However, this cooling effect can be more than countered by the slowing of local matrix groundwater velocities around the VBHE for faster groundwater velocities in the matrix, v_u > 0.01 m day^{-1}. Thus, it increases the probability of negative fracture effects on the VBHE. However, for faster groundwater flows, ΔT_b > 0.3 m day^{-1}, the effect of the fracture starts to diminish significantly and may be ignored.

Matrix dispersivity can significantly change the influence of a nearby fracture for medium (and less so for slow) groundwater velocities in the matrix. Each circled pair of green and orange dots in Figure 7.4 A represents an example of MC results where all fracture parameters are the same for the same v_u, and are different only in the thermal dispersivity (β, see legend). A higher thermal dispersivity increases the adverse effect of fracture when it slows down groundwater flow at the location of the VBHE, which also reduces dispersion in the affected area. Thus the temperature change at the VBHE wall can be increased significantly if the matrix dispersivity is high.

This is shown in example pair 1 (and the nearby pairs) with positive differences between models ($\Delta T_b^{TAF} - \Delta T_b^{TAH}$) highlighted in Figure 7.4 A. The fracture parameters for the example pair 1 is given in Table 7.1. For outliers when ΔT_b is maximum and positive (similar to pair 1), W_f varies from pair to pair of similar

outliers. L_f is > 100 m for all those outliers, S_f is small, D_f was around 20 m for most outliers and R_f is high as for other similar outlier pairs. Outliers that have small D_f (e.g. 3 m) have also smaller L_f and R_f lower by one order of magnitude.

Table 7.1 Results for ΔT_b, fracture parameters, groundwater velocity for the two example pairs circled in Figure 7.4. The results are given for both dispersivity values.

Result or parameter	Symbol	Pair 1		Pair 2	
Thermal dispersivity of aquifer L; T; V (m)	β	0;0;0 m	2;0.2;0.2 m	0;0;0 m	2;0.2;0.2 m
Temperature change at the VBHE wall (K) (TAF-2D)	ΔT_b	17.8	15.8	12.7	12.5
Temperature change TAF-2D – TAH-2D difference (K)		3.8	5.4	-7.9	-7.0
Temperature change TAF-2D – TAH-2D rel. diff. (%)		27.5	51.5	-40.0	-36.1
Groundwater velocity (m d^{-1})	v_u	0.03		0.003	
Fracture rotation angle (°)	A_f	7		50	
Distance from fracture to the VBHE (m)	D_f	14		0.6	
Fracture length (m)	L_f	188		191	
Fracture shift (m)	S_f	5.9		-60	
Fracture width (m)	W_f	0.015		0.019	
Ratio of the hydraulic conductivity of the fracture to the matrix (-)	R_K	991330		99989	

When the groundwater flow velocity is slow, the fracture has a mostly positive effect on VBHE performance – it reduces ΔT_b (see example pair 2 and nearby pairs in Figure 7.4 A). Where a VBHE is installed in a matrix with high dispersivity (for example 2 m), the cooling effect of the fracture is smaller than in scenarios when the matrix dispersivity is small. This is because the temperature at the VBHE wall is already significantly reduced by the groundwater flow and dispersion; therefore, the fracture is not as effective at reducing it further. It is similar to the discussed reduction of fracture importance for scenarios with faster groundwater flow in the matrix (Figure 7.2).

To illustrate this, the second example pair is highlighted in Figure 7.4 A with negative differences between models ($\Delta T_b^{TAF} - \Delta T_b^{TAH}$). The second example pair

2 for slow groundwater flow shown in Figure 7.4 is an example of how the effect of the fracture will vary for cases with and without dispersivity. The second pair has large W_f, small D_f and long L_f, similar to the other outlier pairs with the lowest values for $\Delta T_b^{TAF} - \Delta T_b^{TAH}$. S_f, W_f and A_f values varied among similar outliers.

Additionally, if for medium groundwater flow a VBHE is located in the area with increased local groundwater velocity due to nearby flow into a fracture, the dispersive thermal transport in the matrix is also increased for this area; thus the fracture further reduces temperature change at the VBHE wall. In relative terms, the influence of the presence or absence of thermal dispersivity on the effect of the fracture is larger when the groundwater flow is medium (Figure 7.4 B).

The outliers are more numerous when the fracture parameter ranges are influential. The majority of results (> 50 %) lie around the median value, with 70 % of results lying between +0.05 K (for medium groundwater velocity) and -0.2 K (for slow to medium groundwater velocity).

Figure 7.5 summarises the possible effects of the fracture on the extent of the +2 K isotherm X_{2K}.

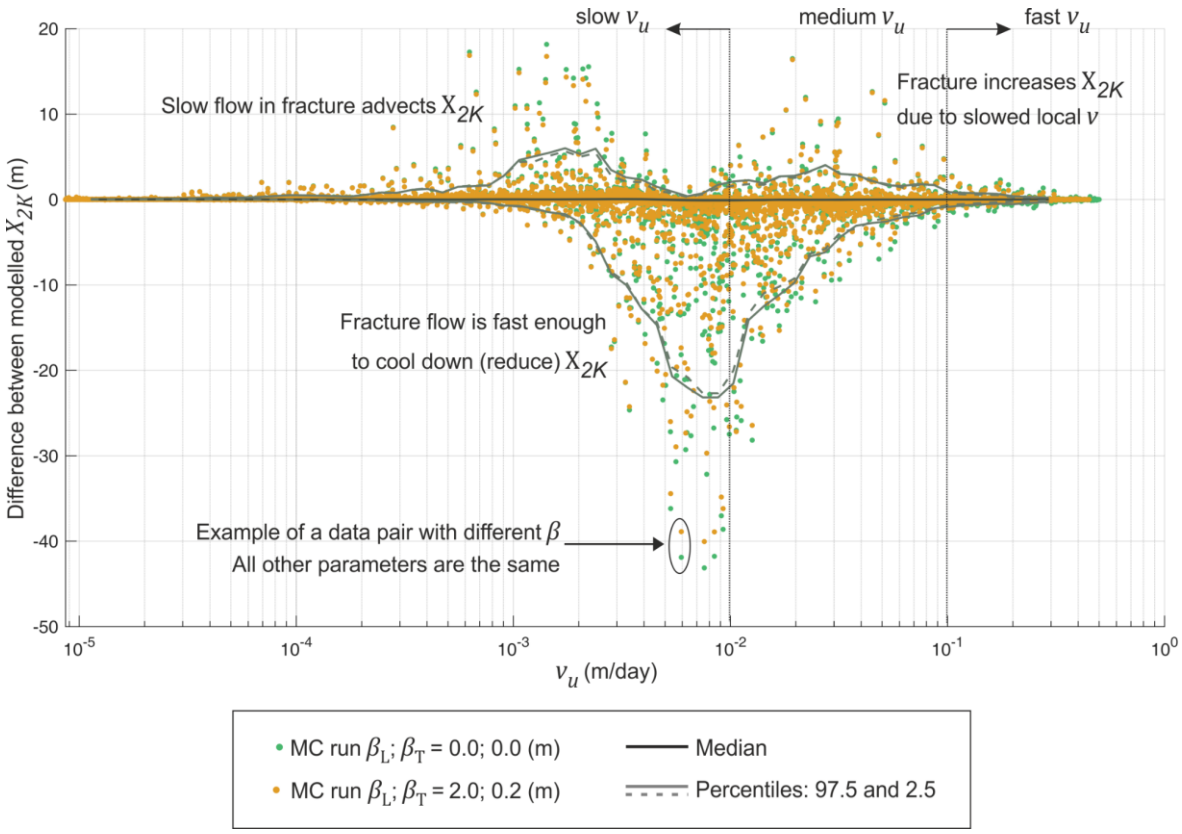

Figure 7.5 Monte Carlo results expressed as difference between models with and without fracture for maximal extent in x-coordinate of the +2 K isotherm ($X_{2K}^{TAF} - X_{2K}^{TAH}$) after 30 years of continuous VBHE operation.

The isotherm can be effectively extended by a fracture in a matrix with slower groundwater velocities (see Figure 7.5 for v_u of around 0.0005 to 0.003 m day^{-1}). This occurs because a fracture in a matrix with slow groundwater flow is only able to reduce the temperature change at the VBHE wall and the extent of the isotherms of high-temperature change.

A second effect occurs when the matrix groundwater flow is faster (see in Figure 7.5 for v_u between 0.003 and 0.05 m day^{-1}) so the flow inside fracture is also enough to reduce X_{2K}. The third type of fracture effect on X_{2K} can be observed for v_u between 0.01 and 0.1 m day^{-1}. In these cases, the effect of locally slowed groundwater velocities due to presence of a fracture is more significant than the fracture cooling effect for isotherms of higher temperature change, for example +2 K (Figure 7.5) which are small enough to be located inside the affected area.

When dispersion in the matrix is high, the fracture does not reduce X_{2K} as much as the 'no dispersion' scenario. This is similar to the effect of dispersion on ΔT_b. A circled pair of green and orange dots represents an example of MC results where all fracture parameters are the same for the same v_u and only values of β are different (see legend).

7.3 Results of parameter sensitivity analysis

This section discusses how the fracture parameters can constrain the modelled uncertainty in the VBHE thermal performance. The sensitivity of the model to each separate fracture parameter is discussed. Figure 7.6 shows dotty plots, a projection of the parameter space into one dimension (Wagener & Kollat 2007). Each subplot shows the results from 10 000 runs of the TAF-2D model represented as dots. Each dot is an MC run result for ΔT_b. The horizontal TAH-2D line represents the result for ΔT_b without a fracture. The groundwater velocity v_u is fixed to either slow or medium value. Figure 7.7 shows the results for X_{2K} in a similar way. The thermal dispersivity is 0 m for the analysis in this section (i.e. for results from Figure 7.6 to Figure 7.10). The influence of the thermal dispersivity was explored in the previous section. The uncertainty discussed here arises only from the presence of a fracture (with varying properties), not from the matrix properties.

To interpret the results of dotty plots in terms of sensitivity of the model result to a certain parameter, the change in the pattern of the dots with the change in the parameter on x-axis should be observed. If the spread of the dots does not change along the x-axis, then the parameter does not influence the model result. If the spread of the dots becomes very narrow around the TAH line for certain values of the parameter on the x-axis, it means that whatever are the values of other fracture parameters, the model result is determined by the value of the parameter on the x-axis, which renders the fracture ineffective to change the thermal performance of the VBHE.

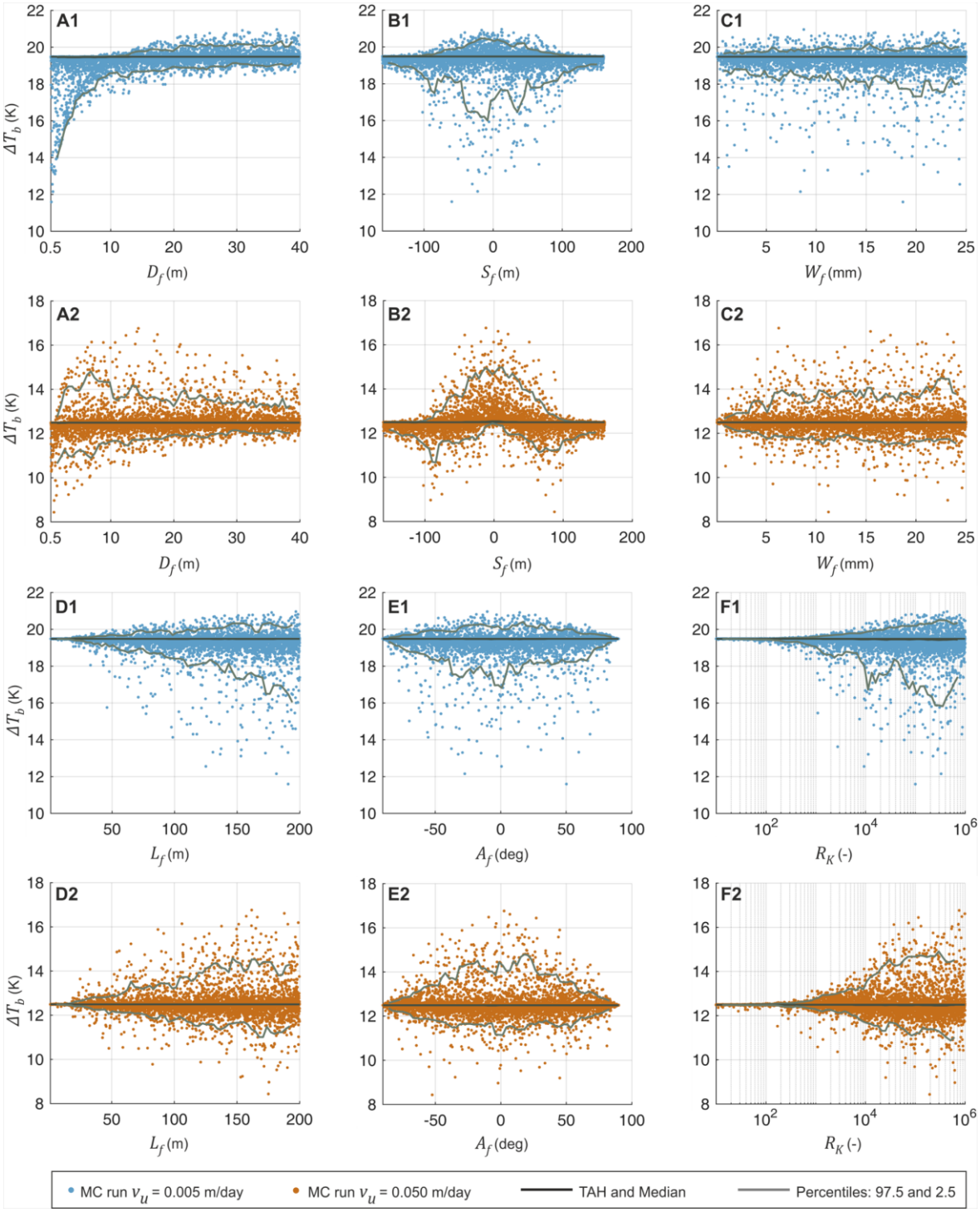

Figure 7.6 Monte Carlo results for temperature change at the borehole wall ΔT_b after 30 years of continuous VBHE operation. A separate varied fracture parameter is shown on the x-axis of each subplot: (A) distance D_f, (B) shift S_f, (C) aperture W_f, (D) length L_f, (E) angle A_f, and (F) hydraulic conductivity ratio R_K. The undisturbed groundwater flow in the matrix v_u is fixed to either 0.005 m day^{-1} (blue dots) or 0.05 m day^{-1} (orange dots). Both cases are with 0 m matrix dispersivity.

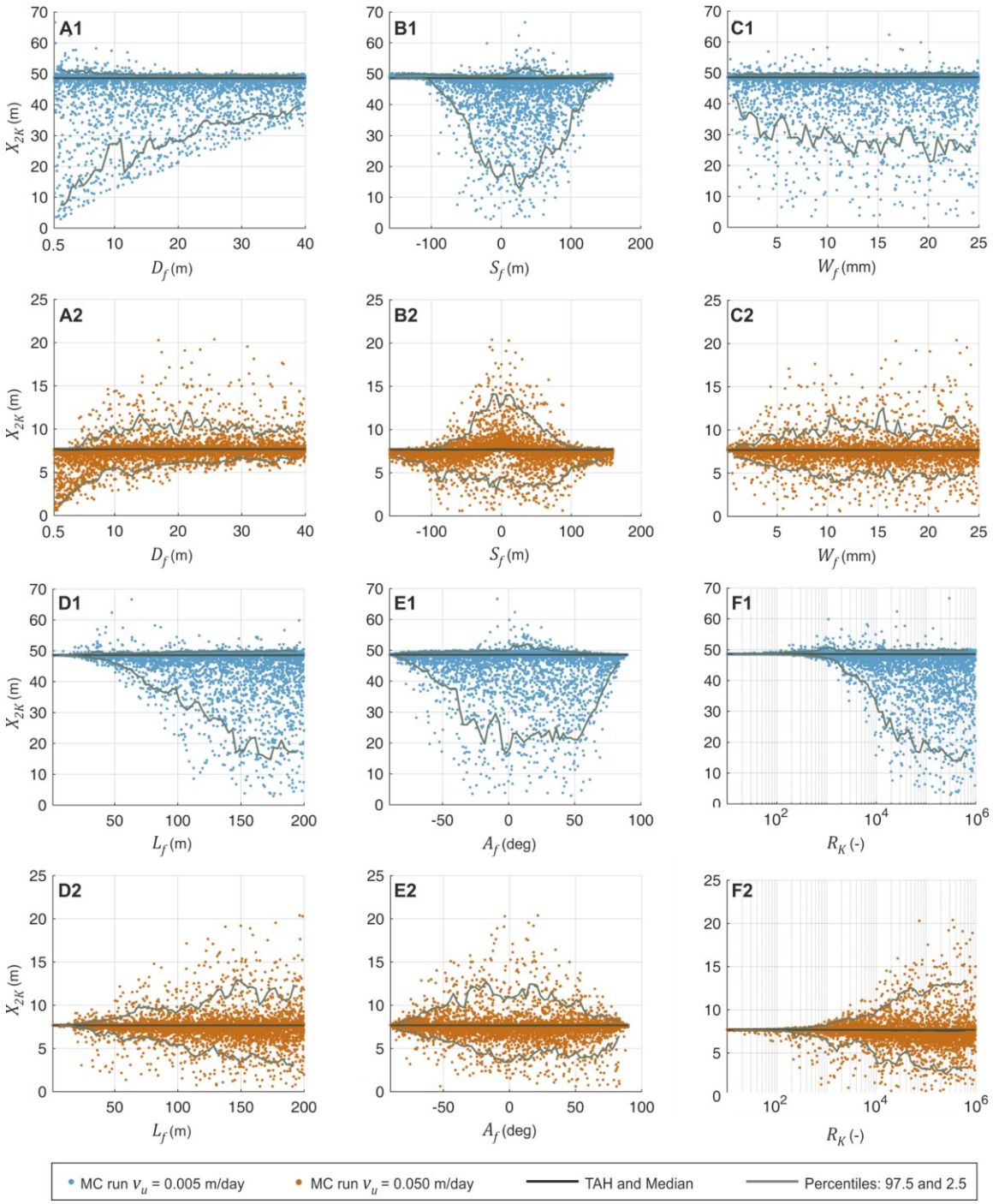

Figure 7.7 Monte Carlo (MC) results for maximal extent in x-coordinate of the ΔT = +2 K isotherm, X_{2K} after 30 years of continuous VBHE operation. A separate varied fracture parameter is shown on the x axis of each subplot: (A) distance D_f, (B) shift S_f, (C) aperture W_f, (D) length L_f, (E) angle A_f, and (F) hydraulic conductivity ratio R_K. The undisturbed groundwater flow in the matrix, v_u , is fixed to either 0.005 m day^{-1} (blue dots) or 0.05 m day^{-1} (orange dots). Both cases are with 0 m matrix dispersivity.

The results for the no-fracture scenario (TAH-2D model) coincide with the median lines for the distribution because the majority of fracture parameter sets result in there being no influence of the fracture on the VBHE ΔT_b.

Knowledge of fracture parameters can significantly reduce the uncertainty in the estimated thermal performance of the VBHE, depending on the groundwater velocity in the matrix (Figure 7.6). When the **fracture distance** (D_f) from the VBHE is relatively small (< 10 m away from VBHE) the fracture reduces ΔT_b in all simulation cases for slow groundwater flow compared with the homogeneous condition (Figure 7.6 A1). However, X_{2K} can be extended (as well as reduced) by fractures at small distances for slow groundwater velocity. For medium groundwater velocity, the fracture influence can go in either direction depending on the other fracture parameters. The median does not vary because the majority (> 50 %) of fracture parameter sets in the MC analysis resulted in there being no change to ΔT_b due to at least one fracture parameter in a set being ineffective. The cases when fracture parameters are ineffective is discussed in Chapter 6.

For medium groundwater velocity, ΔT_b is only reduced for the smallest fracture distances (around or smaller than 1 m) while for larger distances ΔT_b may also increase. X_{2K} is reduced when D_f is < 3 m. When D_f is larger, X_{2K} can be increase by fracture. The uncertainty in ΔT_b due to a fracture when D_f is the smallest is about 5.5 K for slow v_u (Figure 7.6 A1) and about 2 K for medium v_u (Figure 7.6 A2).

Fracture shift (S_f) is also a sensitive parameter both for ΔT_b and for X_{2K} (Figure 7.6 B1, B2, Figure 7.7 B1, B2). This is particularly the case for faster groundwater velocities in the matrix, when the change in groundwater velocities around the fracture is more pronounced: being faster around fracture edges and slower around fracture sides.

In comparison, the **fracture aperture** (W_f) is not a very sensitive parameter (C1 and C2 in Figure 7.6 and Figure 7.7). The uncertainty in ΔT_b and X_{2K} due to other

fracture parameters reduces noticeably only when fracture aperture W_f is less than about 3 mm for medium groundwater flow.

Fracture length (L_f) is a sensitive parameter for both matrix groundwater velocities. The longer the effective fracture, the wider the uncertainty in the thermal performance of a VBHE (Figure 7.6 D1 D2, Figure 7.7 D1 D2). For faster groundwater velocities v_u long fractures (> 100 m) can result in significantly higher temperature change at the VBHE wall compared with the no-fracture scenario. With increasing fracture length for slow v_u, ΔT_b and X_{2K} may be significantly reduced compared with the no-fracture scenario.

The same difference in results between slow and fast v_u is shown for the **fracture angle** (A_f) (Figure 7.6 E1 E2 Figure 7.7 E1 E2). When the fracture is parallel to the groundwater flow direction, the volumetric flow rate in the fracture reaches a maximum, which allows for the largest possible change in local groundwater flow velocities around the fracture. This explains why ΔT_b can be significantly higher relative to the corresponding TAH-2D case at medium v_u.

The **hydraulic conductivity ratio** (R_K) of the fracture and matrix material is a sensitive parameter. For both faster and slower matrix flow velocities, this ratio has to be > 1000 to produce effective difference in the VBHE performance due to presence of a fracture. This effect can be observed in Figure 7.6 (F1 and F2), when R_K < 1000 the width of the 95% confidence interval is less than 1 K for both values of v_u. For high values of the hydraulic conductivity ratio (> 10000), the difference between the results for the medium and slow v_u is similar to that discussed for the parameters of fracture length and fracture angle. Which is when v_u is slow the fracture mostly reduces ΔT_b, while when v_u is medium the fracture can either significantly increase ΔT_b or reduce it. Based on the influence of each separate fracture parameter, the knowledge of even a single sensitive fracture parameter can effectively inform the possible uncertainty in VBHE performance due to the presence of a fracture.

Figure 7.8 shows the distribution of all Monte Carlo simulations with 95 % confidence intervals and the mean for each fixed groundwater velocity: medium and slow (denoted by colour, as for the dotty plots in Figure 7.6).

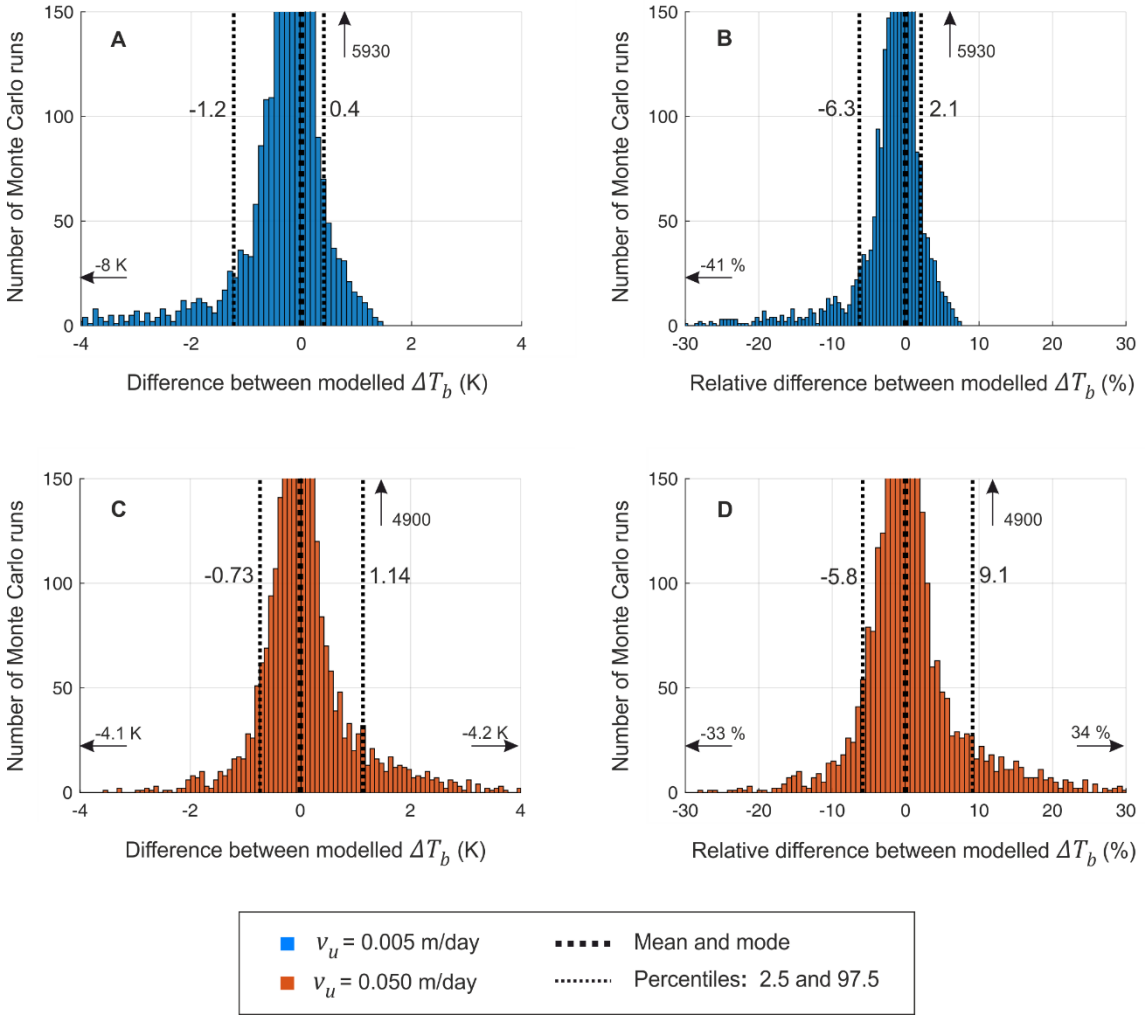

Figure 7.8 Distributions of Monte Carlo simulations (in numbers of runs) of difference in modelled temperature change at the VBHE wall ΔT_b) in real values $\Delta T_b^{TAF} - \Delta T_b^{TAH}$ (A and C) and expressed as relative difference in percentages $\left(\Delta T_b^{TAF} - \Delta T_b^{TAH}\right)/\Delta T_b^{TAH}$ (B and D) for two undisturbed groundwater velocities in the matrix v_u: slow 0.005 m day^{-1} (A and B) and medium 0.05 m day^{-1} (C and D). Thermal dispersivity is zero in all cases. Mode and median values coincide. Plots are truncated (vertically and horizontally) so that less frequent cases are visible - the maximum values for x and y axes are shown on each plot.

Most combinations of fracture parameters resulted in a negligible effect on the VBHE, due to wide value ranges for the selected parameter. This increased the chance of at least one fracture parameter in a set being ineffective.

There is a noticeable difference in distributions between medium and slow groundwater velocity (v_u). For medium v_u there is a positive tail in distribution of

MC runs, which shows that there are possible cases when the fracture significantly increases ΔT_b. There are several cases (outliers) when ΔT_b is increased by the fracture by more than 30 %. Also for medium v_u the 95 % confidence interval is not centred around the zero value of ΔT_b change ($\Delta T_b^{TAF} - \Delta T_b^{TAH}$), but is shifted to the right (i.e. the fracture increases ΔT_b). For slow v_u (Figure 7.8 A and B) the tail is present for negative differences in ΔT_b between models, which is more than 30 % in several cases (outliers). The 95 % confidence interval for slow v_u is narrower and shifted to lower values of model difference in ΔT_b (cases when TAF-2D reduces ΔT_b) compared with medium v_u.

In some cases, ΔT_b is increased by the fracture in the matrix with slow v_u. However, the 97.5 percentile then shows that the increase in ΔT_b due to the fracture is much smaller relative to cases with medium v_u. The outliers for maximum positive relative model difference in ΔT_b (when the fracture increases ΔT_b) do not reach 10 % (Figure 7.8 B). The median and mode values coincide. The majority of the parameter combinations produced ineffective fractures causing no change in ΔT_b.

The method of regional sensitivity analysis described in Wagener & Kollat (2007) was used to estimate the sensitivity of the results to the model parameters, the influence of parameters on the specific output of the model. MCAT toolbox by (Wagener & Kollat) was used to prepare Figure 7.9 and Figure 7.10. These two figures show the model sensitivity to two fracture parameters (D_f and S_f) for slow and medium groundwater flows (v_u) with respect to ΔT_b (Figure 7.9) and X_{2K} (Figure 7.10). Only D_f and S_f are selected for discussion because the model has distinctly different sensitivities to these two parameters depending on the groundwater velocity in the matrix.

For each plot, the ranked parameter populations according to their objective function result (from the best to the worst: the lowest to the highest ΔT_b or X_{2K}) were divided into 10 equally sized groups. Cumulative frequency distributions for each group are plotted as normalised likelihood values. The likelihoods are

normalised by dividing by their total count for each group. If the model result is sensitive to a particular parameter, the cumulative frequency distributions will be different between the 10 groups with varying model parameter. The thick purple line represents the likelihood values for the parameter group which obtained the lowest objective function values (lowest ΔT_b or X_{2K}); the thick blue line represents the cases with the highest values (highest ΔT_b or X_{2K}).

Figure 7.9 shows the sensitivity analysis to D_f and S_f for temperature change at the borehole wall after 30 years of continuous operation, ΔT_b, for two groundwater velocities in the matrix. Figure 7.10 shows the maximum +2 K isotherm extent in the x-coordinate after 30 years of continuous VBHE operation, X_{2K}. It can be interpreted as follows: when all lines are close to each other, and the gradient does not change as D_f or S_f increases, then the model is not sensitive to this parameter. The further the lines are apart (the more their gradient change differs, the more the model is sensitive to the parameter).

This form of analysis allows the MC results (Figure 7.6 and Figure 7.7) to be viewed from a perspective of parameter sensitivity analysis and to quantify at what parameter values the most of the highest or lowest ΔT_b and X_{2K} can be achieved. Figure 7.9 A shows that the lowest temperatures are associated with closest fractures, especially for slow v_u. The fracture parameters are similarly sensitive for both slower and faster v_u, except for fracture distance and fracture shift relative to the VBHE (Figure 7.9 and Figure 7.10).

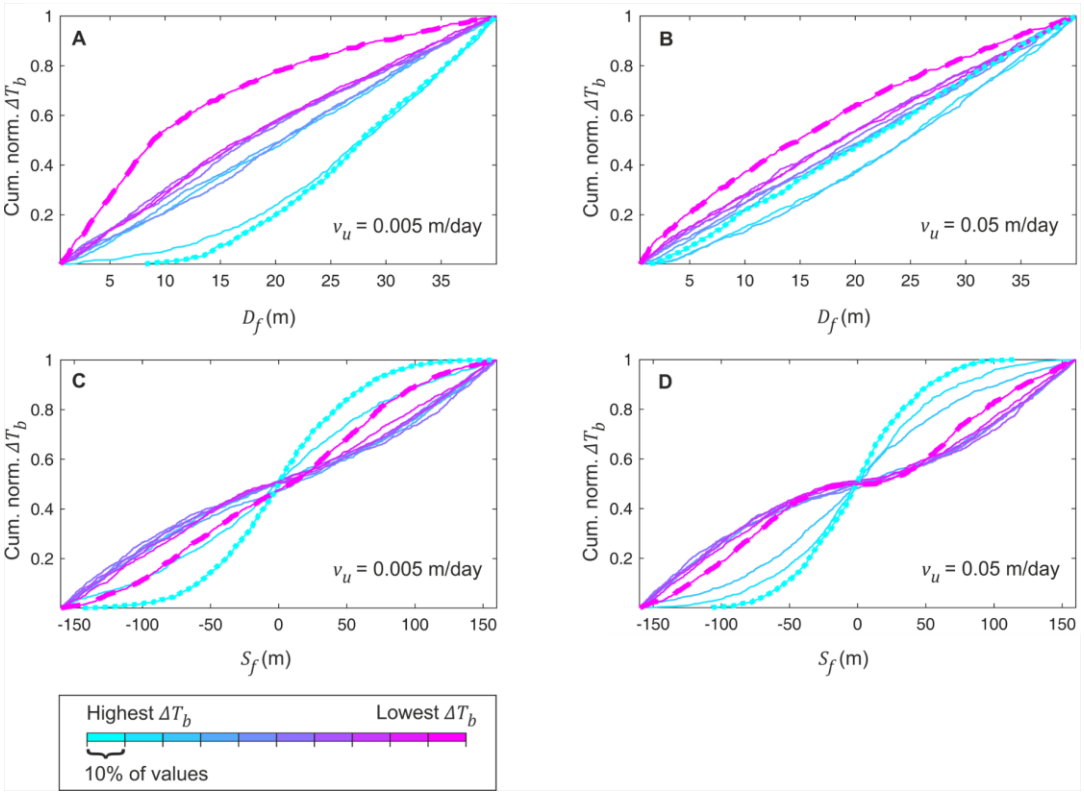

Figure 7.9 Sensitivity analysis for fracture distance from the VBHE D_f (A, B) and fracture shift relative to the VBHE S_f (C, D) for maximal extent in x-coordinate of the +2 K isotherm after 30 years of continuous VBHE operation X_{2K}.

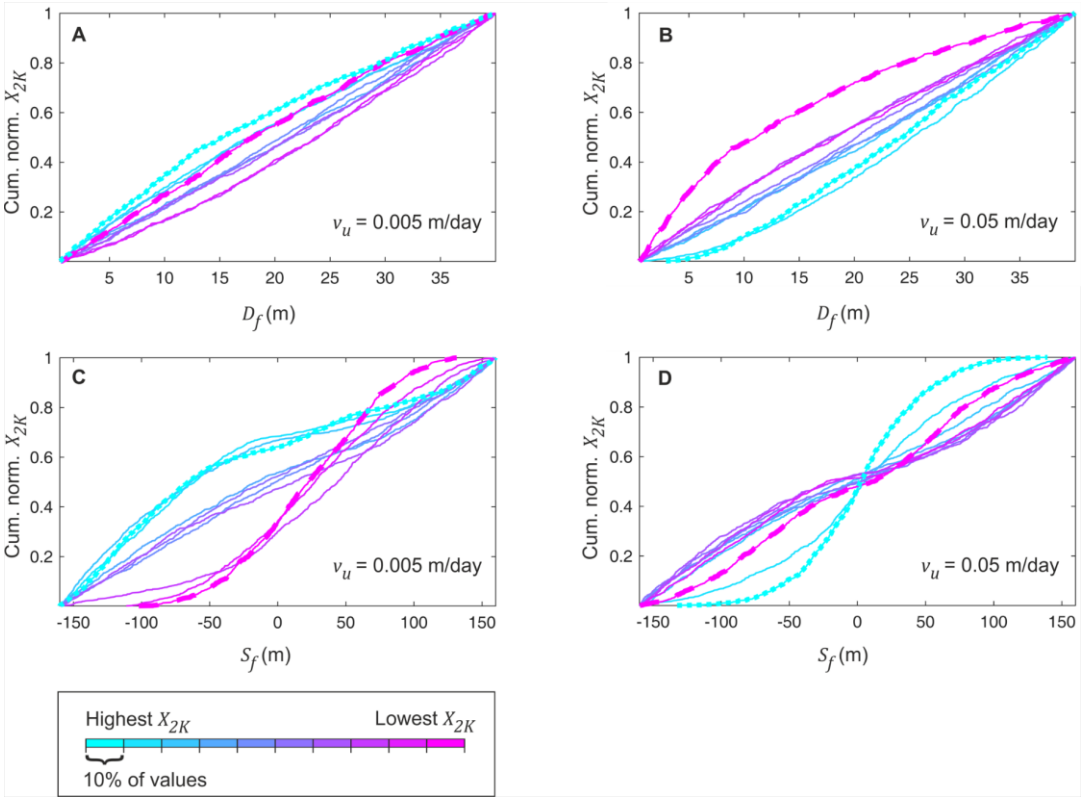

Figure 7.10 Sensitivity analysis for fracture distance from the VBHE D_f (A, B) and fracture shift relative to the VBHE S_f (C, D) for temperature change at borehole wall after 30 years of continuous operation ΔT_b.

The fracture in the matrix with slower groundwater velocity (Figure 7.9 A) is more effective in advecting the heat when the fracture is closer to the VBHE (small D_f). In the matrix with the faster groundwater velocity (Figure 7.9 B) the closer proximity of the fracture to the VBHE also leads to the improved thermal performance. However, it is significantly reduced by the other fracture effects that decrease local groundwater velocities. The cases with the highest temperature change at the borehole wall occur when the VBHE is located near the mid-length of the fracture (fracture shift S_f is close to 0 m), where the fracture significantly slows the local groundwater velocity. Fracture shift has more influence when the groundwater flow in the matrix is faster, when almost none of the cases with low values of ΔT_b (pink lines in Figure 7.9 D) occur for fracture shift values close to 0 m relative to the VBHE.

Most of the lowest values for X_{2K} are reached when the fracture is closest to the VBHE at medium v_u (D_f < 10 m, Figure 7.10 B). For slow v_u the results for X_{2K} are not so sensitive to the fracture distance from the VBHE. The results for X_{2K} are sensitive to the parameter of fracture shift for both values of v_u (Figure 7.10 C and D) but in different ways. For slow v_u the majority of the lowest X_{2K} values (when fracture cools down/shortens the +2 K isotherm) accumulate when fracture shift allows fracture to be close to the VBHE. The highest values of X_{2K} accumulate for large fracture shifts because the fracture is ineffective as it is located far away from VBHE. The majority of such cases are when the fracture is upstream of the VBHE. When v_u is medium, the majority of cases when X_{2K} is highest accumulate when fracture is more or less centred in the VBHE, because it allows X_{2K} to be located in the area of significantly slowed local groundwater velocities.

7.4 Case studies of fracture effects on a multi-VBHE field

VBHE are frequently installed in sets of several boreholes, as a multi-VBHE field. Figure 7.11 explores how a single fracture present in a multi-VBHE field can influence each individual VBHE measured as ΔT_b and the extent of isotherms for

slow (A) and medium (B) groundwater flows after 30 years of continuous operation. All fracture parameters are fixed to the base values used in the single-parameter analysis (Table 6.1). Fracture distance from the central VBHE is 1 m in both subplots.

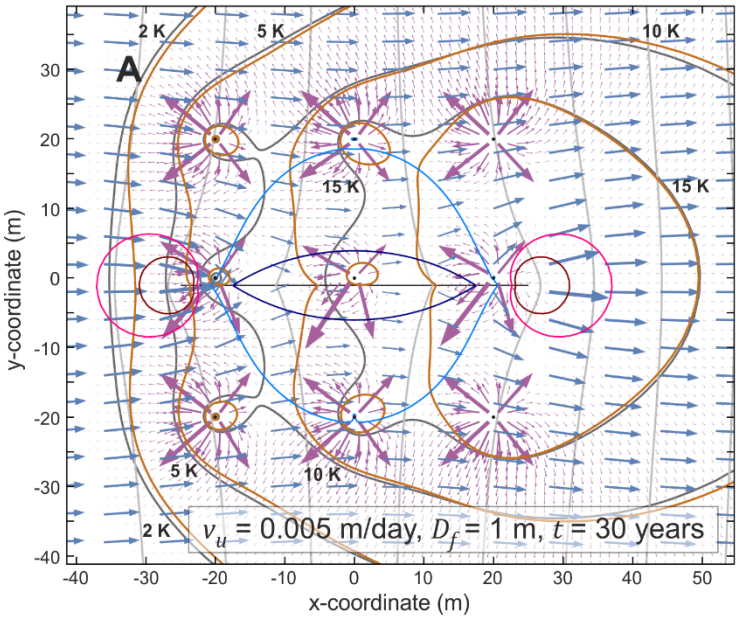

ΔT_b TAH / (TAF-TAH) (K)	-20 m	0 m	20 m
20 m	22.1 / -0.5	30.6 / -0.6	32.1 / -0.5
0 m	23.3 / -3.4	30.6 / **-5.3**	35.3 / -4.2
-20 m	22.1 / -0.6	28.1 / -0.7	32.1 / -0.7

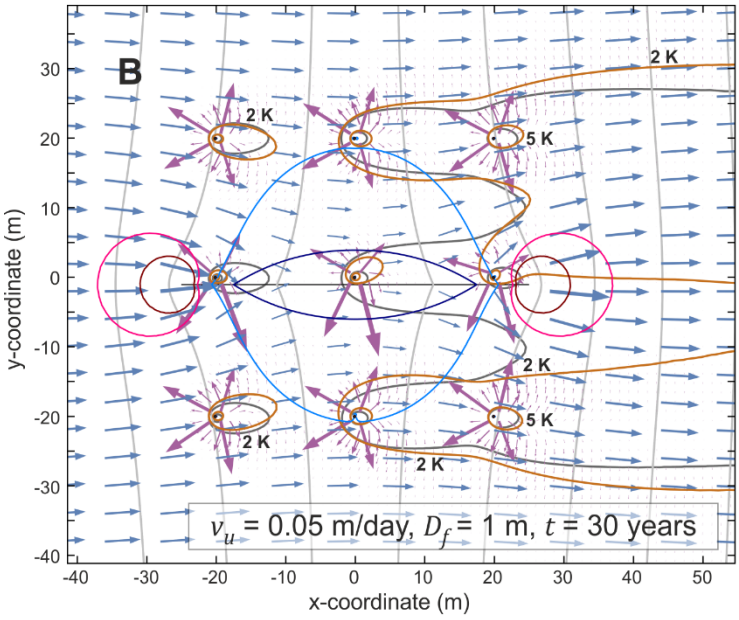

ΔT_b TAH / (TAF-TAH) (K)	-20 m	0 m	20 m
20 m	12.5 / +0.2	13.8 / +0.6	14.7 / +0.4
0 m	12.5 / -1.1	13.8 / -1.4	14.8 / **-2.1**
-20 m	12.5 / +0.2	13.8 / **+0.7**	14.7 / +0.4

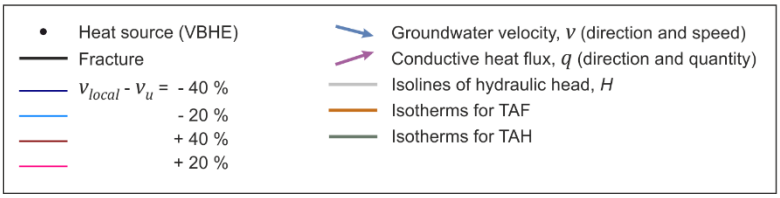

Figure 7.11 Groundwater flow vectors, heat flux vectors and isotherms for a field of 9 VBHE after 30 years of continuous operation (each VBHE continuously injects 5000 W) installed near a vertical flowing fracture located 1 m away from the central VBHE. Groundwater velocity in the undisturbed matrix is (A) slow, v_u = 0.005 m day^{-1} and (B) medium, v_u = 0.05 m day^{-1}.

The values of ΔT_b for each VBHE are shown in the enclosed table for each subplot. The maximum ΔT_b values are highlighted in colour. The fracture effect differs between the boreholes in the field. The VBHE in the upstream row have the lowest values of ΔT_b for both groundwater flows. While the VBHE in the row downstream have the highest ΔT_b values and the thermal performance of these VBHE is undermined. A fracture in the multi-VBHE field with slow groundwater flow significantly increases the thermal transport and improves the thermal performance of the downstream installations. For example, ΔT_b of central VBHE is reduced by a fracture by 5.3 K compared to the case when homogenous aquifer is assumed (see enclosed table in Figure 7.11 A). The practical implication of this is that if the fracture effect is accounted for the VBHE field may have more boreholes or the thermal load on each VBHE can be increased and the system can still operate sustainably.

For the case of medium groundwater flow (Figure 7.11 B) the fracture with the same parameters has relatively smaller beneficial effect. The maximum reduction of ΔT_b is 2.1 K (see enclosed table). However, fracture also has adverse effect on the VBHE located further away (x, y = 0, -20 m). Its ΔT_b is increased by 0.7 K. The illustrated two examples show how groundwater flow changes the significance of fracture in altering the thermal transport within a multi-VBHE field. In the case of medium groundwater flow the fracture significantly changed the local groundwater velocities in the field. Therefore, each VBHE was influenced in a different way by the fracture.

Figure 7.12 shows two example of fracture location within a multi-VBHE field. All fracture parameters are fixed to the base values used in the single-parameter analysis (Table 6.1Table 6.1). Groundwater flow for both cases is medium, 0.05 m day^{-1}.

The first example (Figure 7.12 A) shows the thermal performance of a multi-VBHE field when fracture is located 10 m away from the central VBHE. In the second

example (Figure 7.12 B) the fracture distance to the central VBHE is 1 m and the fracture is rotated 45° to the groundwater flow direction.

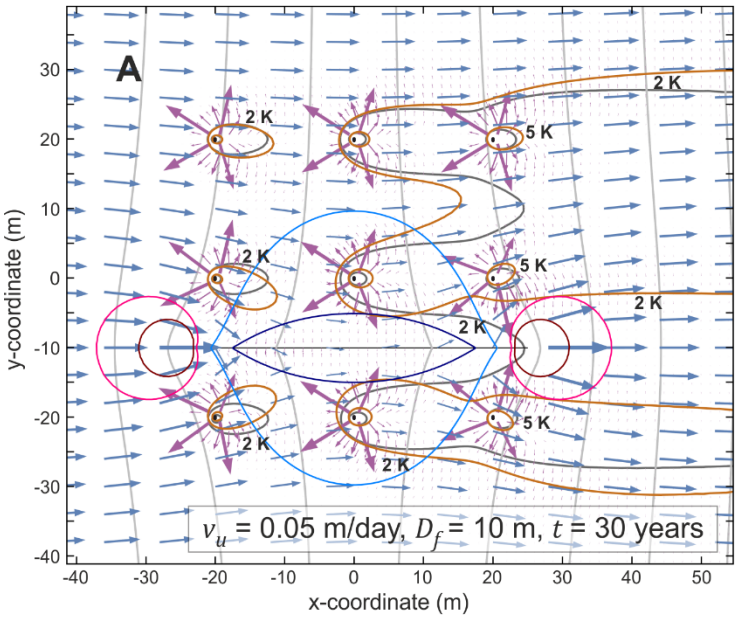

	ΔT_b TAH / (TAF-TAH) (K)		
	-20 m	0 m	20 m
20 m	12.5 / +0.2	13.8 / +0.4	14.7 / +0.4
0 m	12.5 / +0.2	13.8 / +1.1	14.8 / +0.0
-20 m	12.5 / +0.2	13.8 / +1.0	14.7 / +0.0

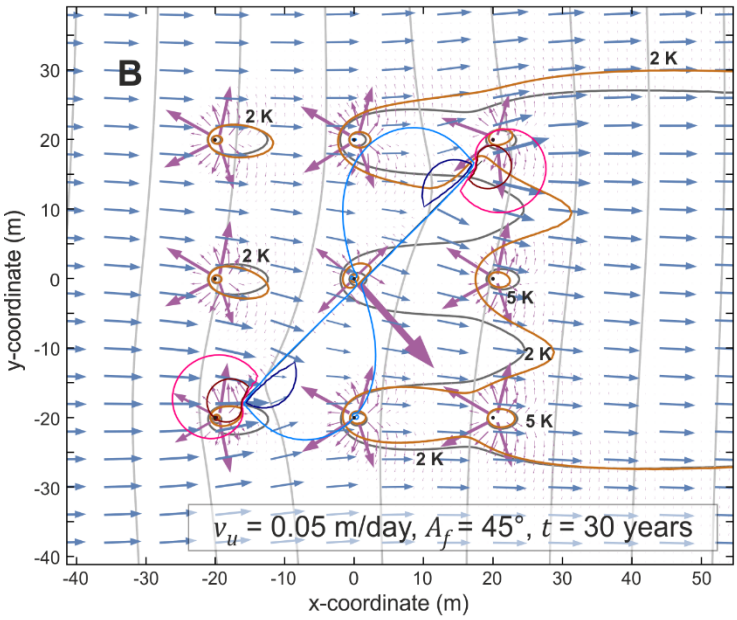

	ΔT_b TAH / (TAF-TAH) (K)		
	-20 m	0 m	20 m
20 m	12.5 / +0.2	13.8 / +0.6	14.7 / -0.8
0 m	12.5 / -0.1	13.8 / -1.2	14.8 / -0.7
-20 m	12.5 / -1.0	13.8 / +0.0	14.7 / +0.0

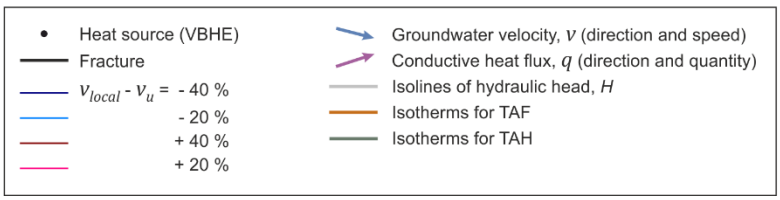

Figure 7.12 Groundwater flow vectors, heat flux vectors and isotherms for a field of 9 VBHE after 30 years of continuous operation (each VBHE continuously injects 5000 W) installed near a vertical flowing fracture, (A) parallel to groundwater flow direction and located 10 m away from the central VBHE and (B) rotated 45° to the groundwater flow direction and 1 m away from the central VBHE. Groundwater velocity in the undisturbed matrix is (A) slow, v_u = 0.005 m day^{-1} and (B) medium, v_u = 0.05 m day^{-1}.

All other parameters are the same between the two examples. The enclosed table for each example shows how ΔT_b is changed by a fracture for each VBHE in the field, compared to the scenario when aquifer is assumed to be homogenous (TAH model).

In the first case (Figure 7.12 A) fracture does not have any beneficial effect. It has small adverse effect on most VBHE in the field. The maximum increase to ΔT_b caused by the fracture is 1.1 K.

The second example (Figure 7.12 B) shows how the thermal performance of each VBHE is changed when the fracture location is different. For example, VBHE located near the fracture (x, y = 0, 0 m) has reduced ΔT_b by 1.2 K, while VBHE located 20 m away (x, y = 0, 20 m) has increased ΔT_b by 0.6 K.

The practical implication of these examples is that the inhomogeneities in an aquifer, for example a fracture, create an uncertainty about the long-term thermal performance of each VBHE in a multi-VBHE field. When the initial field measurements detect a fracture in the field where a multi-VBHE system is planned to be installed, the potential magnitude and direction of fracture effects can be illustrated by several plausible scenarios. In case the maximum estimated fracture effects are within the acceptable uncertainty limits for the design of a VBHE system, the fracture can be ignored.

When the maximal estimated effect of fracture in the long-term renders the system unsustainable, it is advised to conduct further field investigations (described in section 2.3.2). It will help to refine the estimated uncertainty due to fracture influence in the long-term. When the uncertainty due to fracture is considered significant the design of a VBHE system can be optimised (e.g. VBHE locations or thermal load on each VBHE can be adjusted) to maintain the sustainable thermal performance.

7.5 Key messages

The role of groundwater flow in the uncertainty of the thermal performance of a VBHE due to a nearby fracture

The groundwater flow in the matrix determines whether a fracture has a significant effect on VBHE performance. If the matrix groundwater flow is very slow (< 0.001 m day^{-1}) or fast (> 0.3 m day^{-1}), the fracture influence is negligible. For medium matrix groundwater flow (from 0.01 m day^{-1} to 0.1 m day^{-1}) and faster (up to 0.3 m day^{-1}), the cooling effect of the fracture can be more than countered by the slowing of local matrix groundwater velocities and the temperature change at the VBHE wall can be significantly increased by the influence of the fracture. For example, a fracture increased the temperature change at VBHE wall by 5.4 K for medium groundwater flow, as was illustrated on Figure 7.4 and Table 7.1. For slow groundwater flow in the matrix, the fracture in most cases extends the isotherm while for fast groundwater flow it reduces the isotherm length. The divide between fast and slow groundwater flow for the individual isotherm is the point at which the velocity of groundwater is sufficient to extend the given isotherm.

The influence of thermal dispersivity on the uncertainty analysis

Knowledge of the dispersivity in a fast to medium flowing aquifer can reduce the uncertainty in ΔT_b but not the uncertainty in X_{2K}. The faster the matrix groundwater flow, the more effectively knowledge about the matrix dispersivity can reduce the uncertainty in temperature change at the VBHE wall. However, knowledge of the matrix dispersivity is not as useful in estimating the uncertainty in the extent of the isotherm due to a fracture. When dispersion in the matrix is considerable, the positive effect of a fracture on the thermal performance of a VBHE is less than in a no-dispersion scenario.

Significant negative effects of a fracture on a VBHE (when it is located in the area of significantly slowed groundwater velocity) are further exacerbated in cases when an aquifer with medium groundwater flow velocity has considerable

dispersivity, because not only is the groundwater flow is slowed locally by the fracture, the fracture also significantly reduces dispersion in the affected area.

Uncertainty analysis of the VBHE thermal performance influenced by a nearby fracture

Monte Carlo analysis using parameter ranges specific to particular hydrogeological conditions is an effective method to estimate the uncertainty in VBHE thermal performance. The model results were the least sensitive to the fracture aperture unless it was < 3 mm wide for fast groundwater flow and even narrower for slow groundwater flow in the matrix. The model results were sensitive to all other tested fracture parameters. Knowledge about any one of them could inform uncertainty in the VBHE performance, provided the groundwater velocity and the thermal dispersivity are known.

Adverse fracture effects on the VBHE

Reduction in the apparent thermal conductivity is a negative effect that a fracture can have on a nearby VBHE. It occurs in aquifers with medium to fast groundwater velocity (from 0.01 m day^{-1} to 0.5 m day^{-1}). Negative effects of a fracture can be exacerbated when the thermal dispersivity is significant. For these cases, the fracture can reduce the apparent thermal conductivity by slowing local groundwater velocities around VBHE. This occurs when the volumetric flow rate in the fracture is high, and the fracture distance from the VBHE is large enough not to allow for dominance of thermal exchange between the fracture and the VBHE.

Role of fracture parameters for slower and faster groundwater flows

Two fracture parameters that have significantly different sensitivities for slow and medium flow in the matrix are the fracture distance and the fracture shift relative to the VBHE. These two parameters are related to the location of the VBHE relative to areas of locally increased or reduced groundwater velocities caused by the fracture in case of faster groundwater flow in the matrix.

Practical context

The effects of fracture on a VBHE are summarised in Figure 7.13. Fracture nearby a VBHE usually increases thermal transport compared to scenario when aquifer is assumed to be homogeneous. However, when a fracture has high volumetric flow rate and is located further away from the VBHE it can significantly reduce the thermal transport locally to the VBHE due to locally slowed groundwater velocities.

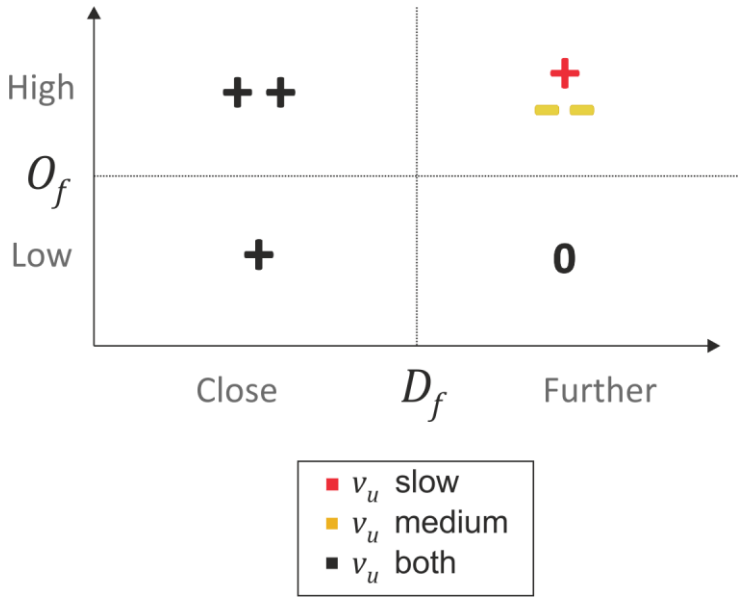

Figure 7.13 Summary of possible fracture effects on the local thermal transport from a VBHE: increase (+), decrease (-) or insignificant effect (0). v_u is groundwater flow in an aquifer, slow (up to 0.01 m day^{-1}) and medium (from 0.01 m day^{-1} to 0.1 m day^{-1}). O_f is the volumetric flow rate in the fracture per unit depth and D_f is fracture distance from the VBHE. Double sign means the effect is relatively greater.

A VBHE is placed somewhere at random into a fractured medium. The rock formation examined is equivalent to a rock type such as sandstone. Here the assumption is made that the VBHE is in a location that is influenced only by an individual fracture, which does not intersect with any other fracture. In reality, depending on the geology, the fractures in the host aquifer (for example, sandstone) may have different orientations and scales and may interact with each other (for instance intersecting to produce interconnected percolating fracture networks). In this hypothetical instance, the installer/designer has no knowledge of the geometrical relationship between the VBHE and the fracture. Therefore, this analysis was undertaken to establish how much such a geological feature might

affect the performance of the device, in principle, under greatly simplified circumstances. This does not provide precise estimates of design uncertainty. The aim was rather to establish insights on how VBHE performance uncertainty may vary due to the fracture, and which hydrogeological aspects it is important to consider. However, these insights could, in principle, be extended to more complex geometries, including interconnected networks.

The uncertainty estimation of the thermal performance of a VBHE system is an essential method to quantify whether it can be sustainable in the long-term. The estimation of hydraulic and thermal properties of an aquifer involve considerable uncertainty even when the aquifer is homogenous. As an engineering rule of thumb, the uncertainties due to estimation of groundwater flow can vary within 30%. The field measurements to estimate the thermal dispersivity in the aquifer also have high uncertainty. Therefore, in relative terms in many cases the uncertainty introduced by a fracture may be within the limits of acceptable uncertainty accounted for in the design of VBHE system as was discussed in section 7.4.

However, for some cases when the fracture is detected near a VBHE and poorly characterized, the preliminary uncertainty estimation for the long-term thermal performance of a VBHE caused by a fracture can exceed the acceptable limits. In this case, additional field measurements have to be undertaken to reduce the estimated uncertainty. A range of methods to identify and characterise a fracture is introduced in section 2.3.2. A combination of geophysical methods can help to identify hydraulically significant fractures in the field. The parameter sensitivity analysis in section 7.3 illustrated how the uncertainty of the fracture influence can be constrained after estimation of even a single fracture parameter. For example, if a fracture is found to be in a close vicinity to a VBHE the range of uncertainty in the long-term thermal performance of a VBHE can be shifted to account only for the beneficial influence of the fracture (Figure 7.6 A1, A2).

Chapter 8 Fracture influence on a VBHE modelled in 3D

This chapter sets out to investigate the effect of a fracture on the thermal performance of a VBHE modelled in 3D.

8.1 Approach

The additional fracture parameters were investigated that are available only in the 3D model, including the angle of fracture inclination and the effect of a horizontal fracture intersecting a VBHE. The methods for single-parameter analysis are outlined in Figure 8.1. The U-pipe was explicitly represented in the 3D model. The methods are described in Chapter 6. This allowed to investigate the relationship between ΔT_b and the mean ΔT of the working fluid inside the U-pipe ΔT_{pm}. The thermal performance of the VBHE was expressed as ΔT_{pm} and the maximum extent of the +2 K isotherm X_{2K}.

The 3D numerical model has four variants:

- **TAF-3D** – **T**hermal transport from a VBHE through an **A**quifer in the presence of a single **F**racture in **3D**.
- **TAFpi** – is the same as **TAF**-3D model but the heat source is modelled explicitly as a grouted U-**pi**pe with water circulating inside it.
- **TAH-3D** – **T**hermal transport through an **A**quifer with **H**omogeneous matrix in **3D**. It differs from TAF-3D only in the aquifer being homogeneous, i.e. the fracture is absent.
- **TAHpi** – is the same as **TAH**-3D model but the heat source is modelled explicitly as a grouted U-**pi**pe.

Chapter 6 describes the details of the models. The 'grout' of TAH-3D has the same hydraulic and thermal properties as the aquifer (i.e. there is no grout). The grout of TAHpi is hydraulically impermeable. Model parameters are listed in Chapter 5. The

TAH-3D model was validated against the moving finite line source analytical solution (MFLS) (Molina-Giraldo *et al.* 2011b) as discussed in Chapter 5. The TAH-3D model is compared with TAHpi in section 8.3.

The questions addressed in this chapter are:

- How do additional fracture parameters (the fracture height H_f, inclination angle I_f and depth beneath the surface Z_f) affect the VBHE?
- How does ΔT_b relate to the mean temperature change of the working fluid ΔT_{pm}? This approximation will help to make practical conclusions based on the previous analyses. Is it practical to explicitly represent the VBHE pipes to model the long-term thermal performance of a VBHE installed near a fracture or influenced by groundwater flow?
- How can a horizontal fracture affect the thermal performance of a VBHE?

8.2 Method

8.2.1 Hydrogeological scenarios

The single-parameter sensitivity analysis for 3D was done similarly to the analysis for the 2D model described in Chapter 6. In the single-parameter analysis, the 3D numerical model was run with individual fracture parameters changed for each model run and the remaining parameters fixed to the base values (Table 6.1). This was carried out for two groundwater velocities in the undisturbed matrix $v_u$of 0.005 m day^{-1} (slow) and 0.05 m day^{-1} (medium). The thermal dispersivity β for this analysis is zero. The effects of the thermal dispersivity were analysed in Chapter 7.

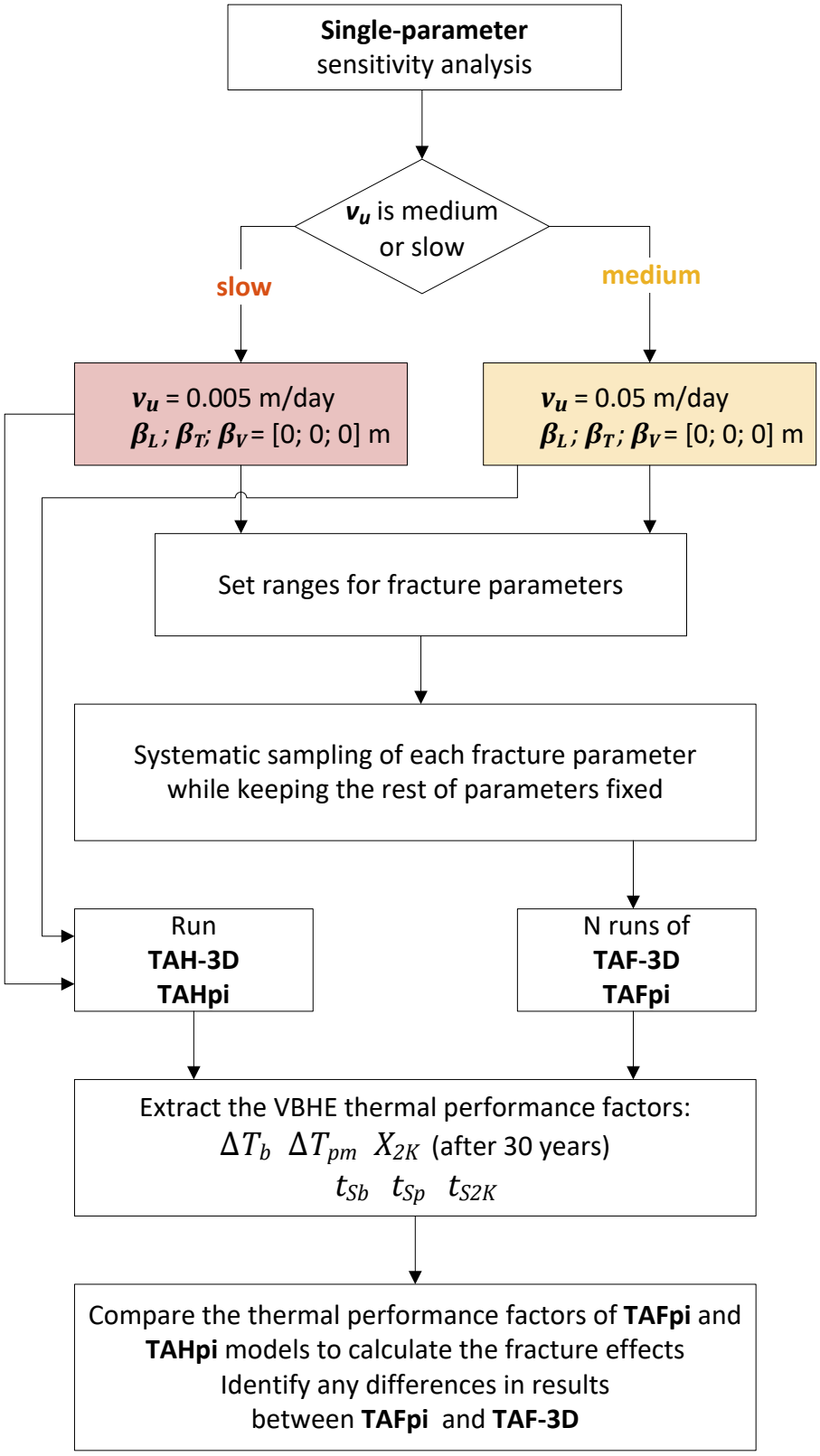

Figure 8.1 The methods outline of the single-parameter sensitivity analysis in 3D. Parameter combinations are in Table 8.1.

8.2.2 Model parameters

The fracture parameters that were investigated in this analysis are listed in Table 8.1. The base values of all other fracture parameters are identical to those for analysis with the 2D model (Chapter 6, Table 6.1). For the analysis in this chapter the fracture rotation angle A_f is fixed to be parallel to groundwater flow direction (A_f = 0°). The base value of the height of the vertical fracture H_f is 100 m so it covers the full length of the VBHE. The range of H_f is selected to start from 10 m as a minimum value. The base value for the fracture inclination angle I_f is selected to be 90° which means that fracture is vertical (perpendicular to the ground surface). The maximum values in the range of I_f for the single-parameter analysis mean that fracture is inclined so that it is close to the ground surface. When fracture inclination is larger than 90° the fracture intersects the VBHE. When fracture inclination is smaller than 90° the fracture is inclined away from the VBHE, and therefore its closest distance to the VBHE equals to D_f (which is the distance between a VBHE the top edge of the fracture, at the ground surface). Figure 5.2 describes how the fracture parameters influence its geometry and its relative position to the VBHE. Additionally, in a separate analysis, I_f was fixed to 0° to test the effects of a horizontal fracture at different depths of intersection with the VBHE.

Table 8.1 Base value and a range for each fracture parameter varied in the single-parameter sensitivity analysis using 3D model.

Parameter	Symbol	Base value	Range (Number of steps)
Fracture height	H_f	100 m	10 m to 190 m (13)
Fracture inclination relative to the horizontal ground	I_f	90°	5° to 175° (16)
Depth from the fracture top edge to the ground surface	Z_f	0 m	0 m to 80 m (12)

8.2.3 Presentation format of the results

The results of the single-parameter sensitivity analysis are discussed with reference to each new fracture parameter which is available in the 3D model (Table 8.1).

The influence of the other fracture parameters (L_f, D_f, A_f, S_f) was discussed in Chapter 7 for the 2D model (which is faster to compute). The results were similar when modelled using the 3D model, therefore they are not discussed here.

The results are presented in the same way as in Chapter 7, according to the indicators of the VBHE thermal performance:

- temperature change at borehole wall ΔT_b
- mean temperature change of the working fluid in the U-pipe ΔT_{pm}
- the maximum longitudinal extent of the +2 K isotherm X_{2K}
- the time to stabilise ΔT_b and X_{2K} (t_{Sb} and t_{S2K})

Both ΔT_b and X_{2K} are calculated after 30 years of continuous operation of the VBHE. ΔT_b is located on the downstream side at the mid-depth of the VBHE (i.e. at x = 0.05 m, y = 0 m, z = 50 m). The extent of X_{2K} was calculated as the maximum value in the x-coordinate determined on the plane in XY axes (at the mid-depth of the VBHE, z = 50 m) and on the plane in XZ axes (y = 0 m). This is because the shape of the isotherm could be asymmetrical both horizontally and vertically due to the presence of a fracture near the VBHE. Finally, how a horizontal fracture affects the thermal performance of the VBHE was discussed.

The thermal performance indicators were calculated for each tested fracture parameter for two fixed values of v_u. The TAFpi results were compared with the results of TAHpi (model without the fracture). In the results that follow, the

relative performance indicators (R, eq. (8.1)) are reported, i.e. the relative difference between the TAFpi and TAHpi models.

$$R = \frac{F^{TAF_{pi}} - F^{TAH_{pi}}}{F^{TAH_{pi}}} \tag{8.1}$$

where F is a performance indicator (for example ΔT_b or X_{2K}) and the superscripts denote the model.

8.3 Results

8.3.1 Effect of the explicit representation of U-pipe in the model for the long-term thermal performance of a VBHE

Figure 8.2 shows how ΔT_b and ΔT_{pm} develop with time. ΔT_b is modelled using TAHpi and TAH-3D. ΔT_{pm} is consistently higher than ΔT_b.

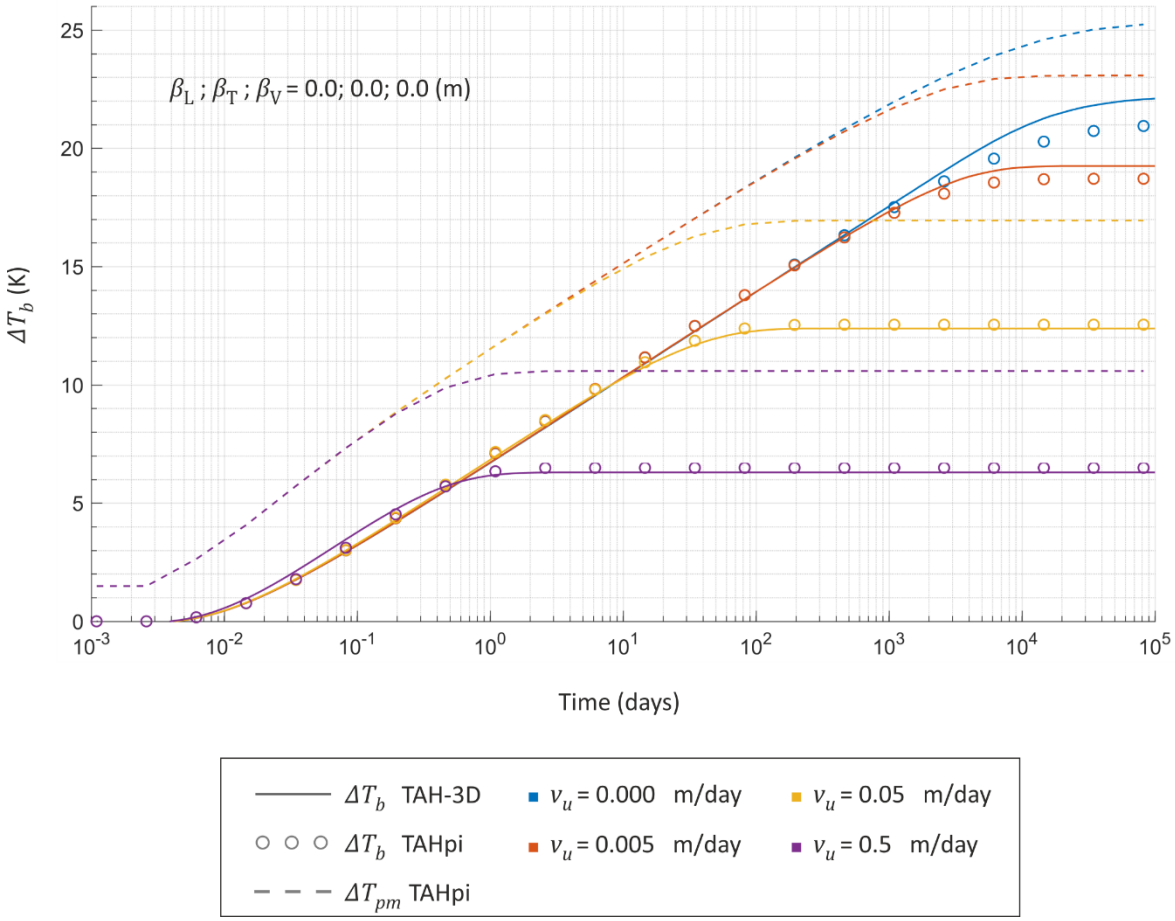

Figure 8.2 Development with time of the temperature change at the VBHE wall ΔT_b and mean temperature change of working fluid inside the U-pipe ΔT_{pm} for four groundwater velocities

v_u. ΔT_b was calculated using the TAH-3D and TAHpi models. All model parameters are listed in Chapter 6.

At long times the difference in ΔT_b between TAH-3D and TAHpi in the absence of groundwater flow is significant (TAH-3D result is higher than TAHpi by about 1 K). This is because the ground surface is fixed to initial temperature and at absent groundwater flow the axial conduction has significant influence on ΔT_b. The pipe circulates the water along the depth of the VBHE. Thus, the change in ΔT_b is more even along the VBHE depth. At mid-depth of the VBHE, ΔT_b is smaller than when modelled using TAH-3D. However close to the surface and bottom of the VBHE, ΔT_b modelled using TAHpi is higher than the result of TAH-3D. This corresponds with the results shown in Figure 8.5.

At fast and medium groundwater flows, ΔT_b calculated using TAH-3D is lower compared to TAHpi. This is because TAH-3D does not have impermeable grout and the groundwater flow directly cools ΔT_b by advection (see Figure 5.3).

Figure 8.3 shows the distribution of differences between ΔT_b and ΔT_{pm} for TAFpi model for L_f, D_f, A_f, S_f, Z_f, H_f, I_f parameter combinations used for single-parameter sensitivity analysis for two groundwater velocities v_u (slow and medium) excluding a case when a horizontal fracture intersects the VBHE at the depth of 50 m. The ranges of used fracture parameters are given in Table 6.1 and Table 8.1. In total 299 TAFpi model runs were used for this figure from the single-parameter sensitivity analysis and 12 TAHpi model runs without the fracture (6 values of v_u with and without thermal dispersivity). The 95 % confidence interval is within 0.5 K.

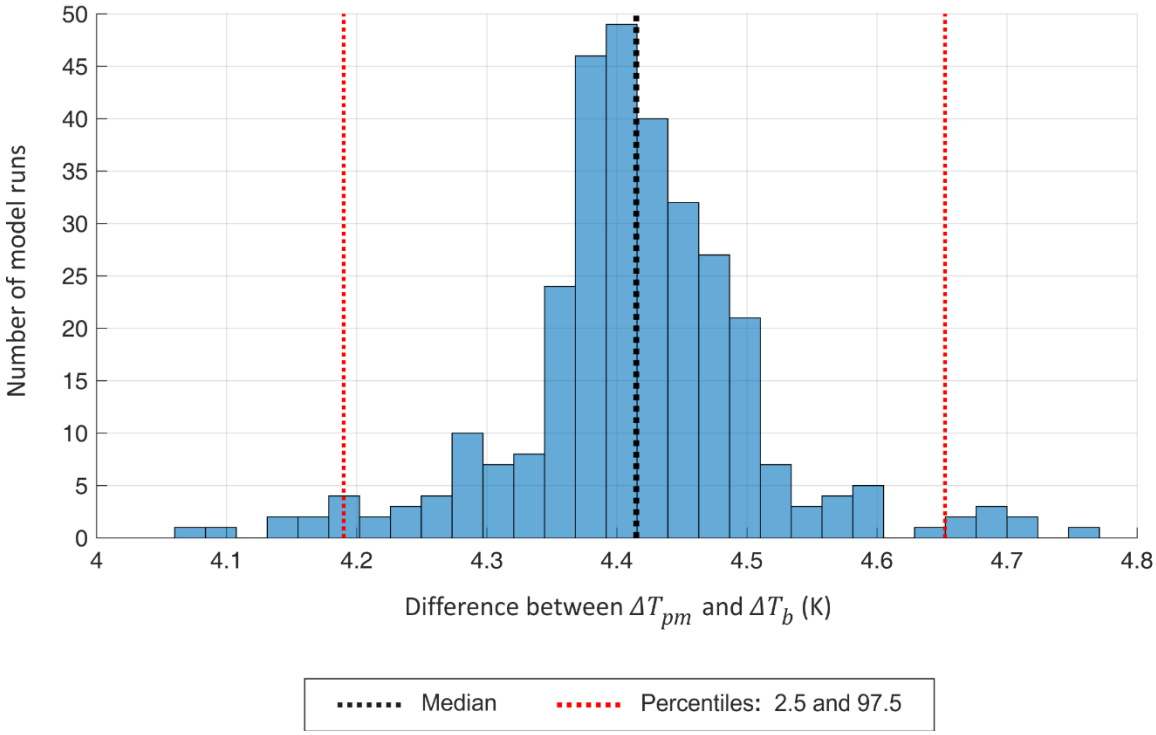

Figure 8.3 The difference between mean temperature change of working fluid in the U-pipe ΔT_{pm} and temperature change at the VBHE wall ΔT_b after 30 years of VBHE operation. The results using TAFpi and TAHpi are combined in this histogram.

The results in Figure 8.2 and Figure 8.3 suggest that the explicit representation of pipes is not necessary to model the long-term thermal performance of a VBHE. Such models have considerably longer execution times and higher memory requirements (on IRIDIS 5 TAFpi required 13 hours and 95 GB, while TAF-3D only 2.5 hours and 55 GB). However, for absent or slow groundwater flow the model TAF-3D can overestimate ΔT_b because it does not explicitly model the pipes. Figure 6.2 and Figure 8.3 show that the hydrogeological settings near the VBHE affect the borehole thermal resistance only by a small amount. The borehole thermal resistance is described in section 2.2.5.

Figure 8.4 shows the temperature change of the working fluid (and its mean value) along the VBHE U-pipe after 30 years of VBHE operation for four v_u. At the inlet pipe the temperature is higher than at the outlet by 3 K. This 3 K difference corresponds to the transfer of 5000 W into the ground, and it is kept constant.

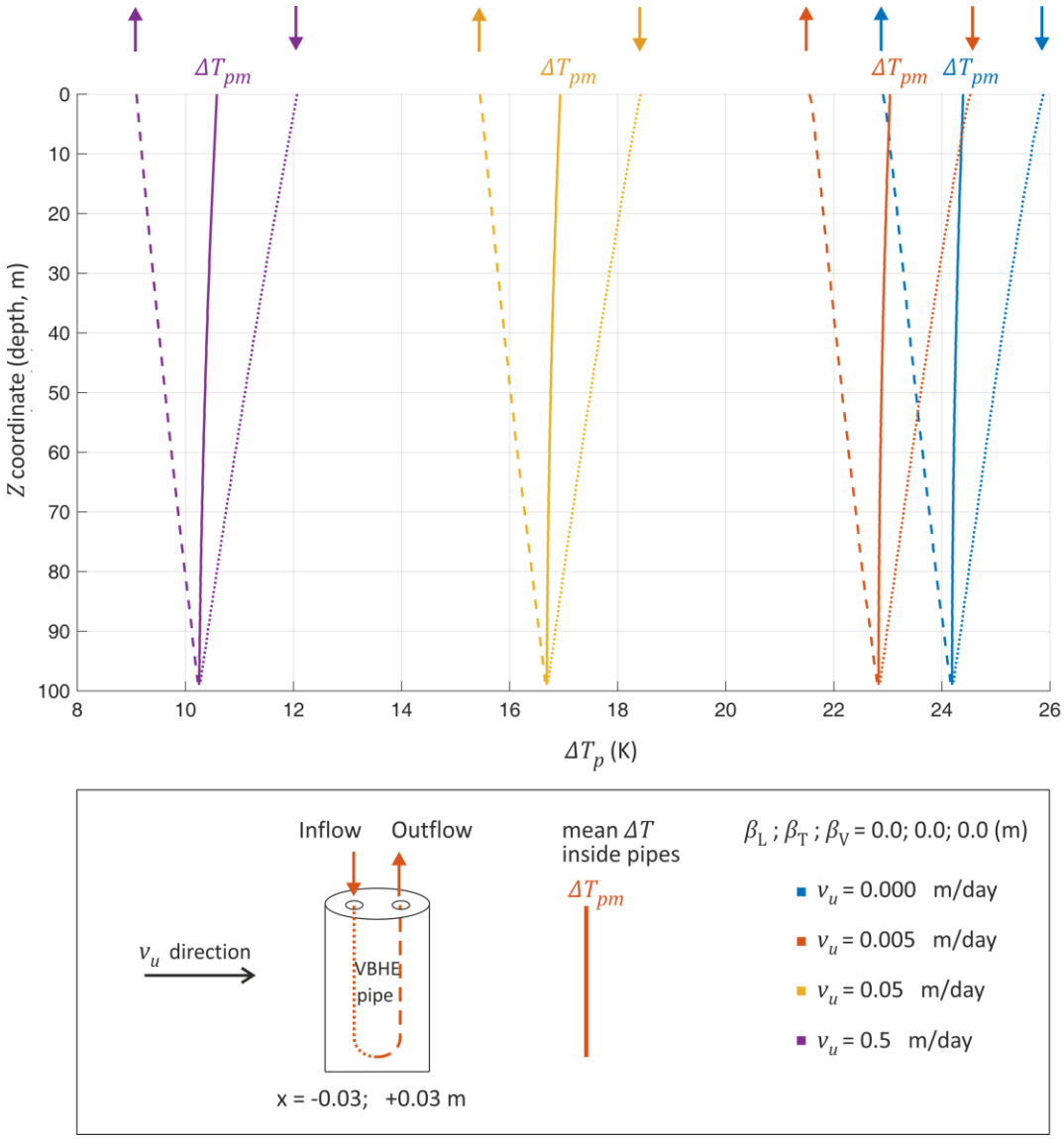

Figure 8.4 Temperature change of the working fluid along the U-pipe ΔT_p after 30 years of VBHE operation at different groundwater velocities v_u. Mean temperature between inlet and outlet of the U-pipe is also shown ΔT_{pm}.

Correspondingly, ΔT_b at the left and right side of the VBHE are also expected to be different for TAHpi compared with TAH-3D. This is because the heat source of TAHpi is the U-pipe, the inlet of which is hotter and is located closer to the VBHE wall than the heat source of TAH-3D. The following discussion is about the change in ΔT_b along the VBHE length on both sides (left and right) of the VBHE.

Figure 8.5 shows how the inclusion of U-pipe in the model can influence ΔT_b along the VBHE depth. The temperature change along the left (upstream) and right (downstream) sides of the VBHE and their mean value are shown after 30 years of

continuous VBHE operation. ΔT_b is presented for both the TAH-3D and TAHpi models to compare the results for different values of v_u.

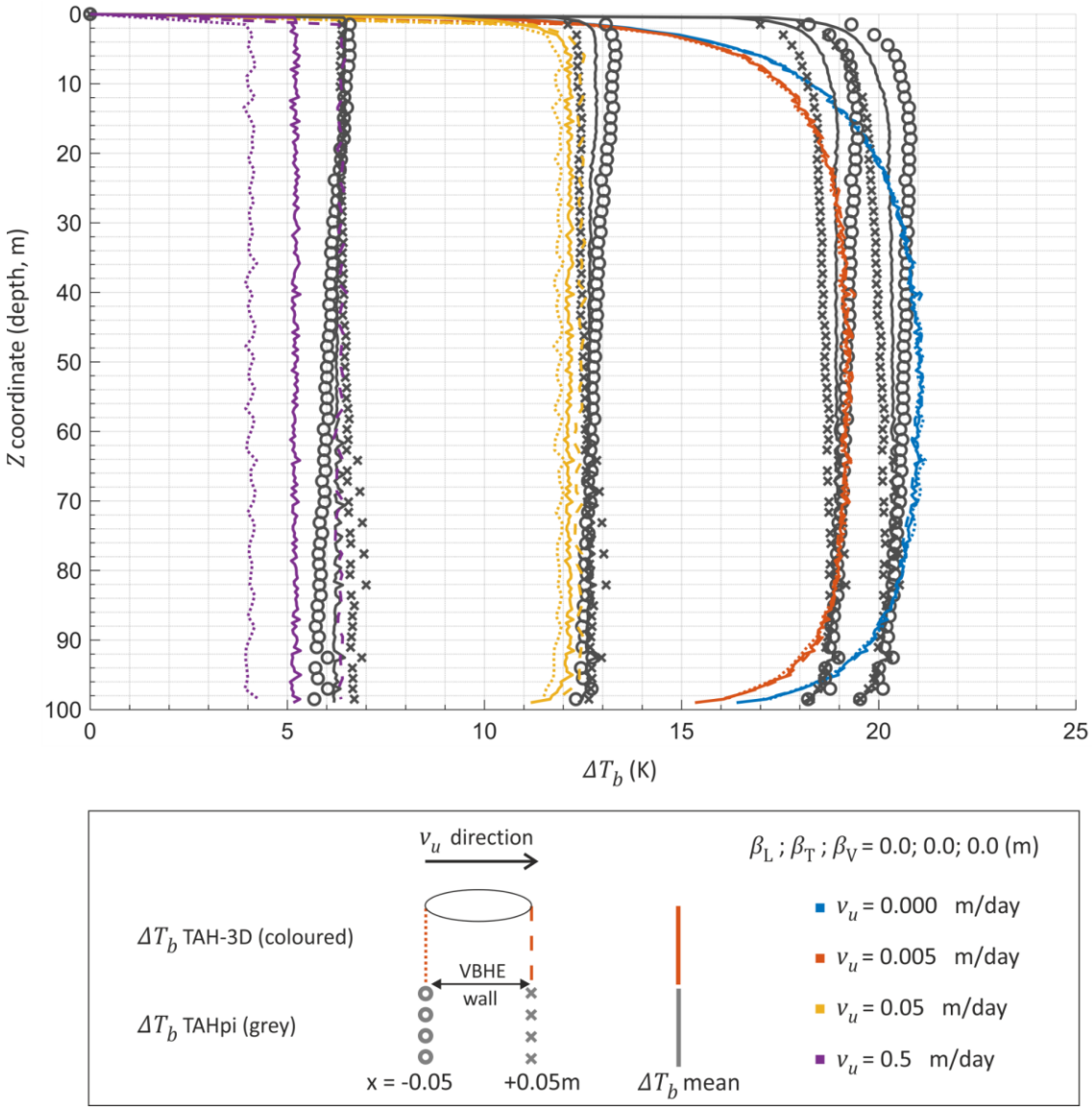

Figure 8.5 Temperature change at the VBHE wall ΔT_b along the VBHE depth after 30 years of VBHE operation for different groundwater velocities v_u. For each v_u the results are presented for TAH-3D (coloured) and TAHpi (grey). Mean temperature between upstream and downstream sides of the VBHE wall at each specific depth is also shown.

The temperature change along the VBHE wall is more evenly distributed for the TAHpi model with U-pipe compared with TAH-3D. For fast groundwater flow v_u the ΔT_b calculated on the left side of the VBHE (upstream) is lower when modelled using TAH-3D compared with TAHpi. This is because TAH-3D does not have grout and the groundwater directly cools down the location where ΔT_b is calculated as sketched in Figure 5.3 A.

When hot water enters the U-pipe (on the left, upstream side of the VBHE) it gradually cools down while it travels down the left side of the VBHE U-pipe (Figure 8.4). For fast v_u the left side ΔT_b modelled using TAHpi decreases similarly, at the bottom it is cooler by about 1 K compared with the left side value at the top of the VBHE. Then water enters the right side of the U-pipe to return to the ground surface. The downstream (right-hand side) value of ΔT_b is noticeably higher. This is because on the right-hand side the VBHE wall receives heat not only by conduction from the U-pipe but also the heat advected with groundwater from the upstream side of the VBHE, as sketched in the Figure 5.3 B.

When groundwater flow is medium or slow, this effect of advection of heat from the left to the right side of the VBHE wall is negligible. Therefore, ΔT_b on the left side is closely related to ΔT_p in the left side of the U-pipe, and similar relation is for ΔT_b on the right side. At the bottom of the VBHE where the left and right side of the U-pipe are connected (and therefore have the same ΔT_p), the values for ΔT_b on both sides of the VBHE are also similar.

8.3.2 Single-parameter sensitivity analysis for fracture parameters in 3D

In this section, the results from single-parameter sensitivity analysis are discussed for fracture parameters which are available only in the 3D model: Z_f, H_f, I_f. The base value for fracture inclination I_f is 90° which means that the fracture is vertical.

Figure 8.6 shows how the changes in the fracture depth below the ground surface Z_f and fracture height H_f influence the mean temperature change of the working fluid in the U-pipe ΔT_{pm} and the time to stabilise it t_{Sp}.

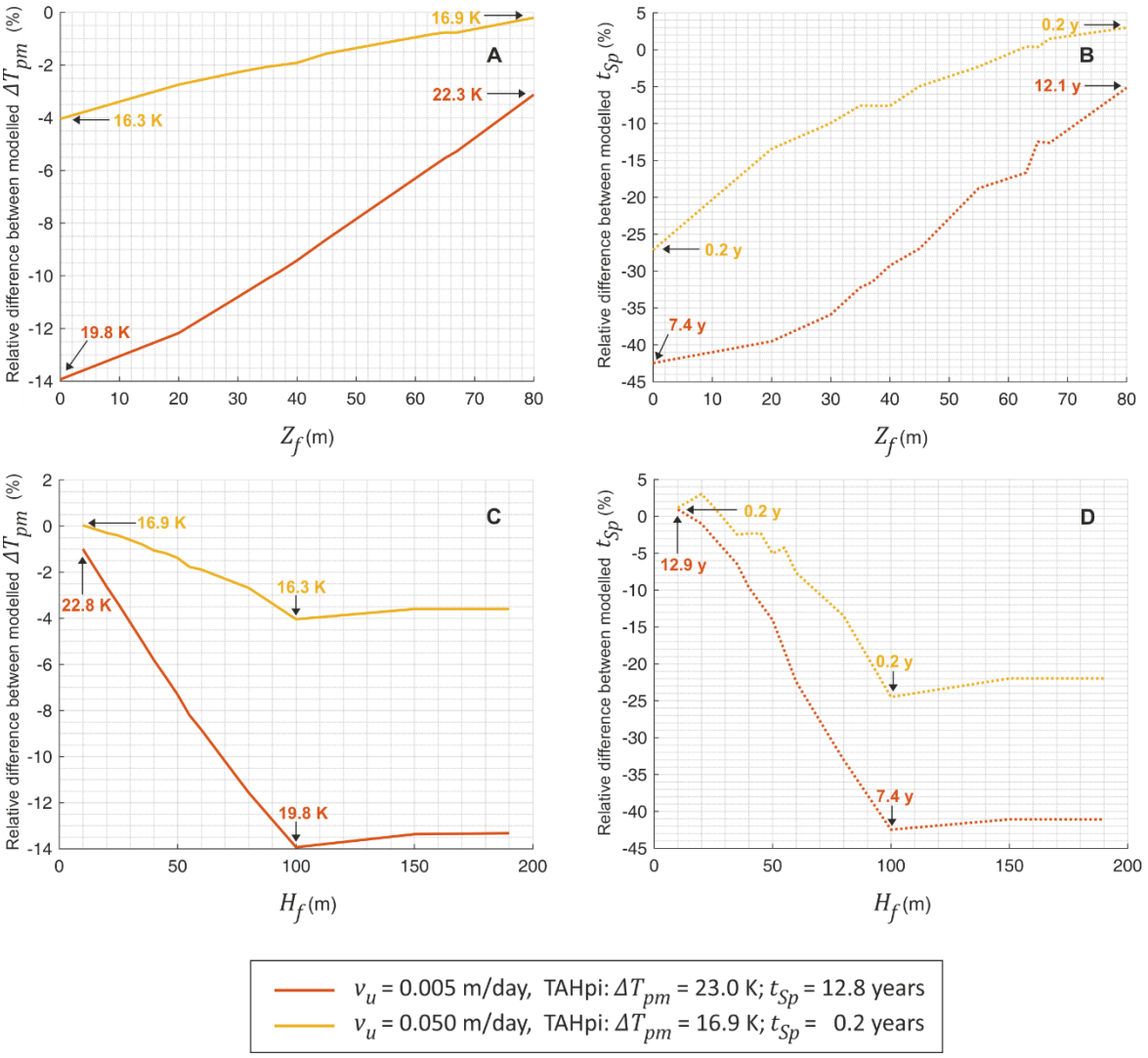

Figure 8.6 The relative difference between the TAFpi and TAHpi models in the mean temperature change of the working fluid ΔT_{pm} after 30 years of VBHE operation and in the time to stabilise it t_{Sp} for two groundwater velocities v_u for (A and B) changing fracture depth below ground surface Z_f and (C and D) changing fracture height H_f.

Clearly, the deeper the vertical fracture is below the ground Z_f, the less is its cooling effect on the ΔT_{pm} and time to stabilise it t_{Sp} (Figure 8.6 A and B). It occurs for both groundwater velocities but especially for slower groundwater flow where the effect of the fracture is more significant.

The height of the vertical fracture H_f has a similar effect, the longer the height of the fracture, the longer is the area of influence between the VBHE and the nearby vertical fracture and the stronger is the influence of the fracture (Figure 8.6 C and D). However, when fracture height is longer than the length of the VBHE (100 m), the fracture effect is slightly smaller. This is because the groundwater velocities at

the fracture bottom edge are faster and the cooling effect of the fracture is milder as the VBHE is further away from the fracture edge. The relative difference between models in time t_{Sp} needed to stabilise ΔT_{pm} follows similar pattern.

Figure 8.7 shows how a fracture near the VBHE changes the longitudinal extent of the +2 K isotherm X_{2K} and time to stabilise it t_{S2K} in the single-parameter analysis for fracture depth below the surface Z_f (A and B) and for fracture height H_f (C and D).

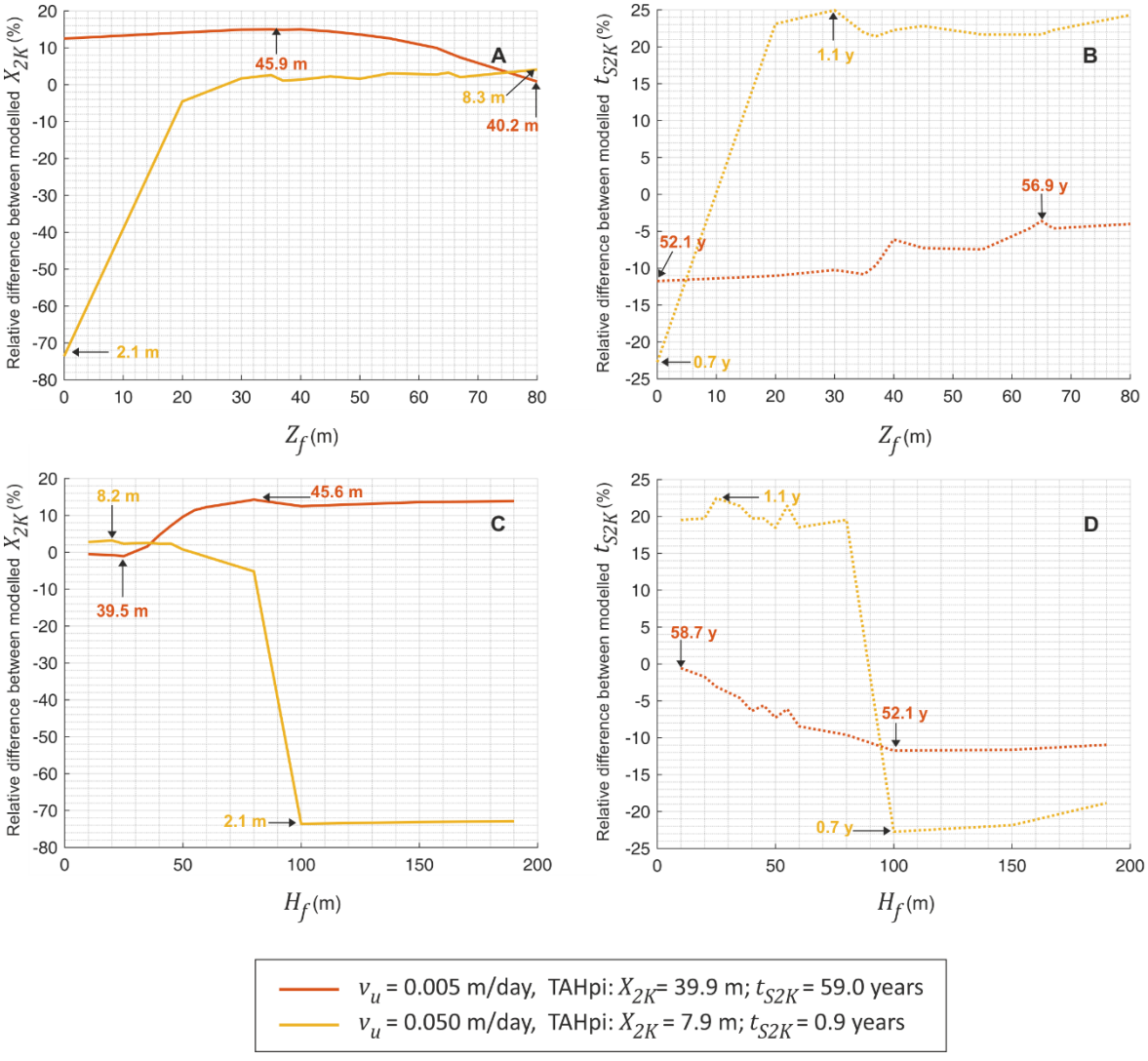

Figure 8.7 The relative difference between the TAFpi and TAHpi models in the longitudinal extent of the +2 K isotherm X_{2K} after 30 years of VBHE operation and in time to stabilise it t_{S2K} for two groundwater velocities v_u for (A and B) changing fracture depth below ground surface Z_f and (C and D) changing fracture height H_f.

For medium groundwater flow when the fracture is just beneath the surface (i.e. Z_f is small), the thermal perturbation is spread further by the fracture, which

causes the X_{2K} to be reduced to the minimal value and the isotherms of the lower ΔT to be extended. H_f has similar effects on the VBHE as Z_f as they change the area of fracture influence in a similar way. Therefore, further discussion of the effects of Z_f is also relevant to H_f.

For slow groundwater flow, X_{2K} is extended as the volumetric flow rate inside fracture O_f is not sufficient to shrink it (insufficient cooling effect of the fracture). For medium groundwater flow, the time to stabilise the isotherm is increased when fracture is deeper beneath the surface (when Z_f value is large). This is because as the fracture is lowered deeper beneath the surface, its cooling effect on the VBHE is reduced. The VBHE is located in the mid-length of the fracture where effect of the locally slowed groundwater is the most significant. Therefore, as Z_f is increasing, t_{S2K} is increasing as well, affected by slowed local groundwater velocities in the mid-length of the fracture whose relative effect compared to the cooling effect is increasing with increasing Z_f.

Figure 8.8 shows how fracture inclination angle I_f affects ΔT_{pm} and t_{Sp}. For explanation of the meaning of I_f values see the sketch in Figure 8.8 A and Figure 5.2.

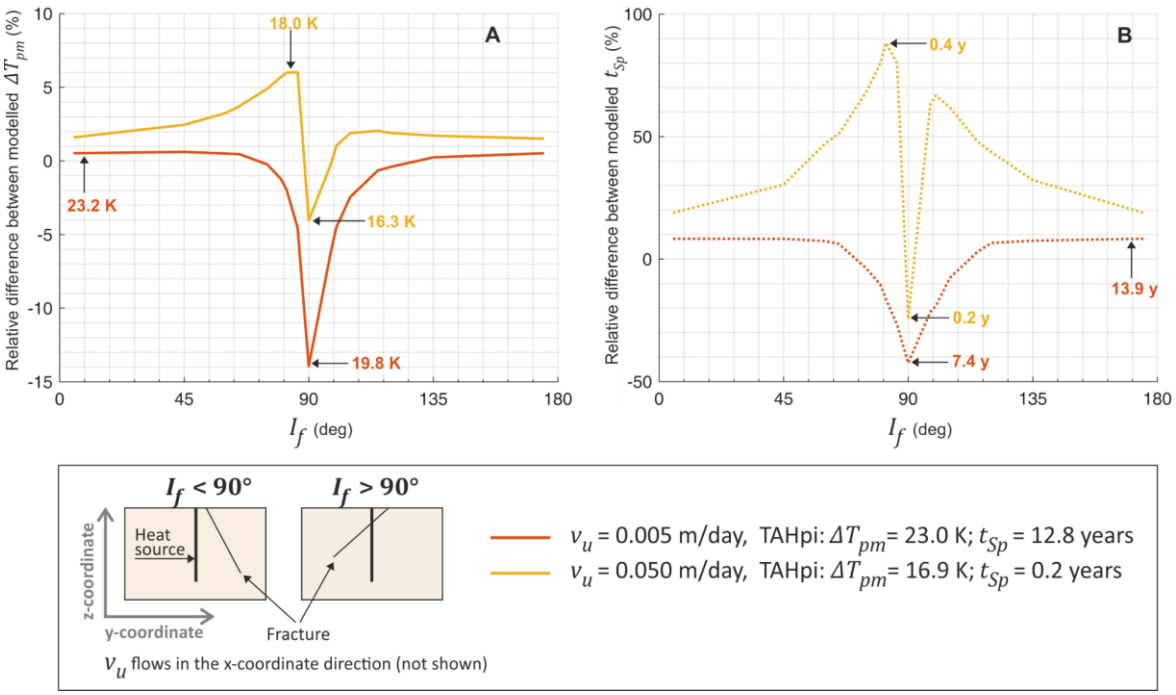

Figure 8.8 The relative difference between the TAFpi and TAHpi models for changing fracture inclination I_f in (A) the mean temperature change of the working fluid in the U-pipe ΔT_{pm} after 30 years of VBHE operation, and (B) time to stabilise it t_{Sp} for two groundwater velocities v_u. When fracture inclination is < 90° the fracture is inclined away from the VBHE, and therefore its closest distance to VBHE equals to D_f at the top edge of the fracture.

When I_f is 90° (fracture is vertical) the fracture has maximum beneficial effect on the VBHE for both groundwater flows. This is because in this case the fracture is closest to the VBHE along its full length. The rapid change in both thermal performance indicators when I_f deviates from 90° is due to the close proximity of the fracture to the VBHE (the base value of D_f = 1 m, similarly to 2D). This causes a large increase in the effective fracture distance from the VBHE when I_f is changed from the base value of 90°.

For slow groundwater velocity when I_f deviates from 90° (when the fracture is not parallel to VBHE) the effect of the fracture diminishes gradually. For medium groundwater velocity when I_f deviates from vertical (e.g. I_f = 80° or I_f = 100°) the fracture increases ΔT_{pm} compared to a result without the fracture (TAHpi). This is especially prominent for I_f < 90°, when fracture is inclined away from the VBHE, so that its cooling effect is smaller. In this case the fracture increases ΔT_{pm} (as well as t_{Sp}) because groundwater local to the mid-length of the fracture (where the VBHE

is located) is slowed and therefore the thermal transport from the VBHE is reduced compared to the results by TAHpi.

The influence of the fracture inclination I_f on X_{2K} and t_{S2K} is shown in Figure 8.9.

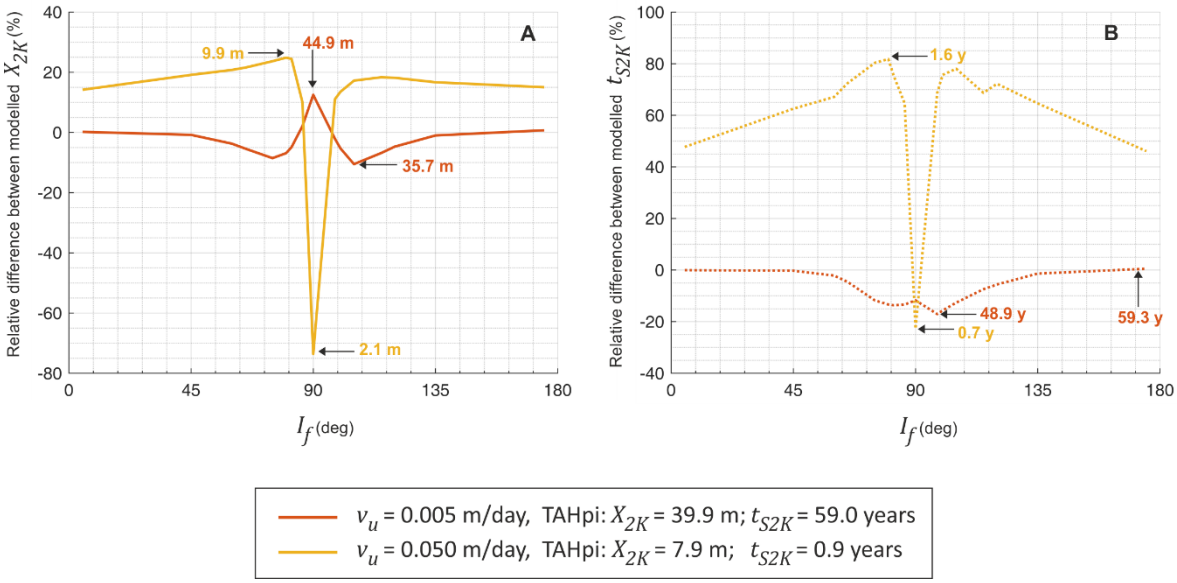

Figure 8.9 The relative difference between the TAFpi and TAHpi models for changing fracture inclination I_f in (A) the longitudinal extent of +2 K isotherm X_{2K} after 30 years of VBHE operation, and (B) in time to stabilise it t_{S2K} Figure 6.3for two groundwater velocities v_u.

When the fracture is vertical (parallel to the VBHE) the fracture effect is maximum. It reduces X_{2K} and t_{S2K} for medium v_u and maximally extends X_{2K} for slow v_u. For medium groundwater velocity the effects of the fracture when it deviates from being vertical are similar to the results for ΔT_{pm} (Figure 8.8).

For slow groundwater flow when I_f is not vertical (deviates from 90°) X_{2K} and t_{S2K} are reduced to their minimum values. This occurs because a non-vertical fracture is less effective in cooling the VBHE as it is effectively further away from the VBHE than when it is vertical. The fracture is too far to be able to advect the +2 K isotherm and to effectively cool ΔT_{pm}. In this case, the fracture advects the isotherms of smaller temperature change and thus reduces X_{2K}.

8.3.3 Effect of a horizontal fracture intersecting the VBHE

The final part of the single-parameter sensitivity analysis is the discussion of the effects of a horizontal fracture on the VBHE. An example of isotherms for two

groundwater velocities when the horizontal fracture intersects the VBHE is shown in Figure 8.10. There is no significant difference in the shape of isotherms between the scenario with and without fracture except for the +0.5 K isotherm for medium groundwater flow. It should be noted that in the single-parameter sensitivity analysis for the 3D model, the maximum downstream extent of the isotherm is reported (maximum value for both the XY and XZ planes).

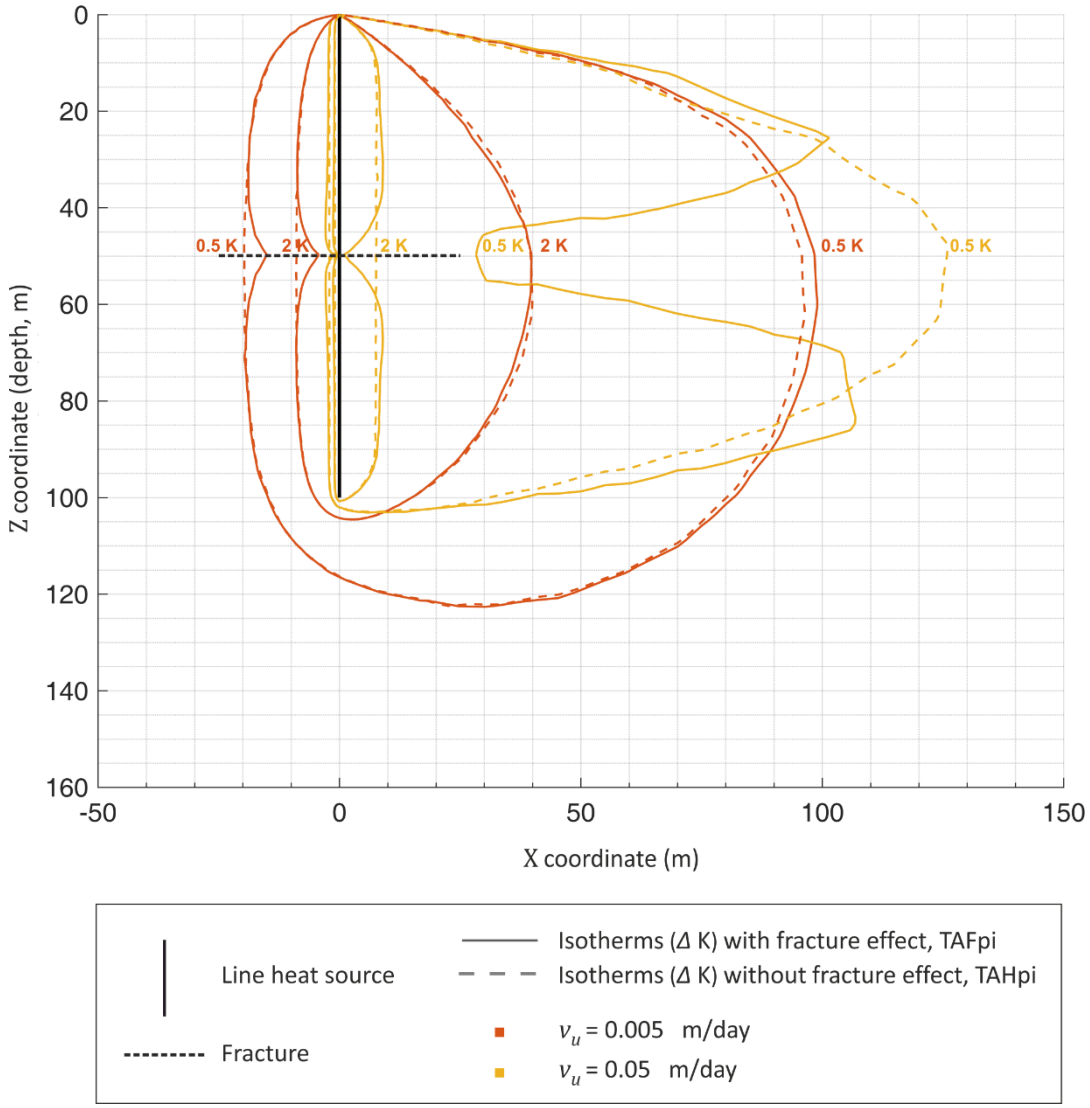

Figure 8.10 Isotherms for temperature change ΔT on XZ plane for the TAFpi and TAHpi models for two groundwater velocities v_u after 30 years of continuous VBHE operation. The fracture is horizontal to the ground surface (I_f = 0°) and intersects the VBHE at depth Z_{fh} = 50 m (mid-length of the VBHE). The fracture has both height H_f and length L_f equal to 50 m and is centred around the VBHE. All other fracture parameters are kept at the base values.

Figure 8.11 shows how the horizontal fracture influences ΔT_{pm} and t_{Sp} for different depths of intersection with the VBHE Z_{fh}.

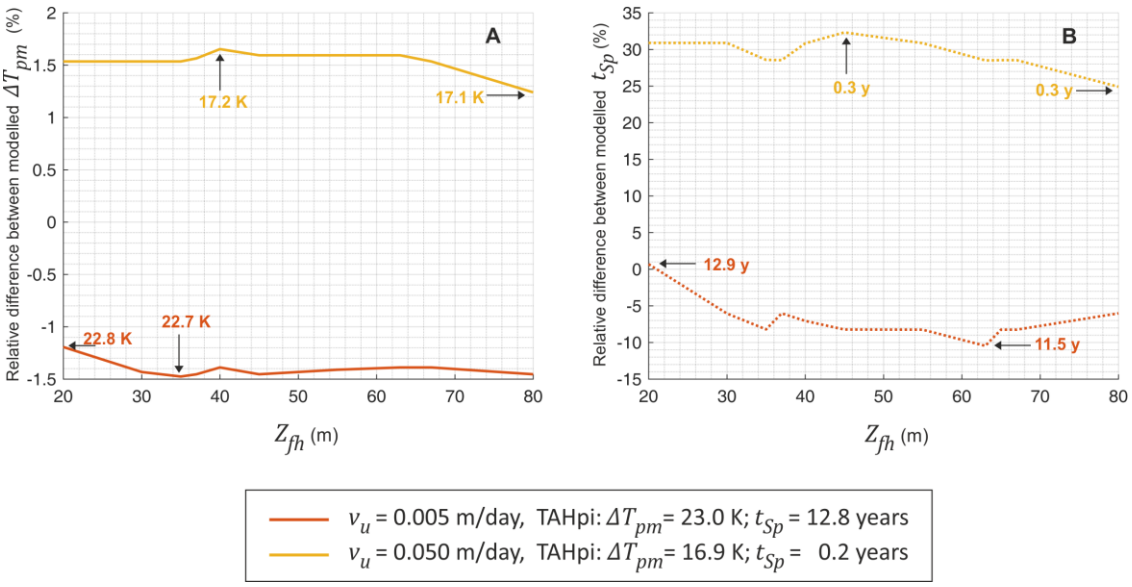

Figure 8.11 The relative difference between the TAFpi and TAHpi models for changing depth of the horizontal fracture below the ground surface Z_{fh} in (A) the mean temperature change of working fluid in the U-pipe ΔT_{pm} after 30 years of VBHE operation, and (B) time to stabilise it t_{Sp} for two groundwater velocities v_u.

Figure 8.11 shows that the model results are not sensitive to the depth at which the horizontal fracture intersects the VBHE Z_{fh} – it does not have a significant influence on ΔT_{pm} which is in accordance with the findings by (Dehkordi *et al.*). Also Z_{fh} does not significantly influence t_{Sp}.

At medium groundwater velocity the horizontal fracture increases ΔT_{pm} by approximately 1.5 K (compared to TAHpi, where the fracture is absent). This effect holds regardless of the depth at which the fracture intersects the VBHE. This is because above and below the horizontal fracture there is an area of significantly reduced local groundwater velocities which hinders the thermal transport. Thus it increases ΔT_{pm} (Figure 8.11 A) and time to stabilise it t_{Sp} (Figure 8.11 B). Whereas when v_u is slow the horizontal fracture reduces ΔT_{pm} by around 1.5 K, because the dominant effect of the fracture in this case is increase in the thermal transport from the VBHE.

Figure 8.12 shows how the depth at which a horizontal fracture intersects the VBHE Z_{fh} influences X_{2K} and t_{S2K}. X_{2K} and t_{S2K} are increased by horizontal

fracture for medium v_u, while they are mostly reduced for slow v_u (Figure 8.12 B). The influence is similar to that on ΔT_{pm} due to the same reasons.

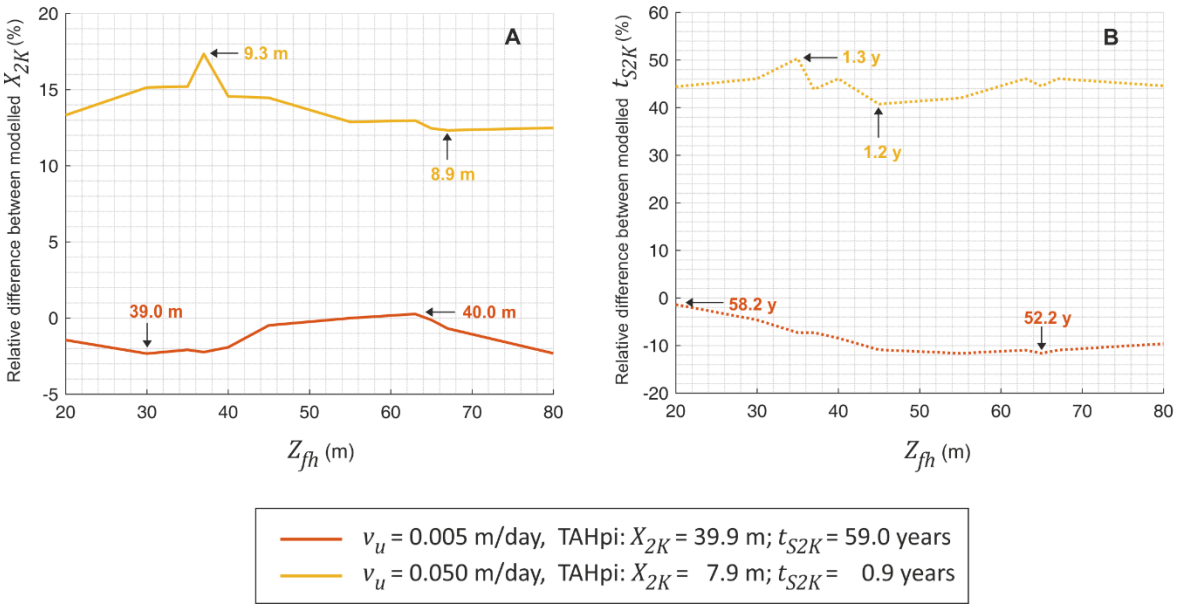

Figure 8.12 The relative difference between the TAFpi and TAHpi models for changing depth of horizontal fracture below ground surface Z_{fh} in (A) the longitudinal extent of the +2 K isotherm X_{2K} after 30 years of VBHE operation and (B) time to stabilise it t_{S2K} for two groundwater velocities v_u.

8.4 Summary and key messages

The influence of a fracture on the thermal performance of a VBHE was examined under different hydrogeological settings: for different fracture parameters available in the 3D model with the explicit representation of the VBHE U-pipe (TAFpi) and for two groundwater flow velocities in the matrix (slow and medium).

8.4.1 Effects of explicit representation of pipes

The temperature change at the VBHE wall is closely related with the temperature change of the working fluid inside the VBHE and determines the sustainability and efficiency of an installation. The international and EU technical limits for the difference between the inlet and outlet temperatures of the working fluid range between 11 to 17 K, for weekly mean load and peak load, respectively (Haehnlein *et al.* 2010).

The results showed that the hydrogeological settings near the VBHE affect the thermal resistance of the VBHE grout only by a small amount (thermal resistance is introduced in section 2.2.5). This is in accordance with the findings about the effect of the thermal conductivity of the ground on the thermal resistance of the VBHE grout (Javed & Spitler 2017). Therefore, when the U-pipe is not modelled, the temperature of working fluid ΔT_{pm} can be estimated using the resistance concept, based on temperature change at the VBHE wall ΔT_b.

Overall the explicit representation of the VBHE U-pipe is not necessary to model the long-term thermal performance of a VBHE. However, when groundwater flow is slow or absent, ΔT_b can be overestimated when VBHE U-pipe is not modelled explicitly. For example, Figure 8.2 shows that in case when groundwater flow is absent the overestimation can reach 1 K. At mid-depth of the VBHE ΔT_b is smaller compared to the result when pipes are ignored (Figure 8.5).

8.4.2 Effects of vertical and horizontal fractures

Fracture height H_f, inclination I_f and fracture depth below the ground surface Z_f control the contact area between the VBHE and the fracture. Therefore the model results (e.g. ΔT_b, ΔT_{pm}) are sensitive to the value of these parameters. When the fracture is vertical (I_f = 90°, Figure 8.8) the beneficial effect of the fracture on the thermal transport is the most significant. It reduced ΔT_{pm} by 14 % (3 K) for slow and by 4 % (0.6 K) for medium groundwater flow. However, when groundwater flow is medium and the fracture inclination slightly deviates from vertical or when the fracture is horizontal and intersects the VBHE (Figure 8.11) it has adverse effect on the ΔT_{pm}. In the first case it increased ΔT_{pm} by up to 6 % (1 K), in the second case, when the fracture is horizontal, the increase was by 1.5 %.

When fracture is inclined, it can increase the mean temperature change of the working fluid ΔT_{pm} as well as the +2 K isotherm X_{2K}. This is because the cooling effect of the fracture, in this case, may not be as significant as its effect on the local groundwater velocities.

It does not make much difference at what depth horizontal fracture intersects with the VBHE. If groundwater flow is medium, the horizontal fracture can increase the mean temperature change of the working fluid ΔT_{pm} as well as the extent of the +2 K isotherm X_{2K}. The contact area between the VBHE and the horizontal fracture is smaller than for the case when the fracture is vertical. But when the horizontal fracture intersects with the VBHE, the locally slowed groundwater velocities in an aquifer with medium groundwater flow caused by this fracture around the VBHE can have significant effect, as was illustrated in Figure 8.11.

8.4.3 Practical messages for VBHE design

From the results of this chapter the following messages can be summarised:

1) The borehole thermal resistance is slightly influenced by the local hydrogeological conditions.

2) When a VBHE model does not represent the pipes explicitly the temperature change at the VBHE wall, when measured at the mid-depth of a VBHE, will be slightly overestimated for slow to medium groundwater flows. This is because the explicit modelling of VBHE with pipes allows for uneven heat flow rate along the VBHE wall.

3) Vertical fracture has the maximal influence on a VBHE relative to all other fracture rotations.

4) Inclined and horizontal fracture intersecting VBHE installed in an aquifer with medium groundwater flow can have adverse effect on the thermal performance of the VBHE.

5) When a horizontal fracture intersects a VBHE, its effect does not depend on the depth of intersection.

Chapter 9 Conclusions, recommendations for practice and future work

This chapter draws the conclusions based on the results and considers the ways in which this work can be extended in the future.

9.1 The thermal performance of a VBHE

The groundwater flow improves the thermal performance of a VBHE, which is estimated with the thermal disturbance that a VBHE causes to the surrounding ground. Ignoring the effects of the advective and dispersive thermal transport in the model is a conservative approach to estimate the sustainable thermal load for a VBHE. This is practised to account for the uncertainty in the local hydrogeological settings. However, such an approach can lead to a significant underestimation of the sustainable thermal load for a VBHE and, consequently, to the overestimation of the installation costs. The estimated groundwater flow at the installation site is often uncertain. In this case the lower value from the estimated range of the groundwater flow should still be considered in the model. The estimated thermal performance of a VBHE is sensitive even to a slow groundwater flow. This is illustrated in Figure 3.4.

The investigation of possible fracture effects on a VBHE installed in an aquifer yielded the following conclusions:

1) An open fracture in an aquifer can either increase or reduce the thermal performance of a VBHE compared with the case when an aquifer is homogeneous. This is because a fracture in an aquifer significantly disturbs the groundwater velocities in the surrounding ground. Therefore, the beneficial effects of the groundwater flow on the thermal transport can be reduced locally to a VBHE due to an adjacent fracture. An example is illustrated in section 6.4.2.

   A fracture close to a VBHE can significantly improve the thermal transport and

intensify the estimated thermal impact further afield, especially in a slow aquifer. This is illustrated in Figure 6.8 and Figure 6.13. Table 7.1 gives examples of cases when a fracture significantly influences the performance of a VBHE. For example, in aquifer with slow groundwater flow a fracture is able to reduce temperature change at the VBHE wall ΔT_b by 8 K compared to no fracture scenario. In another example, for medium groundwater flow and with different fracture parameters, described in Table 7.1, the fracture increased ΔT_b by more than 5 K. This means that in this case the fracture has adverse effect on the thermal transport relative to the case when the aquifer is considered homogenous.

2) Fractures in an aquifer are rarely considered during the site investigation before the installation of a VBHE. Considerable uncertainty in the modelled thermal performance of a VBHE is present even with an assumption that the aquifer is homogeneous. The estimated uncertainty changes due to the influence of a fracture in an aquifer. It depends on the groundwater flow and the thermal dispersivity of the aquifer. The lack of knowledge about the fracture characteristics increases such uncertainty estimated for an aquifer with medium groundwater flow. This key message is discussed in section 7.2. In 95 % of the results, the fracture near a VBHE leads to a variation in the estimated ΔT_b of about +/-20 % compared with a 'no fracture' scenario, equivalent to +/- 2 K (Figure 7.4). At first sight, this change to the overall uncertainty of the model can be regarded as insignificant, considering all the other uncertainties in the full model for a VBHE system — for example, the estimation of the overall thermal and hydraulic properties of the ground. However, the purpose of this study was to evaluate the possible effects of a fracture in a wide range of hydrogeological scenarios. Therefore, the ranges for the fracture parameters in the Monte Carlo analysis were set to be wide.
3) Estimation of some fracture parameters can be used to constrain the uncertainty in the thermal performance of the VBHE due to a nearby fracture (see section 2.3.2 for methods and examples of how to estimate the fracture

parameters). For a fracture to have considerable effect on the thermal transport from a VBHE, the ratio of the hydraulic conductivity between the fracture and the matrix should be > 10 000 to generate a sufficiently high volumetric flow rate inside it. This conclusion is based on Figure 7.6 F1 and F2. The model results are not sensitive to the fracture aperture unless its size is very narrow. The sensitivity of model results to fracture parameters that define the fracture location relative to the VBHE (fracture distance and shift) differs with groundwater velocity in the aquifer (Figure 7.9). The model results are not affected by the depth at which a horizontal fracture intersects with the VBHE when the pipes in the VBHE are explicitly modelled (Figure 8.11).

4) An intersecting horizontal fracture in an aquifer with medium groundwater flow is likely to worsen the thermal performance of a VBHE compared with a scenario that assumes a homogeneous aquifer (without a fracture). This is illustrated in Figure 8.11. When the fracture in an aquifer with medium groundwater flow is inclined (not vertical), it increases ΔT_b and X_{2K} (as well as time taken to stabilise them).
5) For fast groundwater flow in an aquifer, the influence of an open fracture near a VBHE can be disregarded. When the groundwater flow in an aquifer is very slow or fast, the fracture effects are negligible (Figure 7.2). When the VBHE is installed in a slow aquifer near a fracture, its thermal performance is likely to be improved compared to a scenario that assumes the aquifer to be homogeneous (Figure 7.6 and Figure 7.8). ΔT_b can be reduced by a fracture even when its volumetric flow rate is small. Consequently, the downstream thermal impacts of a VBHE adjacent to a fracture in a slow aquifer can be more significant compared with the scenario where the aquifer is assumed to be homogeneous.
6) Knowledge about the thermal dispersivity is more important than knowledge about a nearby fracture to estimate the uncertainty in the thermal performance of a VBHE in a fast aquifer. When the groundwater flow is high (> 0.4 m day^{-1}), the uncertainty in the thermal performance of a VBHE caused

by the estimation of thermal dispersivity is significant. It is likely to be much greater than the uncertainty caused by an adjacent fracture (Figure 7.2).

7) Significant thermal dispersivity in an aquifer enhances the ability of a fracture to reduce the thermal transport estimated with an assumption of a homogeneous aquifer. This is because when a fracture reduces the local groundwater velocity, the dispersive thermal transport at this location is also hindered (Figure 7.4).
8) Model results for the thermal performance of a VBHE can be sensitive to the thermal dispersivity in the vertical direction if an aquifer is heterogeneous. The vertical dispersivity can be disregarded when a VBHE is modelled in a homogeneous aquifer. However, it can be an important parameter for the specific cases in heterogeneous aquifers (Figure 4.10).
9) Ignoring the dispersive thermal transport can significantly underestimate the time needed to stabilise the ΔT_b and X_{2K} for a VBHE installed in an aquifer with medium groundwater flow. This point is illustrated in Figure 4.8. For example, the estimated time to stabilise ΔT_b for a VBHE installed in an aquifer with groundwater flow of 0.03 m day^{-1} is about 230 days without consideration of thermal dispersion. It is about 500 days when thermal dispersion is considered.

9.2 Conclusions for methods

The results showed, in general, that a 2D model is sufficient to estimate the thermal performance of a VBHE under a wide range of hydrogeological conditions. The numerical model in 3D is more computationally expensive than a 2D model which is the obstacle if the uncertainty analysis has to be carried out.

The 3D model is required when a horizontal fracture intersecting a VBHE should be modelled. Also, a 3D model can account for the axial thermal transport which has an important role in the estimation of the extent of isotherms but only for certain groundwater flows (Figure 3.8).

There may be no difference between the estimated extent of an isotherm at the steady state when comparing the results for two different groundwater flows: slow with fast. However, the time needed to reach the steady state in a slow aquifer can be considerably longer: much longer than the actual lifespan of a VBHE installation (Figure 3.12). Therefore, it is more practical to estimate the extent of an isotherm in a slow aquifer in the transient state, which is after a certain time of the VBHE operation rather than at the steady state.

The explicit modelling of pipes allows for the thermal exchange between the VBHE and the ground to be vertically uneven. It does not improve the modelling of the thermal performance of the VBHE in a homogeneous aquifer, except when the groundwater flow is absent or slow. When the VBHE pipes are not explicitly modelled, the temperature of the working fluid ΔT_{pm} can be estimated with acceptable accuracy based on the temperature change at the VBHE wall, ΔT_b.

However, when the VBHE pipes are not modelled explicitly for a case when the groundwater flow is slow or absent, in the long term the ΔT_b at the VBHE mid-depth can be overestimated. This is because at zero or slow groundwater flow the vertical conduction has more significant influence on the ΔT_b. The model with pipes accounts for the increased thermal exchange between a VBHE and the ground surface due to the circulation of the working fluid. Thus, the change in ΔT_b is more evenly distributed along the length of a VBHE. At the VBHE mid-depth the ΔT_b is smaller compared with the result when the VBHE pipes are not explicitly modelled.

9.3 Recommendations for practice

Based on the results, the following recommendations are offered for modelling a VBHE installed in an aquifer. The groundwater flows were classified in this study into three categories: fast groundwater flow is ≥ 0.1 m day^{-1}, slow groundwater flow is ≤ 0.01 m day^{-1} and medium are the values in between.

9.3.1 Groundwater flow

Even slow groundwater flow can influence the thermal performance of a VBHE, and therefore it is an important factor to consider in the uncertainty analysis. The groundwater flow can significantly improve the thermal performance of an individual VBHE by reducing the magnitude of the thermal disturbance that VBHE causes to the ground. This increases the thermal load that VBHE can sustainably deliver. However, this beneficial effect of groundwater flow exacerbates potential adverse downstream impacts of the VBHE, which may lead to undermined thermal performance of the installations downstream. Therefore, it is recommended to account for the uncertainty in thermal performance of VBHE due to groundwater flow. This is especially relevant for multi-VBHE installations because it will help to adjust the VBHE locations to avoid significant adverse thermal impacts on the neighbouring VBHE installations downstream.

9.3.2 Thermal dispersion

The thermal dispersivity in an aquifer with medium to fast groundwater flow is an important model parameter to constrain the uncertainty in the thermal performance of a VBHE. In cases when the groundwater flow is fast, the uncertainty caused by the estimates in the thermal dispersivity is greater than the uncertainty due to a fracture near the VBHE. Therefore, it is recommended to account for dispersive thermal transport when modelling VBHE system installed in an aquifer with fast groundwater flow. The effect of an individual fracture in this case can be ignored.

9.3.3 Fracture

The effect of a fracture on the thermal performance of a VBHE can be disregarded for an aquifer with fast groundwater flow.

When the advective and dispersive thermal transport are accounted for in a VBHE model, the assumption for an aquifer to be homogeneous should be justified. This can be done by field investigations to determine whether the aquifer can be

assumed homogenous on the site to be affected by the VBHE installation. The methods to identify the presence of a fracture are described in section 2.3.2.

If a fracture is identified, its characterisation is recommended, because if a fracture has high volumetric flow rate, it can locally reduce the groundwater velocity and thermal dispersion near a VBHE. This will lead to the overestimation of the sustainable thermal load compared to the estimation with assumption that the aquifer is homogenous.

On the other hand, an open flowing fracture adjacent to a VBHE will always increase the estimated thermal transport in an aquifer with slow groundwater flow. This means that an adjacent fracture is likely to improve the estimates of the VBHE thermal performance when the groundwater flow is not considered in the model. However, this is relevant only to an individual VBHE, because consequently the fracture also exacerbates the downstream thermal impacts of the VBHE. This has implications for the overall thermal performance of a multi-VBHE system.

9.3.4 Uncertainty

Uncertainty analysis is a useful practice to estimate the long-term thermal performance of a VBHE and its thermal impacts. The estimation of groundwater flow and the thermal dispersivity can significantly constrain this uncertainty.

It is resource-intensive to collect field data about the fractures in an area where a VBHE is planned to be installed. Therefore, such an undertaking requires justification. However, ignoring the uncertainty due to a fracture adjacent to a VBHE may lead to a significant underestimation of the sustainable thermal load of a VBHE. Even partial information about a fracture can constrain the uncertainty in the thermal performance of a VBHE. For example, the estimation of the fracture location relative to a VBHE and the direction of the groundwater flow.

Additionally, if the groundwater flow is medium and the model accounts for it, the assumption for an aquifer to be homogeneous should be justified based on field measurements (section 2.3.2). Because in this case, the uncertainty in the

estimated thermal performance of a VBHE can be widened in both directions due to an adjacent fracture. The possible changes in the uncertainty for different groundwater flows is schematically illustrated in Figure 9.1.

9.3.5 Model complexity

Modelling in 2D is sufficient to estimate the thermal performance of a VBHE under a wide range of hydrogeological conditions. Modelling in 2D is useful when the vertical thermal transport can be neglected (when a VBHE is long enough, e.g. > 50 m) and groundwater flow is present. See details in section 9.2.

9.3.6 Summary of practical recommendations to aid borehole thermal design

Based on the practical findings in Chapters 6, 7 and 8 the practical recommendations can be given for the following cases when a VBHE is installed in an aquifer with slow, medium and fast groundwater flow.

A VBHE system installed in the ground with slow or absent groundwater flow

If a fracture is present near a VBHE, it will likely have a significant beneficial effect on the thermal performance of an individual system. When VBHE is installed in an aquifer with slow groundwater flow (in this study it is considered to be < 0.01 m day^{-1}), the beneficial fracture effect can be significant and can influence the decisions about the VBHE design (Figure 6.18). The decision to install the VBHE system can be supported and go forward if a nearby fracture is identified, which significantly increases the estimated thermal transport compared to the case when the slow aquifer is assumed to be homogeneous. Thermal response test can be conducted to estimate whether the thermal performance of the VBHE system will be enhanced by a nearby flowing fracture.

The examples of beneficial fracture effects in slow aquifers are illustrated in Figure 7.4. For slow aquifer, a fracture was able to reduce the temperature at the VBHE wall by up to 8 K compared to no fracture scenario. A fracture near a VBHE in slow

aquifer was able to reduce the extent of the +2 K isotherm by up to 40 m (Figure 7.5). Such change in the estimated extent of the generated thermal plume would influence the planned locations (density) of the VBHE in a multi-VBHE system. Therefore, despite likely beneficial effects of a fracture on the thermal transport in a slow aquifer, the downstream thermal effects of a VBHE may become an issue in case of multi-VBHE installation, especially if the fracture is vertical, which maximises the fracture effect as was illustrated in Figure 8.8.

Adverse downstream fracture effects are shown in Figure 7.5. In the illustrated cases a fracture was able to extend the +2 K isotherm by up to 19 m compared to a no fracture scenario. The regulations for the allowed thermal disturbance of the ground should be consulted to make the decision of whether to proceed with the field measurements to characterise the fracture to avoid the adverse thermal effects on the downstream aquifer users.

A VBHE system installed in an aquifer with medium groundwater flow

The medium groundwater flow in this study is considered to range between 0.01 m day^{-1} and 0.1 m day^{-1}. In case when a VBHE is installed in an aquifer with medium groundwater flow the relative beneficial fracture effect on the thermal transport from a VBHE may be smaller compared to the case with slow groundwater flow. However, the uncertainty in the thermal performance of a VBHE due to presence of a nearby fracture is significant and goes both ways: a fracture may have either beneficial or adverse effect on a VBHE. The summary of when and how a fracture is likely to change the uncertainty in the thermal performance for a VBHE installed in an aquifer is summarised by Figure 9.1.

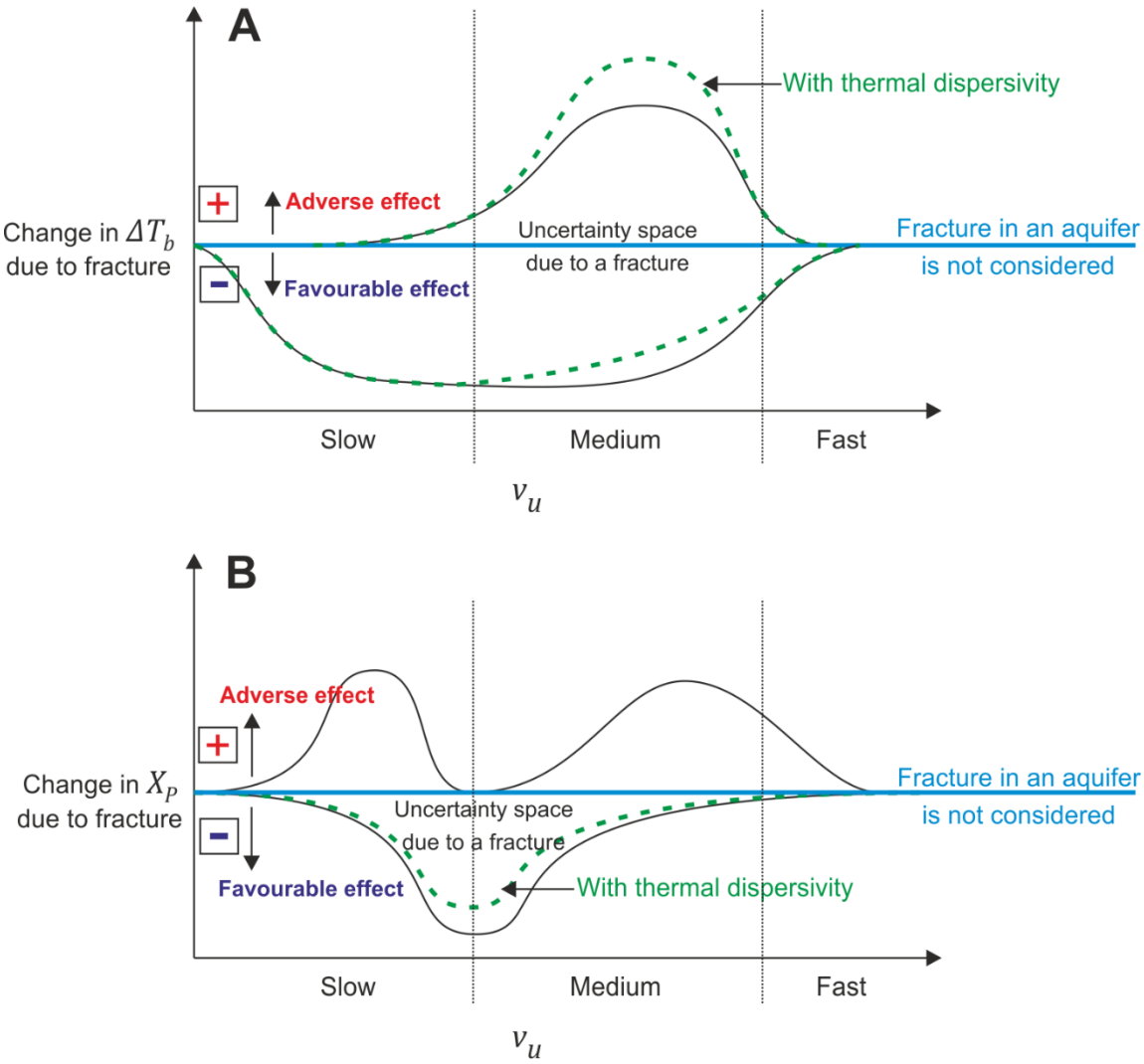

Figure 9.1 Schematic representation of the possible change in the uncertainty bounds in the thermal performance indicators for a VBHE caused by an adjacent fracture in an aquifer. Based on the results from Monte Carlo analysis in Figure 7.4 (for A) and Figure 7.5 (for B). The given change in the uncertainty is in relation with the result when the aquifer in a model is considered to be homogeneous. The illustrated thermal performance indicators are: (A) the change in ΔT_b (the temperature change at the VBHE wall) and (B) the change in X_p (the downstream extent of the isotherm of interest). v_u is groundwater flow in a homogeneous aquifer.

The fracture effect of a VBHE can go both ways (either beneficial or adverse effect on thermal transport compared to the scenario when fracture is disregarded and homogeneous aquifer is assumed). It is summarised in Figure 7.13. The effect of fracture on the thermal transport depends on the combination of the volumetric flow rate in the fracture and its distance relative to the VBHE. The effective fracture distance is the distance of fracture from the VBHE, along its whole length, which means that a horizontal fracture intersecting a VBHE has large effective distance from the VBHE, resulting in the smaller effect of the fracture (Figure 8.8).

Volumetric flow rate of a fracture depends on its dimensions, rotation relative to groundwater flow direction and the ratio of hydraulic conductivities between the fracture and matrix (i.e. aquifer material). In the case when the uncertainty in the thermal performance of a VBHE is too large, the assumption that ground is homogeneous during the design of the VBHE system is not justified and further field investigations are necessary to narrow the uncertainty in the thermal performance of a VBHE.

For example, in an aquifer with medium groundwater flow, depending on the fracture parameters, a fracture was able to reduce the temperature change at the VBHE wall by up to 5 K. In cases with different fracture parameters, a fracture was able to increase the temperature change at the VBHE wall by up to 5.4 K, which equals to an increase by 50 % compared to a no fracture scenario (Figure 7.4, Table 7.1). This suggests that when a VBHE is installed in an aquifer with medium groundwater flow and there is a likelihood of a fracture present nearby, the field measurements to characterise this fracture can be justified. The brief overview of methods to identify and characterise a fracture is given in section 2.3.2.

A VBHE system installed in an aquifer with fast groundwater flow

When a VBHE is installed in an aquifer with fast groundwater flow (in this study it is > 0.1 m day^{-1}) the relative effect of a fracture can be disregarded. This is because the uncertainty in the thermal performance of a VBHE caused by a fracture is much smaller compared to the case when groundwater flow is medium. This is schematically shown in Figure 9.1 and it is based on the results from the uncertainty analysis (Figure 7.2, Figure 7.4 and Figure 7.5). In case of the fast groundwater flow (and for the higher values from the range of medium groundwater flow), the uncertainty due to estimation of the thermal advection and dispersion by far outweighs the uncertainty due to a fracture.

9.4 Future work

9.4.1 Field measurements

This study was theoretical and simplified the geological reality, for example, the geometry of a fracture. It would be useful to conduct a **field experiment** with a real fracture and see how a VBHE would perform under real conditions with different values of induced groundwater flows.

A model for the VBHE thermal performance influenced by a fracture should be developed based on a case study. This would allow **validation of model results** using measurements of the thermal performance indicators. The method used to quantify the uncertainty in the thermal performance of a VBHE due to local hydrogeological conditions could be based on the site-specific narrowed parameter ranges.

9.4.2 Upscaling to a real case of a VBHE design

This study assumed a constant **thermal load** on the VBHE, but in practice, it varies with demand, and it can involve both seasonal cooling and heating. It would be useful to estimate the thermal performance of a VBHE under the effect of a nearby fracture with a real case of thermal loading.

The method of this study can be repeated for a **multi-VBHE system** to quantify the effects of a fracture on the thermal interactions.

An extended analysis of the thermal performance of a VBHE can be made to **include an above-ground heat pump** in the model to estimate the change in Coefficient of Performance (COP) of a VBHE under the influence of a fracture. Design limits can be added to the model, for example, a limit for the temperature difference of the working fluid.

9.4.3 Fracture networks

This study can also be extended to estimate the thermal performance of a VBHE installed in an aquifer with several fractures. Furthermore, other modelling approaches can be used to model the thermal performance of a VBHE installed within a fracture network.

A model with a **discrete fracture network** (DFN) can be developed to carry out a sensitivity analysis with varying fracture parameters and varying density of a fracture network, its connectivity and the distribution (homogeneous or heterogeneous). There will be a point at which the fracture network is such that the aquifer can be considered homogeneous. Despite requiring relatively high computational and site investigation efforts and having little practical use, this framework can be used **to evaluate the performance of simpler models**.

The heat transfer through fractured aquifers differs from that of homogeneous aquifers. The reason for this is that fractures in an aquifer cause varying advection velocities, which produce a broad spectrum of transport rates. This results in a wider thermal breakthrough curves with long tailing and an early peak. The Fourier type equation cannot capture this behaviour, especially for **heterogeneous fracturing** with significant advection, where the heat transfer rate can span several orders of magnitude (Geiger & Emmanuel 2010). Therefore, to model the thermal interactions in a heterogeneously fractured aquifer, other model approaches can be tested to account for the complexity of hydrogeological settings. For example, for an aquifer where there is a network of fractures, the stochastic model framework can be applied, as the continuum time random walk (CTRW). A homogeneous well-connected fracture network can be modelled using an advection-diffusion equation (ADE) with macro-dispersivities. The CTRW can outperform the ADE to model the thermal transport in the heterogeneous, poorly connected fracture patterns. The CTRW approach captures the anomalous heat transfer in the fractured aquifers – long tailing as well as early arrival of the

thermal breakthrough curve for aquifers with a low matrix permeability (Geiger & Emmanuel 2010).

The length of a VBHE can cover several geological layers in an aquifer with different hydraulic properties. For example, a top layer of an aquifer can be fractured due to weathering. An analysis can be carried out to test when the usual model assumption that the aquifer is homogeneous still gives a reasonable result for the estimated thermal performance of a VBHE installed in a layered aquifer. The field data could be used to validate a numerical model. Each significant layer of an aquifer that is intersected by a VBHE could be assigned its own thermal and hydraulic properties. The analytical solution for a VBHE installed in a **layered aquifer** developed by Erol & François (2018) can also be tested in the analysis.

Appendix A Produced posters and presentations

Based on the work presented in this thesis, the following contributions were made during conferences.

Poster presentations:

- Poster: Comparison of different heat modelling frameworks in fractured aquifers; Conference title: Groundwater in Fractured Bedrock Environments: Managing catchment and subsurface resources, organised by the Geological Society; Conference date: 10 June 2016, QU Belfast
- Poster: How does groundwater flow change the thermal performance of borehole heat exchangers?; Conference title: Groundwater: Managing our Hidden Asset; Subtopics: Groundwater and energy (Groundwater in renewable and nuclear energy, Groundwater as an energy source); Conference date: 13-14 September 2016, University of Birmingham, UK
- Poster: The impact of fractures on heat transfer in an aquifer used for shallow geothermal energy applications; Poster ID: EGU2018-914; Conference: European Geosciences Union, General Assembly 2018, Session HS8.2.3/ERE6.4; Topic: Thermal and mechanical processes and energy storage in porous and fractured aquifers. Conference date: 9 April 2018, Vienna.

Other presentations:

- The international sustainability conference organised by the University of Southampton, 15th April 2016
- At the working group meeting in Romania of the European network for shallow Geothermal energy Applications in Buildings and Infrastructures (GABI action), 22nd March 2016

- At the working group meeting in Turin of the European network for shallow Geothermal energy Applications in Buildings and Infrastructures (GABI action), 6th December 2016
- GSHPA technical seminar, Leeds: When does a fracture matter for a borehole heat exchanger?, 24th May 2018
- CDT SIS conference 2018: Improving the way we harvest the heat beneath our feet (The Centre for Doctoral Training in Sustainable Infrastructure Systems at the University of Southampton), 14th November 2018
- European Geothermal congress 2019, Hague: Quantifying the effect of single fractures on the thermal performance of borehole heat exchangers, 13th June 2019

Appendix B Classification for fracture apertures

Table B.1 Classification of fractures by openness from works of Barton (1973), ISRM (1978) and Ulusay and Hudson (2007), taken from Dehkordi *et al.* (2015).

Aperture (mm)	Category
< 0.1	Very tight
0.1 – 0.25	Tight
0.25 – 0.5	Partly open
0.5 – 2.5	Open
2.5 – 10.0	Moderately wide
> 10.0	Wide

Appendix C Additional analysis of advection effects

C.1 Effect of the advection on the optimisation of the VBHE design

The length of a planned VBHE changes the cost of the system installation. Even slow groundwater flow can significantly reduce the estimated optimal length of the VBHE (Liuzzo-Scorpo *et al.* 2015). Figure C.1 shows how groundwater flow in an aquifer can influence the optimal (minimal needed) length of the VBHE H_b to produce (and not exceed) the target value of ΔT_b (+10 K and +15 K) and ΔT_{20m} at 20 m from the VBHE (+2 K and +5 K) after 30 years of operation for a given VBHE heat flow rate J = 5000 W.

Slow groundwater flow of 0.01 m day^{-1} already causes visible reduction in the required VBHE length when optimising for ΔT_b of +10 K and +15 K (Figure C.1). The VBHE can be 30 m or 50 m shorter if such groundwater flow is present depending on the target (maximum allowed) ΔT_b.

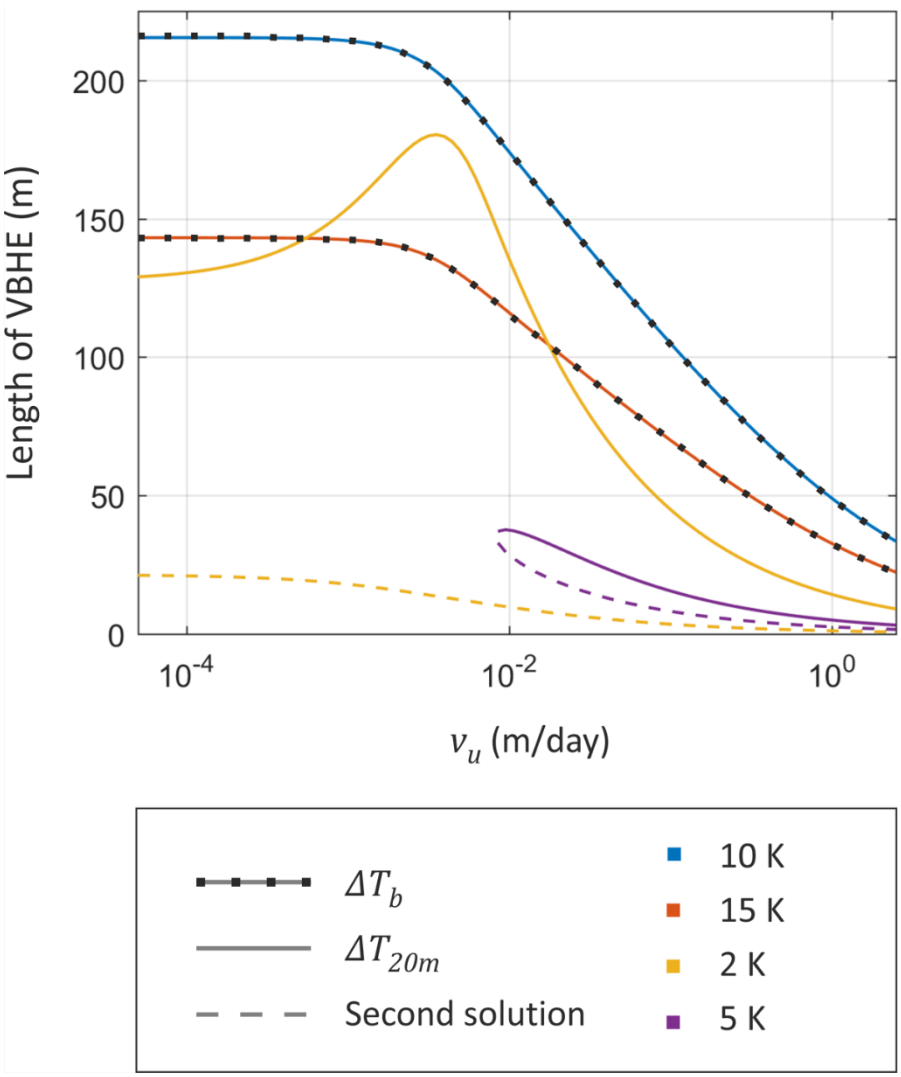

Figure C.1 The calculated VBHE length H_b depending on the groundwater velocity v_u to produce the specified temperature change at the VBHE wall ΔT_b (+10 K and +15 K) and at 20 m distance from the VBHE ΔT_{20m} (+2 K and +5 K) after 30 years of continuous VBHE operation. Note that a second solution (possible VBHE length) is present for ΔT_{20m} for both 2 K and 5 K (the VBHE can be either very short or long to produce +2 K at 20 m distance). MFLS model is used. Model parameters are given in Table 5.3.

The temperature changes at the VBHE wall ΔT_b and at 20 m distance from the VBHE ΔT_{20m} were chosen as an example of requirements for the VBHE design. The fixed maximum temperature change at 20 m from the VBHE corresponds to the EU minimum distance between VBHE installations according to the legal requirements in some countries of the EU, Table 2.1 (Haehnlein *et al.* 2010).

Figure C.1 shows that if there is a requirement not to exceed ΔT_{20m} of +2 K ground temperature change at 20 m from the VBHE then the optimal (minimal needed) VBHE length is about 130 m for a negligible v_u and increases with increasing

groundwater flow to about 170 m for v_u = 0.004 m day^{-1}. This is because at these slow to medium groundwater velocities ΔT_b is reduced while the +2 K isotherm is advected downstream, and the extent of this isotherm becomes larger. Therefore, longer VBHE is needed to provide less heat flow rate per unit length of the borehole while the VBHE heat flow rate remains the same (J = 5000 W). Note that if both $\Delta T_b \leq$ 15 K and $\Delta T_{20m} \leq$ 2 K should be met, the value of VBHE length should meet both requirements and can be longer than if modelled only to meet the limit for ΔT_b.

The groundwater flow faster than 0.01 m day^{-1} reduces the required length of the VBHE for ΔT_{20m} = +2 K compared with no groundwater flow case. This is because faster groundwater is able to reduce the extent of the +2 K isotherm (while increasing the extent of isotherms of smaller temperature change).

The required VBHE length for ΔT_{20m} = +5 K exists only for faster groundwater flows, because for slower groundwater flows it is not possible to achieve ΔT of +5 K at 20 m distance from the VBHE for any VBHE length H_b.

Note that there is a second solution to achieve ΔT_{20m} = +2 K (and also +5 K): the VBHE length can be very short. In such case the axial conduction helps it to reach the goal. But for such a short VBHE ΔT_b would be extremely high, so in practice it is not viable.

C.2 Effect of the VBHE heat flow rate on time to steady state

Figure C.2 shows how time to stabilise ΔT_b and $X_{0.5K}$ depends on the VBHE heat flow rate J and groundwater flow v_u. Increasing VBHE heat flow rate J causes larger extent of the +0.5 K isotherm $X_{0.5K}$. Thus, the time needed to stabilise this isotherm is increasing as well. J does not influence the time to reach steady state at the VBHE wall t_{Sb}). For fast groundwater flow, time to stabilise the isotherm $t_{S0.5K}$ is very short (< 100 days), while for slower groundwater flows (e.g.

v_u = 0.05 m day^{-1}) the difference between time needed to stabilise ΔT_b and $X_{0.5K}$ can be significant, especially for higher J.

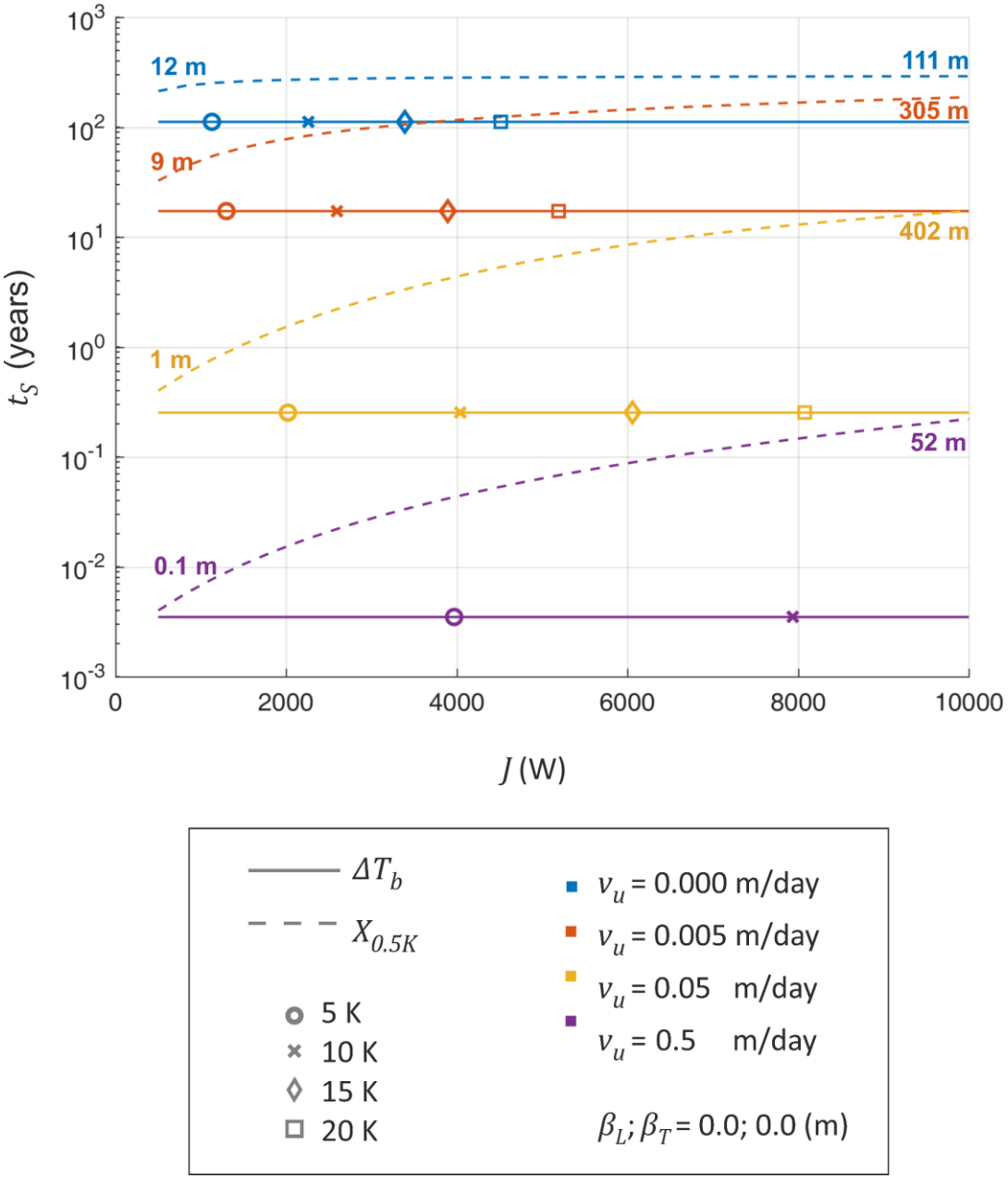

Figure C.2 Time to reach steady state at the VBHE wall t_{Sb} and for the 0.5 K isotherm $t_{S0.5K}$ versus VBHE heat flow rate injection J for a range of groundwater flows v_u. Modelled using MFLS. Numbers above lines for $X_{0.5K}$ are the longitudinal extent of the +0.5 K isotherm at steady state for J = 500 W and J = 10000 W. Model parameters are given in Table 5.3.

However, it does influence the time needed to stabilise the isotherm of interest (e.g. +0.5 K). For fast groundwater flow the time needed to stabilise an isotherm is very short while for slower groundwater flow (e.g. 0.05 m day^{-1}) the difference

between the time needed to stabilise ΔT_b and $X_{0.5K}$ can be significant, especially for higher heat flow rates.

C.3 Effect of advection on the extent of isotherms and time to stabilise them

Figure C.3 shows how the extent of the +2 K and +0.5 K isotherms grows with time for different groundwater velocities. For slow groundwater flow (0.005 m day^{-1}) the extent of the +0.5 K isotherm $X_{0.5K}$ grows at slower rate compared with the same isotherm for medium groundwater flow (0.05 m day^{-1}). Also, it takes much longer to reach steady state compared with the same isotherm at medium groundwater flow due to comparatively reduced thermal transport. Slow groundwater flow causes the largest extent for both isotherms (at steady state) compared with the other cases with absent and medium groundwater flow.

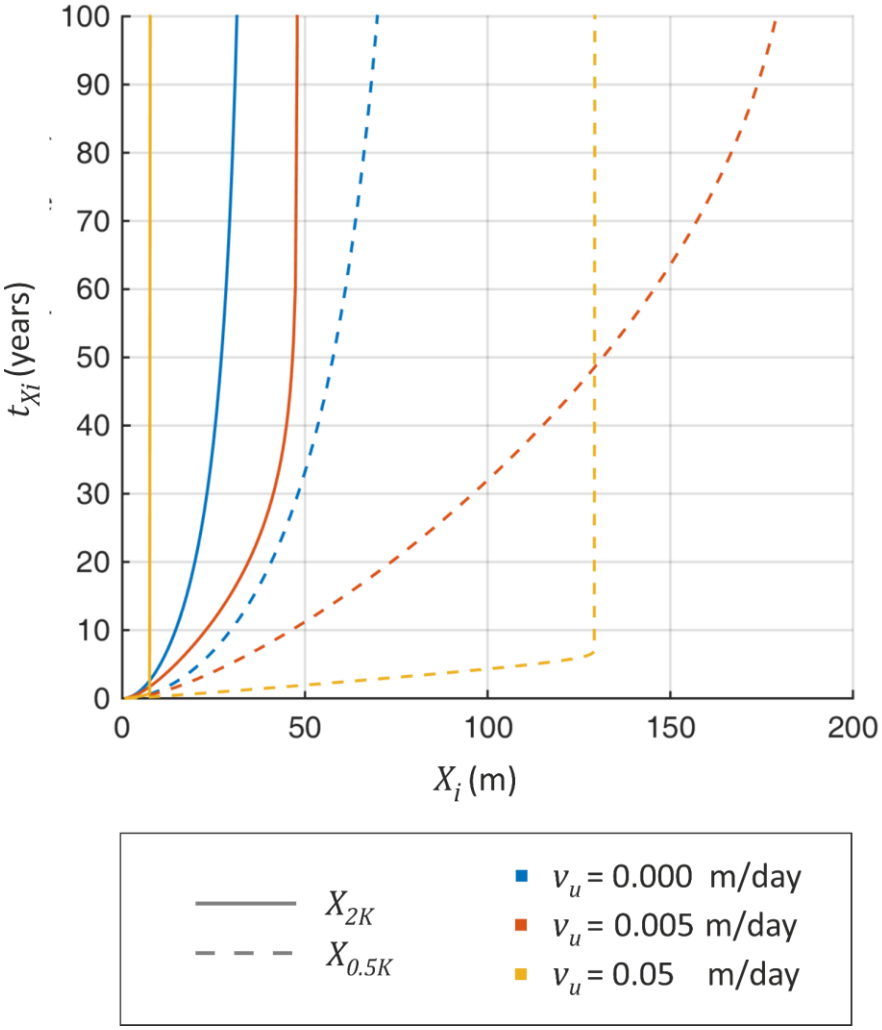

Figure C.3 Longitudinal extent in the x-coordinate of the +2 K and +0.5 K isotherms (X_{2K} and $X_{0.5K}$) with respective times needed for their development for different groundwater velocities v_u. Modelled using MFLS. When the lines become vertical, the isotherm is considered to be stabilised. Model parameters are listed in Table 5.3.

Appendix D The influence of longitudinal and vertical thermal dispersivity on the +0.5 K isotherm generated by a VBHE

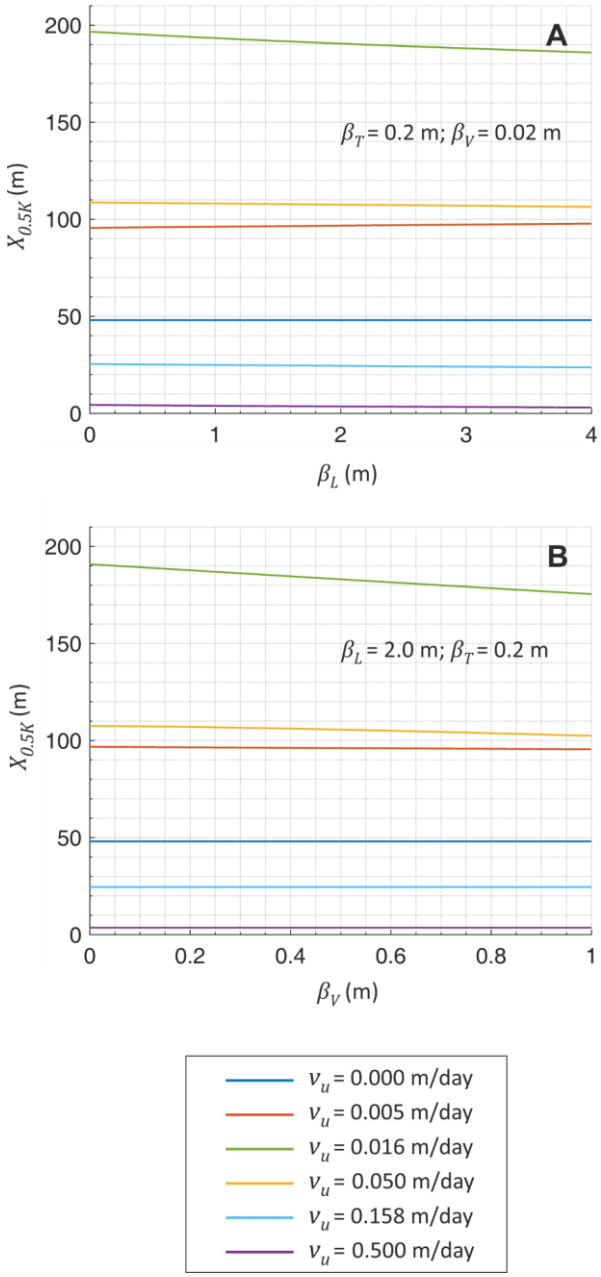

Figure D.1 Longitudinal extent of the +0.5 K isotherm $X_{0.5K}$ after 30 years of continuous VBHE operation versus changing dispersivity in single direction: (A) longitudinal β_L and (B) vertical β_V. The transverse dispersivity is marked as β_T. Modelled using MFLS – the moving finite line source analytical solution, adapted for 3D dispersion. v_u is Darcy groundwater velocity. The pattern of groundwater velocity increase is logarithmic: v_u = 5×10^{-3}, 5×10$^{-2.5}$, 5×10^{-2}, 5×10$^{-1.5}$, 5×10^{-1} m day^{-1}.

Appendix E Supplementary analysis of the influence of a single fracture on a VBHE in 2D

E.1 Case study for the effect of volumetric flow rate in the fracture

When volumetric flow rate in the fracture O_f is high, it increases the thermal transport between the VBHE and the fracture by enhanced conduction due to the enhanced temperature gradient between the fracture and the VBHE and the ability of the fracture to advect more heat downstream. A high value of O_f will change local groundwater velocities around the fracture, as the matrix groundwater is effectively transported inside the fracture. For the base parameter values, the VBHE is located in the area of fracture mid-length where the fracture can significantly reduce local groundwater velocities. When groundwater velocities around the VBHE are reduced, it reduces the thermal transport between the VBHE and the matrix by reducing the thermal advection. Thus, it lessens the cooling effect of the fracture on the VBHE wall for the highest tested values of O_f (Figure E.1).

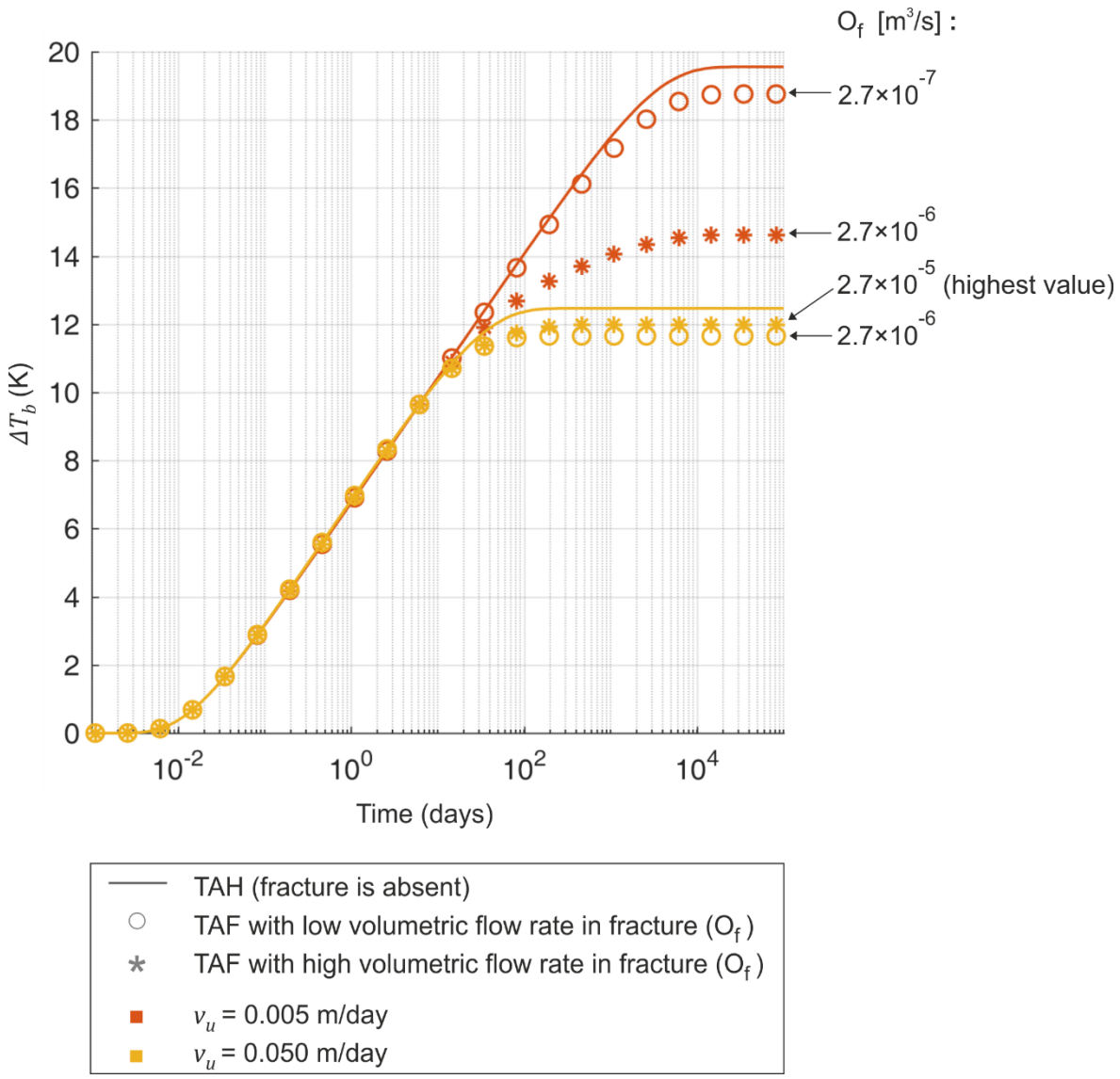

Figure E.1 Temperature change at the VBHE wall ΔT_b versus time for model without fracture (TAH-2D) and model with fracture (TAF-2D) with high and low volumetric flow rate in the fracture O_f. Results are for two groundwater velocities in undisturbed matrix v_u. Models are with impermeable grout and zero aquifer dispersivity β. The ratio of the hydraulic conductivity between the matrix and the fracture R_K is fixed. Low O_f is for R_K = 1000, high O_f is for R_K = 100 000. The other fracture parameters are set to the base values given in Table 6.1.

E.2 Effect of fracture location relative to the VBHE

The location of a fracture relative to the VBHE was changed by systematically varying the fracture shift S_f parallel to the fracture orientation for two fracture distances D_f from the VBHE (1 and 5 m). The results for ΔT_b for the VBHE installed in aquifers with medium and slow groundwater flow (Figure E.2) can be explained by the interplay of two fracture effects on the ATC. Note that when S_f is increased beyond the fracture half-length, the edges of the fracture move away from the

VBHE, and the fracture has a rapidly diminishing effect. The fracture can only increase the ATC local to VBHE compared with the TAH-2D results when D_f = 1 m (Figure E.2). Additionally, when there is medium groundwater flow in the matrix (0.05 m day^{-1}, Figure E.2), the nearby fracture (D_f = 1 m) significantly accelerates the local groundwater flow around its edges, improving the thermal performance of the VBHE (reducing ΔT_b) if it is located near the fracture edge (when S_f is around $\pm L_f/2$, Figure E.2).

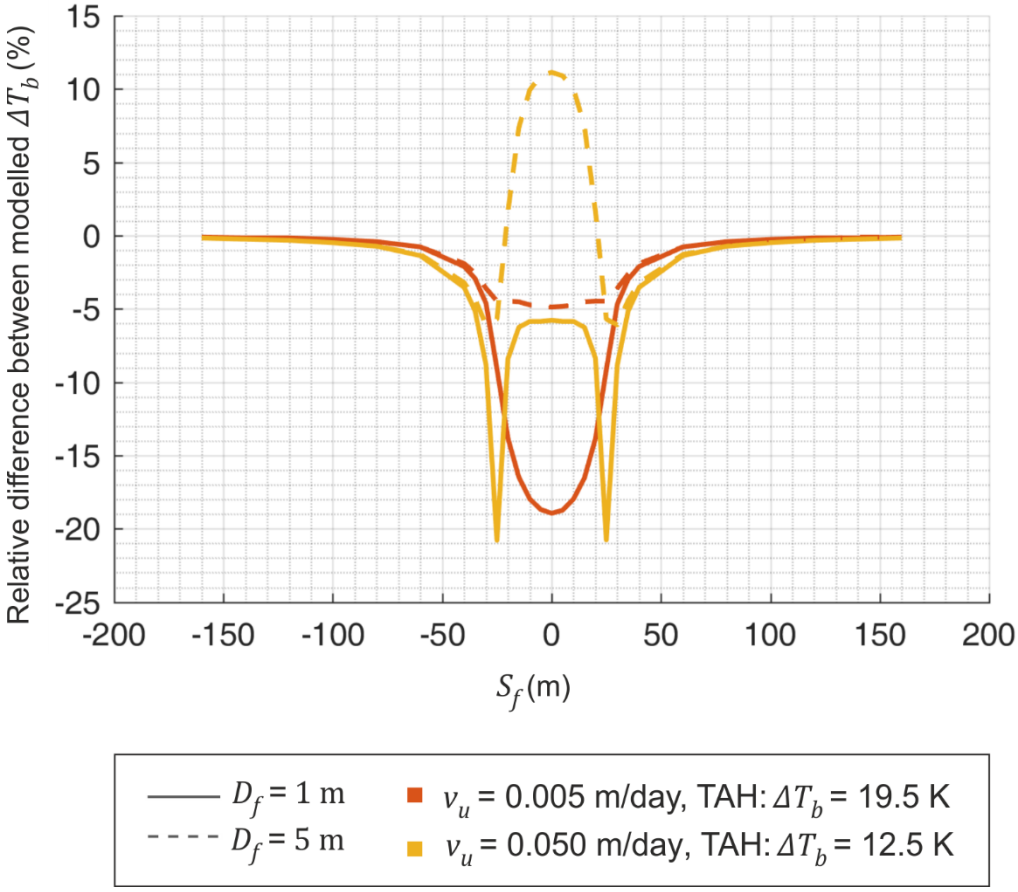

Figure E.2 Relative difference $(\Delta T_b^{TAF} - \Delta T_b^{TAH})/\Delta T_b^{TAH}$ in temperature change at the VBHE wall after 30 years of continuous operation for varying fracture shift relative to the VBHE S_f.

For all S_f, when D_f is fixed to 5 m, the fracture can either increase or reduce the ATC local to the VBHE compared with the TAH-2D model. This depends on the groundwater velocity in the matrix (Figure E.2). If the matrix has a medium groundwater flow (0.05 m day^{-1}) the fracture effect on the VBHE is negative when it is located in the area of reduced local groundwater velocities (when S_f is

between -20 m and +20 m, Figure E.2). The fracture shift relative to VBHE changes time to stabilise ΔT_b (Figure E.3) in the similar way as it changes ΔT_b (Figure E.2).

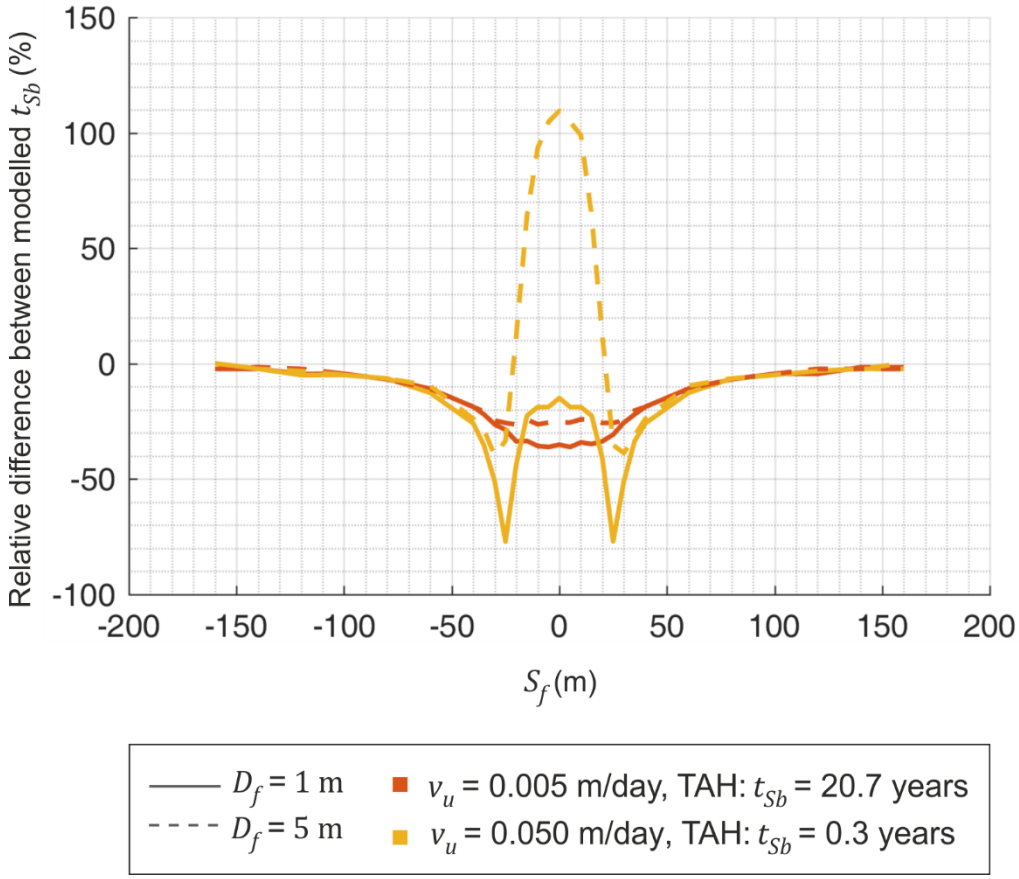

Figure E.3 Relative difference between the TAH-2D and TAF-2D models $(t_{Sb}^{TAF_{2D}} - t_{Sb}^{TAH_{2D}})/t_{Sb}^{TAH_{2D}}$ in time to stabilise temperature change at the VBHE wall for varying fracture shift relative to the VBHE S_f. Two undisturbed groundwater velocities v_u are used. The actual t_{Sb} values for TAH-2D are in the legend.

Figure E.4 shows how fracture shift relative to the VBHE S_f affects X_{2K} for two groundwater velocities v_u and two fracture distances from the VBHE D_f. The effect of fracture shift S_f on ΔT_b is symmetric both upstream and downstream of groundwater flow direction (Figure E.2). However, its effect on X_{2K} is not symmetric. The maximum effect of the fracture on X_{2K} occurs when fracture shift is downstream by half of the fracture length (S_f = +25 m), which means that full length of the fracture is downstream from the VBHE.

For medium groundwater flow in the matrix, if S_f = +25 m and fracture distance is 1 m the VBHE is located near the fracture edge where local groundwater velocities are increased by the fracture, ΔT_b is significantly reduced (Figure E.2), and

therefore X_{2K} is also significantly reduced. The fracture effect for this case is not as significant for D_f = 5 m (dashed yellow line in Figure E.4).

When S_f = 0 m, for medium groundwater flow in the matrix, for D_f = 5 m, X_{2K} is increased (similarly to ΔT_b, see Figure E.2) compared with TAH-2D, due to reduced local groundwater velocities in the area of +2 K isotherm. For the same case, but when the fracture is closer to the VBHE, i.e. D_f = 1 m, X_{2K} is reduced (cooled down by fracture) similarly to ΔT_b (Figure E.2) but not as much as when the VBHE was near the fracture edge (S_f = +25 m).

When S_f = -25 m, for medium groundwater flow in the matrix, again, fracture which is closer to the VBHE cools down ΔT_b and reduces X_{2K} more efficiently than the fracture, which is further away. However, compared with S_f = +25 m, fracture effect on X_{2K} is not symmetrical with respect to the fracture shift (see S_f = +25 m and S_f = -25 m in Figure E.4), unlike the fracture effect on ΔT_b (Figure E.2). When S_f = -25 m the fracture effect on X_{2K} is not as pronounced as when S_f = +25 m. This is because when S_f = -25 m the VBHE is located near fracture edge with increased local groundwater velocities and thus is cooled down effectively by conduction and advection. However, as the heat from the VBHE is advected downstream, there is no fracture downstream of the VBHE, i.e. the fracture cooling effect is absent; thus, the heat transport is less efficient.

For slow groundwater flow in the matrix, ΔT_b is maximally reduced by nearby fracture (Figure E.2) when S_f = 0 m, more significantly so when the fracture is closer. This is because the groundwater velocity inside the fracture is maximum at its mid-length. The insignificant change in local groundwater velocities around the fracture does not affect ΔT_b. Due to slow groundwater flow in the matrix, the fracture does not have sufficient volumetric flow rate to reduce the +2 K isotherm extent. Thus, the fracture cools down ΔT_b by extending X_{2K} for both fracture distances D_f from VBHE (Figure E.4). Both ΔT_b and X_{2K} are changed less by the more distant fracture. Unlike ΔT_b, the maximum fracture effect on X_{2K} is not when

S_f = 0 m, but when S_f = +25 m. This is because in this case the fracture is fully downstream of the VBHE, which allows the heat from the VBHE (+2 K and higher) to enter the fracture edge and then it is transported further away along the fracture and enters the cooler matrix via conduction along the fracture length.

Note that as the fracture shift S_f increases beyond half of the fracture length, the base value of fracture distance from the VBHE also increases (the fracture edge moves away from the VBHE).

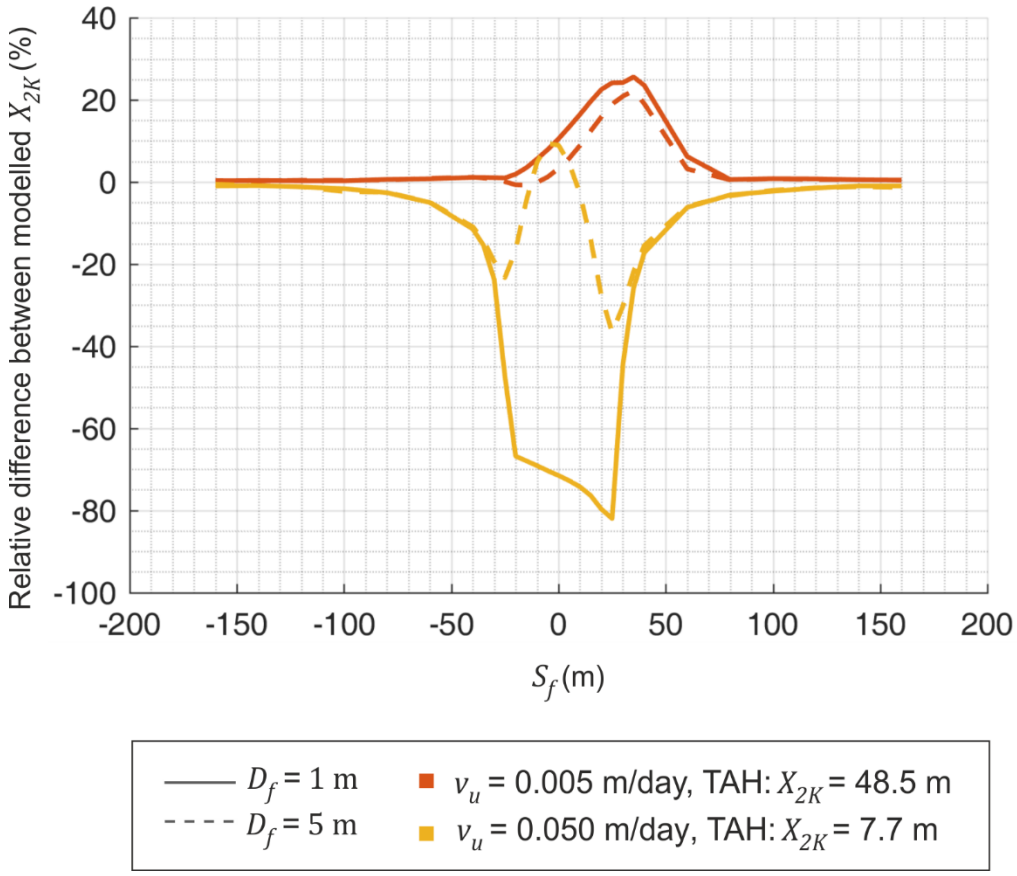

Figure E.4 Relative difference $\left(X_{2K}^{TAF_{2D}} - X_{2K}^{TAH_{2D}}\right)/X_{2K}^{TAH_{2D}}$ in the maximum extent in x-coordinate of the +2 K isotherm after 30 years of continuous operation for varying fracture shift relative to the VBHE S_f and for two fracture distances D_f. Two undisturbed groundwater velocities v_u are used. The actual values for TAH-2D are in the legend.

Figure E.5 shows how the fracture shift relative to the VBHE S_f affects t_{S2K} for two groundwater flows in the matrix v_u and for two fracture distances from the VBHE D_f. The relationship is similar as for t_{Sb} in Figure E.3. While the relative model difference is larger for the faster groundwater flow, the actual time to stabilise the +2 K isotherm, t_{Sb}, is larger for slow v_u (for TAH-2D t_{Sb} = 84 years).

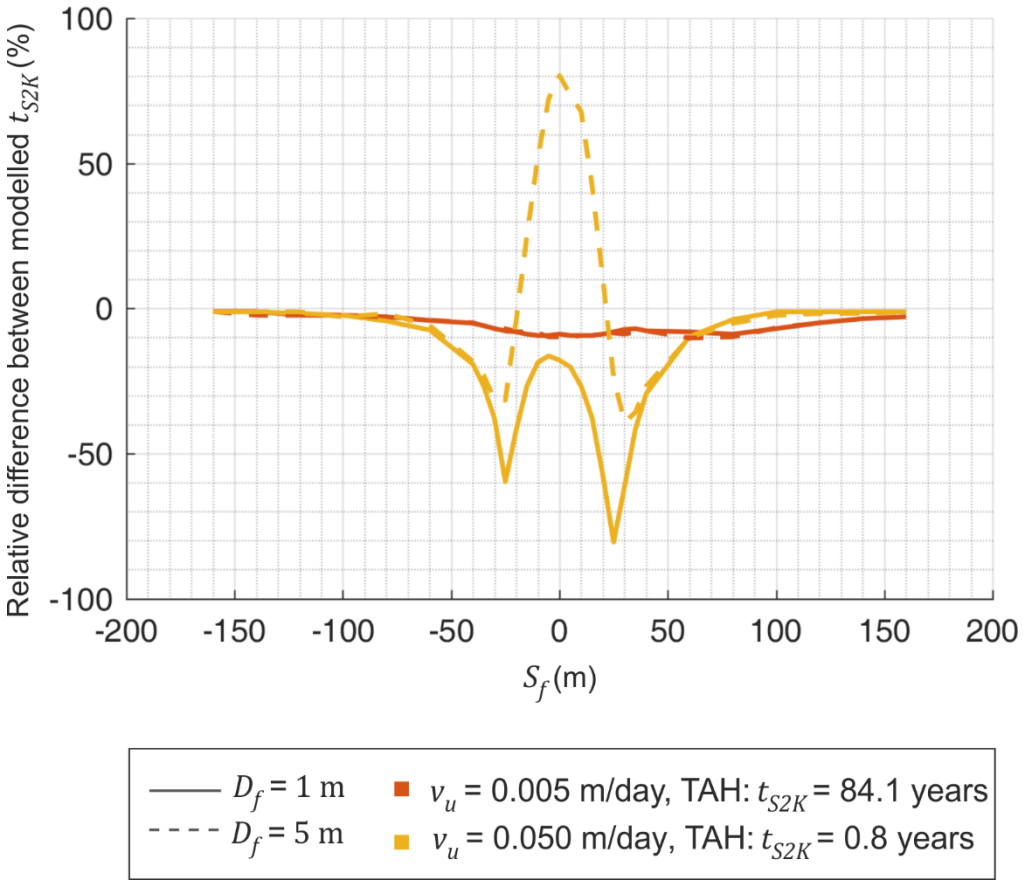

Figure E.5 Relative difference between the TAH-2D and TAF-2D models $\left(t_{S2K}^{TAF_{2D}} - t_{S2K}^{TAH_{2D}}\right)/t_{S2K}^{TAH_{2D}}$ for varying fracture shift relative to the VBHE S_f for two fracture distances from the VBHE D_f. t_{S2K} is the time to stabilise the maximum extent in x-coordinate of the +2 K isotherm. Two undisturbed groundwater velocities v_u are used. The actual t_{S2K} values for TAH-2D model are in the legend.

List of References

Abdelaziz, S. L., T. Y. Ozudogru, C. G. Olgun and J. R. Martin. 2014. Multilayer finite line source model for vertical heat exchangers. *Geothermics* **51:** 406-416.

Acworth, R. 1987. The development of crystalline basement aquifers in a tropical environment. *Quarterly Journal of Engineering Geology and Hydrogeology* **20:** 265-272.

Alcaraz, M., A. García-Gil, E. Vázquez-Suñé and V. Velasco. 2016. Advection and dispersion heat transport mechanisms in the quantification of shallow geothermal resources and associated environmental impacts. *Science of The Total Environment* **543:** 536-546.

Allen, D., L. Brewerton, L. Coleby, B. Gibbs, M. Lewis, A. Macdonald, S. Wagstaff and A. Williams. 1997. The physical properties of major aquifers in England and Wales.

Arbogast, T., J. Douglas, Jim and U. Hornung. 1990. Derivation of the double porosity model of single phase flow via homogenization theory. *SIAM Journal on Mathematical Analysis* **21:** 823-836.

Atam, E. and L. Helsen. 2016. Ground-coupled heat pumps: Part 2—Literature review and research challenges in optimal design. *Renewable and Sustainable Energy Reviews* **54:** 1668-1684.

Banks, D. 2015. A review of the importance of regional groundwater advection for ground heat exchange. *Environmental Earth Sciences* **73:** 2555-2565.

Bayer, P., D. Saner, S. Bolay, L. Rybach and P. Blum. 2012. Greenhouse gas emission savings of ground source heat pump systems in Europe: A review. *Renewable and Sustainable Energy Reviews* **16:** 1256-1267.

Bear, J. 1988. *Dynamics of fluids in porous media.* Dover Publications, Inc.**,** New York.

Bear, J., C.-F. Tsang and G. D. Marsily. 1993. Flow and contaminant transport in fractured rock. in. Academic Press, Inc., San Diego, California.

Beyer, M. and U. Mohrlok. 2007. A double continuum approach for determining contaminant transport in fractured porous media. In: *Groundwater in fractured rocks. Selected papers from the Groundwater in Fractured Rocks International Conference, Prague, 2003,* J. Í. Krásny & J. J. M. Sharp (eds.). London: Taylor & Francis Group**;** 646. Ch. 37.

Blum, P., G. Campillo and T. Kölbel. 2011. Techno-economic and spatial analysis of vertical ground source heat pump systems in Germany. *Energy* **36:** 3002-3011.

Blum, P., G. Campillo, W. Münch and T. Kölbel. 2010. CO 2 savings of ground source heat pump systems–a regional analysis. *Renewable Energy* **35:** 122-127.

Brielmann, H., T. Lueders, K. Schreglmann, F. Ferraro, M. Avramov, V. Hammerl, P. Blum, P. Bayer and C. Griebler. 2011. Shallow geothermal energy usage and its potential impacts on groundwater ecosystems. *Grundwasser* **16:** 77-91.

British Plastics Federation. 2019. *Polyethylene (High Density) HDPE*. British Plastics Federation. Available from https://www.bpf.co.uk/plastipedia/polymers/hdpe.aspx (Accessed 03 September 2019).

Bruderer, C. and Y. Bernabé. 2001. Network modeling of dispersion: Transition from Taylor Dispersion in homogeneous networks to mechanical dispersion in very heterogeneous ones. *Water Resources Research* **37:** 897-908.

Busato, F., R. Lazzarin and M. Noro. 2015. Ground or solar source heat pump systems for space heating: Which is better? Energetic assessment based on a case history. *Energy and Buildings* **102:** 347-356.

Cansino, J. M., M. D. P. Pablo-Romero, R. Román and R. Yñiguez. 2011. Promoting renewable energy sources for heating and cooling in EU-27 countries. *Energy Policy* **39:** 3803-3812.

Capozza, A., M. De Carli and A. Zarrella. 2013. Investigations on the influence of aquifers on the ground temperature in ground-source heat pump operation. *Applied Energy* **107:** 350-363.

Carslaw, H. and J. Jaeger. 1959. *Conduction of heat in solids, (Method of images on page 273).* Second ed. Clarendon Press**,** Oxford.

Carvalho, A. D., D. Mendrinos and A. T. De Almeida. 2015a. Ground source heat pump carbon emissions and primary energy reduction potential for heating in buildings in Europe—results of a case study in Portugal. *Renewable and Sustainable Energy Reviews* **45:** 755-768.

Carvalho, A. D., P. Moura, G. C. Vaz and A. T. De Almeida. 2015b. Ground source heat pumps as high efficient solutions for building space conditioning and for integration in smart grids. *Energy Conversion and Management* **103:** 991-1007.

Chai, T. and R. Draxler. 2014. Root mean square error (RMSE) or mean absolute error (MAE)? *Geoscientific Model Development Discussions* **7:** 1525-1534.

Chaudhry, M. A. and S. M. Zubair. 1994. Generalized incomplete gamma functions with applications. *Journal of Computational and Applied Mathematics* **55:** 99-123.

Chen, S. H., A. J. Jakeman and J. P. Norton. 2008. Artificial intelligence techniques: an introduction to their use for modelling environmental systems. *Mathematics and Computers in Simulation* **78:** 379-400.

Chiasson, A. and A. O'connell. 2011. New analytical solution for sizing vertical borehole ground heat exchangers in environments with significant groundwater flow: Parameter estimation from thermal response test data. *HVAC&R Research* **17:** 1000-1011.

Cold Climate Housing Research Center. 2016. *Heat pump scheme*. Cold climate housing research center,, online. Available from http://www.cchrc.org/weller_school/wp-content/uploads/2011/05/weller_heat_pump_graphic.jpg (Accessed 5 April 2016).

Comsol 5.2a. 2016. *User's Guides and Application Library Manuals.*

Comte, J.-C. 2016. Catchment-scale heterogeneity of hydraulic properties in the Irish weathered/fractured bedrock aquifers: Implications for aquifer typology and groundwater flowpaths. *Groundwater in Fractured Bedrock Environments: Managing Catchment and Subsurface Resources, Year of Water series Conference in Belfast by the Geol. Soc. 10th June*. The Geological Society.

Comte, J.-C., R. Cassidy, J. Nitsche, U. Ofterdinger, K. Pilatova and R. Flynn. 2012. The typology of Irish hard-rock aquifers based on an integrated hydrogeological and geophysical approach. *Hydrogeology Journal* **20:** 1569-1588.

Cook, P. G. 2003. *A Guide to regional groundwater flow in fractured rock aquifers.* CSIRO Land and Water**,** Glen Osmond, SA, Australia.

Curtis, R., J. Lund, B. Sanner, L. Rybach and G. Hellström. 20052005. Ground source heat pumps–geothermal energy for anyone, anywhere: current worldwide activity. Pages 24-29. *Proceedings World Geothermal Congress* Antalya, Turkey.

Daly, K. R. and T. Roose. 2014. Multiscale modelling of hydraulic conductivity in vuggy porous media. *Proceedings of the Royal Society of London A: Mathematical, Physical and Engineering Sciences* **470**.

De La Bernardie, J., O. Bour, T. Le Borgne, N. Guihéneuf, E. Chatton, T. Labasque, H. Le Lay and M. F. Gerard. 2018. Thermal attenuation and lag time in fractured rock: theory and field measurements from joint heat and solute tracer tests. *Water Resources Research* **54:** 10,053-10,075.

Dehkordi, S. E., B. Olofsson and R. A. Schincariol. 2015. Effect of groundwater flow in vertical and horizontal fractures on borehole heat exchanger

temperatures. *Bulletin of Engineering Geology and the Environment* **74:** 479-491.

Dehkordi, S. E. and R. A. Schincariol. 2014. Effect of thermal-hydrogeological and borehole heat exchanger properties on performance and impact of vertical closed-loop geothermal heat pump systems. *Hydrogeology Journal* **22:** 189-203.

Department of Communications Energy and Natural Resources of Ireland. 2016. *Geological survey of Ireland. Geothermal suitability map for vertical closed loop systems*. Ordnance Survey Ireland, online. Available from http://dcenr.maps.arcgis.com/apps/webappviewer/index.html?id=9ee46bee08de41278b90a991d60c0b9e (Accessed 11 June 2016).

Diao, N., Q. Li and Z. Fang. 2004. Heat transfer in ground heat exchangers with groundwater advection. *International Journal of Thermal Sciences* **43:** 1203-1211.

Dietrich, P., R. Helmig, M. Sauter, H. Hötzl, J. Köngeter and G. Teutsch. 2005. Flow and Transport in Fractured Porous Media. in. Springer, Heidelberg.

Ene, H. I. and D. Poliserverski. 1987. *Thermal flow in porous media.* Kluwer Academic Publishers**,** Norwell, MA.

Energy Saving Trust. 2007. *Domestic Ground Source Heat Pumps: Design and installation of closed-loop systems – A guide for specifiers, their advisors and potential users, CE82.* Energy Saving Trust, London.

Erol, S. 2016. *Near Field Investigation of Borehole Heat Exchangers.* A dissertation submitted in fulfillment for the degree of Doctor of Philosophy in Engineering Sciences. The Université Libre de Bruxelles Bruxelles.

Erol, S. and B. François. 2014. Efficiency of various grouting materials for borehole heat exchangers. *Applied Thermal Engineering* **70:** 788-799.

Erol, S. and B. François. 2016. Freeze damage of grouting materials for borehole heat exchanger: Experimental and analytical evaluations. *Geomechanics for Energy and the Environment* **5:** 29-41.

Erol, S. and B. François. 2018. Multilayer analytical model for vertical ground heat exchanger with groundwater flow. *Geothermics* **71:** 294-305.

Erol, S., M. A. Hashemi and B. François. 2015. Analytical solution of discontinuous heat extraction for sustainability and recovery aspects of borehole heat exchangers. *International journal of thermal sciences* **88:** 47-58.

Eskilson, P. 1987. *Thermal analysis of heat extraction boreholes.* PhD thesis. University of Lund, Lund, Sweden.

EU Council. 2009. *Directive 2009/125/EC of the European Parliament and of the Council of 21 October 2009 establishing a framework for the setting of ecodesign requirements for energy-related products, OJ L 285 , 31.10.2009*. EU Council.

EU Council. 2010a. *Directive 2010/30/EU of the European Parliament and of the Council of 19 May 2010 on the indication by labelling and standard product information of the consumption of energy and other resources by energy-related products, OJ L 153 , 18.6.2010*. EU Council.

EU Council. 2010b. *Directive 2010/31/EU of the European Parliament and of the Council of 19 May 2010 on the energy performance of buildings (recast), OJ L 153 , 18.6.2010*. EU Council.

EU Council. 2018a. *Directive (EU) 2018/2001 of the European Parliament and of the Council of 11 December 2018 on the promotion of the use of energy from renewable sources (recast), OJ L 328/82 , 21.12.2018*. EU Council.

EU Council. 2018b. *DIRECTIVE (EU) 2018/2002 of the European Parliament and of the Council of 11 December 2018 amending Directive 2012/27/EU on energy efficiency. OJ L 328/210, 21.12.2018*.

European Commission. 2016. *Communication from the Commission to the European Parliament, the Council, the European Economic and Social Committee and the Committee of the Regions on an EU Strategy for Heating and Cooling.*

European Council for an Energy Efficient Economy. 2019. *EU's 2030 policy framework*. ECEEE, online. Available from https://www.eceee.org/policy-areas/2030-policy-framework/ (Accessed 03 September 2019).

European Geothermal Energy Council. 2015. *ReGeoCities, Developing Geothermal Heat Pumps in Smart Cities and Communities. Final Report*. Available from http://regeocities.eu/wp-content/uploads/2012/08/ReGeoCities-Final-Report_web.pdf.

Ferguson, G. 2007. Heterogeneity and Thermal Modeling of Ground Water. *Ground Water* **45:** 485-490.

Ferguson, G. 2015. Screening for heat transport by groundwater in closed geothermal systems. *Groundwater* **53:** 503-506.

Fetter, C. W. 2001. *Applied Hydrogeology.* 4th ed. Pages 598. Prentice-Hall**,** New Jersey.

Florides, G. and S. Kalogirou. 2007. Ground heat exchangers—A review of systems, models and applications. *Renewable energy* **32:** 2461-2478.

Freeze, R. A. and J. A. Cherry. 1979. *Groundwater.* Prentice-Hall**,** Englewood Cliffs, NJ.

Fujii, H., T. Inatomi, R. Itoi and Y. Uchida. 2007. Development of suitability maps for ground-coupled heat pump systems using groundwater and heat transport models. *Geothermics* **36:** 459-472.

García-Gil, A., E. Vázquez-Suñe, M. M. Alcaraz, A. S. Juan, J. Á. Sánchez-Navarro, M. Montlleó, G. Rodríguez and J. Lao. 2015. GIS-supported mapping of low-temperature geothermal potential taking groundwater flow into account. *Renewable Energy* **77:** 268-278.

Gehlin, S. 2002. *Thermal response test: Method development and evaluation.* Doctoral thesis. Lulea University of Technology, Sweden, Lulea.

Gehlin, S. and G. Hellström. 2003. Influence on thermal response test by groundwater flow in vertical fractures in hard rock. *Renewable energy* **28:** 2221-2238.

Geiger, S. and S. Emmanuel. 2010. Non-Fourier thermal transport in fractured geological media. *Water Resources Research* **46:** n/a-n/a.

Gelhar, L. W., C. Welty and K. R. Rehfeldt. 1992. A critical review of data on field-scale dispersion in aquifers. *Water Resources Research* **28:** 1955-1974.

Geological Survey of Ireland. 2015. *Ground Source Heat and Shallow Geothermal Energy. Homeowner manual.* Geological Survey of Ireland and Department of Communications Energy and Natural Resources, Dublin.

Giordano, N., C. Comina, G. Mandrone and A. Cagni. 2016. Borehole thermal energy storage (BTES). First results from the injection phase of a living lab in Torino (NW Italy). *Renewable Energy* **86:** 993-1008.

Gustafsson, A. M. and L. Westerlund. 2010. Multi-injection rate thermal response test in groundwater filled borehole heat exchanger. *Renewable Energy* **35:** 1061-1070.

Haehnlein, S., P. Bayer and P. Blum. 2010. International legal status of the use of shallow geothermal energy. *Renewable and Sustainable Energy Reviews* **14:** 2611-2625.

Hardebol, N., C. Maier, H. Nick, S. Geiger, G. Bertotti and H. Boro. 2015. Multiscale fracture network characterization and impact on flow: A case study on the Latemar carbonate platform. *Journal of Geophysical Research: Solid Earth* **120:** 8197-8222.

Hecht-Méndez, J., N. Molina-Giraldo, P. Blum and P. Bayer. 2010. Evaluating MT3DMS for heat transport simulation of closed geothermal systems. *Groundwater* **48:** 741-756.

Hein, P., O. Kolditz, U.-J. Görke, A. Bucher and H. Shao. 2016. A numerical study on the sustainability and efficiency of borehole heat exchanger coupled ground source heat pump systems. *Applied Thermal Engineering* **100:** 421-433.

Hénault, B., P. Pasquier and M. Kummert. 2016. Financial optimization and design of hybrid ground-coupled heat pump systems. *Applied Thermal Engineering* **93:** 72-82.

Hidalgo, J. J., J. Carrera and M. Dentz. 2009. Steady state heat transport in 3D heterogeneous porous media. *Advances in water resources* **32:** 1206-1212.

Ho, C. (Technical report, Sandia National Laboratories, Albuquerque, NM (US)). 2000. *Dual porosity vs. dual permeability models of matrix diffusion in fractured rock.*

ISRM. 1978. International Society for Rock Mechanics, Commission on standardization of laboratory and field tests: Suggested methods for the quantitative description of discontinuities in rock masses. *International Journal of Rock Mechanics and Mining Sciences & Geomechanics Abstracts* **15:** 319-368.

Javed, S. and J. Spitler. 2017. Accuracy of borehole thermal resistance calculation methods for grouted single U-tube ground heat exchangers. *Applied Energy* **187:** 790-806.

Javed, S. and J. D. Spitler. 2016. 3 - Calculation of borehole thermal resistance. In: *Advances in Ground-Source Heat Pump Systems,* S. J. Rees (ed.). Woodhead Publishing**;** 63-95.

Klenk, I. and P. Grathwohl. 2002. Transverse vertical dispersion in groundwater and the capillary fringe. *Journal of Contaminant Hydrology* **58:** 111-128.

Koohi-Fayegh, S. and M. A. Rosen. 2013. A review of the modelling of thermally interacting multiple boreholes. *Sustainability* **5:** 2519-2536.

Kuzmic, N., Y. L. E. Law and S. B. Dworkin. 2016. Numerical heat transfer comparison study of hybrid and non-hybrid ground source heat pump systems. *Applied Energy* **165:** 919-929.

Lee, C. and H. Lam. 2012. A modified multi-ground-layer model for borehole ground heat exchangers with an inhomogeneous groundwater flow. *Energy* **47:** 378-387.

Lee, T.-C. 1998. *Applied mathematics in hydrogeology.* CRC Press**,** Boca Raton.

Li, Q., K. Ito, Z. Wu, C. S. Lowry and S. P. Loheide Ii. 2009. COMSOL Multiphysics: A Novel Approach to Ground Water Modeling. *Ground Water* **47:** 480-487.

Liebel, H. T. 2012. *Influence of Groundwater on Measurements of Thermal Properties in Fractured Aquifers.* Thesis for the degree of Philosophiae Doctor. Norwegian University of Science and Technology, Trondheim.

Liebel, H. T., K. Huber, B. S. Frengstad, R. K. Ramstad and B. Brattli. 2012. Thermal response testing of a fractured hard rock aquifer with and without induced groundwater flow. *Bulletin of Engineering Geology and the Environment* **71:** 435-445.

Liuzzo-Scorpo, A., B. Nordell and S. Gehlin. 2015. Influence of regional groundwater flow on ground temperature around heat extraction boreholes. *Geothermics* **56:** 119-127.

Lord, J. A., C. R. I. Clayton and R. N. Mortimore. 2002. *Engineering in chalk. Section 2 The engineering geology of chalk (Plate 2.16b page 51).* Pages 350. CIRIA**,** London.

Loveridge, F., G. Holmes, W. Powrie and T. Roberts. 2013. Thermal response testing through the chalk aquifer. *ICE Proceedings Geotechnical Engineering* **166:** 197-210.

Lund, J. W. and T. L. Boyd. 2016. Direct utilization of geothermal energy 2015 worldwide review. *Geothermics* **60:** 66-93.

Marcotte, D., P. Pasquier, F. Sheriff and M. Bernier. 2010. The importance of axial effects for borehole design of geothermal heat-pump systems. *Renewable Energy* **35:** 763-770.

Molina-Giraldo, N., P. Bayer and P. Blum. 2011a. Evaluating the influence of thermal dispersion on temperature plumes from geothermal systems using analytical solutions. *International Journal of Thermal Sciences* **50:** 1223-1231.

Molina-Giraldo, N., P. Blum, K. Zhu, P. Bayer and Z. Fang. 2011b. A moving finite line source model to simulate borehole heat exchangers with groundwater advection. *International Journal of Thermal Sciences* **50:** 2506-2513.

Morris, D. A. and A. I. Johnson (US Government Printing Office). 1967. *Summary of hydrologic and physical properties of rock and soil materials, as analyzed by the hydrologic laboratory of the US Geological Survey, 1948-60.*

Mottaghy, D. and L. Dijkshoorn. 2012. Implementing an effective finite difference formulation for borehole heat exchangers into a heat and mass transport code. *Renewable Energy* **45:** 59-71.

National Research Council. 1996. *Rock fractures and fluid flow: contemporary understanding and applications.* National Academies Press.

Neuman, S. P. and D. M. Tartakovsky. 2009. Perspective on theories of non-Fickian transport in heterogeneous media. *Advances in Water Resources* **32:** 670-680.

Pambou, C. H. K., J. Raymond and L. Lamarche. 2019. Improving thermal response tests with wireline temperature logs to evaluate ground thermal conductivity profiles and groundwater fluxes. *Heat and Mass Transfer* **55:** 1829-1843.

Panfilov, M. 2000. *Macroscale models of flow through highly hetrogeneous porous media.* Kluwer Academic Publishers**,** Dordrecht, The Netherlands.

Pedchenko O., Loveridge F., N. Woodman and W. Powrie. 2019. Quantifying the effect of single fractures on the thermal performance of borehole heat exchangers. *European Geothermal Energy Council*. To be confirmed.

Pehme, P. E., B. L. Parker, J. A. Cherry, J. W. Molson and J. P. Greenhouse. 2013. Enhanced detection of hydraulically active fractures by temperature profiling in lined heated bedrock boreholes. *Journal of Hydrology* **484:** 1-15.

Plumas-Sierra Rural Electric Cooperative. 2016. *How does GeoExchange work?* . Online. Available from http://www.psrec.coop/geothermal.php (Accessed December 2016).

Radioti, G., S. Delvoie, R. Charlier, G. Dumont and F. Nguyen. 2016. Heterogeneous bedrock investigation for a closed-loop geothermal system: A case study. *Geothermics* **62:** 79-92.

Rau, G. C., M. S. Andersen and R. I. Acworth. 2012. Experimental investigation of the thermal dispersivity term and its significance in the heat transport equation for flow in sediments. *Water Resources Research* **48**.

Raymond, J., S. Mercier and L. Nguyen. 2015. Designing coaxial ground heat exchangers with a thermally enhanced outer pipe. *Geothermal Energy* **3:** 7.

Retkowski, W., G. Ziefle and J. Thöming. 2015. Evaluation of different heat extraction strategies for shallow vertical ground-source heat pump systems. *Applied Energy* **149:** 259-271.

Rivera, J. A., P. Blum and P. Bayer. 2015a. Analytical simulation of groundwater flow and land surface effects on thermal plumes of borehole heat exchangers. *Applied Energy* **146:** 421-433.

Rivera, J. A., P. Blum and P. Bayer. 2015b. Ground energy balance for borehole heat exchangers: Vertical fluxes, groundwater and storage. *Renewable Energy* **83:** 1341-1351.

Rouleau, J., L. Gosselin and J. Raymond. 2016. New concept of combined hydro-thermal response tests (H/TRTS) for ground heat exchangers. *Geothermics* **62:** 103-114.

Saito, T., S. Hamamoto, T. Ueki, S. Ohkubo, P. Moldrup, K. Kawamoto and T. Komatsu. 2016. Temperature change affected groundwater quality in a confined marine aquifer during long-term heating and cooling. *Water Research* **94:** 120-127.

Saner, D., R. Juraske, M. Kübert, P. Blum, S. Hellweg and P. Bayer. 2010. Is it only CO 2 that matters? A life cycle perspective on shallow geothermal systems. *Renewable and Sustainable Energy Reviews* **14:** 1798-1813.

Sarbu, I. and C. Sebarchievici. 2014. General review of ground-source heat pump systems for heating and cooling of buildings. *Energy and Buildings* **70:** 441-454.

Sauty, J., A. Gringarten, A. Menjoz and P. Landel. 1982. Sensible energy storage in aquifers: 1. theoretical study. *Water Resources Research* **18 (2):** 245-252.

Self, S. J., B. V. Reddy and M. A. Rosen. 2013. Geothermal heat pump systems: status review and comparison with other heating options. *Applied Energy* **101:** 341-348.

Singhal, B. B. S. and R. P. Gupta. 2010. *Applied hydrogeology of fractured rocks.* Springer Science & Business Media.

Somogyi, V., V. Sebestyén and G. Nagy. 2017. Scientific achievements and regulation of shallow geothermal systems in six European countries–A review. *Renewable and Sustainable Energy Reviews* **68:** 934-952.

Soni, S. K., M. Pandey and V. N. Bartaria. 2015. Ground coupled heat exchangers: A review and applications. *Renewable and Sustainable Energy Reviews* **47:** 83-92.

Soni, S. K., M. Pandey and V. N. Bartaria. 2016. Hybrid ground coupled heat exchanger systems for space heating/cooling applications: A review. *Renewable and Sustainable Energy Reviews* **60:** 724-738.

Stauffer, F., P. Bayer, P. Blum, N. M. Giraldo and W. Kinzelbach. 2014. *Thermal Use of Shallow Groundwater.* Taylor & Francis.

Suresh Kumar, G. 2014. Mathematical modeling of groundwater flow and solute transport in saturated fractured rock using a dual-porosity approach. *Journal of Hydrologic Engineering* **19:** 04014033.

Sutton, M. G., D. W. Nutter and R. J. Couvillion. 2003. A ground resistance for vertical borehole heat exchangers with groundwater flow. *Journal of Energy Resources Technology* **125:** 183-189.

The MathWorks Inc. 2017. *Matlab*. R2017a. The MathWorks Inc.,**,** Natick, Massachusetts, United States.

Tye-Gingras, M. and L. Gosselin. 2014. Generic ground response functions for ground exchangers in the presence of groundwater flow. *Renewable Energy* **72:** 354-366.

Wagener, T. and J. Kollat. 2007. Numerical and visual evaluation of hydrological and environmental models using the Monte Carlo analysis toolbox. *Environmental Modelling & Software* **22:** 1021-1033.

Wagner, V., P. Bayer, G. Bisch, M. Kübert and P. Blum. 2014. Hydraulic characterization of aquifers by thermal response testing: Validation by large-scale tank and field experiments. *Water Resources Research* **50:** 71-85.

Yang, H., P. Cui and Z. Fang. 2010. Vertical-borehole ground-coupled heat pumps: a review of models and systems. *Applied Energy* **87:** 16-27.

Yang, W., Y. Chen, M. Shi and J. D. Spitler. 2013. Numerical investigation on the underground thermal imbalance of ground-coupled heat pump operated in cooling-dominated district. *Applied Thermal Engineering* **58:** 626-637.

Zarrella, A. and P. Pasquier. 2015. Effect of axial heat transfer and atmospheric conditions on the energy performance of GSHP systems: A simulation-based analysis. *Applied Thermal Engineering* **78:** 591-604.

Zeng, H., N. Diao and Z. Fang. 2003. Heat transfer analysis of boreholes in vertical ground heat exchangers. *International Journal of Heat and Mass Transfer* **46:** 4467-4481.

Zimmerman, R. W. and I.-W. Yeo. 2000. Fluid Flow in Rock Fractures: From the Navier-Stokes Equations to the Cubic Law. In: *Dynamics of Fluids in Fractured Rock,* B. Faybishenko, P. A. Witherspoon & S. M. Benson (eds.). Washington, D. C.: American Geophysical Union.

Zubair, S. and M. A. Chaudhry. 1996. Temperature solutions due to time-dependent moving-line-heat sources. *Heat and Mass Transfer* **31:** 185-189.